Assessment of the Role of Clusterin/Apolipoprotein J in Cellular Homeostasis

A doctoral dissertation
submitted in partial fulfillment
of the requirements for the degree of
doctor rerum naturalium

at the

Faculty of Biology

Johannes Gutenberg-University Mainz

by

Philipp Rohne, Dipl.-Biol.

Born on September 7th 1983 in Wippra

Mainz 2017

The present thesis has been drafted in the period between September 2012 and March 2017 in the Work Group Cellular Biochemistry at the Institute of Pharmacy and Biochemistry – Therapeutical Life Sciences – Johannes Gutenberg University, Mainz.

Dean:

Thesis Advisor:
Primary Reviewer:
Secondary Reviewer:

Date of oral exam: 17.11.2017

The author attests that permission has been obtained for the use of any copyrighted material appearing in this thesis (other than brief excerpts requiring only proper acknowledgement in scholarly writing) and that all such use is clearly acknowledged. Furthermore, the author assures that he has independently produced this work and has not used any sources and aids other than stated, with quotations duly marked as such.

_____

Signature of Author

Permission is herewith granted to the Faculty of Biology of the Johannes Gutenberg-University Mainz to circulate and to have copied for non-commercial purposes, at its discretion, the above title upon the request of individuals or institutions.

The author reserves other publication rights, and neither the thesis nor extensive extracts from it may be printed or otherwise reproduced without the author's written permission.

Contents

Assessment of the Role of Clusterin/Apolipoprotein J in Cellular Homeostasis

Philipp Rohne, Dipl.-Biol.

Abstract

Clusterin (CLU) is a highly glycosylated extracellular chaperone with a nearly ubiquitous expression in vertebrates and tissues. Since its discovery more than three decades ago, especially the secretory form of CLU (sCLU) was considered being a cytoprotective protein with high correlation to certain diseases, such as cancer, atherosclerosis and Alzheimer's disease. Despite of intense research activity (almost 2500 articles in PubMed), its exact role in diseases is still unknown. This thesis focuses primarily on the role of sCLU in the cellular homeostasis and proteostasis. Underlying important properties of human sCLU are the glycosylation and the proteolytic cleavage into two separate chains held together by disulfide bonds. Therefore, at first the role of these structural properties on the folding and chaperone activity of sCLU will be addressed. This will be predominately conducted by using human and mouse sCLU. In this context, it will be further assessed in which way CLU is conserved among the animal kingdom and whether the CLU protein indeed can be considered as a conserved secretory molecular chaperone. Based on findings concerning the chaperone activity of sCLU, a potential role in cell biology will be addressed. Noticeable, in past studies an elevated abundance of CLU and sCLU was identified by virtue of its occurrence in pathologies with uncontrolled or detrimental cell death, such as in ischemia, inflammation or wounding. The second section therefore investigates the expression of CLU in an *in vitro* necrosis model to understand its function in harmful cellular settings. Intriguingly, this approach led to new insights concerning CLU's role in the unfolded protein response (UPR) and revealed CLUs' interplay with various proteostatic pathways. Moreover, a new cellular mechanism called *Necrosis-induced Proliferation* (NiP) will be proposed, which might have important implications for treatment of cancer. In summary, this thesis discusses basic aspects of CLU biochemical and cell biological properties to understand its role in death and disease.

Publication List

The doctoral thesis is based on the following publications (*Corresponding Author)

(1) "Non-Secreted Clusterin Isoforms Are Translated in Rare Amounts from Distinct Human mRNA Variants and Do Not Affect Bax-Mediated Apoptosis or the NF-κB Signaling Pathway."

Prochnow H, Gollan R, **Rohne P**, Hassemer M, Koch-Brandt C, Baiersdörfer M*
PLoS One, 2013

---

(2) "The Chaperone Activity of Clusterin is Dependent on Glycosylation and Redox Environment."
Rohne P*, Prochnow H, Wolf S, Renner B, Koch-Brandt C
Cellular Physiology and Biochemistry, 2014

---

(3) "Clusterin/Apolipoprotein J: How glycosylation, proteolytic cleavage and redox environment determine the function of an extracellular chaperone"
Rohne P*, Renner B, Koch-Brandt C
Poster presentation, DGZ Meeting 2015, Cologne

---

(4) "The CLU-Files: Disentanglement of a Mystery"
Rohne P*, Prochnow H, Koch-Brandt C
Biomolecular Concepts, 2016

---

(5) "Exposure of Vital Cells to Necrotic Cell Lysates Induce the IRE1α Branch of the Unfolded Protein Response and Cell Proliferation"
Rohne P*, Wolf S, Dörr C, Ringen J, Holtz A, Gollan R, Renner B, Baiersdörfer M, Prochnow H, Koch-Brandt C
Cell Stress and Chaperones, 2017

1 Introduction

1.1 Clusterin (CLU): Discovery of a multifaceted glycoprotein

The first hit of the term „clusterin“ in PubMed was found in the year 1979 in a study which characterized a glycoprotein in the salvia shown to aggregate *Streptococcus sangius* [1]. However, the first occurrence of the word “clusterin” in an article is from 1983. In this year two studies have found a cell-aggregating factor in the rete testis fluid of the ram and characterized it as an 80 kDa glycoprotein terming it clusterin (CLU) [2, 3]. In the following years, further groups independently found CLU in various contexts leading to an extensive repertoire of names, such as glycoprotein of 80 kDa (gp80) [4], complement lysis inhibitor (CLI) [5], testosterone repressed message-2 (TRPM-2) [6] or apolipoprotein J (apoJ) [7]. However, to prevent confusion in 1992 the name clusterin (CLU) was generally accepted [8].

1.2 Human CLU: Biosynthesis

In humans, the *clu* gene is located on the p-arm of chromosome 8 at the location 8p21-p12 as a single-copy gene [9, 10]. From this gene, at least three transcript variants are known [11]. These transcripts all bear exon 2 to 9 but have alternative exon 1 (1a, 1b and 1c). Located on exon 2 is the so-called signal sequence coding region (SSCR). This region consists of an endoplasmic reticulum (ER) leader sequence (ER leader) with a double AUG acting as an upstream translation start site. Originating at this area, CLU follows the canonical pathway of secretory proteins [12]. The preproprotein consists 449 amino acids (aa) including the 22 aa ER leader sequence which is cleaved off after entering the ER. Within the ER four to five disulfide bonds are formed [13] and an N-linked core glycosylation occurs at six asparagine residues generating the so-called presecretory CLU (psCLU) [4, 14, 15]. Subsequently, psCLU is transferred to the Golgi apparatus (Golgi) and complex carbohydrate moieties are attached. These carbohydrate moieties are composed of galactose, fucose, mannose, N-acetylglucosamine and N-acetylneuraminic acid, and differ in a tissue-dependent manner [14, 16]. Eventually, the resulting approximately 80 kDa protein is cleaved by a furin-like proprotein convertase (FC) between Arg227 and Ser228 at the recognition site RIVR|S resulting in an N-terminal α-chain and a C-terminal β-chain [17]. Finally, the heterodimeric glycoprotein with 40-45 kDa per chain is secreted from the cell, representing secretory clusterin (sCLU). Importantly, under conditions of cellular stress or in malign transformed cells, intracellular CLU forms are occasionally emerging. These intracellular CLU forms are either the result of failed translocation, alternative splicing of exon 2 or were translated from alternative

translation initiation start sites [11]. Further, under ER stress conditions the ER key chaperone BiP (GRP78) is able to retrotranslocate CLU forms residing in the ER or Golgi back into the cytosol [18]. An overview of CLU expression and maturation is depicted in Fig.1.

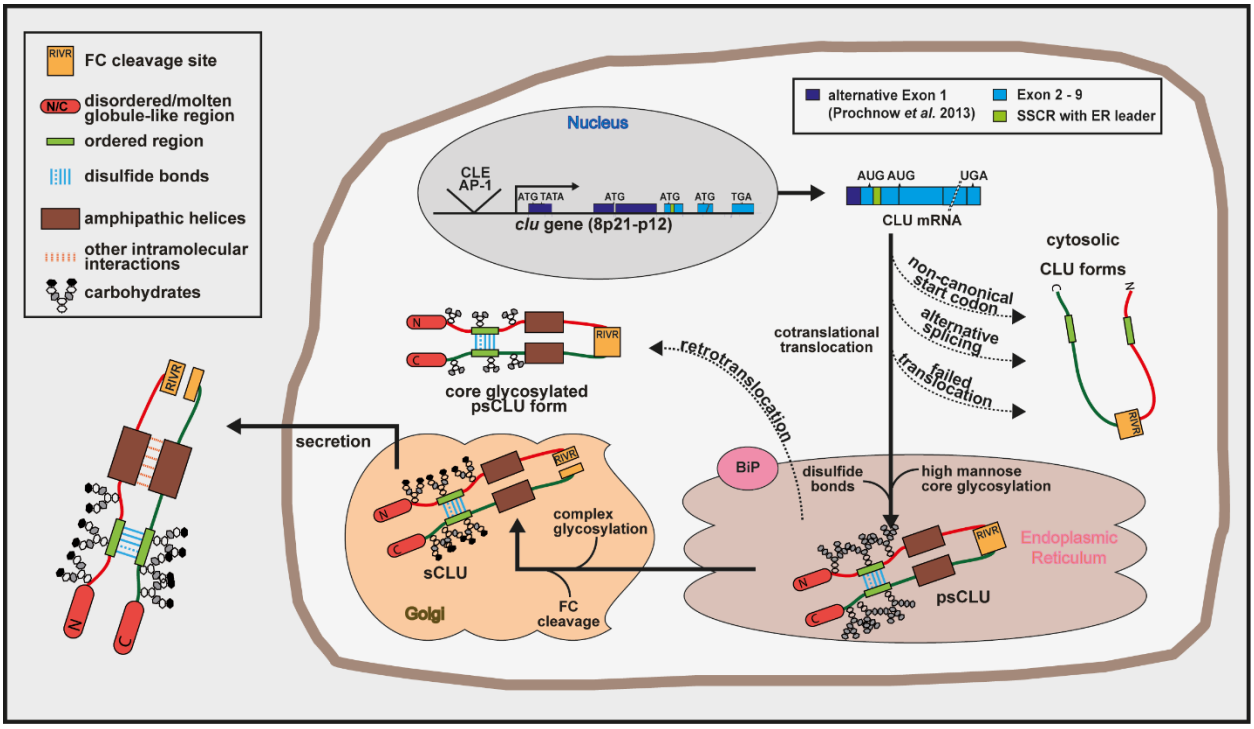

Fig.1 CLU biosynthesis adapted from [19]. SSCR signal sequence coding region; FC furin-like proprotein convertase cleavage site; BiP Binding immunoglobulin protein. Further details see text above.

1.3 Human CLU: Structure

CLU is considered to be a so-called intrinsically misfolded protein [20]. The advantage of intrinsically misfolded proteins is a broad spectrum of potential client proteins since they are feasible to adjust to various structures. This notion holds true for sCLU which was eventually described as the first extracellular chaperone found in 1999 [21]. In numerous studies, it was confirmed that CLU binds different proteins while they are in their off-folding pathway in an ATP-independent manner, such as insulin, catalase, GST, albumin, lysozyme, ovotransferrin, alcohol dehydrogenase, IgG, γ-crystalline and many more [21-23]. Structural predictions revealed that CLU bears at least five amphipathic α-helices where two of them are located at the C- and the N-terminus, which are conserved among humans, rats and bovine [24]. Further, the CLU protein has wide stretches of disordered regions, especially at the C- and N-terminus, and a partially increased hydrophobicity which is compensated by up to 30% glycosylation [12, 21, 24]. An overview of basic structural elements can be found in Fig.2.

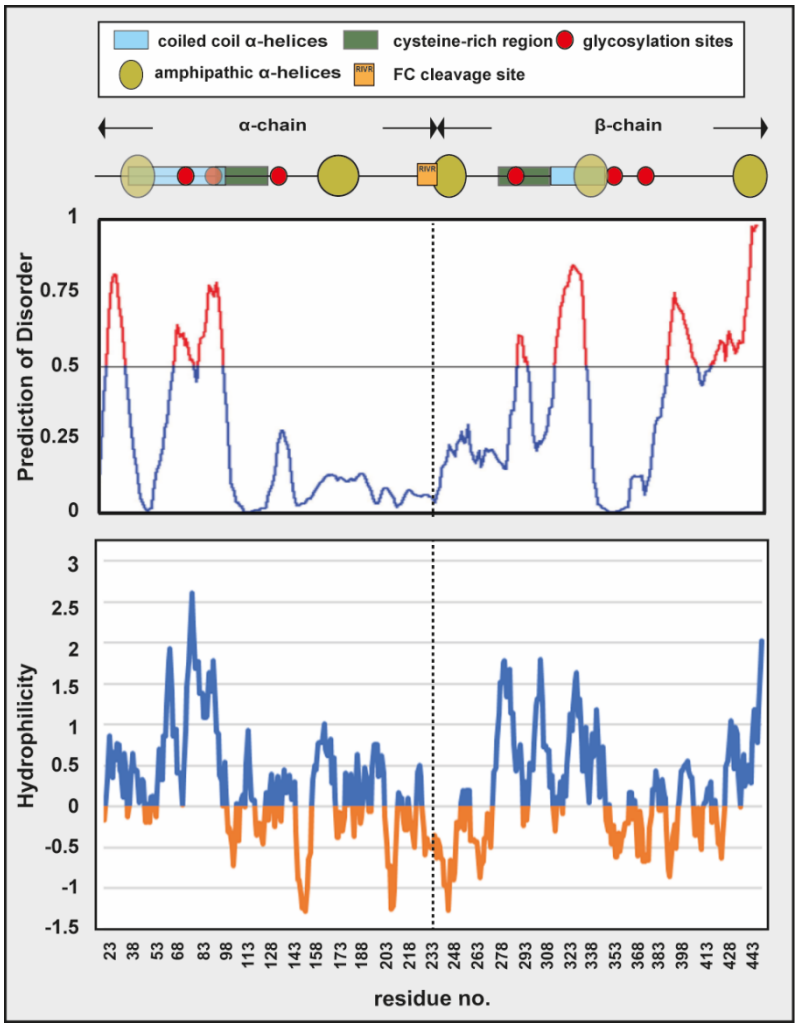

Fig.2 CLU structural properties, disorder and hydrophobicity adapted from [21, 24-26].

From these findings, it was suggested that CLU interacts via its amphipathic α-helices with mainly hydrophobic molecules [21]. A confirmation for a distinct binding model however is pending due to a lack of reliable X-ray structures or NMR data thus far [23, 27]. The reason for the lack of structural data relies on the aggregating nature of CLU. CLU tends to oligomerize with itself by forming di-, tetra and higher oligomers depending on the pH-value [2, 22, 23, 28, 29]. In combination with ligands such as fibrinogen, CLU even forms high molecular weight complexes (HMWC) up to 40,000 kDa [29]. Additionally, the complex and heterogeneous glycosylation pattern of CLU renders structural data hard to obtain [14, 16]. Moreover, even findings from CD spectra analysis are not consistent with studies ranging from 25% to 43% α-helices, 16% to 23% β-sheets, 14% to 20% β-turns and 26% to 31% random coils or disordered regions [28-31]. Moreover, it is still contentious or unclear which influence the glycosylation and the proteolytic cleavage have on structure and chaperone activity [31].

1.4 Murine CLU

Even though mice are common model animals to study a plethora of biological aspects (for instance by generating knockout mice), the biochemical characterization of murine CLU has not been made yet. As in the case of humans, *clu* is a single-copy gene in mice. It is encoded on chromosome 14 at location 14qD1 and spans about 13,066 bp (NC_000080.6 [65968483..65981548]) [32]. In contrast to humans, there is only one mRNA variant known (NM_013492.3). Mouse CLU mRNA contains about 1,832 bp and is therefore 1,045 bp shorter than the comparable human CLU mRNA variant 1 (NM_001831.3). On the protein level, however, they show an identity of about 77% (Needleman-Wunsch alignment of two sequences with full-length CLU of mouse and human). Intriguingly, it is known that human and rat CLU have a comparable order of their basic structural elements (Fig. 3), namely amphipathic helices and disordered regions [24], FC recognition site [7], cysteine-rich regions [13], and have also an identity in the aa sequence of about 77% (see above).

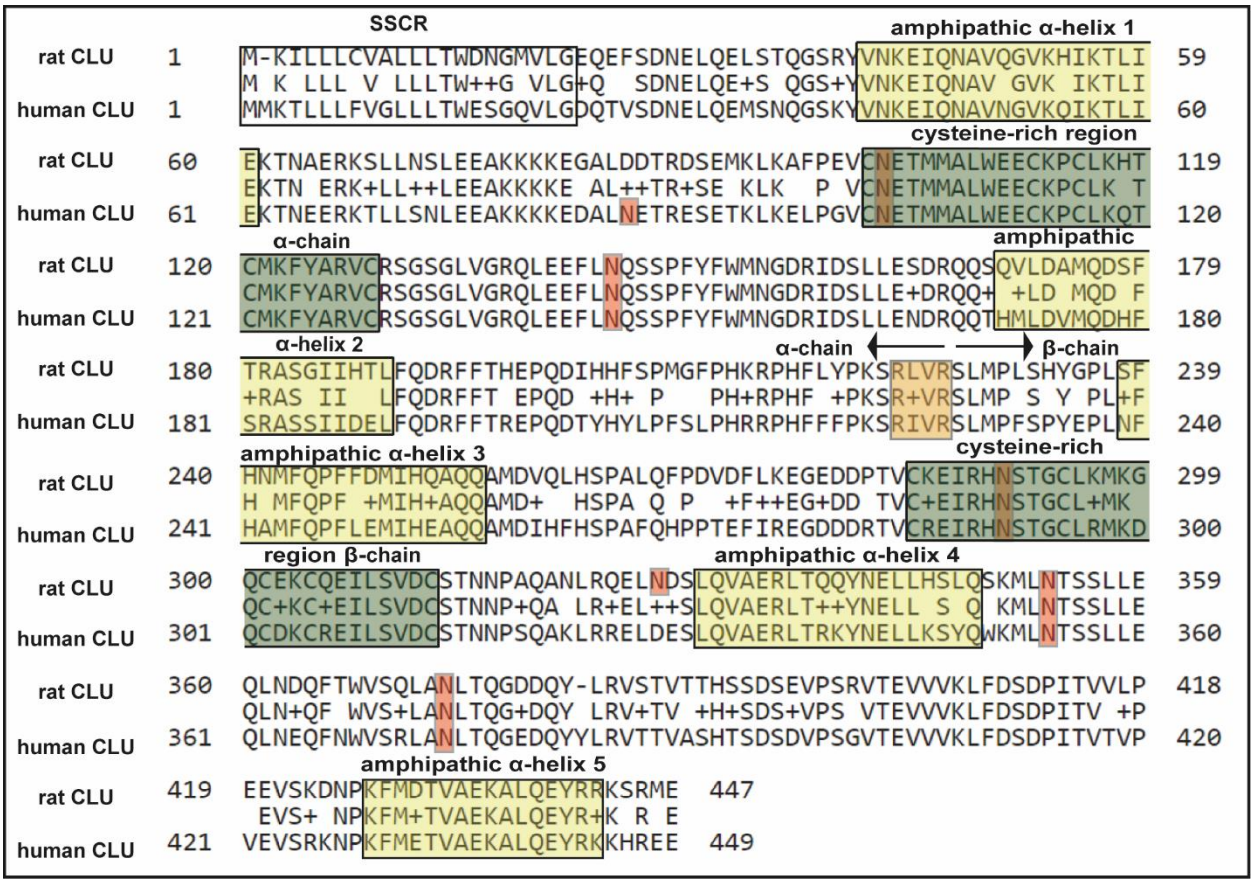

Fig.3 Comparison of the aa sequence of rat (NP_444180.2) and human (NP_001822.3) full-length CLU based on findings of [7, 13, 14, 21, 24, 25] using a Needleman-Wunsch alignment (NCBI). SSCR signal sequence coding region; yellow: amphipathic α-helices; green: cysteine-rich regions; orange: furin-like proprotein convertase recognition site; red: N-glycosylation sites.

Only the glycosylation sites differ between humans and rats [7, 14, 24]. Furthermore, just as human CLU, rat CLU has been found at highest concentrations in semen and on sperm cells [33-38]. Moreover, rat CLU also has complement inhibitory activity such as human CLU [5, 34]. However, it was never investigated whether mouse CLU has the same properties as rat CLU (Identity between rat and mouse in aa sequence is 93%). If mouse CLU has a similar structure and function as human CLU, it would be an indication that the conserved features indeed are involved in verified CLU functions, such as complement inhibition or chaperone activity.

1.5 Regulation of CLU expression

The human *clu* gene promoter (NC_000008.11 [27596917..27616717]) consists of multiple potential and confirmed binding sites for transcription factors and other regulatory elements. Intriguingly, beside the TATA box there are at least two binding sites which are associated with cellular stress conditions, namely CLE (clusterin element) [39, 40] and the AP-1 (activator protein-1) binding site [39, 41]. Additionally, a B-MYB binding site was also confirmed [42] (Fig.4).

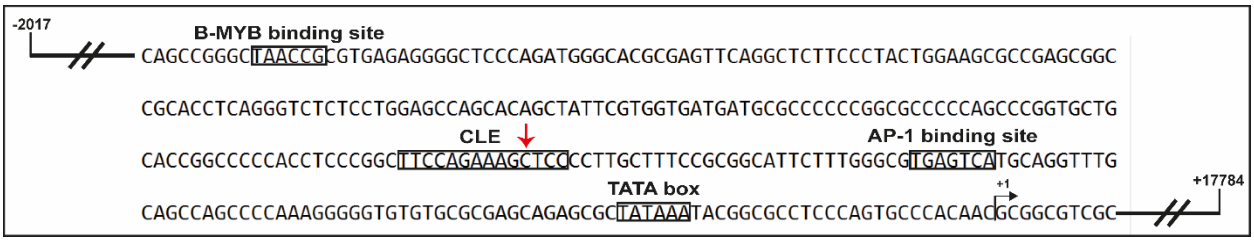

Fig.4 Schematic depiction of confirmed binding sites within the human *clu* gene promoter based on previous findings [11, 39, 40, 42]. +1 indicates the transcriptions start site of CLU variant 1. The red arrow indicates the base which is different from CLE (clusterin element) to the conserved heat shock element (HSE) (T/C).

CLE is a homologue to the highly-conserved consensus sequence HSE (heat shock element) that differs only in one base (red arrow Fig.4) but still serves as an efficient binding site for HSFs during a heat shock response [39, 40]. The AP-1 binding site for its part, is recognized by multifaceted transcription factors, namely Jun, Fos, Maf and ATF [43]. Upon various stimuli, these transcription factors dimerize, forming homo- and heterodimers. Possible inducers are, among others cytokines and neurotransmitters [43] but also physical and chemical stresses, such as UV light [44] or oxidative stress [45]. B-MYB is a transcription factor which belongs to the oncogenic MYB family which is involved in cell survival, proliferation and differentiation [46]. Apart from the well-investigated binding sites, additional elements were found as listed below (Tab.1).

Tab.1 Additional regulatory elements within the *clu* gene promoter.

Transcription factor(s)	Binding site(s)	Species found/predicted	Reference
AP-1	**AP-2**	***Rattus norvegicus***	**[47]**
TCF-1	**TCF-1**	***Homo sapiens***	**[48]**
YB-1; Twist1; SREBP-1c	**E-box**	***Homo sapiens***	**[49-51]**
SP1	**SP1**	***Mus musculus; Rattus norvegicus, Homo sapiens***	**[39, 47, 52]**
NF-κB	**NF-κB response element**	***Mus musculus***	**[53]**
CBF	**CBF**	***Rattus norvegicus***	**[54]**
GRE	**GRE**	***Rattus norvegicus***	**[55]**
CRE	**CRE**	***Rattus norvegicus***	**[55]**
HIF-1a	**HREs**	***Homo sapiens***	**[56]**
AR	**AREs**	***Homo sapiens***	**[57]**

Additionally, to *cis*-regulatory elements, epigenetic modifications were reported within the *clu* gene. In humans, at least two CpG-rich methylation domains were reported upstream and downstream of the transcription start site of variant 1 [52, 58, 59]. The amount of methylation within prostate cancer cells varies from about 10% up to 50% [58]. In a recent study, it was shown that the expression of CLU is elevated upon DNA demethylation and histone acetylation, especially of a promoter region located upstream of the transcription start site of variant 1 [59]. Similar observations were made in neural cells [60] and retinal pigment epithelial cells [61].

The complexity of multiple promotor elements as well as the superior epigenetic modifications underlie the complex nature of CLU. Therefore, this thesis will mainly highlight the role of the stress-related promoter regions, especially of AP-1.

1.6 CLU, its biological function(s) and role in diseases

1.6.1 Multifaceted functions of a single protein?

For years, since its discovery, CLU has been implicated to be involved in a plethora of various biological roles. The extracellular form, sCLU, is among others involved in tissue- and cytoprotective mechanisms such as complement inhibition [5], sperm maturation [62], lipid trafficking [7, 63], tissue remodeling [64], membrane recycling [65], removal of cellular debris, misfolded proteins [16, 65-69] (mediated by DC-SIGN, scavenger & LDL receptors) and apoptotic cells [70], signal transduction via the ERK1/2 [71] and PI3K/AKT [72] pathways, cell-cell interaction [73], protection against oxidative stress and heat stress [74], the clearance of Aβ [75], protection of the ocular surface [76] and many more, as well as interaction with foreign molecules such as nanoparticles [77, 78]. On the other side, intracellular CLU forms are reported to be involved in both cell death [79] and survival [80]. However, despite the abundance of various potential functions a distinct mechanism of CLU action is still missing. Moreover, plenty mechanisms as listed above are still contentious, e.g. the complement inhibition only holds true at very high sCLU concentrations under physiological conditions [81]. Furthermore, the signal transducing activity of CLU has never been distinguished from potential side effects. Additionally, the concentration of sCLU applied in some studies is below the average concentration in human tissues. For instance, on astrocytes an effect was obtained after application of 1 ng/mL sCLU [71], but the concentration of sCLU within cerebrospinal fluid is between 100 ng/mL to 10 µg/mL [82]. Nevertheless, even the term apoJ is still challenging due to sCLU accounting for only 2% of plasma HDL, indicating a potential unspecific interaction [7]. Moreover, especially the role of unglycosylated intracellular CLU forms is very contentious as reviewed previously [19].

1.6.2 CLU a key player in diseases?

In accordance with numerous potential functions, CLU has been found to be involved in various pathological conditions. Predominately, CLU is associated with amyloidosis-related pathologies such as Alzheimer's disease (AD). It was suggested that sCLU binds Aβ and facilitates its removal across the blood brain barrier mediated by LRP2/megalin [75, 83]. Furthermore, it has been shown that sCLU prevents Aβ aggregation but in turn stabilizes Aβ fibers once they are established. These actions are dependent on the ratio of CLU to substrate proteins whereby a low CLU to Aβ ratio promotes Aβ oligomerization [84]. Based on various laboratory findings, multiple clinical and genomic studies have been undertaken to confirm CLU as a risk factor and/or

biomarker for AD. As reviewed recently, a hint for a clear role of CLU in AD has not yet been verified [85].
Another prominent clinical CLU research field is its involvement in cancer. For almost 25 years, CLU has been found to correlate with the occurrence of cancer and poor prognosis. Noteworthy, is its role in prostate cancer [86], breast cancer [87], colorectal cancer [88], pancreatic cancer [89], ovarian cancer [90], hepatocellular carcinoma [91], renal cell carcinoma [92], lung cancer [93] and various other cancer types. In cancer disease, CLU seems to be primarily involved in chemoresistant mechanisms e.g. by inducing prosurvival or proliferatory signal transduction pathways [72, 94, 95], enhancement of metastasis by increased MMP9 expression [96], by preventing BAX-mediated apoptosis [97] and even by interacting with chemotherapeutic drugs such as Paclitaxel [98]. Based on these findings in 2005 an antisense oligonucleotide strategy was established targeting CLU in cancer [99]. The goal was to decrease the amount of the potential cancer-promoting CLU to advance current cancer therapies. Within the past 10 years OGX-011 emerged as a promising tool for cancer therapy in Phase I and II clinical trials. Unfortunately, the Phase III clinical trials of 1000 patients with castrate-resistant prostate cancer have shown either no benefit or even negative results [100].
Other pathologies with CLU involvement, such as atherosclerosis show also contradictory results as in the case of AD and cancer [32, 101, 102]. It is therefore questionable, whether CLU actually has a defined role in these settings or is just a bystander and the result of other disease-specific mechanisms.

1.7 CLU and tissue protection

Except for a host of activities as described above the most convincing findings are CLU in relation to tissue damage. Based on mouse models it was found that a gene knockout of CLU shows no difference in the phenotype of wild type animals as long as they suffer no stress or damage [103]. Intriguingly, CLU knockout mice show a threefold elevated severity after induction of a myocarditis opposed to wild type mice. Moreover, the CLU knockout mice show elevated postinflammatory tissue destruction [103]. In additional studies, it was observed that the infarct size was significantly reduced after intravenous administration of CLU in rats after myocardial infarction [104]. Moreover, the induction of an ischemia-reperfusion injury (IRI) in the kidneys of CLU knockout mice decreases the survival rate from 90% to about 30% [105]. In line with IRI in kidneys it was observed that in CLU knockout mice the rejection after heart transplantation is increased [106] and supplemental CLU prolongs the handling-time until organ transplantation by increasing membrane fluidity [107]. Furthermore, after induction of permanent focal cerebral ischemia in wild type, CLU overexpressing and CLU knockout mice, it was found that CLU

has neuroprotective properties after stroke [108]. Similar findings have been seen elsewhere [109] but also contradictory observations have been made [110]. Another interesting finding was published most recently [76]. In a dry-eye model it was shown that supplemented sCLU is capable to prevent air draft-triggered disruption of the ocular surface. By examining the protective mechanism, they have found that sCLU generates high molecular weight aggregates on the ocular surface at the size of cells. Moreover, the age-dependent accumulation of potentially harmful protein deposits in the kidneys of CLU knockout mice has been reported [111]. Taken together, these findings indicate that CLU is an indispensable tool to counteract and prevent tissue damage.

1.8 CLU and necrosis

Based on the findings from animal models (see 1.7) the term of necrosis has emerged occasionally in CLU research. Necrosis is distinct from apoptosis defined as uncontrolled cell death with tremendous consequences to tissues [112]. The main difference of necrosis to apoptosis is that the plasma membrane swells and finally disrupts, whereas in the case of apoptosis the plasma membrane remains intact. The consequence of the disintegrated cells in necrotic cell death is the accumulation of various so-called danger-associated molecular patterns (DAMPs) as well as reactive oxygen species (ROS) and free radicals within the extracellular space [113-115]. DAMPs for their part are acting as alarmons guiding immune cells to the area of damage and priming the release of proinflammatory cytokines and chemokines [116]. Examples for common DAMPs are heat shock proteins (HSPs), HMGB1, S100 proteins, uric acid, ATP, RNA and Chromatin/DNA [113, 116]. DAMPs are mostly indirectly detrimental due to an overshoot in activation of the immune system. In contrast to DAMPs, ROS and free radicals are capable to directly harm the cells, for instance by reacting with lipids within the cellular membrane [117]. As described in section 1.7 the most promising animal CLU models are based on ischemic conditions such as upon stroke, heart attack or transplantation. These pre-clinical settings are characterized by an impaired supply with oxygen and nutrients due to occluded blood vessels or interrupted blood stream. Under these conditions, cellular ATP is degraded to hypoxanthine which is for its part oxidized to xanthine, urea and further to ROS by the xanthine oxidase when the blood stream is reestablished (Fig.5A) [115]. Finally, neutrophil invasion, the overload with ROS and the inflammatory response trigger the rapid destruction of cells causing necrosis (Fig.5B) [116].

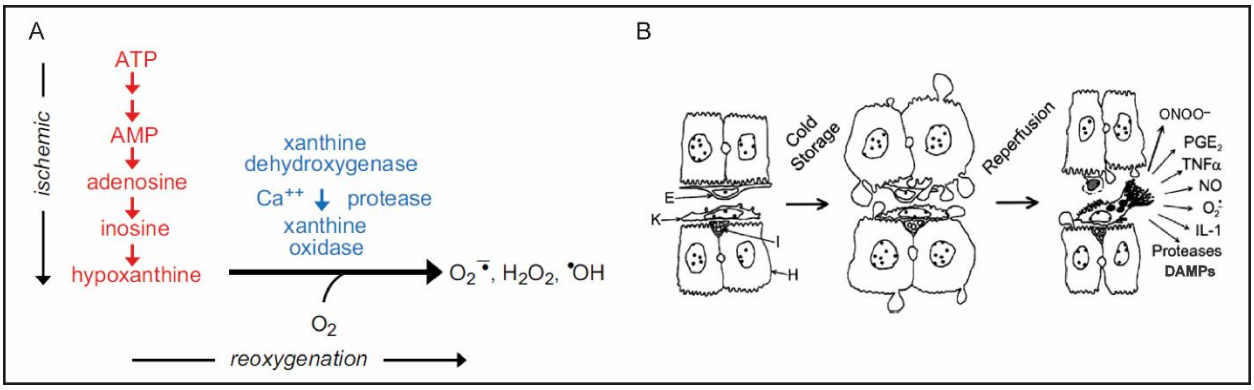

Fig.5 (A) Potential mechanism of ischemia-mediated generation of ROS and (B) following IRI (ischemia-reperfusion injury) adapted from [115].

Intriguingly, under conditions as described above, CLU has been found to be upregulated and secreted in acute phase [118]. Initially it has been found that phosphoatidylserine(PtdSer)-loaded lipid vesicles successfully induce upreguation of CLU expression in Rat1 cells [119]. Further studies have shown that CLU can be upregulated via TLR3/TRIF, induced by dsRNA released from necrotic cells. This finding was confirmed following intravenous application of the synthetic RNA analogue poly(I:C) in mice, in which the elevated serum concentration of sCLU was significantly abrogated in the absence of TRIF [67]. Moreover, it has been shown that necrotic cell debris is cleared from the extracellular space via LDL receptors in the presence of sCLU [66, 67]. Additionally, more recently it was reported that HMGB1 released from necrotic cells induces CLU upregulation via the RAGE/TLR4/NF-κB signaling pathway in prostate cancer cells promoting cell survival [120]. Nonetheless, distinct actions of CLU and all participating pathways in the face of necrosis are still poorly understood. For the assessment and treatment of necrosis-based pathologies, it is therefore important to highlight CLUs' role.

1.9 CLU and proteostasis

As already mentioned above, one of the main and probably the most thoroughly proved function is the chaperone activity of CLU and the scavenging function. Correlated with the chaperone activity is the term "proteostasis" which describes a cellular control network for maintaining the order within the proteome in- and outside of a cell. The underlying mechanisms of CLU chaperone activity was discussed intensively in previous paragraphs. Therefore, this section will primarily discuss mechanisms of the cellular proteostasis, especially of the unfolded protein response (UPR), and the role CLU might play.

1.9.1 Mechanisms of proteostasis

The proteostatic system is often reduced on the level of molecular chaperones and proteases acting mainly inside of living cells. Nonetheless, the proteostatic networks encompasses far more branches as expected. For a detailed overview, the reader should be referred to the plethora of review articles available in the database [26, 117, 121-128]. Fig.6 summarizes the most intriguing aspects of proteostasis and the proteostatic network.

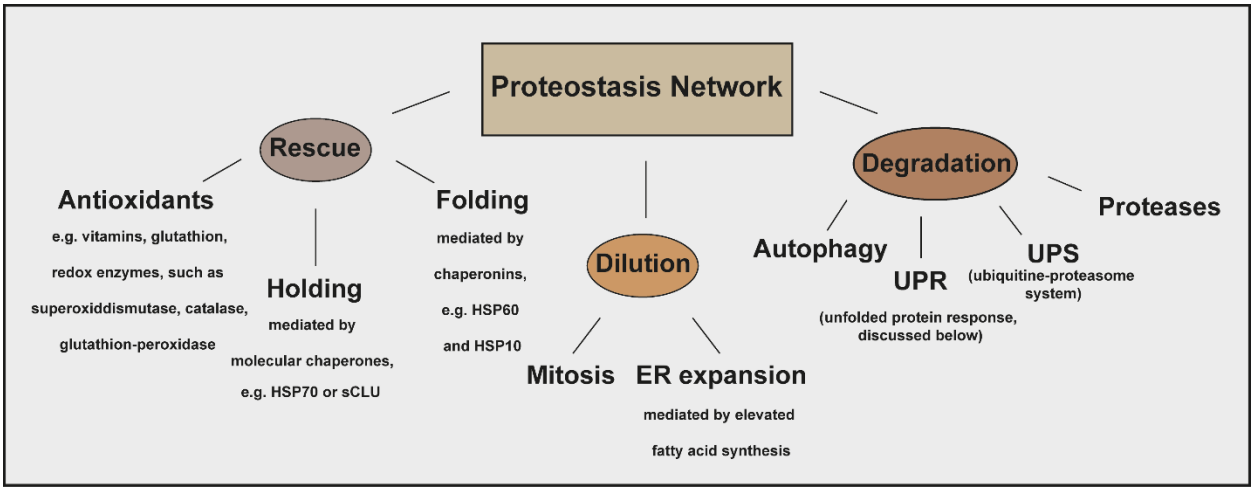

Fig.6 Overview of branches of the proteostasis network to counteract proteostatic imbalances.

Components of the proteostasis network are not working on their own, they are embedded in a fine-tuned crosstalk with other parts of the network. As an extracellular chaperone, sCLU passes the ER. It is therefore of interest how CLU and the ER-resident proteostatic signaling network UPR are related one another (1.9.2). Further, CLUs' role within the proteostatic network will be discussed (1.9.3).

1.9.2 The unfolded protein response (UPR): A sole intracellular protective pathway?

The UPR is a cellular surveillance program located in the ER to prevent misfolding and aggregation of mainly ER-resident proteins. An overview of all UPR branches is illustrated in Fig.7.

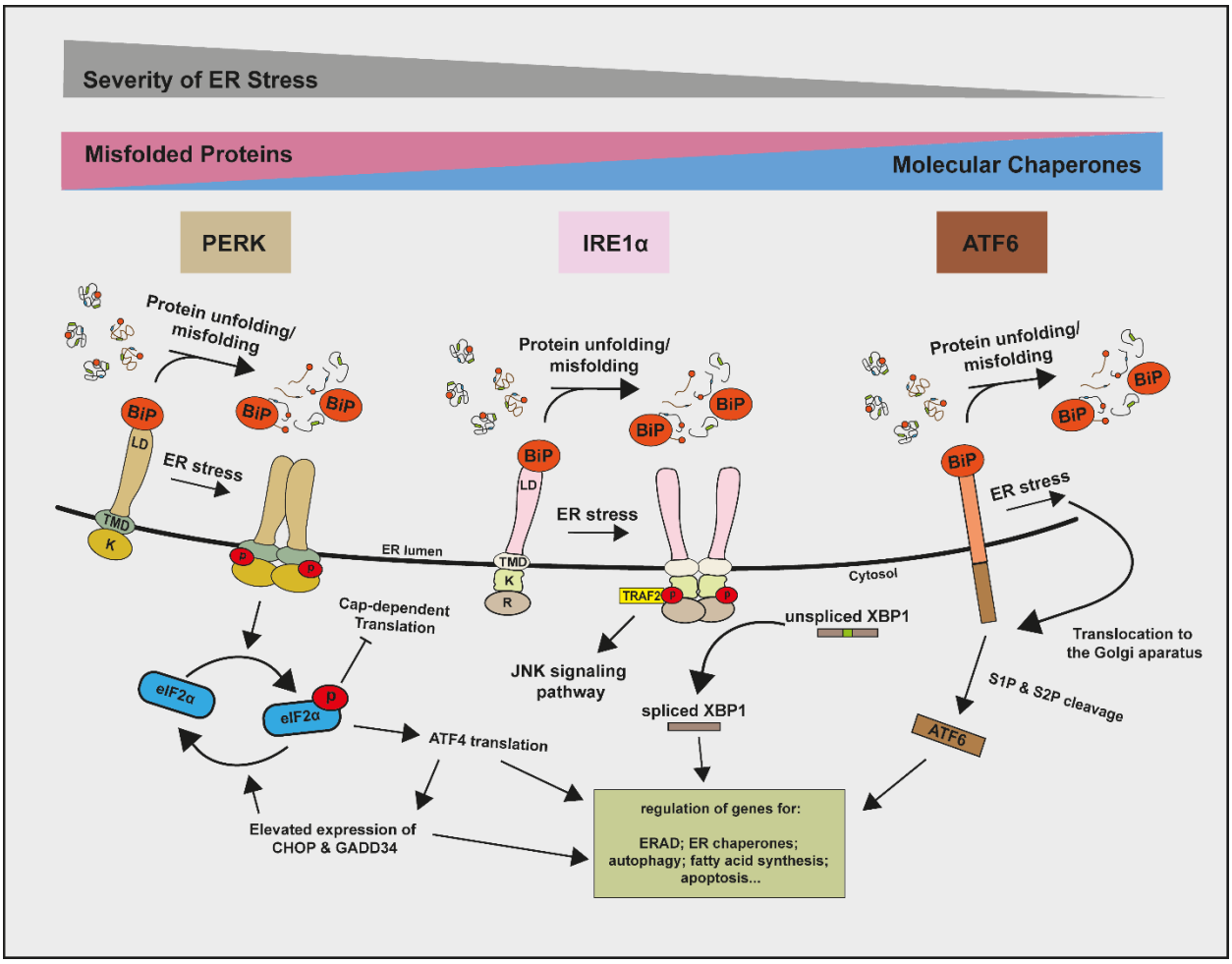

Fig.7 Branches of the UPR based on findings as cited above and [129]. LD luminal domain; TMD transmembrane domain; K kinase domain; R RNase domain. For further information see text.

The existence of an UPR was first confirmed in the late 1980s by overexpressing mutant ER-resident proteins which are prone to misfolding [130]. Due to the upregulation of the glucose-regulated proteins GRP78 (also known as BiP or HSP5A) and GRP94, it was suggested that they might counteract the misfolding of the mutant proteins. Subsequently, it was found, that the transmembrane kinase IRE1α (ERN1) is responsible for the upregulation of BiP [131, 132]. The transcription factor HAC1 in yeast or XBP1 in mammals was characterized as the mediator between IRE1α and BiP [133-137]. Today, IRE1α is considered as a transmembrane kinase located in the ER membrane with RNase activity once IRE1α is autophosphorylated, [138-140] or at least once ADP is bound to its kinase domain [141, 142], with concomitant IRE1α oligomerization [138, 141]. XBP1 mRNA, for its part, contains a 26 nucleotide (nt) intron which is removed by IRE1α RNase activity and spliced together spliceosome-independent [133, 134, 143]. The spliced XBP1 can then be translated and migrate to the nucleus to transcribe UPR-related genes. Additionally, beside IRE1α RNase activity, phosphorylated IRE1α also interacts

with the adaptor protein TRAF2 to activate the JNK signaling pathway [144]. Today, however, the exact mode of activation of IRE1α is not fully understood. Nonetheless, it is suggested that IRE1α interacts with the ER chaperone BiP in a monomeric inactive state [145, 146]. Upon ER stress and accompanied accumulation of misfolded proteins, BiP dissociated from IRE1α enabling IRE1α to oligomerize and finally to phosphorylate. In contrast to yeast [147], however, mammalian IRE1α is not able for directly interact with misfolded proteins [148].

Like IRE1α another BiP-associated transmembrane kinase, called PERK was found in the ER membrane. Different from IRE1α, PERK however, directly phosphorylates its target protein eIF2α preventing further expression of cap-dependent protein translation [128, 149, 150]. In contrast, the translation of the transcription factor ATF4 and thus the transcription/translation of CHOP [150] and GADD34 [151] are upregulated counteracting eIF2α phosphorylation. The induction of the PERK signaling pathways ultimately leads to cell death if the ER stress is not abolished [128], whereas the IRE1α branch is considered as a rather more pro-survival signaling pathway [152], even though also pro-death pathways, such as the JNK signaling pathway may occur [128, 144].

An additional mainly pro-survival ER stress pathway is the ATF6 branch. In contrast to PERK and IRE1α, ATF6 is no transmembrane kinase. ATF6 is a basic Leu zipper (bZIP) transcription factor which is activated upon cleavage (mediated by S1P and S2P) within the Golgi after induction of ER stress [128, 153, 154]. The translocation of ATF6 to the Golgi is repressed by BiP [155] indicating a comparable mode of activation such as in the case of PERK and IRE1α.

The UPR collectively promotes the transport of misfolded proteins from the ER to the cytosol for proteasomal degradation, a mechanism which is called ERAD (ER-associated degradation). Moreover, IRE1α mediates the degradation of RNA via its RNase activity to prevent further protein influx [156]. A mechanism which is called RIDD (Regulated Ire1-dependent decay) [128, 156, 157].

As described above, the UPR is generally accepted as a signaling network inside of cells, which mainly reacts to disturbances caused by intracellular/ER-resident events. However, the fact that the ER is the path to the extracellular space renders it likely that the UPR may also be influenced by changes outside of the cell or may even affect the extracellular homeostasis. Importantly, there is only one chaperone known today that is upregulated and secreted upon ER stress, namely ERdj3, counteracting prion-mediated cytotoxicity [158]. This finding is remarkable due to an increasing amount of publications reporting UPR induction by extracellular factors/settings (Tab.2).

Tab.2 Observations of the induction of the UPR by extracellular factors.

Factor	species/cell	pathway/event	Reference
LPS	J774 mouse macrophages and XBP1 knockout mice	IL-6 & TNF upregulation/secretion mediated by TLR4/IRE1α/XBP1	[159]
AApoAII	AApoAII fibril administration in mice	Primarily BiP upregulation and XBP1 splicing in liver and kidneys	[160]
oxLDLs & HDLs	human HMEC-1 endothelial cells	HDLs preventing oxLDLs induced IRE1α, JNK and eIF2α phosphorylation	[161]
TNF	HeLa, L929 and MEF cells	TNF activates all UPR branches by inducing ROS production	[162]
TTR oligomers	DRGs, ND7/23, SG, SH-SY-5Y and HSF-1 knockout animals	TTR oligomers inducing eIF2α phosphorylation and BiP	[163]
HMGB1	dendritic cells of mouse	BiP expression and XBP1 splicing is enhanced	[164]
VEGF	HUVECs	All UPR branches are activated by the VEGFR/mTOR signaling pathway	[165]
High glucose	Rat insulinoma cells, INS-1 & INS-2, mouse islet cells	Stimulation of all UPR branches, especially IRE1α	[166]
Aβ1-40	RBE4 (rat brain epithelia cells)	Aβ induces all UPR branches	[167]

1.9.3 CLUs' role in intra-and extracelluar proteostasis

Secretory CLU (sCLU) is a unique protein due to its characterization as the first molecular chaperone acting outside of the living cell [21]. In cells however, the role of CLU is much more contentious as reviewed recently [19]. Nevertheless, there are reports concerning CLUs' role in intracellular proteostasis. As in the case of sCLU, intracellular CLU is described to be pro-survival (except of unglycosylated isoforms). Initially, it was found that CLU can escape secretion from the Golgi upon severe ER stress induced by Thapsigargin (Tg) [17]. Retrotranslocation in this study however, seems to belong to the UPR mechanism of ERAD (see above), as CLU has subsequently been ubiquitinylated. In a further study concerning retrotranslocated CLU, it was observed that BiP is the mediator for ER stress-induced CLU retrotranslocation [18]. Moreover, they observed the accumulation of both, sCLU and psCLU in the cytosol. Eventually, retrotranslocated CLU stabilizes the mitochondrial membrane, thus preventing ER stress-induced apoptosis in

prostate cancer cells. Based on the findings of ER stress-mediated CLU retrotranslocation it was further confirmed that cytosolic CLU promotes autophagy in prostate cancer and kidney cells [18, 168]. In these studies, it was found that CLU is a prerequisite for LC3 lipidation. Lipidated LC3 for its part facilitates the maturation of the autophagosome, a membrane-shrouded structure which collects cellular waste, such as misfolded proteins, for subsequent degradation after fusion with a lysosome [121]. UPR and autophagy are highly correlated to each other, e.g. by supporting ERAD of the UPR [169]. Furthermore, it was found that IRE1α phosphorylation decreases in the absence of CLU, suggesting a supporting role of CLU in the UPR [168]. Moreover, it was suggested that unglycosylated CLU still exerts chaperone activity [31]. This notion renders it likely that even unglycosylated CLU forms emerged from failed translocation, alternative translation initiation or alternative splicing may act as chaperones inside of the cell.
In summary, CLU is suggested to be a widespread multifunctional protein that acts in various cellular settings, mainly embedded in the proteostasis network. An overview of CLU functions is illustrated in Fig.8.

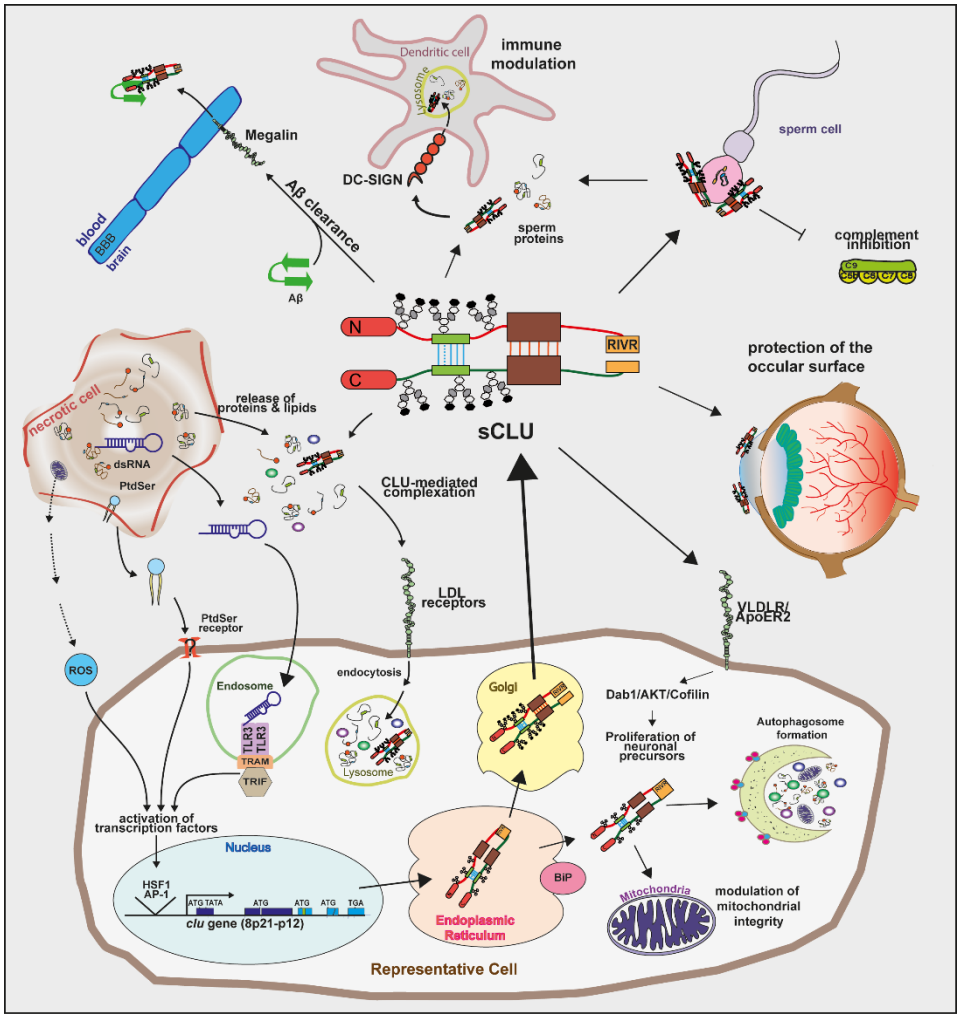

Fig.8 Depiction of various CLU functions as described above, adapted from [19, 76].

2 Objectives

The aim of this thesis is to elucidate in which way CLU might act and which impact this would have on the cellular homeostasis. As one component of HDLs it was reported that secretory CLU (sCLU) interacts with receptors of the LDL receptor gene family, namely LRP2, ApoER2 and VLDLR. Even though the transport/removal of ligands such as lipids and proteins is well characterized (see above), presumed cellular signaling processes of sCLU via these receptors were not observable (data not shown). Therefore, it was assumed that CLU executes a function distinct from signal transduction. The most verified function is the chaperone activity of sCLU. Consequently, this thesis will first examine the chaperone activity of CLU and the underlying structural features, namely the proteolytic cleavage and the glycosylation. Information of the CLU structure might be of relevance to find possible roles in cellular physiology. In this context, it is of interest whether CLU structure and function are conserved among animals. To assess whether sCLU chaperone activity is a feature primarily of mammals (especially humans) or might be conserved throughout the evolution, a comprehensive analysis of the CLU protein among various CLU-expressing animal classes will be conducted. Therefore, in the first section the cloning, expression and characterization of mouse sCLU in comparison to human sCLU will be described. Further, the CLU protein of up to 108 various species will be analyzed in a bioinformatic approach and the role of proteolytic maturation and glycosylation will be experimentally investigated in the case of human sCLU. The second section, will based on findings of the first section, assess CLU's role in tissue damage by conducting necrosis cell death assays. The purpose of these analyses is to characterize mechanisms of CLU upregulation in necrotic tissue and effects of CLU upregulation as to the fate of the surrounding vital cells. Moreover, it is of interest how various signal transduction pathways and proteostatic network components act together to counteract situations when neighboring cells are accidentally disrupted. Eventually, this thesis encompasses multiple approaches to highlight the importance of CLU and provides potential explanations concerning problems in CLU research these days.

3 Material

3.1 Chemicals & Supplements

The names, IDs and manufacturers/suppliers of chemicals and supplements for buffers, cell culture, analytics etc. are enumerated below.

Alexis Biochemicals: LPS *Samlmonella minnesota* R595 (581-008-l002) **Applichem:** Imidazole (A1073,0500) **Bio-Rad:** Bromophenol Blue (1610404); Triton® X-100 (A1388,1000) **Biochrom:** Sodium bicarbonate ($NaHCO_3$, L1713); Non-essential amino acids (NEAs, K0293); Phosphate buffered saline (PBS, L182-10) **Carl Roth:** 1,4-Dithiothreitol p.a. (DTT, 6908.1); 8-Anilino-1-naphthalenesulfonic acid (ANS, A1028); Albumin Fraktion V protease-free (BSA, T844.2); Albumin Fraktion V endotoxin-free (BSA, CP84.1); Ammonium persulfate p.a. (APS, 9592.3); Ampicillin (K029.2); Blasticidin S hydrochloride (CP14.2); Calcium chloride dihydrate ($CaCl_2$ x $2H_2O$, C7902); Dietylpyrocarbonat 97% (DEPC, K028.3); Dimethylsulfoxid (DMSO, A994.1); Disodium phosphate dihydrate p.a. (Na_2HPO_4 x $2H_2O$, 4984.3); Ethidium bromide solution (HP47.1); Ethylenediaminetetraacetic acid p.a. (EDTA, 8043.2); Formic acid p.a. (4724.3); Glutathione (oxidized, 6378.1); Glutathione (reduced, 6832.1); Glycerol p.a. (3783.1); Glycin p.a. (3908.3); Lysogeny broth agar (X969.2); Lysogeny broth medium (X968.2); Methanol (99.5%, CP43.3); Milk powder (T145.2); Monosodium phosphate dihydrate p.a. (NaH_2PO_4 x $2H_2O$, T879.2); Nickel(II) sulfate p.a. (T111.1); Ponceau S (5938.2); Preservative for water baths (9025.1); Roti®-Blue (A152.1); Roti®-Quant (K015.1); Rotiphorese® Gel 30 (30% Acrylamide/Bis Solution, 3029.2); Sodium chloride p.a. (3957.2); Sodium dodecyl sulfate p.a. (SDS, 4360.2); Tetramethylethylenediamine p.a. (TEMED, 2367.3); Trichloroacetic acid (TCA, 8789.2); Tris(hydroxymethyl)aminomethane p.a. (Tris, 4855.5); Tris hydrochloride (9090.3);Tween 20® (9127.1); Urea p.a. (3941.2) **Chemical storage University Mainz:** Ethanol denatured; Glacial acid; Sodium azide **FMC:** Seakam® LE Universal Agarose (28649) **Macherey-Nagel:** Protino® Ni-IDA Resin (745210.30) **PerkinElmer:** Western Lightning® Plus-ECL (Lumino, NEL104001EA) **Sigma:** Dulbecco's Modified Eagle's Medium, 4.5 g/L glucose (DMEM, D5671); Ethanol p.a. (32205); Fetal Bovine Serum (FBS, F0804); L-Glutamine (G7513); N-(2-Hydroxyethyl)piperazine-N′-(2-ethanesulfonic acid) (HEPES solution, H0887); Paraformaldehyde (PFA, 158127); Penicillin-Streptomycin solution (P0781); Phorbol 12-myristate 13-acetat (PMA, P8139); Poly-L-lysine hydrobromide (P6282); Sodium Pyruvate solution (S8636); Trypan Blue Solution (T8154); Trypsine-EDTA solution (T4174) **Thermo Fisher:** dCTP Set 100 mM Solution (R0151); dNTP Set 100 mM Solutions (R0181); GeneRuler 100 bp Plus DNA Ladder (SM0321); Lipofectamine® RNAiMAX Transfection Reagent (13778030); MassRuler Express Forward DNA Ladder (SM1283); Opti-MEM® (31985047); PageRuler™ Prestained Protein Ladder (26616); TurboFect Transfection Reagent (R0531)

3.2 Buffers

Self-made buffers prepared are enumerated below. If not indicated otherwise all buffers were prepared in ddH_2O. Details of the constituents are listed in 2.1.1.

50x TAE buffer: 2 M Tris, 50 mM EDTA pH 8.0, 1 M glacial acid **5x SDS-PAGE sample buffer:** 0.225 M Tris hydrochloride pH 6.8, 50% glycerol, 5% SDS, 0.05% Bromophenol blue, ad 10 mL. For reducing SDS-PAGEs 50 µL 2 M DTT were added to 1 mL SDS-PAGE sample buffer **5x Electrophoresis buffer:** 0.5 M Tris, 1.92 M glycine, 0.5% SDS, pH 8.8 **Stacking gel buffer for SDS-PAGEs** 3 M Tris, pH 8.8 **Separating gel buffer for SDS-PAGEs:** 1 M Tris, pH 6.8 **1x Tank-blotting transfer buffer:** 25 mM Tris, 150 mM glycine, 20% (v/v) methanol, pH 8.3 **1x Ponceau S staining solution:** 0.5% (w/v) Ponceau S, 1%

(v/v) glacial acid Stripping buffer: 100 mM NaOH, 2% (w/v) SDS, 33.3 mM DTT (added immediately prior use) **1x Staining/destaining solutions for Coomassie gels:** Staining with 10% (v/v) and 10% Roti-Blue®. Destaining with 25% (v/v) methanol **25x Tris-buffered saline (TBS):** 1.25 M Tris, 3.75 M NaCl, pH 7.6 **1x LEW buffer:** 5.8 mM Monosodium phosphate dihydrate, 44.2 mM Disodium phosphate dihydrate, 300 mM NaCl, pH 8.0 **1x Elution buffer:** 50 mM Monosodium phosphate dihydrate, 300 mM NaCl, 250 mM Imidazol, pH 8.0 **Phosphat buffer:** 0.95 mM Monosodium phosphate dihydrate, 9.05 mM Disodium phosphate dihydrate, pH 7.0 **Cell lysis buffer:** 50 mM Tris/HCl pH 8.0, 150 mM NaCl, 1% (v/v) Triton® X-100 **Tailing buffer:** 50 mM Tris/HCl pH 8.4, 125 mM KCl, 7.5 mM $MgCl_2$ **10x Precipitation buffer:** 0.5 M Na_2HPO_4/NaH_2PO_4 pH 7, 1.5 M NaCl, 0.2 M DTT (in reducing assays)

3.3 Consumable Materials

The names, IDs and manufacturers/suppliers of consumable materials for cell culture and analytics are enumerated below.

BD Bioscience: BD Falcon Round-Bottom Tubes Polystyrene (FACS tubes, B4-BE-352058) **Beckman:** Microfuge® Tube Polyallomer (ultracentrifugation tubes, P91103) **Buddeberg:** Filters for accu-jet® controller (9.281.091), 50 mL syringes (9.410 050) **ELGA:** ultrapure water from ELGA Purelab Flex **General Electric:** Amersham Protran Supported 0,45µm NC (Protein blotting membrane, 10600016) **Greiner:** Cell culture flasks (TC) small (T25, 690175), medium (T75, 658175), large (T175, 660175); Cryo tubes in various colors (126279, 126278, 126277, 126280); Culture multiwell plates 96 well unsterile (655101), 96 well white plates (655075); 96 well sterile TC (655980), 48 well sterile (677 180), 24 well sterile (662160), 6 well sterile (657160); Petri dishes (632180) Pipet tips 200 µL (739290), 1 mL (740290); Reaction tubes 0.2 mL (683201), 0.5 mL (682201), 1.5 mL (616201), 2mL (623201), 15 mL (188271), 50 mL (227261) **Millipore:** Amicon® Ultra-15 Centrifugal Filter Unit, 30 & 50 NMWL (UFC903008 & UFC905008) **PALL:** MinimateTM TFF Capsule with 30 or 50 kDa Omega Membrane (membrane filter unit) **Sarstedt:** multiwell plates lumox multiwell, 96 (sterile black 96 well plate, 94.6000.024), black micro test plate (sterile black 96 well plate, 82.1581.220); serological pipettes 5 mL (86.1253.001), 10 mL (86.1254.001), 20 mL (86.1685.001); Cell scraber 39 cm (83.1831) **Sartorius Stedim Biotech:** Blotting Paper / Grade BF 4 (FT-2-521-580600G), Cellulose Acetate (CA) Membrane Filter (11107--47----CAN), Vivaspin Turbo 4, 5.000 MWCO PES (VS04T11) **Starlab:** Semi-Skirted PCR Plate with Raised Rim (for qRT-PCRs, E1403-7700); Advanced Polyolefin StarSeal, X-Clear (for qRT-PCR plates, E2796-9795); 10µl RPT Graduated Tip (S1160-3700-C)

3.4 Laboratory Equipment

The names and companies of devices and tools used in the laboratory are enumerated below.

Alpha Innotech: AlphaImager™ Gel Imaging System (for analyzing DNA gels) **Beckman:** L7-65 (ultracentrifuge); 45Ti rotor (serial number: 94Ei565) **BD Bioscience:** BD FACS Canto II (for FACS analyses) **BDK:** UVF 6.12 S (sterile bench) **Binder:** CB 210 (CO_2 incubator for eukaryotic cells) **Biometra:** Powerpack P25 T (power supply; TPersonal (PCR cycler) **Bio-Rad:** VersaDoc™ MP Imaging System (Western blot imager); Mini-PROTEAN® Tetra Vertical Electrophoresis Cell (1-D vertical gel electrophoresis); Mini Trans-Blot® Electrophoretic Transfer Cell (Tank blotter) **BioTek:** PowerWave™ XS (ELISA reader) **BMG Labtech:** LUMIstar OPTIMA (Microplate reader) **Brand:** 5mL and 10 mL micropipettes; accu-jet® (pipetting aid) **Canon:** CanoScan LiDE 210 (flatbed scanner) **CAT:** ST 5 (Shaker) **Chyo:** JL-200 (micro scale) **CMV:** CMV-Rom (roll mixer) **Electronic:** IKA-VIBRAX-VXR (vibrating table) **Eppendorf:** BioPhotometer® plus; Concentrator plus (Lyophilizer); Multipette® Stream **FVA:** Fedegari Autoclavi SpA (autoclave) **G.Heinemann:** HTU SONI130 (Sonifier) **General Electric:** ÄKTApurifier 10

(Fast protein liquid chromatography, FPLC); HiLoad™ 16/60 Superdex™ 200 prep grade (size exclusion chromatography); XK16/20 (FPLC column) **GFL:** 3018 (swiveling table) **Gilson:** 2 µL, 10 µL, 20 µL, 100 µL and 200 µL micropipettes; Macroman™ (pipetting aid) **Heidolph:** Reax1 (vortexer) **Hellma:** quartz cuvettes suitable for photometry, CD and fluorescence spectroscopy **Horiba:** Fluoromax4 (Fluorescence spectrometer) **Hund:** Wilovert S (Optical microscope) **Infors HT:** Ecotron (Shaking incubators) **Ismatec:** MP-GE (peristaltic pump) **Janke & Kunkel:** VF2 (vortexer) **Jasco:** J-815 (Circular Dichroism Spectropolarimeter) **Knick:** 765 Calimatic (pH meter) **Kratos Analytica:** Shimadzu CFR Axima (MALDI-TOF MS) **Motic:** Motic AE21 (Biological Inverted Microscope); Moticam1000 (USB Camera) **Labnet:** AccuBlock™ Digital Dry Baths (heating block); Spectrafuge™ 24D and Spectrafuge™ Mini (tabletop centrifuges) **Memmert:** BM600 (incubator for prokaryotic cells) **PEQLAB:** peqSTAR Gradient (PCR cycler) **Raytest:** Stella 3200 (Western blot imager) **Roth:** Neubauer Counting Chamber **Sartorius:** BP 2100 S (scale) **Self-made:** 10 cm x 5 cm and 13 cm x 10 cm agarose gel electrophoresis chambers **Sigma:** Bioblock scientific 3K15 (Cooling centrifuge) **Thermo Fisher:** 7500 Fast Real-Time PCR System (qRT-PCR cycler); Bioblock Scientific (heating block); Multifuge 1S-R (Cooling centrifuge); Nalgene® Polysulfone Reusable Bottle Top Filters; Safe 2020 (Biological Safety Cabinet) **VWR:** VWR® PCR plate spinner (521-1648) **Wisa:** SUC-O-MAT (aspirator)

3.5 Enzymes & Proteins

Enzymes and proteins as well as the IDs and manufacturers/suppliers are enumerated below.

NEB: α2-3 Neuraminidase (P0728); β1-4 Galactosidase (P0730); β-N-Acetylglucosaminidase (P0732); Histone $H1^0$ Human, Recombinant (M2501); Histone H2A Human, Recombinant (M2502); Histone H2B Human, Recombinant (M2505); Histone H3 (H3.1) Human, Recombinant (M2503); Histone H4 Human, Recombinant (M2504); NcoI (R0193); PNGase F (P0704); XbaI (R0145) **PEQLAB:** KAPA SYBR Fast Rox low (qRT-PCR Master Mix, KAPBKK4619-02); KAPAHiFi PCR Kit (07-KK2100-01) **R&D Systems:** Recombinant Human HMGB1 Protein (1690-HMB-050); Recombinant Human S100A8/S100A9 Heterodimer Protein (8226-S8-050) **Roth:** Chymotrypsin (0238.1) **Sigma:** Apoferritin for gel filtration (105K6114); Catalase (C9322); Gel Filtration Cal Kit Low Molecular Weight (28-4038-41); Tumor Necrosis Factor-α human (TNF, H8916) **Thermo Fisher:** BamHI (ER0051); HindIII (ER0501); Maxima Hot Start Green PCR Master Mix (2X, K1062); Pfu DNA Polymerase, native (EP0571); RevertAid Reverse Transcriptase (EP0441); T4 DNA Ligase (EL0014); Terminale Desoxynucleotid Transferase (EP0161)

3.6 Antibodies

The names, IDs, manufacturers/suppliers, species of origin and dilutions of used antibodies are enumerated below.

Abcam: Anti-IRE1 (phospho S724) (rabbit, 1:1,000, ab48187) **Epitomics:** GAPDH (rabbit, 1:5,000, 2251-1) **Thermo Fisher:** 6x-His Epitope Tag Antibody (HIS.H8) (mouse , 1:2,000, MA1-21315); Anti-V5-Antibody (mouse, 1:5,000, R960-25); **Millipore:** Anti-Clusterin α chain (human) Antibody, clone 41D (mouse, 1:1,000, 05-354) **NEB:** Anti-mouse IgG, HRP-linked Antibody (1:10,000, 7076); Anti-rabbit IgG, HRP-linked Antibody (1:5,000, 7074); BiP (C50B12) (rabbit, 1:1,000, 3177); eIF2α (D7D3) (rabbit, 1:1,000, 5324); IRE1α (14C10) (rabbit, 1:1,000, 3294); JNK2 [56G8] (rabbit, 1:1,000, 9258); LC3A/B (D3U4C) (rabbit, 1:1,000, 12741); p44/42 MAPK (Erk1/2) (137F5) (rabbit, 1:1,000, 4695); p70 S6 Kinase (49D7) (rabbit, 1:1,000, 2708); Phospho-eIF2α (Ser51) (D9G8) (rabbit, 1:1,000, 3398); Phospho-p44/42 [Erk1/2] [T202/Y2049] (rabbit, 1:1,000, 4377); Phospho-p70 S6 Kinase (Thr389) (108D2) (rabbit, 1:1,000, 9234); Phospho-p70 S6 Kinase (Thr421/Ser424) (rabbit, 1:1,000, 9204); Phospho-S6 Ribosomal Protein

(Ser235/236) (D57.2.2E) (rabbit, 1:1,000, 4858); Phospho-SAPK/JNK [Thr183/Tyr185] (rabbit, 1:1,000, 9251); Phospho-Src (Tyr527) (rabbit, 1:1,000, 2105); Phospho-Src Family (Tyr416) (rabbit, 1:1,000, 2101); S6 Ribosomal Protein (5G10) (rabbit, 1:1,000, 2217); Src (32G6) (rabbit, 1:1,000, 2123); TRAF2 (C192) (rabbit, 1:2,000, 4724) **R&D Systems:** Human TLR4 Antibody (O00206); Normal Goat IgG Control (AB-108-C) **Santa Cruz:** Clusterin-α (C-18) (goat, 1:1,000, sc-6419); Clusterin-α (B-5) (mouse, 1:500, sc-5289); ERdj3 (C-7) (mouse, 1:1,000, sc-271240); IRE1α (B-12) (mouse, 1:1,000, sc-390960) **Sigma:** Anti-goat IgG (whole molecule)-Peroxidase antibody (1:10,000, A5420); Anti-α-Tubulin Clone B-5-1-2 (mouse, 1:10,000, T5168) **StressMarq Biosciences Inc.:** Anti-Calreticulin (rabbit, 1:2,000, SPC-122A)

3.7 Inhibitors

The names, IDs and manufacturers/suppliers of used antibodies are enumerated below. Additionally, the main function, solvent, concentration of the stock solutions (all stored on -20°C) and working concentrations (w.c.) are also indicated. For details concerning incubation times and concentrations please refer to the Method and Result Section.

Applichem: Actinomycin D (transcription inhibitor, 2 mg/mL in methanol, 2 µg/mL w.c., A1489.0005) **Calbiochem:** Kira6 (IRE1α kinase inhibitor, 50 mg/mL in DMSO, 1 µM to 10 µM w.c., 532281); MG-132 (proteasome inhibitor, 10 mM in DMSO, 10 µM w.c., 474790) **InvivoGen:** Rapamycin (mTOR inhibitor, 100 mM in DMSO, 20 nM to 100 nM w.c., tlrl-rap) **Merck:** Phosphatase Inhibitor Cocktail V (50x stock diluted to 1x in cell lysis buffer, US1524629) **R&D Systems:** APY29 (IRE1α kinase inhibitor, 30 mM in DMSO, 0.3 µM to 3.0 µM w.c., 4865/10) **Roche:** cOmplete™, Mini, EDTA-free Protease Inhibitor Cocktail (one tablet in 10 mL cell lysis buffer) **Roth:** Phenylmethylsulfonyl fluoride (PMSF) (serine protease inhibitor, 0.1 M in isopropanol, 1 µM w.c., 6367.1) **Sigma:** Cycloheximide (translation inhibitor, 10 mg/mL in DMSO, 5 µg/mL w.c., C1988); Parthenolide (NF-κB inhibitor, 10 mM in DMSO, 25 µM w.c., P0667); Q-VD-OPh hydrate (pan caspase inhibitor, 14 mg/mL in DMSO, 5 µM w.c., SML0063); SP600125 (JNK inhibitor, 9.1 mM, 10 µM w.c., S5567); Thapsigargin (SERCA inhibitor, 1 mg/mL in DMSO, 1 µM w.c., T9033)

3.8 Oligonucleotides & siRNAs

Oligonucleotides and siRNAs were obtained from Roth, Sigma, Eurofins, Santa Cruz, Thermo Fisher and RealTimePrimers.com. The names, sequences, purpose and additional information are listed below.

Tab.3 Primers for cloning, *in vitro* mutagenesis, oligo hybridization, colony PCR; sequencing, quantitative RT-PCR (qRT-PCR) and semiquantitative RT-PCR (sqRT-PCR). (H.P. indicates constructs cloned by Hans Prochnow).

Oligo(s)	Forward (location)	Reverse (location)	Purpose	Notice/ Reference
CLU mouse Fusion 1	ATATTAAAGCTTACCCGCGTCACCAGG AGGAG	GAAAGAGCGTGTCTATGATGC	Cloning Primer	
CLU mouse Fusion 2	AGGCCACACCATGAAGATTC	AGTGGGATCCTTCCGCACGGCTTTTC CTG	Cloning Primer	
pcDNA-CLU-KDEL	AAAGATGAGTTGTGAGTTTAAACCCGC TGATC	CAACTCATCTTTATGGTGATGGTGAT GATGAC	Cloning Primer	cloned by H.P.
HSP72 human	AAATTTAAGCTTATGGCCAAAGCCGCG	ATTAATGGATCCATCTACCTCCTCAAT G	Cloning Primer	

IRE1α human	**TTTAAACTTAAGCTTCAGTTCTGCGTCC GCTGA**	**TGGACTAGTGGATCCGAGGGCGTCT GGAGTCACT**	**Cloning Primer**	
CLU human RIVR/RITR	**GTCCCGCATCACCCGCAGCTTG**	**ATTAATGGATCCATCTACCTCCTCAAT G**	***In-vitro* mutagenesis**	
CLU human RIVR/RIVQ	**CCGCATCGTCCAGAGCTTGATGC**	**GCATCAAGCTCTGGACGATGCGG**	***In-vitro* mutagenesis**	
AP-1 Reporter	**CTTACGCGTGCTAGCTGAGTCAGTGAG TCACTGACTCACTGACTCATGAGTCAG CTGACTCA**	**GATCTGAGTCAGCTGACTCATGAGTC AGTGAGTCAGTGACTCACTGACTCAG CTAGCACGCGTAAGAGCT**	**Primer for AP-1 in pTAL-Luc - oligohybridiz-ation**	**cloned by H.P.**
CLU in pTAL-NF-κB- & pTAL-AP-1-Luc	**GTAAAGCCACCATGGGAACCCACTGCT TACTGGCTTATC**	**CGCCCCGACTCTAGAAACAGATGGCT GGCAACTAGAAGG**	**Primer for substitution of Luc by CLU**	
pcDNA	**TAATACGACTCACTATAGGG**	**CTGGCAACTAGAAGGCACAG**	**colony PCR/ sequencing**	
pTAL-Luc	**GTTCGTCACATCTCATCTACCTCC**	**CAAACTCATCAATGTATCTTATC**	**colony PCR/ sequencing**	
pTAL	**CAG GTG CCA GAA CAT TTC TCT ATC G**	**CAAACTCATCAATGTATCTTATC**	**colony PCR/ sequencing**	
IRE1α	**GCTGGTGGTGACTGTGGAC GCTGCCCTTCCACCC GCAGACACAGTTTCAGCC**	**GTCTCCACAGCGACATTG GCGAGTGGTTGGAGGC GTCCATTTGATTGAGCC**	**sequencing**	
mouse CLU specific 1st strand		**TGCGGCTTTTCCTGCGGTATTCC**	**first step of 5'-RACE**	
AAP (abridge anchor primer) & mouse CLU-R1	**GGC CAC GCG TCG ACT AGT ACG GGI IGG GII GGG IIG**	**GACTTGGCTCTGCTGCC**	**fourth step of 5' RACE (1st RACE PCR)**	
AUAP (abridge universal amplification primer) & mouse CLU-R2	**GGC CAC GCG TCG ACT AGT AC**	**CCA GGA CCA AGC CAT TGT C**	**fifth step of 5' RACE (2nd RACEPCR) /sequencing**	
Poly D(T) 12-18 Primer			**Reverse Transcription**	
BiP	**CGAGGAGGAGGACAAGAAGG**	**CACCTTGAACGGCAAGAACT**	**qRT-PCR**	**[170]**
CHOP	**AGCCAAAATCAGAGCTGGAA**	**TGGATCAGTCTGGAAAAGCA**	**qRT-PCR**	**[171]**
CLU	**GGAGGAGTGAGATGTGGATG**	**ATGCAGGAGCAATTCTGTTC**	**qRT-PCR**	
ERdj3	**GGGTGCTGCTTATGAGGTTCTG**	**CCAAAATCCCCAAAGAAGTGTG**	**qRT-PCR**	
GADD34	**TGAGGCAGCCGGAGATAC**	**GTAGCCTGATGGGGTGCTT**	**qRT-PCR**	**[171]**
HPRT11	**TGACACTGGCAAAACAATGCA**	**GGTCCTTTTCACCAGCAAGCT**	**qRT-PCR**	
XBP1	**TGCTGAGTCCGCAGCAGGTG**	**GCTGGCAGGCTCTGGGGAAG**	**qRT-PCR**	**[172]**

BiP	CGAGGAGGAGGACAAGAAGG	CACCTTGAACGGCAAGAAC	sqRT-PCR	
CHOP	TTGCCTTTCTCCTTCGG	CACTTTCCTTTCATTCTCCTG	sqRT-PCR	
CLU	AAAATGCTGTCAACGGGGTG	TTCAGGCAGGGCTTACACTCT	sqRT-PCR	
ERdj3	TTTATTGGAGAAGGTGAGCC	CTGTTTGATACCTTCTCTCGC	sqRT-PCR	
FXYD5	TCTACACAGAACTCCAGCCCAC	TGCTTTGGTGCTCTTGTGTG	sqRT-PCR	
GADD34	CGAGGAAGAGGGAGTTGC	GTTGGCACCACCAGGAC	sqRT-PCR	
GAPDH	TGGGGCCAAAAGGGTCATCATCTC	GCCGCCTGCTTCACCACCTTCTT	sqRT-PCR	
HSP27	GGAGTGGTCGCAGTGGTTAGG	GGGAGGAGGAAACTTGGGTG	sqRT-PCR	
IP-10	CTGATTTGCTGCCTTATCTTTCTG	CTTGGAAGATGGGAAAGGTGAG	sqRT-PCR	
XBP1	CCTTGTAGTTGAGAACCAGG	GGGGCTTGGTATATATGTGG	sqRT-PCR	[143]

Tab.4 siRNAs

siRNA	Sense	Antisense	Purpose	Note
Scramble	upon request	upon request	unspecific control siRNA (human)	AM4611 (ambion)
IRE1α	CAACCUCUCUUCUGUAUCUtt GGAAGGUGAUGCACAUCAAtt CUGGAGGAGACGAAUGAUAtt CUGUACUCUUGGAGUAACAtt	AGAUACAGAAGAGAGGUUGtt UUGAUGUGCAUCACCUUCCtt UAUCAUUCGUCUCCUCCAGtt UGUUACUCCAAGAGUACAGtt	Knockdown human IRE1α	sc-40705

3.9 Plasmids

The plasmids used are pcDNA6/V5-His B (Thermo Fisher), pNF-κB-Luc (Takara) and its variations pLuc and pAP-1-Luc (see Primer Section and Appendix), as well as pTER-EGFP [173]. A brief overview is illustrated in Fig. 9.

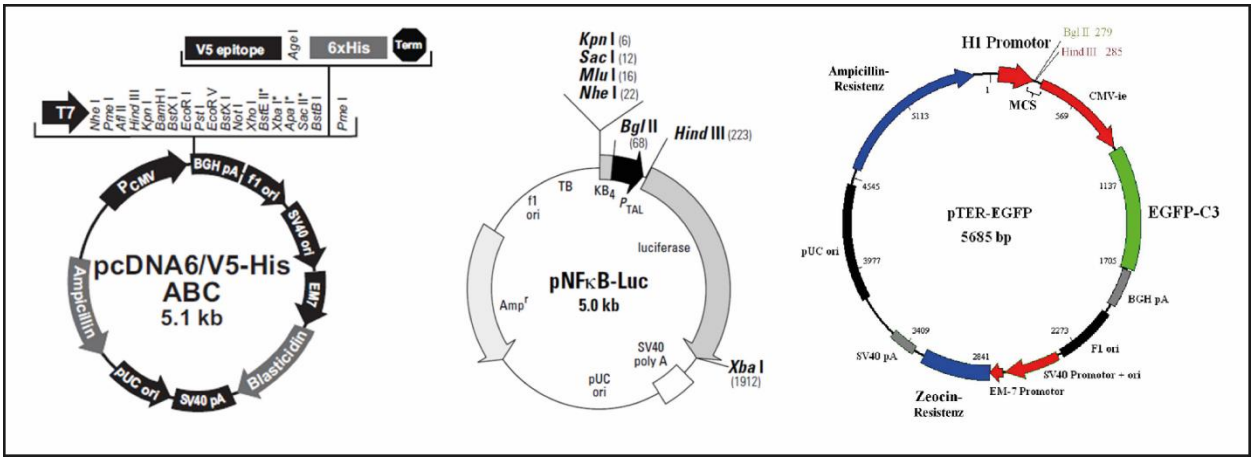

Fig.9 Utilized plasmids adapted from [173, 174].

3.10 Kits & Assays

The names, IDs and companies of used kits are enumerated below.

Analytik Jena: innuPrep Gel Extraction Kit (845-KS-5030250); innuPrep RNA Mini Kit (845-KS-2040050) **Baseclick:** EdU-HTS Kit 555 (BCK-HTS555-2) **BD Biosciences:** PE Annexin V Apoptosis Kit I (559763) **Promega:** Cell Titer 96® Aqueous one solution (G3580); Luciferase Assay System (E1500) **Roche:** High Pure PCR Product Purification Kit (11732668001) **Takara:** In-Fusion HD Cloning plus (638909) **Thermo Fisher:** GeneJet Plasmid Minipräp-Kit (K0503)

3.11 Cell lines & Bacteria

Enlisted below (Tab.4) are the used eukaryotic cell lines and the composition of their growth medium. Primarily, human cell lines, except of yolk sac cells (10A, 6A & 6A3 from mouse as described previously [175, 176]) were used.

Tab.4 Eukaryotic cell lines and growth medium used.

Reagents	HEK-293	SK-N-MC	HeLa	MCF-7	PC-3	HepG2	EA.hy926	yolk sac
DMEM	500 mL	500 mL	500 mL	500 mL	500 mL	500 mL	500 mL	500 mL
L-glutamine (200 mM)	5 mL	5 mL	5 mL	5 mL	5 mL	5 mL	10 mL	10 mL
Sodium bicarbonate (7.5% w/v)			15 mL					
Sodium pyruvate (100 mM)	5 mL	5 mL				5 mL		
NEAs (100x)			5 mL			5 mL		5 mL
HEPES (1.0 M)			5 mL				5 mL	5 mL
Penicillin (10,000 U/mL)-Streptomycin (10 mg/mL)	5 mL	5 mL	5 mL	5 mL	5 mL	5 mL	5 mL	5 mL
FBS	50 mL	50 mL	50 mL	50 mL	50 mL	50 mL	50 mL	50 mL

Bacterial strains DH5α (Thermo Fisher) and Stellar competent bacteria (see In-Fusion HD Cloning plus kit by Takara) were cultivated on standard agar plates and in LB medium (see 3.1.1 & 4.2.3).

3.12 Software

Software for data collection and analyses, project management, illustration, manuscript preparation as well as the developer are enumerated below.

Adobe Systems: Illustrator CC 2015.3 **Alexis Dereeper & Valentin Guignon:** Phylogeny.fr platform **Bio-Rad:** Quantity One 4.40 **BD Bioscience:** FACSDiva **BioTek:** Gen5 **Clarivate Analytics:** EndnoteX7 **Des Higgins & Fabian Sievers:** Clustal Omega (v1.2.4) **General Electric:** UNICORN TM Version 3.21 **Geospiza:** FinchTV 1.4.0 **GraphPad Software:** GraphPad Prism 5 & 6 **Horiba:** Fluorescence 1.3.5 **IBIVU**: PRALINE **Jasco:** Spectra Manager II Software **JustBio:** Complementor **Microsoft:** Microsoft Office 2016 **Motic:** Motic Images Plus 2.0 **NCBI:** BLAST; Batch Web CD-Search Tool **PREMIER Biosoft:** NetPrimer **Raytest:** StellaX **SerialCloner:** SerialCloner2.6.1 Stella: **Technical University of Denmark:** SignalP 4.1 Server; NetNGlyc 1.0 Server; ProP 1.0 Server **Thermo Fisher:** 7500 Fast Software v2.3 **Tree Star:** FlowJob **UT Southwestern Mecial Center:** AL2CO **VIB/UGent:** Venn **Wayne Rasband:** ImageJ

4 Methods

In this section, the methods will be described to collect the results of this thesis. Basic techniques will not be described in any detail, for instance Western blotting is a standard laboratory technique established almost four decades ago [177], the fundamental principles are therefore already textbook knowledge [178]. The Method Section will primarily focus on the exact implementation and notable differences to standard protocols. Further information is also included in the Figure Legends and the Material Section.

4.1 Cell culture

This paragraph will describe how eukaryotic cells were cultured, passaged and conserved during the thesis. Furthermore, cell-based assays will be described. Occasionally, the reader will be referred to the Material Section, publications in the Reference List or to the corresponding Figures in the Result Section.

4.1.1 Cultivation of eukaryotic cells and beyond

Eukaryotic cells (see 3.11) were cultured using common cell culture flaks, well plates and dishes (3.3) with verified culture media and supplements (3.1 and 3.11) in suitable cell culture incubators and handled under sterile conditions (3.4). The following paragraphs will describe general conducted procedures.

4.1.1.1 Seeding, passaging, counting and conservation of eukaryotic cells

All cells were seeded in the following way: Cryo vials containing $1.5*10^6$ to $3.0*10^6$ cells (diluted in FBS w/ 10% DMSO) were thawed in a water bath for approximately 5 minutes, diluted in 10 mL serum-rich culture medium and centrifuged for 15 minutes at 1,000xrpm at RT. Subsequently, the supernatant was removed and the cell pellet was resuspended in 15 to 20 mL serum-rich medium for further cultivation in T75 flasks. After receiving full confluency, the medium was removed, and the cells were washed once with 15 mL PBS. After aspiration of PBS, 3 mL Trypsin (3.1) was added, subsequently removed and the flasks were incubated in an CO_2 incubator for 15 minutes at 37°C. Afterwards, the cells were detached with full-medium (3.11) and passaged to fresh culture vessels. Depending of the utilized cell line the growing time varied. For instance, HEK-293 receive a confluency after seeding within approximately 5 days, whereas other lines such as MCF-7 need up to two weeks. Please note, that cell lines such as SK-N-MC tend to grow to over-confluency with concomitant cell death and must therefore be passaged at a higher ratio or more often. For reproducible results or for the creation of cryo stocks it is important to count the cell number. For cell counting the removed cells were diluted in PBS (1:10 in the case of HEK-293 cells to 1:2 in the case of SK-N-MC after removal from T75 flasks) and subsequently stained with trypan blue (1:2) for 5 minutes. Afterwards, 8 µL of the suspension was added to a Neubauer counting chamber (3.4) with an approximate cell number of at least 15 cells per large square. Only trypan blue negative cells were taken into consideration for further experiments or cryo stock preparation. To create cryo stocks the desired cell number (at least $1.5*10^6$ per vial) was centrifuged for 15 minutes at 1,000xrpm and RT. Subsequently, the pellet was diluted in ice-cold FBS with 10% DMSO, transferred to cryo vials and immediately stored at -80°C.

4.1.1.2 Transfection of eukaryotic cells and isolation of single clones

For transfection of cells two strategies were used, forward and reverse transfection. Forward transfection was carried out for transferring plasmid DNA into cells as follows: $1.0*10^6$ HEK-293 cells diluted in 2 mL serum-rich medium were plated into a 6-well and grown for 24 hours. After reaching about 60 to 70% confluency, 4 µg DNA, 4 µL Turbofect (3.1) and 188 µL OptiMEM® (3.1) were mixed together and incubated for 30 minutes at room temperature. Subsequently, 1 mL in the 6-wells was removed and the transfection reagent mix was dropped onto the cells. After a transfection time of 6 to 18 hours, the cells were further processed (depending on the purpose, see Figures and below). For stable transfection, transfected cells were passaged 1:3, using 10 µg/mL Blasticidin into fresh 6-well plates. After an initial dying phase of un-transfected cells the remaining cells were again passaged in Blasticidin-rich full medium, either in T75 flasks (mixed clones) or in 96-well plates with one cell in 100 µL (single clones). In the latter case, the cells were observed for the next few weeks to make sure that only one cell population is growing. After receiving a sufficient confluency (demands occasional Blasticidin-rich medium change), the cells were passaged first into 48-well plates and further into 24- and 6-well plates. In accordance with the cell passaging, the expression level of the desired protein was controlled via Western blot (4.3.4).
For transfecting siRNA, the reverse transfection strategy was carried out using Lipofectamine® (3.1). Briefly, 150 µL OptiMEM with 5 µL Lipofectamine® and 150 µL OptiMEM (3.1) with 7.5 µL siRNA (10 µM, see Tab.4) were incubated at room temperature for 5 minutes and mixed together for an incubation time of 30 minutes at room temperature. In the meantime, at least 300,000 but not more than 500,000 HEK-293 cells were diluted in 1.7 mL antibiotic-free full medium. Finally, the transfection cocktail was equally distributed in a 6-well and the cell suspension was dropped onto the prepared cocktail. The success of transfection was observable within 48 hours.

4.1.1.3 Preparation of whole cell lysates

To prepare whole cell lysates the supernatants of cells in 6-well plates were removed and ice-cold cell lysis buffer (see 3.2) containing protease inhibitor (3.7) and in the case of phosphorylated proteins, additional phosphatase inhibitor (3.7) was applied. The amount of the lysis buffer used depends on the desired final protein concentration and varies depending on the used cell line and approaches between 50 and 150 µL. After application of the cell lysis buffer the cells were removed using a cell scraber (3.3), lysed for 30 minutes using a roll mixer (3.4) at 4°C and subsequently centrifuged for at least 30 minutes at 20,000xg and 4°C. Finally, the supernatants were separated from the pellet and further analyses were conducted.

4.1.1.4 Preparation of necrotic cell lysates

For preparation of necrotic cell lysates, cells grown in various culture vessels and, removed by trypsin treatment as already described (4.1.1.1), diluted in serum-free medium (volume depends on culture vessel, for instance 20 mL for T75 flasks or 1 mL for a 6-well) and centrifuged for 20 minutes, at 1,000xg and room temperature. Afterwards, the supernatant was aspirated and the pellet diluted into fresh serum-free medium. Please note, that the volume for resuspension also depends on the culture vessels. An appropriated working concentration for necrotic cell lysates was 5 mg/mL. For instance, to achieve a concentration of 5 mg/mL, the resuspension volume should not exceed 1 mL in the case of cells removed from one fully confluent T75 flask. After obtaining a homogenous cell suspension four freeze/thaw cycles were carried out in liquid nitrogen and a water bath. Subsequently, the necrotic cells were centrifuged at 20,000xg for at least 30 minutes on 4°C, the supernatant was then transferred to fresh sterile tubes, the protein concentration was determined using the Bradford assay (see 4.3.1) and the concentration was

adjusted to 5 mg/mL. To remove protein aggregates and other higher molecular weight components, the necrotic preparation was additionally centrifuged 100,000xg for 30 minutes at 4°C in an ultracentrifuge (3.4).

4.1.2 Cell-based assays

In this section, experiments conducted with eukaryotic cells will be described. Please note that procedures such as cell cultivation, cell counting and passaging are already described in 4.1.1. Some variations of the protocols below are indicated in the corresponding Figure Legends.

4.1.2.1 Phosphorylation assays

Phosphorylation is a major modification of proteins in cellular signal transduction [179]. To assess the activation or inhibition of signal transduction pathways, protein phosphorylation was measured using Western blots (see 4.3.4). For protein phosphorylation experiments, cells were plated into 6-well plates and grown to full confluency (for instance $1.5*10^6$ HEK-293 cells in 2 mL are fully confluent within 24 hours of growth). After receiving full confluency, the cells were set serum-free (800 µL) for 4 hours in the presence or absence of inhibitors and respective controls, e.g. DMSO (see also 3.7 and the Result Section), subsequent experiments were conducted (see Result Section) and the cells were finally lysed as described in 4.1.1.3. Characteristic features concerning the handling and detection of phosphorylated proteins have already been described (4.1.1.3) or will be discussed below (4.3.3, 4.3.4).

4.1.2.2 Transcription analyzing assays

The procedure in this section is comparable to the procedure described above (4.1.2.1). The main difference however, is that the cells were not lysed after finishing the experiments, instead they were trypsinized with 50 µL trypsin for 15 minutes in a CO_2 incubator at 37°C (3.4). Afterwards, the cells were removed using 1 mL PBS, collected in 2 mL Eppis and were centrifuged for 15 minutes at 1,000xg (room temperature). Subsequently, PBS was removed and the cell pellet was either processed immediately (see 3.10 and 4.2.2.3) or stored at -80°C.

4.1.2.3 Cell viability assays

The viability of cells was measured using MTS (Cell titer solution in 2.10). To determine how the viability of cells is changed upon various conditions 5,000 to 10,000 cells per well (see Figures Legends) were passaged in 96-well plates in a total of 100 µL and grown for 24 hours. Subsequently, the cells were either transfected (see corresponding Figure Legends and 4.1.1.2 with adjusted amount of OptiMEM, DNA and Turobfect), set on serum-free for 4 hours or were pre-incubated on serum-free in the presence or absence of inhibitors and respective controls (DMSO) for 4 hours (see 3.7 and corresponding Figure Legends). Afterwards, the cells were stimulated with necrotic cell lysates (see Figures) in the presence or absence of inhibitors for 12 hours to 24 hours (see Figure Legends). One exception is the experiment with Q-VD-OPh where the inhibitor was applied directly after the initial growth phase and the transfection was carried out the entire time until the assay was measured. Please note, the cells in 96-wells have never been washed to prevent detachment. Further, after setting the cells serum-free the medium was not exchanged for stimulation. Moreover, transfection as well as serum-free cultivation and pre-incubation always occurred in 50 µL. That means the stimulation was carried out in a total of 100 µL by adding 50 µL to the 50 µL medium already present in the wells. Finally, after stimulation the medium was removed, the cells set on 50 µL fresh serum-free medium, 10 µL MTS were added and the plates were measured within 4 hours at a wavelength

of 490 nm and 630 nm, whereas the value at 630 nm was subtracted from 490 nm value afterwards. Please note, that the 2 hours-value always displayed the most reliable absorbance which has been used for evaluation as shown in the Result Section. The relative cell viability was calculated based on the cell viability measured after 24 hours of initial growth phase (50 µL serum-free with 10 µL MTS).

4.1.2.4 Flow cytometry: Fluorescence-activated cell sorting (FACS)

For measurement of apoptotic cell death, FACS in combination with annexin V and 7-AAD staining was used as described previously [180]. By using flow cytometry, the scattering of light by cells and the fluorescence of dyes, connected to specific antibodies/proteins bound to the cells, can be measured. For apoptosis measurements, the PE Annexin V Apoptosis Kit I was used (3.10). By application of annexin V the exposure of phosphatidylserine to the extracellular space upon cellular apoptosis can be monitored. Further, relative cell injury is detectable due to 7-AAD only enters the cell after damage of the cellular membrane and eventually intercalates into genomic DNA. To elucidate the relative apoptosis rate, FACS analyses were performed with 500,000 HEK-293 cells seeded in 6-well plates and grown for 24 hours. Subsequently, the cells were washed once and set serum-free as well as were stimulated with 1 mg/mL necrotic cell lysates. After additional 24 hours, supernatants were collected and centrifuged for 10 minutes (1,000xg at 4°C). While centrifugation, the remaining cells were washed once with 1 mL PBS and 200 µL trypsin were added for 15 minutes. Subsequently, the trypsinized cells were removed using 300 µL binding buffer containing 10% FBS and were united with the centrifuged cell pellet. 150 µL of the obtained cell solution was mixed with 5 µL annexin V and 3 µL 7-AAD in FACS tubes (3.3), vortexed gently once and kept in the dark for 20 minutes at room temperature. Finally, the dilution was filled up to 500 µL with binding buffer, vortexed gently again and FACS measurements were carried out. With the FACS Canto II (3 lasers, 3.4) the simultaneous detection of the annexin V and 7-AAD fluorescence is detectable. Additionally, the cell size (FSC = forward scatter) and cell granularity (SSC = sideward scatter) was measured. Thus, the cell populations positive for annexin V and/or 7-AAD were quantified using FlowJo (gating strategy, Fig.10).

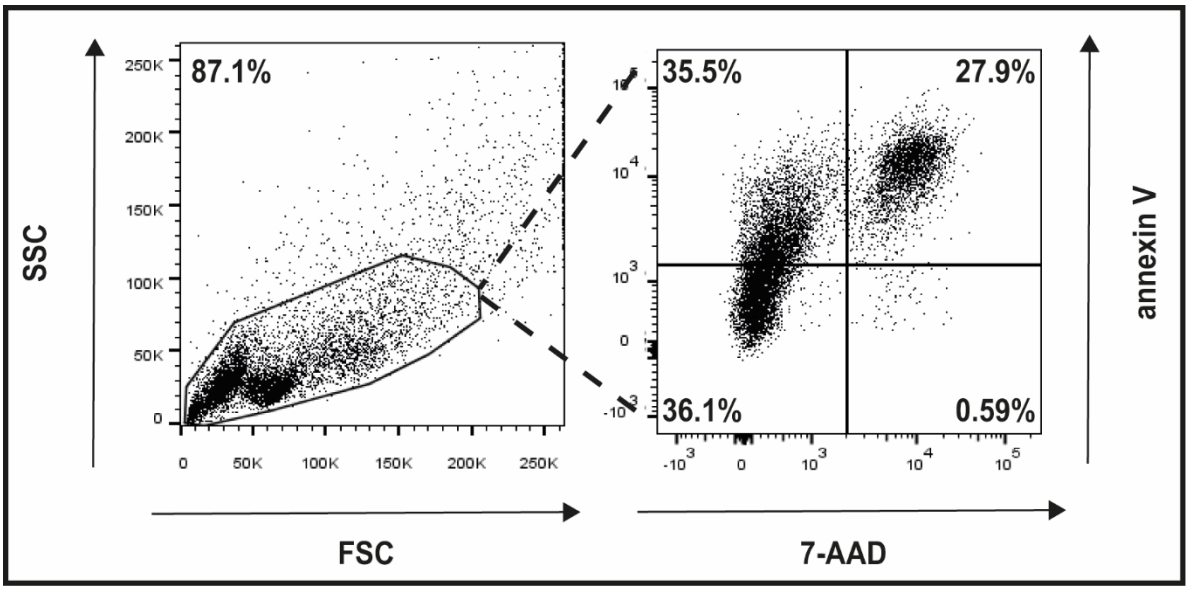

Fig.10 Gating strategy at a representative experiment.

4.1.2.5 Luciferase reporter assays

The luciferase reporter assays were conducted similary as previously described [181]. As vehicle, the pAP-1 reporter cloned by Hans Prochnow (Tab.3) was used. Briefly: 300,000 HEK-293 cells were seeded, diluted in 500 µL per well into 24-well plates and grown for 24 hours. Subsequently, the cells were washed once with 1 mL PBS per well and were co-transfected using 1 µg pAP-1-Luc or pTAL-Luc and 0.4 µg pTER-EGFP for 6 hours. Subsequently, the cells were treated as indicated in Fig.26B. At last, the cells were washed once with PBS, treated with the lysis buffer shipped with the respective kit (see 3.10) and stored at -80°C for at least 30 minutes. Afterwards, the plate was thawed on a vibrating table at room temperature for about 30 minutes and 5 µL to 10 µL were transferred to white plates for detection of luciferase or 20 µL lysate with 80 µL ddH_2O in black plates for detection of fluorescence (3.3). Finally, the cell's luciferase activity was measured using the Luciferase Assay System (3.10) according to the manufacturer's protocol and the FLUOstar Omega luminometer (3.4) with the following adjustments: Position delay 1 second; measurement start time 5 seconds; no. of intervals 25 seconds; interval times 1 second; 50 µL volume of substrate; shaking frequence 300 rpm; shaking time 2 seconds; pump speed 300 µL/second. The pTER-EGFP fluorescence was measured at a position delay of 0.2, with 10 flashes per well with the following filters: λ_{abs}= 485 nm / λ_{em} = 520 nm. Values were expressed relative to the fluorescence intensity of the respective cell lysates. All measurements were performed in triplicate.

4.1.2.6 Cell proliferation assays

For direct detection of the cell proliferation the EdU HTS555 kit was used (3.10). The advantage of this method is that the thymidine analog EdU is directly incorporated into genomic DNA during replication and can be detected by a click chemical reaction coupled with the fluorescent dye TAMRA-PEG3-Azide (λ_{abs}= 546 nm / λ_{em} = 579 nm). The whole procedure was carried out according to the manufactures protocol but will be described briefly: Fluorescence 96-well plates (lumox, see 3.3) were coated with 30 µL 0.1 mg/mL Poly-L-Lysine (3.1) in PBS. Subsequently, 40,000 HEK-293 cells were seeded in a volume of 100 µL (full medium) and grown for 24 hours. After the initial growth phase, the medium was substituted by 100 µL either serum-free medium or 1 mg/mL necrotic cell lysates in serum-free medium. Following 24 hours of stimulation, the medium was removed once more and the cells were labeled with 10 µM EdU in serum-free medium for another 4 hours. Note that one well remains unlabeled and served as a negative control. Subsequently, the cells were washed with 100 µL sterile PBS containing 1% endotoxin-free BSA (3.1) and were fixed with 100 µL 3.7% PFA in PBS for 20 minutes in the dark at room temperature. Afterwards, the cells were washed again with 200 µL PBS containing 1% BSA (twice!) and were permeabilized with 100 µL 0.5% Triton-X 100 in PBS for 20 minutes in the dark at room temperature. Subsequently, the permeabilization solution was removed and 100 µL of the click assay cocktail (containing all buffers for the click reaction and the fluorescence dye) was added (incubation for 30 minutes in the dark at room temperature). Afterwards the solution was removed, the wells were washed twice with 150 µL rinse buffer, 100 µL PBS containing 1% BSA was added and the plate was ready for measurement (FLUOstar Omega with the following filters: λ_{abs}= 544 nm / λ_{em} = 580 nm). For evaluation, all test samples were set relative to the EdU negative control. All measurements are representatives of five individuals.

4.1.2.7 Cell dying assays

To trigger necrotic cell death without completely disrupting cells, cell injury was induced based on [182]. Fully confluent HEK-293 cells grown in T175 flasks were trypsinized and diluted in 20 mL serum-free HEK-293 medium. After centrifugation for 30 minutes at 1,000xrpm the supernatant was removed and the

pellet was resuspended in 1 mL serum-free medium. Subsequently, 350 µL (approximately 20*10^6 cells) of the suspension were either kept at 37°C or were heated up to 45°C for 10 minutes in a water bath. After heat shock, the cells were added into fresh 24-well plates for 3 hours in a CO_2 incubator (3.4) and were centrifuged afterwards for 15 minutes at 1,000xg at room temperature. The supernatant was eventually added to fresh confluent vital HEK-293 cells (already kept on 700 µL serum-free for 4 hours) for 2 hours. As controls either 250 µg/mL necrotic cell lysates or serum-free medium was used. The cells were further processed as described in 4.1.1.3.

4.1.2.8 Cell aggregation assays

To determine the cell aggregating potential of CLU as described [2], cell aggregation assays were conducted based on protocols published previously [183, 184]. The cell aggregation assays were performed as follows: 0.66% agarose/LB agar (3.1) diluted in 5 mL PBS was heated in a microwave. The bumping was compensated by sterile water and the entire hot solution was aliquoted into five sterile 1.5 mL Eppis. After aliquot preparation, the Eppis were heated up to 90°C for sterilization in a heating block (3.4) for 10 minutes. Subsequently, the heated, sterile Eppis were stored at 55°C in a water bath (3.4). Eventually, 50 µL of the agarose/LB agar solution was added into 96-wells. In the meantime, CLU knockdown and scramble HEK-293 cells (shCLU & shScr, see [173]) were removed from T25 culture flasks by trypsinization using full HEK-293 medium. After centrifugation (1,000xrpm) for 15 minutes, the cell pellet was diluted in HEK-293 cell medium containing 1% FBS and 20,000 cells (100 µL) were added to the fresh coated 96-well plates. After keeping the cells in the coated 96-well plates for 48 hours the wells were photographed (Motic, see 3.4) and the relative aggregate size was determined using ImageJ as follows: Analyze → Set Scale (set Distance in Pixels on 100 and click Global); Image → Type → 8-bit; Process → Binary → Make Binary; Edit → Invert; Analyze → Analyze Particles (Size 20; Show Outlines; Display Results; Summarize; Record Starts).

4.2 Nucleic acid analyses

In the following section the work with nucleic acids will be described. For basic technique concepts such as PCR, molecular cloning, DNA sequencing and others, the reader should be referred to standard text books of molecular biology/genetics.

4.2.1 Isolation, quantification of nucleic acids and agarose gel electrophoresis

For isolation of nucleic acids, the kits in paragraph 3.10 were used. The elution of DNA was carried out with 10 mM Tris pH 8.5, RNA was eluted with RNase-free H_2O and kept on ice or frozen anytime. Agarose gel electrophoresis was carried out with the components and equipment listed above (3.1, 3.2 & 3.4). Ethidium bromide stock solution (0.07% in ddH_2O) was added to gel immediately after melting. Electrophoresis was carried out with 80 V. The concentration of nucleic acid was determined in a photometer (3.4) with a dilution of 1:100 using the following equation (X_{DNA} = 40; X_{RNA} = 50):

$$c_{(nucleic\ acids)} = OD_{260nm} * X \frac{ng}{\mu L} * dilution\ factor$$

4.2.2 Polymerase chain reaction (PCR)

The PCR (polymerase chain reaction) protocols and programs described in this section are primarily for human gene targets. Exceptions are indicated.

4.2.2.1 PCR protocols/programs

For various applications, the following PCR programs were utilized. Please note, that for molecular cloning various DNA polymerases were used. All programs are listed in the following order: Initially heating; heating phase; primer annealing; elongation phase; final elongation; number of cycles and particularities. Please note, that the lid of the PCR cycler was heated up to 110°C.

sqRT-PCR: sqRT-PCRs were prepared as follows: 10 µL Hot Start Mix (3.5); 1 µL forward primer (10 µM); 1 µL reverse primer (10 µM); 1 µL cDNA (25 ng/µL); 7 µL ddH_2O. All sqRT-PCRs except of IP-10 and FXYD5 were performed using the following basic program: 95°C 15 minutes; 95°C 30 seconds (IP-10 1 minute); 30 seconds annealing (IP-10 1 minute); 72°C 30 seconds elongation (IP-10 1 minute); 72°C 5 minutes final elongation (IP-10 & FXYD5 10 minutes); annealing temperature & cycles: BiP 55°C & 23 cycles; CHOP 45°C & 40 cycles; CLU 60°C & 23 cycles; ERdj3 55°C & 23 cycles; FXYD5 55°C & 30 cycles; GADD34 50°C & 23 cycles; GAPDH 60°C & 20 cycles; HSP27 58°C & 24 cycles; IP-10 55°C & 26 cycles; XBP1 45°C & 27 cylces. **qRT-PCR:** qRT-PCRs were prepared in qPCR plates (3.3) as follows: 5 µL qRT-PCR Master Mix (3.5); 2.5 µL Primer mix (0.2 µM); 2.5 µL cDNA (25 ng/µL). The utilized program for all qRT-PCRs was: 95°C 15 minutes; 40 cycles of 95°C 15 seconds, 60°C 30 seconds & 72°C 30 seconds; 2 final cycles of 95°C 15 seconds & 60°C 60 seconds. **RACE PCR:** RACE PCRs were prepared as follows: 25 µL Hot Start Mix (3.5); 5 µL forward and reverse primer (10 µM) for the 1st RACE PCR and 1 µL forward and reverse primer (10 µM) for the 2nd RACE PCR; 5 µL cDNA (1st) or 5 µL of 1:100 diluted c-tailed DNA (2nd), the reactions were finally filled up to 50 µL with ddH_2O. All RACE PCRs were performed using the following basic program: 95°C 15 min; 95°C 30 seconds; 53°C for fourth step of the 5' RACE or 48°C for fifth step of the 5' RACE; one minute elongation; 10 minutes of final elongation at 72°C; 35 cycles **Cloning PCRs:** For cloning of various constructs different DNA polymerases were used. Cloning CLU mouse: *Preparation of cloning PCR for fragment amplification:* 0.5 µL Pfu DNA polymerase (3.5); 5 µL Pfu buffer + $MgSO_4$; 1 µL dNTPs (3.1); 1 µL forward primer (10 µM); 1 µL reverse primer (10 µM); 5 µL cDNA (mouse yolk sac cells); 36.5 µL ddH_2O. *Preparation of fusion PCR:* 0.5 µL Pfu DNA polymerase (3.5); 5 µL Pfu buffer + $MgSO_4$; 1 µL dNTPs (3.1); 1 µL forward primer Exon1 (10 µM); 1 µL reverse primer Exon9 (10 µM); 0.5 µL of each purified PCR fragment (eluted in 30 µL); 40.5 µL ddH_2O. *The following PCR program was utilized for CLU mouse cloning:* 95°C 3 minutes; 95°C 30 seconds; 51°C 30 seconds; 72°C 5 minutes; 5 minutes of final elongation; 40 cycles for fragment amplification and 35 cycles for fusion PCR. Site-directed *in vitro* mutagenesis (RIVR/RIVQ & RITR): *Preparation of cloning PCR for fragment amplification:* See also cloning of CLU mouse but with 1 µL full-length human CLU in pcDNA6 (250 ng/µL by Hans Prochnow), with both pcDNA6 sequencing primers as terminal primers. *Preparation of fusion PCR/PCR program:* See cloning of mouse CLU but with different annealing temperatures (55°C for RIVQ and 50°C for RITR). Cloning HSP72: *Preparation of cloning PCR for fragment amplification:* 0.5 µL KAPA HiFi DNA polymerase (3.5); 10 µL 5x KAP HiFi Fidelity buffer; 1 µL dNTPs; 1 µL forward primer (10 µM); 1 µL reverse primer (10 µM); 1 µL cDNA (25 ng/µL) obtained from HEK-293 cells. *The following PCR program was used:* 95°C 3 minutes; 95°C 30 seconds; 55°C 30 seconds; 72°C 30 seconds; 10 minutes for final elongation; 35 cycles. Cloning IRE1α; Sub-Cloning CLU in pTAL-AP-1/NF-κB & FXYD5: PCRs were prepared as follows: 12.5 µL Takara Clone Amp HiFi PCR 2x Mix (3.10); 1 µL forward primer (10 µM); 1 µL; reverse primer (10 µM); 1 µL cDNA (25 ng/µL) obtained from HEK-293 cells or plasmid DNA (2.5 ng/µL); 9.5 µL ddH_2O. For all PCRs, the following program was utilized: 98°C 1 minute; 98°C 30 seconds; 65°C 30 seconds; 72°C 2.5 minutes (except for IRE1α with 5 minutes); 72°C 15 minutes of final elongation; 35 cycles. **Colony PCR:** Colony-PCRs were prepared as follows: 10 µL Hot Start Mix (3.5); 1 µL forward primer (10 µM); 1 µL reverse primer (10 µM); 5 µL of clone suspension (one colony in 30 µL ddH_2O see below); 2 µL ddH_2O. The following program was performed: 95°C 15 minutes; 95°C 30 seconds; 51°C (pcDNA) or 48°C (pTAL) 30 seconds; 72°C one minute; 72°C 10 minutes for final elongation; at least 20 cycles.

4.2.2.2 Determination of transcription start sites via 5' RACE PCR

For determination of transcription start sites, the 5' rapid amplification of cDNA ends PCR (5' RACE PCR) was performed. A schematic depiction of the principle has been illustrated previously [174]. This paragraph will solely describe how the 5' RACE PCR was carried out for determining the transcription start site of mouse CLU.
The 5' RACE consists of at least six steps: 1) Gene-specific cDNA synthesis, 2) Purification of the specific cDNA, 3) C-tailing of the specific cDNA, 4) 1st RACE-PCR for amplification of the 5' end, 5) 2nd RACE-PCR for more yield and higher specifity of the amplified cDNA (nested PCR) and 6) Final purification and DNA sequencing.
Step 1) 2.5 µg RNA from yolk sac cells of the mouse were lyophilized, diluted in 6 µL RNase-free H_2O, mixed with 0.5 µL of a mouse CLU specific reverse primer (10 µM, Tab.3), heated up to 70°C for 10 minutes and kept on ice for one minute. Afterwards, 2 µL RevertAid buffer (3.5), 1 µL dNTPs (10 mM) were added and an initial warming for 2 minutes at 42°C was carried out. Subsequently, 0.5 µL RevertAid Reverse Transcriptase (3.5) was added and the cDNA synthesis was conducted for 50 minutes at 42°C with a subsequent denaturation step of 10 minutes at 70°C. In Step 2) the obtained CLU-specific cDNA was purified using the PCR Product Purification Kit (3.10) with subsequent elution of the cDNA in 50 µL Tris pH 8.5. In the C-tailing step number 3) 10 µL of the purified cDNA, 5 µL tailing buffer (3.2), 2.5 µL dCTP (2 mM, 3.1) and 6.5 µL ddH_2O were mixed, heated to 94°C, kept on ice for 1 minute, 1 µL Terminale Desoxynucleotid Transferase (TdT, see also 3.5) was added and the C-tailing reaction was carried out at 37°C for 10 minutes with a subsequent denaturation step at 65°C for 10 minutes. Step 4 & 5) comprised the two RACE PCR (1st & 2nd) reactions as described above (4.2.2.1). In the final step 6) the obtained RACE PCR products were again purified and sequenced as described below (4.2.3.4) using a reverse mouse CLU primer (Tab.3).

4.2.2.3 Reverse transcription of mRNA

The cell samples obtained in various experiments (see 4.1.2.2) were processed with the innuPrep RNA Mini Kit (3.10) according to the manufacturers' protocol. The RNA concentration was measured photometrically (3.3 & 3.4) at a dilution of 1:100 in RNase-free H_2O and cDNA synthesis was carried out as follows: 5 µg purified RNA was filled up to a total of 12 µL with RNase-free H_2O, 1 µL oligo-dT primer were added, the mixture was heated up to 65°C for 5 minutes and kept on ice for 2 minutes. Afterwards, 4 µL RevertAid buffer and 2 µL dNTPs were added and the solution was warmed to 42°C for another 2 minutes. Subsequently, 1 µL Reverse Transcriptase (3.5) was added to the solution and the reverse transcription was carried out for 60 minutes at 42°C with a subsequent denaturation step at 70°C for additional 10 minutes. Finally, the solution was filled up to 200 µL at a final concentration of 25 ng/µL.

4.2.2.4 Semi quantitative reverse transcription PCR (sqRT-PCR)

Semiquantitative Reverse Transcriptase PCRs (sqRT-PCRs) were carried out with primers listed in Tab.3 according to the PCR protocols as listed above (4.2.2.1). The necessary number of cycles was determined empirically by testing various cycles and choosing the cycle number where expression differences can be deduced from the band intensity or according to the qRT-PCR analyses (see below). To visualize sqRT-PCR, 2% agarose gels were used as described above (4.2.1). One exception were sqRT-PCRs of XBP1. To visualize the splicing of XBP1, 4% agarose gels were conducted with a running time of approximately 2.5 hours.

4.2.2.5 Quantitative Reverse Transcription PCR (qRT-PCR)

To quantify the expression of genes quantitative RT-PCRs (qRT-PCRs) were performed in a specialized light cycler (3.4), using a DNA polymerase cocktail (master mix) with a DNA intercalating dye (SYBR green, see also 3.5). The more DNA was amplified the higher was the SYBR fluorescence. As reference, a non-intercalating dye was also present in the master mix (ROX). By dividing the SYBR fluorescence from the ROX fluorescence, so-called Rn values were obtained. The further subtraction of the fluorescence without detectable increase (baseline) from the Rn values lead to the ΔRn value which was plotted against the cycle number. The cycle number where all the samples for comparison are in their exponential phase is defined as the c_T value. To obtain information of the relative change in the expression of a defined gene in comparison to a control housekeeping gene (HPRT in this case) the analyses were carried out as described previously [185]. The preparation of qRT-PCR (3.3, 3.4, 3.5, 4.2.2.1), the utilized machines (3.4) and PCR programs (4.2.2.1), as well as the software for qRT-PCR analyses (3.12) were already listed/described above.

4.2.3 Molecular cloning & *In vitro* mutagenesis

The creation of recombinant DNA molecules for expression of proteins or modulation of the cellular homeostasis is summarized here under the term “molecular cloning”. Mutagenizing of recombinant DNA molecules *ex vivo* is termed “*in vitro* mutagenesis”. Utilized plasmids for both approaches are illustrated in Fig.9.

4.2.3.1 Restriction enzyme-based cloning

One of the most prominent and wide performed cloning approach is the restriction enzyme-based cloning. The following constructs cloned in this thesis are based on this approach: mouse CLU in pcDNA6, human CLU in pcDNA6 (cloned by Hans Prochnow), BAX in pcDNA6 (cloned by Markus Baiersdörfer) and HSP72 in pcDNA6. Exact details of the PCR strategy are described above (4.2.2.1) and in the Primer List (Tab.3), in this section the general procedure will be depicted.

After obtaining the wanted purified PCR product carrying restriction sites (here HindIII and BamHI) dedicated for integration in the vector of choice, both (vector and PCR fragment) were restricted: 20 µL BamHI buffer, 2 µL HindIII, 2 µL BamHI (3.5), between 50 and 100 µL DNA (50 ng/µL), added to a final volume of 200 µL with ddH_2O and kept on 37°C overnight. The next day the whole restriction reaction was loaded on a 1% agarose gel, respective bands were cut out and the DNA was extracted using a gel extraction kit (3.10) with subsequent elution in 40 µL ddH_2O. On another gel (2%) the concentration of the purified DNA was determined using a Mass Ruler DNA marker (3.1) and the necessary amount of DNA was calculated using the following equation:

$$m_{(Integrate)} = 3 * m_{(Vector)} * \frac{bp\ Integrate}{bp\ Vector}$$

After calculating the necessary amount, the DNA has either been lyophilized or was directly used for ligation: 1 µL T4 DNA Ligase (3.5), 0.5 µL T4 DNA Ligase buffer, a final volume of 10 µL containing water, integrate and vector. The ligation reaction was carried out at room temperature for 2 hours. Afterwards, 200 µL competent DH5α bacterial cells (already prepared as described previously [186]) and 10 µL ligation reaction were mixed and kept on ice for 30 minutes. Subsequently, the cells were heat-shocked in a water bath for 90 seconds at 42°C and transferred on ice for another 5 minutes. The heat-shocked bacteria were finally suspended in 1 mL warm LB medium (3.1), kept on 37°C for one hour, were centrifuged for 10 minutes at 4,600xg, 1 mL supernatant was removed, the remaining bacteria were resuspended and

plated onto agar plates containing 100 µg/mL ampicillin (3.1 & 3.3). The next day respective clones were isolated, diluted in 30 µL sterile ddH_2O and colony PCRs were performed as described (4.2.2.1). Positive clones were further diluted in 5 mL LB medium containing ampicillin (100 µg/mL), grown overnight, 500 µL of the dense bacterial solution were mixed with 500 µL sterile 50 % glycerol in LB medium (v/v) and stored on -80°C. The remaining bacterial solution was used for plasmid isolation with subsequent agarose electrophoresis, concentration determination, DNA sequencing and further approaches.

4.2.3.2 In-Fusion™ cloning

Compared to restriction enzyme-based cloning, digestion with restriction enzymes is no prerequisite for In-Fusion cloning. The basic principles are well described in the literature [187] and will be described here just briefly. The so-called In-Fusion Enzyme bears a 3'-5' exonuclease activity of the poxvirus DNA polymerase. This feature allows the digestion of DNA in 3'-5' direction creating 5' overlapping single stranded DNA ends. When applying two DNA molecules with a complementary overlap of 15 bp the single-stranded DNA overlapping sites are hybridizing. After transforming the obtained hybridized DNA molecule into competent cells the gaps within the construct (results of the 3'-5' exonuclease activity) will be repaired and a fully intact recombinant DNA molecule is replicated within the cells. The only prerequisite for the reaction are linear DNA fragments which can be obtained either by digestion with restriction enzymes or by PCR. The primers for the In-Fusion reaction should display the following features (excluding overlap): Only two purines, melting point between 58°C to 65°C and a GC content of 40 to 60%. After purification of the linearized target vector and the PCR fragment between 40 and 100 ng of DNA, 2 µL In-Fusion Enzyme in a total of 10 µL filled up with ddH_2O was utilized for the In-Fusion Reaction which was carried out for 15 minutes at 50°C. Afterwards, the fused DNA construct was transformed into commercially available competent bacteria supplied with the kit (Stellar™ competent cells). The transformation protocol was basically comparable to the transformation as described in 4.2.3.1 with a few alterations: 2.5 µL of the DNA construct + 50 µL competent cells, 45 seconds of heat shock, 100 µL warm SOC medium. The isolation of clones and further processing was equal to 4.2.3.1.

4.2.3.3 Site-directed *in vitro* mutagenesis

The site-directed mutagenesis was conducted according to the illustration as published previously [174]. As a template, the already cloned full-length human CLU cDNA was used. The utilized primers (RIVQ/RITR) are listed in Tab.3 and the PCR preparation/protocol is shown in 4.2.2.1. In principle, the entire strategy was in accordance with 4.2.3.1.

4.2.3.4 Sanger DNA sequencing

The sequencing of constructs created was carried out by the company SeqLab in Göttingen. Each run contains approximately 750 ng of purified DNA with 2 µL primer (10 µM) in a total of 7 µL. The average sequencing length was approximately 1,500 bp. The analyses of the sequence data were carried out using FinchTV (3.12).

4.3 Protein analytics

The preparation of proteins from cells was already described (4.1.1.3 and 4.1.1.4). Therefore, this section will primarily explain how proteins were purified, how their concentrations were measured, how proteins

and protein modifications were visualized, how protein activity assays were performed and how protein folding was assessed. Please note, that proteins were primarily kept on ice or frozen.

4.3.1 Bradford assay

The measurement of the protein concentration was carried out using the Bradford assay. The Bradford assay was performed in unsterile 96-well plates (3.3) using an ELISA reader (3.4). Briefly: 10 µL of a BSA standard diluted in water was used in duplicates (0, 40, 120, 200, 300 und 400 µg/mL). 10 µL of samples diluted in water (1:10 in the case of purified proteins and 1:30 for cell lysates) were used in triplicates. After adding standards and samples in the 96-well plates, 10 µL formic acid was added to each well followed by 180 µL Roti®-Quant (diluted 1:5, see 3.1). The absorbance was measured within 30 minutes ($OD_{595\ nm}$).

4.3.2 TCA precipitation

In the case of insufficient protein concentration, the proteins were precipitated using TCA (Trichloroacetic acid, see 3.1). Briefly: 50% ice-cold TCA were mixed with 250 µL of the sample in a ratio of 1:2 and kept on ice for 30 minutes. Hereafter, the sample was centrifuged (20,000xg, 4°C, 15 minutes) and the supernatant was discarded. Subsequently, the protein pellet was washed with 1 mL ice-cold acetone and kept once more on ice for 5 minutes. After an additional centrifugation step as described above, the supernatant was discarded again and the pellet was kept on room temperature for one hour (tube lid open). Afterwards, the dry protein pellet was diluted in 30 µL 1x SDS-PAGE sample buffer (3.2) and heated up to 60°C for 10 minutes. In the case of a low pH value due to remaining acetone, 1-2 µL 1M NaOH was added. Occasionally, the pellet was insoluble, therefore the pellet was sonified until full dilution (3.4).

4.3.3 SDS-PAGE & Coomassie staining

For separation of proteins depending on their molecular weight SDS-PAGEs (sodium dodecylsulfate poly acryl amide gel electrophoresis) were performed. The principle of the SDS-PAGE has been described previously [188]. SDS-PAGEs were prepared as followed according to the manufacturers' protocol (Bio-Rad see 3.4):

Tab.5: Composition of SDS-PAGEs (Components are listed in 3.1)

Reagents	separating gel					stacking gel
	7.5%	9%	10%	12.5%	15%	5%
water (mL)	6.1	5.6	5.3	4.5	3.68	3.45
acryl-/bisacrylamide (mL)	2.5	3.0	3.3	4.1	4.92	0.85
1 M Tris pH 8.8 (mL)						0.63
3 M Tris pH 8.8 (mL)	1.25	1.25	1.25	1.25	1.25	
10% (w/v) SDS (µL)	100	100	100	100	100	50
APS (µL)	75	75	75	75	75	37.5
TEMED (µL)	15	15	15	15	15	7.5

After gel preparation, samples of various protein concentrations with the addition of SDS-PAGE sample buffer under reducing or non-reducing conditions were applied (3.2). Please note, that if not indicated otherwise the SDS-PAGEs were performed under reducing conditions. Depending on the pocket size the voltage and sample size was between 15 V, 25 µL (small pockets, 15 lanes) and 100 V, 40 µL (large pockets, 10 lanes). After completing the SDS-PAGEs the stacking gel was removed and the separating gel

has either been blotted (see below) or stained with Coomassie Brilliant Blue (18 mL ddH_2O, 3 mL Roti®-Blue, 3 mL methanol) overnight and destained with 25% methanol (v/v). Finally, Coomassie gels were scanned for documentation. If not indicated otherwise, 10% SDS-PAGEs were used.

4.3.4 Western blotting

As already mentioned at the beginning of section 4, Western blotting is a standard technique first published almost 40 years ago [177]. Western blots were used in this thesis to address various issues such as recombinant protein expression, monitoring of protein purification or signal transduction. The basic protocol however, was comparable for all applications. After adjustment of an appropriate protein concentration, the proteins obtained of various sources (see 4.1.1.2, 4.1.1.3, 4.1.1.4, 4.3.5) were separated by SDS-PAGE (4.3.1) and blotted (400 mA, 100 V, approximately 1 hour in a Tank blot, see 3.4) onto nitrocellulose membranes (3.3). Subsequently, the membranes were blocked for 1 hour using 5% milk powder in PBST and washed afterwards at least 4 times with PBST (non-phosphorylated proteins) or TBST (phosphorylated proteins) (see also 3.1, 3.2). After removing all the remaining milk powder, the membranes were incubated with antibodies (3.6) diluted in PBST (for non-phosphorylated proteins, with 5% milk powder if the antibody is cross-reactive) or TBST containing protease-free 2% BSA (phosphorylated proteins, see 3.1) for at least 16 hours overnight at 4°C on a shaking table (3.6). Afterwards, the antibodies were removed thoroughly and the membranes were washed with PBST or TBST (depending on phosphorylation) for 4 times, 5 minutes each washing step and were incubated with the respective secondary antibodies (diluted in PBST/5% milk powder or TBST/2% BSA) for 1 hour. Subsequently, the washing steps were repeated once more and eventually the respective bands were visualized using a Western blot imager (3.4) and ECL (3.1) with the membrane between two foils. The blots were finally evaluated using ImageJ (3.12). Loading controls were performed afterwards on the same membrane comparable to the procedure of the primary antibody. By visualizing multiple targets on one blot the membranes were cut into slides at the corresponding molecular weight.
Occasionally, the controls were hard to distinguish from the background of the primary antibodies, in this case it was necessary to remove the primary antibody or at least the secondary antibody from the membrane before adding the loading control. For this purpose, stripping buffer (3.2) was heated to 60°C and added to the membrane on a vibrating table for 20 minutes. Afterwards, the membrane was washed at least 5 times with PBST and the fresh antibody was applied. Additional blocking steps were not required.

4.3.5 Fast protein liquid chromatography (FPLC)

For purification of recombinant sCLU as well as for the separation of necrotic cell lysates the FPLC was utilized.

4.3.5.1 Protein purification with FPLC

The purification of recombinant sCLU has already been described [174, 176] and published [189]. Furthermore, other groups also presented a purification strategy [27]. Moreover, an exact protocol for the sCLU purification has been given to the MPI for Polymer Research in Mainz (Volker Mailänder). Nonetheless, the basic principle will be described briefly according to [189]. HEK-293 cells overexpressing mouse sCLU or human sCLU (cleaved & uncleaved) were cultivated to a confluency of 100% and were subsequently serum-starved for at least 60 hours. Dead or detached cells were removed from the supernatant by centrifugation (1,000xg, 30 minutes, 4°C). The DMEM-based buffer of the cleared sCLU-enriched supernatant, was substituted by LEW buffer containing 7% glycerol (3.2) via a membrane filter

unit (30 or 50 kDa, see 3.3) connected to a peristaltic pump (3.4). The obtained solution was subjected to a FPLC column packed with 2g Ni-IDA Resin (3.1). After two washing steps with 100 mL LEW buffer (the second step with additional 25 mM Imidazol), the bound sCLU fractions were eluted by using elution buffer containing 250 mM Imidazole (three fraction á 10 mL). Finally, the elution buffer was substituted with PBS (at least 4 times) by using a centrifugation filter unit (30 or 50 kDa). The final protein concentration was adjusted to 1 µg/µL as determined by a Bradford assay (4.3.1).

4.3.5.2 Size exclusion chromatography

The size exclusion chromatography of necrotic cell lysates has already been described previously [190] and is graphically depicted in Fig.34. The size exclusion has been carried out as follows: HEK-293 cells, grown to full confluency in at least five T175 flaks, were removed as described above (4.1.1.1) and were freeze/thawed in 5 mL phosphate buffer (3.2) and further processed (4.1.1.4). After obtaining the clear supernatant, the necrotic cell lysate was applied to an ultracentrifuge (4.1.1.4). The supernatant obtained after ultracentrifugation was hereafter utilized to a centrifugation filter unit (50 kDa, see 3.3) twice (5 minutes and 20 minutes, each at 4,600xg on 4°C). The flow through was used for further experiments and the non-filtrated remaining was applied to a size exclusion column (see 3.4, Superdex200) in the following manner: A 2 mL *Loop* was connected between vault 2 and 6 to an ÄKTA system (3.4). Hereafter, the size exclusion column was connected, equilibrated with phosphate buffer (3.2) and the flow path was adjusted to load. Approximately 2.5 mL of the prepared necrotic cell lysates (with or without ultracentrifugation) were loaded into a scissor and injected into vault 4. After changing the option to flow path inject, the sample passed the column with an approximate flow rate lower than 1 mL/minute. The fractions were collected, further processed (4.3.1 & 4.3.2), and applied to the cells (4.1). Please note, that fractions which were applied on living cells have never been precipitated. A standard calibrate curve was obtained in a comparable manner (3.5).

4.3.6 Chaperone activity assays

The chaperone activity assays of sCLU have already been described [174] and published [189]. Nevertheless, the basic principle will be described briefly according to [189]. Additional information is also included in the respective Figure Legends. Necrotic cell lysates were obtained from HEK-293 cells as already described (4.1.1.4) and diluted in phosphate buffer (3.2). Catalase (1 mg/mL) or necrotic cell lysates (750 µg/mL) was mixed with sCLU (see above, 75 µg/mL or 100 µg/mL depending on the experiment, respectively) or BSA (83 µg/mL) as a non-chaperone control in a total volume of 100 µL with 1x precipitation buffer (3.2). The assay was performed at 50°C for 150 minutes, respectively, while protein precipitation was concomitantly monitored by detecting the OD at 360 nm (turbidity) using an ELISA reader (3.4). All data were corrected, by the absorption of plain assay buffer.

4.3.7 Deglycosylation and reduction of sCLU

The deglycosylation of sCLU has already been described/published [189] and was carried out as follows: Partial deglycosylation was achieved by treatment of sCLU together with three exoglycosidases. 100 µg sCLU diluted in 100 µL PBS was incubated with 4.2 U/µL α2,3-neuraminidase, 0.7 U/µL β1,4-galactosidase and 0.3 U/µL β-N-acetylglucosaminidase at 37°C for 12 hours under gentle agitation at pH 6. Subsequently, the buffer was substituted by PBS using a membrane filter unit (5 kDa). For full deglycosylation, sCLU (25-400 µg) was treated with various concentrations of PNGase F in PBS (see Figures). Please note that the deglycosylation is more successful by using smaller volumes. The reduction of sCLU was carried out

concomitantly with sCLU deglycosylation or separately for 6 to 12 hours as described above with various concentrations of DTT. Additional information is also included in the respective Figure Legends.

4.3.8 Circular dichroism spectroscopy (CD spectroscopy)

Information of a protein's folding is important to explain changes in the behavior of proteins, such as alterations in the activity. CD spectra however, provide solely information of the content of secondary structure and do not allow a final assessment of the protein folding. The basic principle is the measurement of the absorption of left and right circular polarized light by a protein. The relative mean residual ellipticity (MRE) measured is specific for certain secondary structure elements within a defined wavelength under standard conditions (20°C, thickness 1 mm) and at defined molecular weight and concentration of the protein solution. By using algorithms, the relative secondary structure elements within a protein can be calculated. More as to the principle of CD spectroscopy can be found elsewhere [188, 191]. The CD spectroscopy of sCLU has already been described/published [189] and was carried out as follows: The measurements were carried out in a CD spectrometer (3.4) with 0.1 µg/µL protein diluted in phosphate buffer (3.2) in a step-scan mode using 1.0 mm path length quartz cells (3.4) at 20°C. CD spectra were obtained via a step resolution of 1.0 nm and a bandwidth of 5.0 nm at a sensitivity of 100 mdeg. The correction of an average spectrum acquired from three scans was performed in relation to the blank buffer and smoothed with a Savitzky-Golai convolution using Spectra Manager (3.12). The prediction of secondary structures was carried out on the Dichroweb website (http://dichroweb.cryst.bbk.ac.uk/) using the CDSSTR algorithm and the reference data set 7 (optimized for 190 nm to 240 nm) [192]. Molecular masses of 70 kDa for fully glycosylated, 61.4 kDa for partially and 55.6 kDa for fully deglycosylated sCLU were assumed. All sCLU forms are considered to have a length of 478 aa (427 aa+51 aa tag), except for mouse sCLU with 484 aa.

4.3.9 Fluorescence spectroscopy

To measure relative changes in the overall folding of proteins, fluorescence measurements of molecules which enter the hydrophobic core of proteins were carried out. The organic compound ANS (3.1) is capable to bind hydrophobic areas within a protein accompanied by increased fluorescence. Therefore, an elevated fluorescence signal upon ANS application is an indicator for protein unfolding. The procedure was carried out as follows: sCLU was reduced as described in 4.3.7. Hereafter, 1 µM sCLU was mixed with 7.5 µM ANS (molar excess) for 30 minutes, the entire solution was filled up to 200 µL with phosphate buffer and measured in a fluorescence spectrometer (3.4). The excitation wavelength was 370 nm and the emission was measured between 400 nm and 600 nm, with a gap width of 5 nm at 25°C (temperature control).

4.3.10 MALDI-TOF MS

To determine the success of full sCLU deglycosylation, MALDI-TOF MS (Matrix-assisted laser desorption/ionization time of flight mass spectroscopy) analyses were carried out by dilution in a sialic acid matrix. The analyses occurred using a Shimadzu CFR Axima (Kratos Analytica) and were carried out by Dr. Berger-Nicoletti at the Institute for Organic Chemistry (University of Mainz).

4.4 Bioinformatics

4.4.1 Alignments

For the comparison of two or more nucleotide or protein sequences non-commercial alignment tools were used (Nucleotide BLAST, Protein BLAST and Clustal Omega). To conduct alignments, the default settings were applied. Data for alignments and further analyses were collected via DNA sequencing (4.2.3.4), obtained from NBCI or UniProt (experimental verified and predicted sequences, see App.1 & App.2).

4.4.2 Prediction/determination of SSCR, N-glycosylation, furin cleavage sites, homolog protein domains and protein sequence identity

To predict SSCRs (signal sequence coding regions), N-glycosylation, furin-like proprotein convertase cleavage sites and homologies, SignalP 4.1 [193], NetNGlyc 1.0 [194], ProP 1.0 [195] and the Batch Web CD-search tool [196-199] were used. The default settings of all programs were unaltered. In the case of NetNGlyc predictions, only glycosylation sites without proline at Xaa in the sequon Asn-Xaa-Ser/Thr and a relative potential > 0.5 were used for further evaluations.
To determine the identity/conservation of various protein sequences, the AL2CO tool [200] was used with default settings.
Additional analyses (such as for hydrophobicity, residual type and conservation) were conducted with the multiple sequence alignment program PRALINE utilizing the default settings [201-203]. For all PRALINE analyses the full-length protein sequences (excluding *Chelonia mydas*, *Nomascus leucogenys* and *Loxodonta africana*) were applied.

4.4.3 Prediction of disorder tendency

The relative disorder tendency was predicted using IUPred [204, 205]. For comparison of all animal classes 84 species with the CLU full-length protein of 445 aa (+17 aa) were chosen and the protein length was adjusted to 445 aa by truncating the N-terminus. As a putative intrinsically disordered protein [20, 24] the prediction type for long-disorder proteins were chosen. After prediction of all species, the mean of all animal classes was separately calculated and plotted together with the mean of other animal classes in one diagram. For single comparison, the untruncated CLU full-length protein was used.

4.4.4 Prediction of secondary structures

Secondary structure elements were calculated using JPred [206]. As in the case of disorder prediction, 84 species with an average length of 445 aa were used (see above) and all sequences were aligned to obtain an average distribution of putative secondary structure elements. For single comparison, the untruncated CLU full-length protein was used. The secondary structures indicated in the corresponding Figures were obtained by Jnet prediction and coiled-coil domains were deduced from Lupas Coil Prediction at a window size of 28 with at least 50% probability.
Additional analyses were conducted with the multiple sequence alignment program PRALINE utilizing the default settings [201-203]. For all PRALINE analyses the full-length protein sequences (excluding *Chelonia mydas*, *Nomascus leucogenys* and *Loxodonta africana*) were applied.

4.4.5 Generation of phylogenetic trees

The description of this method, is adopted by the output of Phylogeny.fr. The analysis was performed on the Phylogeny.fr platform [207-213] and comprised the following steps. Sequences were aligned using MUSCLE (v3.8.31) configured for highest accuracy (MUSCLE with default settings). After alignment, ambiguous regions (i.e. containing gaps and/or poorly aligned) were removed with Gblocks (v0.91b) using the following parameters: minimum length of a block after gap cleaning 10, no gap positions were allowed in the final alignment, all segments with contiguous non-conserved positions bigger than 8 were rejected, minimum number of sequences for a flank position were 85%. The use of Gblocks were enounced in the case of poor-aligned sequences or in the case of sequences with an input of less than 200 aa. The phylogenetic tree was reconstructed using the maximum likelihood method implemented in the PhyML program (v3.1/3.0 aLRT). The WAG substitution model was selected assuming an estimated proportion of invariant sites (of 0.061) and 4 gamma-distributed rate categories to account for rate heterogeneity across sites. The gamma shape parameter was estimated directly from the data (gamma=0.999). Reliability for internal branch was assessed using the aLRT test (SH-Like). Graphical representation and edition of the phylogenetic tree were performed with TreeDyn (v198.3). All branches with a support value smaller than 50% were collapsed.

4.4.6 Transcriptomics

To find factors are expressed in cells which might be responsible for the observed effects transcriptome data obtained from TRON in Mainz (http://celllines.tron-mainz.de/) were used. Since more than 20,000 potential genes exist, the threshold for the search was set at the first 1,000 highest expressed targets. The assumption was that the observed effect must correlate with a sufficient expression of the gene. After removing of all genes except of the first 1,000 genes, the data of 5 various cell lines were compared using a Venn Diagram (see 3.12 & http://bioinformatics.psb.ugent.be/webtools/Venn/). After finding only genes which remain in cell lines with the observed effects, the genes were analyzed using the Webgestalt server (http://www.webgestalt.org/) concerning the cellular location the gene product resides. Additionally, the genes were co-checked using PhosphoSitePlus (http://www.phosphosite.org/) and Uniprot (http://www.uniprot.org/). After finding candidate genes which are in frame, the relative expression of the candidate genes (no threshold!) was calculated relative to the expression of all transcripts in a cell. Afterwards, the relative expression was compared to the relative expression in PC-3 cells. Only gene targets in negative cells with a relative expression rate lower than 0.1 relative to PC-3 were taken into further analyses due to genes with a higher expression level can be detected in PCR reactions (data not shown) and are therefore probably expressed in a sufficient manner even in “negative” cells.

4.5 Statistical analyses

For assessment of the statistical significance of the obtained data various statistical tests were performed. Whenever possible, all statistical tests were performed using the mean of various experiments and the standard error. However, by using data sets obtained from single experiments or data whose values were independently collected from one another (e.g. obtained from various species) the standard deviation was calculated to shows how the individuals differ from the calculated mean. By comparing two data sets (e.g. Ctrl vs. stimulated) the unpaired, two-tailed Student’s t test were used. By increasing the amount of data sets a one-way ANOVA either followed by Dunnett’s test for multiple comparison (by comparing data sets with one control), Tukey’s multiple comparison test or Bonferroni multiple comparison test was performed. All statistical analyses were carried out using GraphPad Prism (3.12).

5 Results

In this paragraph results obtained from experimental findings and bioinformatic approaches will be presented. Note that some of the results might be part of articles published during the course of the present doctoral thesis [19, 189].

5.1 Evolution, structure and chaperone activity of the CLU protein

The CLU protein is still considered to be enigmatic due to no reliable structural information or discrete function is known yet. Nevertheless, CLU is described as a natively unfolded or intrinsically disordered protein which displays chaperone-like activity. Based on these finding, the first section will focus on the chaperone activity of CLU, the comparison of structural components of the CLU protein of various species and a subsequent experimental validation.

5.1.1 Cloning and characterization of mouse CLU

The chaperone activity of CLU is one of the most reliable CLU-based assays ever performed [21]. However, it was never addressed whether CLU, except of human origin, also displays chaperone activity. Therefore, in this section mouse CLU was cloned and further analyses were conducted.

5.1.1.1 Determination of the transcription start site of mouse CLU mRNA

The exact determination of the transcription start site of a gene is important for further molecular biological approaches. Even though a predicted mRNA sequence is available in the database it has never been figured out where the transcription of the CLU mRNA starts. Fig.11 shows the result of a 5' RACE PCR of cDNA reverse transcript by mRNA obtained from mouse yolk sac cells followed by Sanger sequencing as described in the Methods Section.

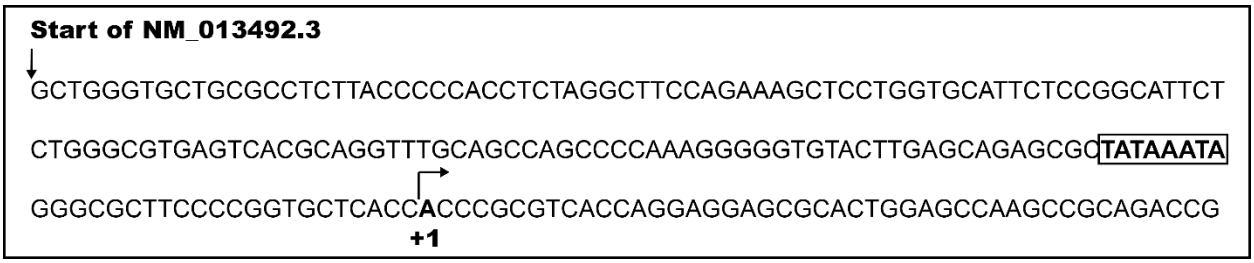

Fig.11 Result of the 5' RACE PCR and Sanger sequencing of reverse transcribed mouse yolk sac cell cDNA. +1 indicates the first base downstream the amplified cDNA end.

As expected, the mouse CLU mRNA starts 23 bp downstream of the TATA box. Similar results were obtained in the case of human CLU elsewhere [11, 174].

5.1.1.2 Purification of sCLU mouse

Based on the determined start site of mouse mRNA the full-length mouse cDNA was cloned in pcDNA6/V5-His B, stably transfected into HEK-293 cells and finally purified via affinity chromatography. The purification of mouse sCLU is depicted in Fig.12.

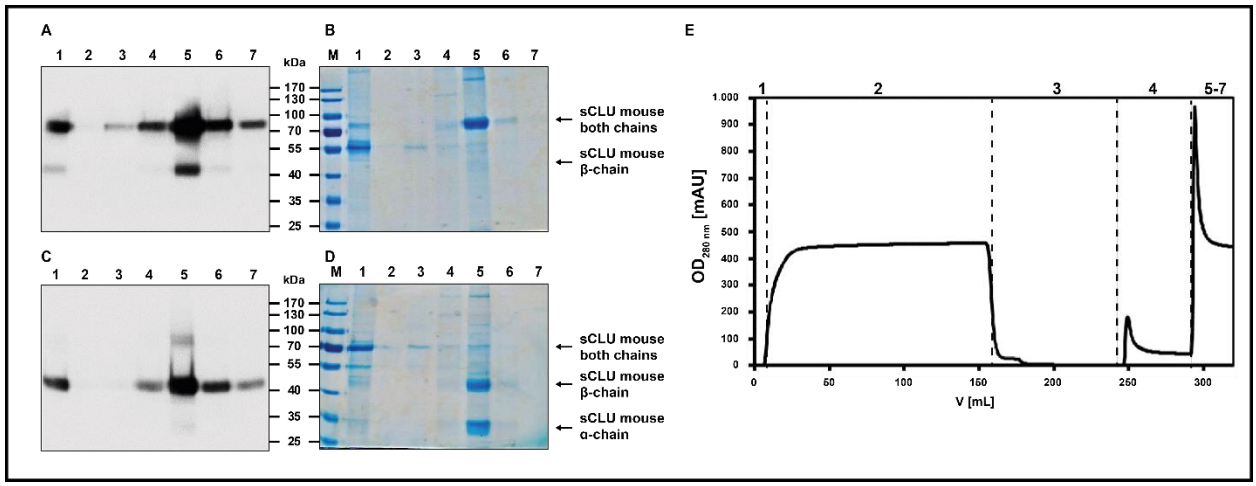

Fig.12 Purification of sCLU mouse. A Stable transfected single clone of sCLU mouse overexpressing HEK-293 cells were seeded 1:10 in ten T175 flasks, grown for five days and set serum-free after reaching more than 90% confluency for 60 hours. Subsequently, the supernatants were processed as described in the Methods Section. The numbers indicate the following purification steps: 1 buffer-exchanged supernatant prior to FPLC; 2 FPLC flow through; 3 first washing step with LEW buffer; 4 second washing step with LEW buffer + 10% elution buffer; 5-7 elution steps with 100% elution buffer, 10 mL each fraction. Western blot (anti-V5 antibody) and Coomassie analyses of the purification steps under non-reducing (A,B) and reducing (C,D) conditions on 10% SDS-PAGEs with 30 µL of the corresponding fraction per lane. (E) Chromatogram of the corresponding FPLC run shown in A-D.

Fig.12 shows the success of the purification of recombinant secretory mouse CLU (sCLU mouse). Intriguingly, both chains are only weakly attached to one another since a band was observable corresponding to the β-chain visible in Fig.12A under non-reducing conditions. However, in Coomassie-stained SDS-PAGEs (Fig.12B), no intense bands in the size of both single chains visually emerged, indicating that the vast amount of the sCLU protein is intact. Nevertheless, it must be mentioned that similar observations had not been made in the case of recombinant human sCLU [27, 174, 176]. Further, it must be noted that similarly to human sCLU purifications impurities are present that might be the result of sCLU chaperone activity. The yield of ten T175 flasks with more than 90% confluency and 60 hours on serum-free is about 1.3 mg protein. In contrast, blank purification with solely pcDNA6 transfected cells but in the same way as in case of sCLU overexpressing cells, is leading to a yield of about 34 µg protein. The co-purified proteins in the fractions are therefore most likely not a result of unspecific protein binding to the column (see also App.8).

5.1.1.3 Chaperone activity and CD spectroscopy of human & mouse sCLU

After purifying recombinant mouse sCLU, it was of interest whether the structure and activity of mouse sCLU is comparable to human sCLU (Fig.13).

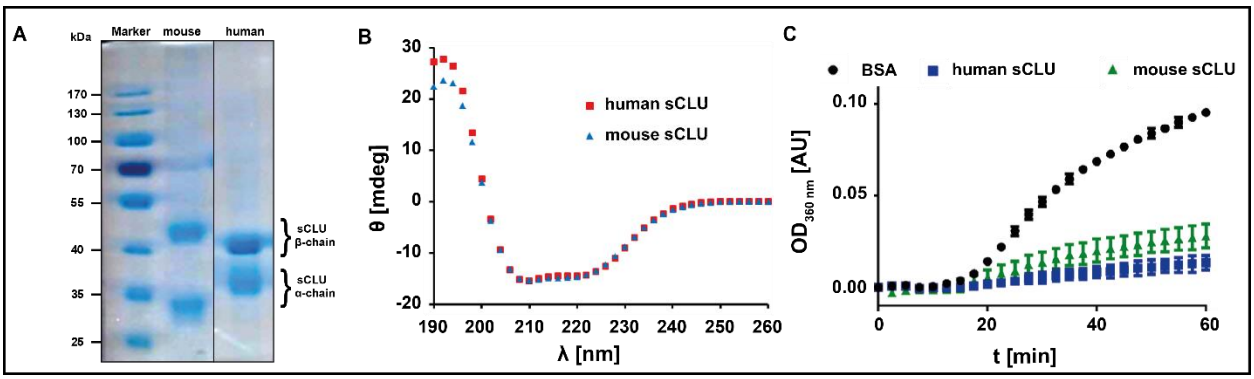

Fig.13 Comparison of human and mouse sCLU. (A) Reducing Coomassie gel (10% SDS-PAGE) with 3 µg recombinant sCLU mouse and human per lane. Note that the lanes were on the same gel but not in neighboring lanes. (B) CD spectra of human and mouse sCLU. All CD spectra were obtained at wavelengths ranging from 190 to 260 nm in 1 nm intervals. The spectra shown illustrate the means of three consecutive scans. Plotted is the ellipticity θ (mdeg) against the wavelength λ (nm), whereas intervals of 2 nm were chosen for a better illustration (n=3). (C) Chaperone activity assay using 75 µg/mL sCLU (mouse and human) or 83 µg/mL BSA with 1 mg/mL catalase as client protein under reducing conditions. Data plotted in intervals of 5 min. The represented data were obtained from a single experiment using triplicates. Error bars correspond to standard deviation. The data shown are representative for three independent experiments.

As shown in Fig.13A, both chains of mouse sCLU have a different molecular weight in comparison to human sCLU. The β-chain of mouse sCLU is approximately 3 kDa larger and the α-chain 3 kDa smaller than the corresponding bands of human sCLU. This result was expected due to human sCLU has three N-glycosylation on each chain, whereas mouse sCLU displays four N-glycosylation on the β-chain and only two N-glycosylation on the α-chain (determined with NetNGlyc, see 4.4.2). The average size of all six N-glycosylation (assuming standard glycosylation, [14, 16]) is 14.4 kDa. One glycosylation therefore has a size of approximately 2.4 kDa. Nonetheless, CD spectroscopic analyses reveal a comparable CD spectrum to human sCLU (Fig.13B). The average content of secondary structures is: 62.0±13.4% α-helices, 9.3±3.4% β-sheets, 12.0±4.2% turns and 17.3±6.0% unordered/random coiled. Finally, mouse sCLU also displays a chaperone activity comparable to human sCLU (Fig.13C), even though the activity of the mouse sCLU is slightly impaired. In summary, mouse sCLU is almost identical to human sCLU pointing to a conserved role as an extracellular chaperone.

5.1.2 Comparison of the CLU protein between various species

Encouraged by the findings above (5.1.1) it was of interest how conserved the CLU protein itself and its structural properties really are. Indeed, the mouse and human full-length CLU protein has an identity in the aa (amino acid) sequence of 77% but are comparable in their structure and chaperone activity. It was therefore of interest whether basic concepts of the CLU protein are conserved among CLU-bearing animals ranging from fishes to higher mammalians.

5.1.2.1 Identity/conservation of the aa sequence among various species

Initially, the Conservation Index of the CLU protein within the protein sequences obtained from 105 various species was calculated using AL2CO (4.4.2). Fig.14 shows the conservation of the CLU protein. Further information is listed in App.1.

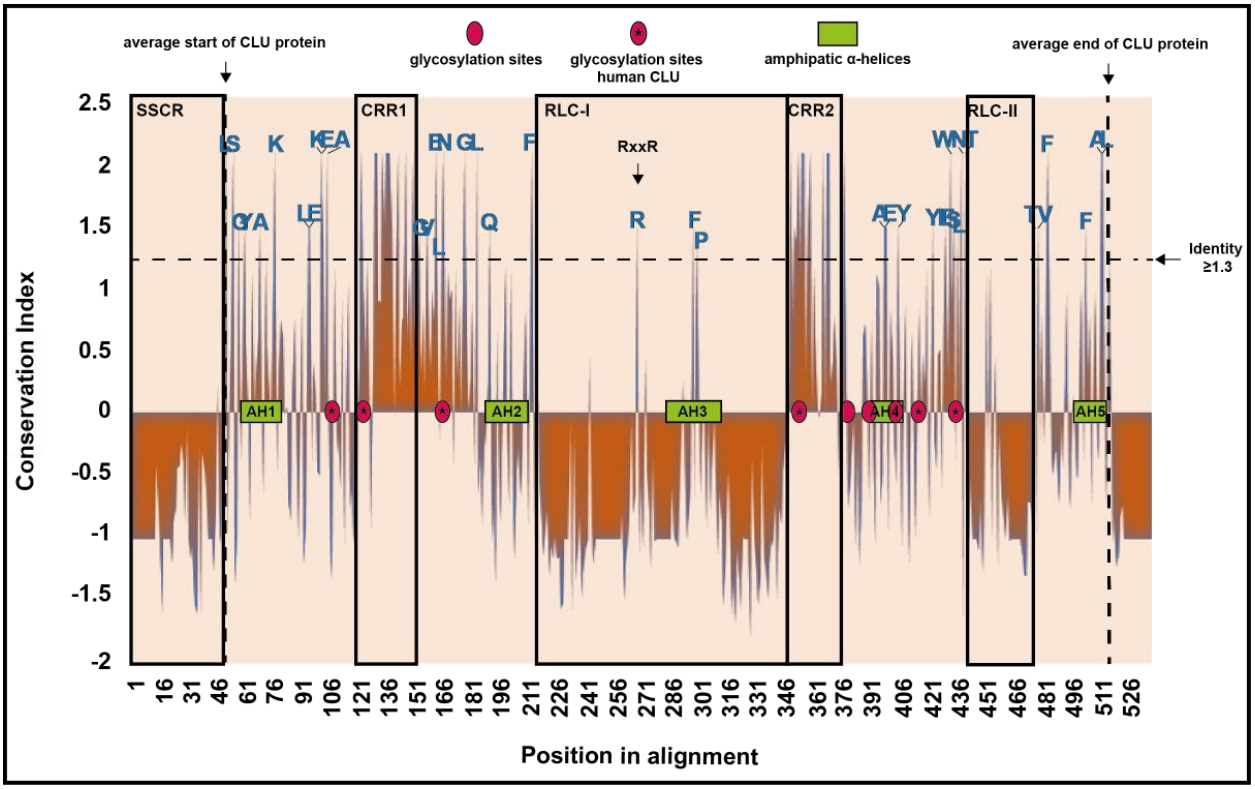

Fig.14 The conservation of the CLU protein between various species calculated with AL2CO after alignment with Clustal O (v1.2.4). Also included are the average SSCR (SignalP 4.1.), the putative FC recognition site RxxR (ProP & [195]) and putative glycosylation sites (NetNGlyc 1.0). Positions of amphipathic α-helices and cysteine-rich regions were adopted from [24]. The blue letters are indicating aa of an identity ≥1.3. Identical aa within the CCR are not indicated due to lack of space. Note that 40 highly identical aa are located outside of the CCRs and 25 within the CCRs. SSCR signal sequence coding region; CRR cysteine-rich region; RLC region of low conservation.

For a reliable alignment *Chelonia mydas*, *Nomascus leucogenys* and *Loxodonta africana* were excluded from the analysis. The conservation of the remaining 105 species, including 33 fishes (“Pisces”), 3 amphibians (Amphibia), 11 reptiles (Reptilia), 7 birds (Aves) and 54 mammals (Mammalia) is illustrated in Fig.14. The overall calculated identity is about 39%. All 105 tested protein sequences displaying CLU-like domains of the CLa and CLb superfamily. Moreover, all CLU proteins show a high conservation within the cysteine-rich regions (CCRs). Five disulfide bonds are potentially possible in every tested species. The length of the signal sequence coding region (SSCR) differs between 19 aa (*Xaenopus tropicalis*) and 36 aa (*Ophiophagus hannah*). Two species, included in the analysis, show no evidence for a SSCR, namely *Oncorhynchus mykiss* and *Alligator mississippiensis*. Furthermore, *Nomascus leucogenys* and *Loxodonta africana* (both excluded from the analysis above) also show no SSCR. The average length of the preproprotein is 451 aa and the mature CLU protein has an average size of about 429 aa. Regions of the N-glycosylation sites also show high levels of conservation, whereas the positions of the N-glycosylation sites on the α-chain are more conserved than the N-glycosylation on the β-chain, displaying a higher variability. The average number of N-glycosylation is about 5.2. Intriguingly, the amount of potential glycosylation sites differs between animal classes (see below). Beside low identity at the C- and N-terminus, which might be an artifact of the alignment, at least two areas (RLCs, regions of low conservation) are displaying a tremendous impaired conservation. First, the area approximately between position 212 and 345 (RCL-I) and second the area between position 438 and 472 (indicated as RLC-II in Fig.14). Interestingly, the recognition site for furin-like proprotein convertases (FC recognition site) is located within the RLC-I but shows high conservation (see arrow RxxR). Moreover, the putative amphipathic α-helices [24] are located at least in partially conserved regions.

5.1.2.3 Prediction of disorder tendency and secondary structures

Due to the notion that CLU is an intrinsically disordered protein with putative amphipathic α-helices it was of interest whether the order within the CLU protein and putative secondary structure elements are conserved among species. To determine the disorder tendency and to predict secondary structure elements, candidate proteins with an average length of 445 aa + 17 aa were chosen and truncated to 445 aa at the N-terminus to obtain equal protein size. The remaining 84 species (2 of 3 amphibians, 7 of 7 birds, 43 of 54 mammals, 27 of 33 fishes and 5 of 11 reptiles) were used for further analyses. Note that the average identity with 84 species instead of 105 species was not significantly altered (data not shown). After predicting the disorder tendency and secondary structures as shown in Fig.15, an evolutionary tendency for fluctuating order/disorder was revealed. The most extensive stretch of disorder was obtained at the N-terminus downstream the SSCR which is in accordance with an extended α-helical/coiled-coil structure and

encompasses an area of approximately 80 aa with one glycosylation site. The area within RLC-II (approximately 20 aa) also shows a high disordered tendency but β-sheets instead of α-helices. The sections of the CCRs and of the glycosylation sites show mostly low disorder tendency except for the first glycosylation site on the α-chain upstream the CCR1 and the second glycosylation site of the β-chain downstream the FC recognition site (RxxR). Intriguingly, the glycosylation sites on the β-chain are located within an α-helical/coiled-coil area. Furthermore, RLC-I shows a mixed disorder tendency. The area upstream and around the putative FC recognition site (RxxR) shows low disorder tendency whereas the section containing the putative amphipathic helix 3 (AH3 [24]) shows an immediate increase in disorder. Finally, the C-terminus of the CLU protein shows a comparable low disorder tendency and the presumed amphipathic α-helix 5 (AH5 [24]).

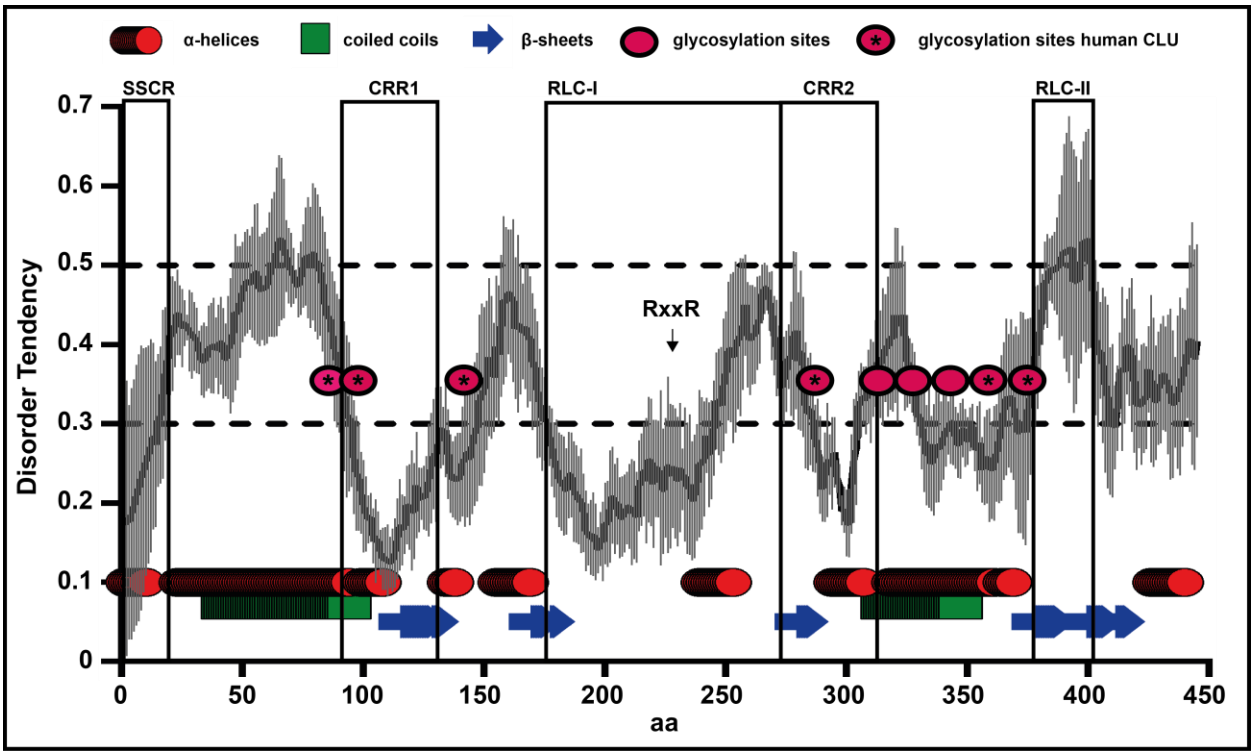

Fig.15 Prediction of disorder tendency and secondary structures. 84 animals with equal CLU protein length were selected for prediction of disorder tendency and secondary structure content using IUPred and JPred. For depiction, the mean of each class (Mammalia, “Pisces”, Aves, Amphibia and Reptilia) were plotted together and error bars correspond to the standard deviation. Putative furin-like proprotein recognition sites RxxR and glycosylation sites were predicted as shown in Fig.14. SSCR signal sequence coding region; CRR cysteine-rich region; RLC region of low conservation.

Taken together, areas of importance in processing the CLU expression (CCRs, FC recognition site & glycosylation sites) are more present in sections of low disorder tendency, whereas areas potentially involved in CLU chaperone activity and other

presumed functions display higher disorder tendencies. Moreover, the overall rate of predicted α-helices among species is 46.3% versus 10.5% β-sheets, renders CLU in summary as a predominately α-helical/unordered protein as already suggested [20, 24].

5.1.2.4 Phylogenetic tree based on the CLU aa sequence of various species

Encouraged by findings of various aa identity but similar structural organization it was of interest whether the full-length aa sequence of CLU or the sequence of RLC-I and other areas with low aa identity are specific evolutionary adaptions within the tested animals. Phylogenetic trees based on the full-length CLU protein (Fig.16) and after truncation (App.2) were calculated.

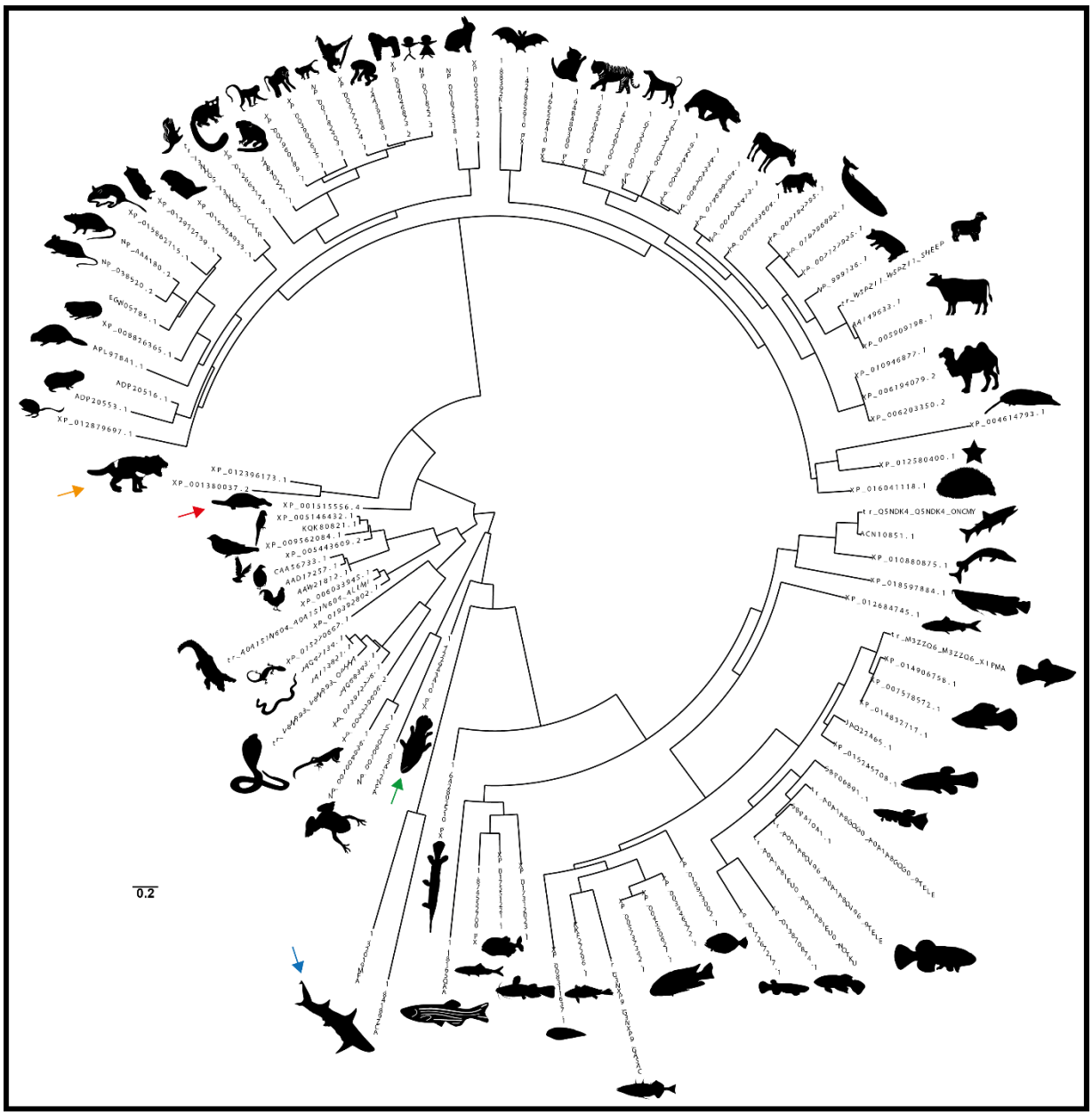

Figure 16 Circular phylogenetic tree based on the full-length CLU protein sequence of 105 species calculated as described above (4.4.5). The meaning of colored arrows will be discussed below. Please note that the illustrated animals are either copy free or were designed by the author of this thesis.

The phylogenetic tree in Fig.16 show that based on the aa sequence of CLU full-length protein, a lineage between species can be deduced. The majority of animals tested can be found in the groups they usually belong [214]. Three major mammalian branches/infraclasses can be found: Marsupialia (represented by *Monodelphis domestica* and *Sarcophilus harrisii*, orange arrow), Monotremata (represented by *Ornithorhynchus anatinus*, red arrow) and Placentalia (represented by the remaining mammals). Birds and reptiles are emerging from a common origin and are dividing into two branches with sub-branches/orders for Squamata (lizards and snakes) at the one hand and Crocodylia together with Psittaciformes, Falconifirmes, Cuculiformes and Galliformes on the other hand. Furthermore, fishes are organized in distinct classes: Sarcopterygii (*Latimeria chalumnae*, green arrow) and Actinopterygii (represented by *Lepisosteus oculatus* and remaining teleosts) as representatives of the Osteichthyes and Chondrichthyes (represented by *Chiloscyllium plagiosum* and *Callorhinchus milii*, blue arrow). The basic phylogenetic order derived from the sequence of the CLU full-length protein approximately remains after solely using RLC-I (minor changes) for analysis or after excluding the SSCR, RLC-I, RLC-II and the C-termini, respectively (App.2). Taken together, the phylogenetic analyses are indicating that the CLU protein even without the highly variable areas can be used for assessment of ancestry.

5.1.2.5 Comparison of the FC recognition site among various species

Nonetheless, even though the RLC-I shows a high variability across the species, the RxxR motif seems to be highly conserved as depicted in Fig.14. From 108 species tested only three species (all fishes!) do not display the putative FC recognition site motif RxxR [195] (Fig.17C). Two of them are belonging to the class of Chondrichthyes (*Chiloscyllium plagiosum* and *Callorhinchus milii*) and one to the class of Osteichthyes (*Ictalurus punctatus*). Nevertheless, *Ictalurus punctatus* shows a motif comparable to RxxR (PIYR|S) which also show the conserved serine residue downstream of the putative FC recognition site motif (see also App.1 and [195]). Intriguingly, fishes show the highest diversity of putative FC recognition sites with a ratio, of potential various FC recognition sites towards species tested, of 0.45 (15/33). In comparison reptiles and birds both display a ratio of approximately 0.275 (3/11 and 2/7, respectively). The ratio of amphibians is 1, whereas the extent of tested species was minor (only three species). Nevertheless, the lowest ratio can be found in mammals 0.15 (8/54). The most frequent FC recognition sites in all species is the motif RFAR (21%), RVVR (11%) and RIVR (10%). Interestingly, the RIVR motif occurs predominately in mammals with the exception of *Esox lucius* (fish). Moreover, all primates, except for *Pongo abelii* (RIIR), are carrying the RIVR

motif. Additionally, only two mammals tested show two putative FC recognition sites (*Castor fiber* and *Dipodomys ordii*). The ratio of double motifs to single motifs within the mammalian class is therefore lower than 0.04. In all other animal classes (except for amphibians) the ratio of double motifs to single motifs is 0.36 (fish), 0.83 (reptiles) and 1.33 (birds).

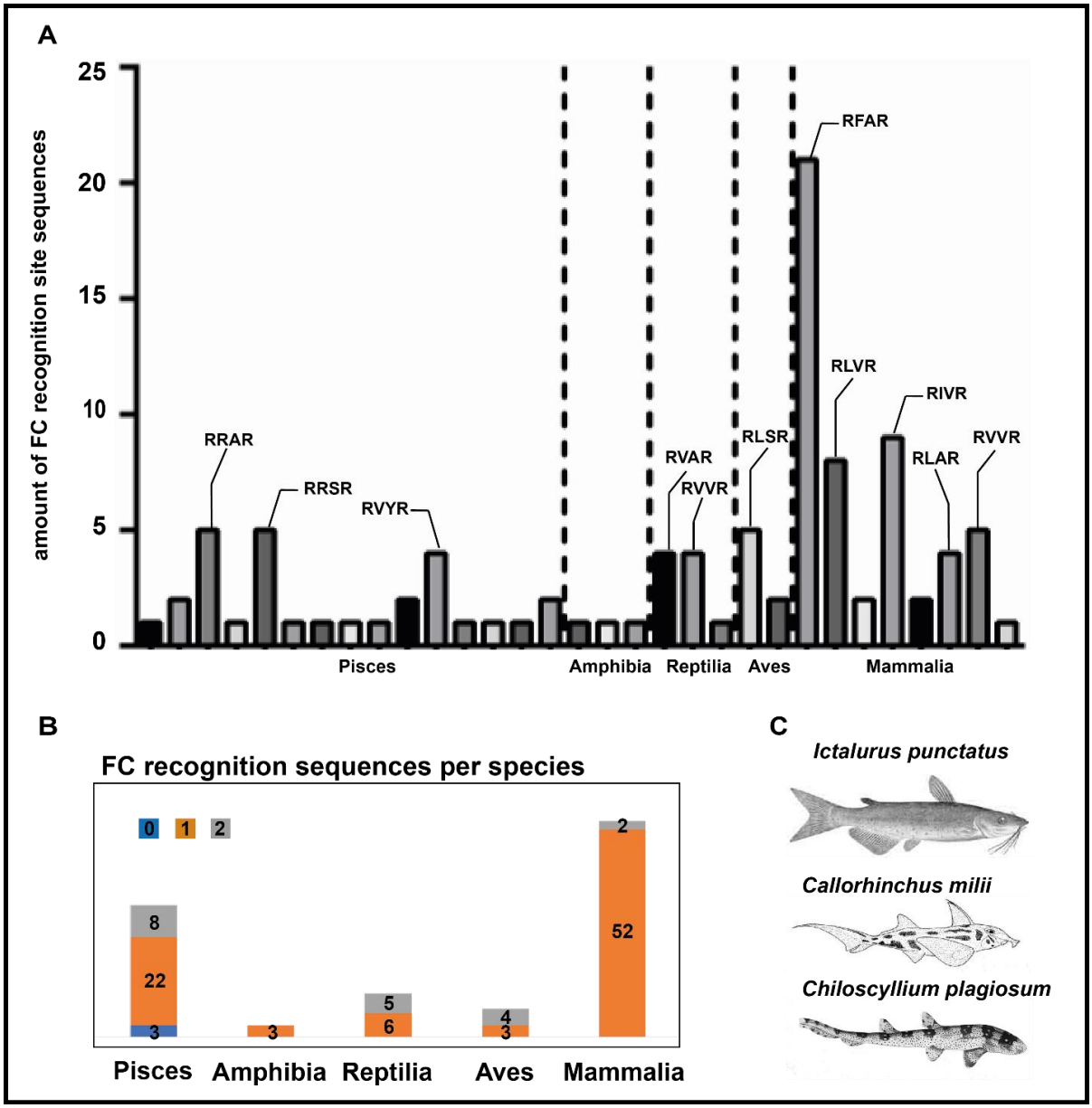

Fig.17 Comparison of FC recognition sites of 108 species of various animal classes. (A) Amount of various FC recognition sites within animal classes based on [195]. (B) FC recognition sequences within single species. (C) Three of 108 tested animals without RxxR consensus sequence. *Ictalurus punctatus* were taken from [215] under the terms and conditions of the Government of Canada. Illustrations of *C.milii* and *C.plagiosum* are copyright free and can be found here [216, 217].

In summary, more than 97% of all species tested bear at least one putative FC recognition motif. The motif is conserved within an area of low aa identity (RLC-I) but is not present in Chondrichthyes. Furthermore, a tendency to a single recognition site and a decreased variability of potential FC recognition sites can be observed in mammals. Fishes are the most heterogeneous animal class concerning FC recognition site motifs.

5.1.2.6 Comparison of the N-glycosylation among various species

After finding the CRR, the FC recognition site, structural elements such as α-helices, coiled-coil domains and an overall increased structural disorder, to be fundamental features of the CLU protein among various vertebrate classes, the glycosylation remains to be proved. Indeed, the glycosylation of sCLU is probably one of the most important structural components due to up to 30% of human sCLU variant being glycosylated [14, 16].
Fig.18 compares the amount of glycosylation sites between various vertebrate classes.

A

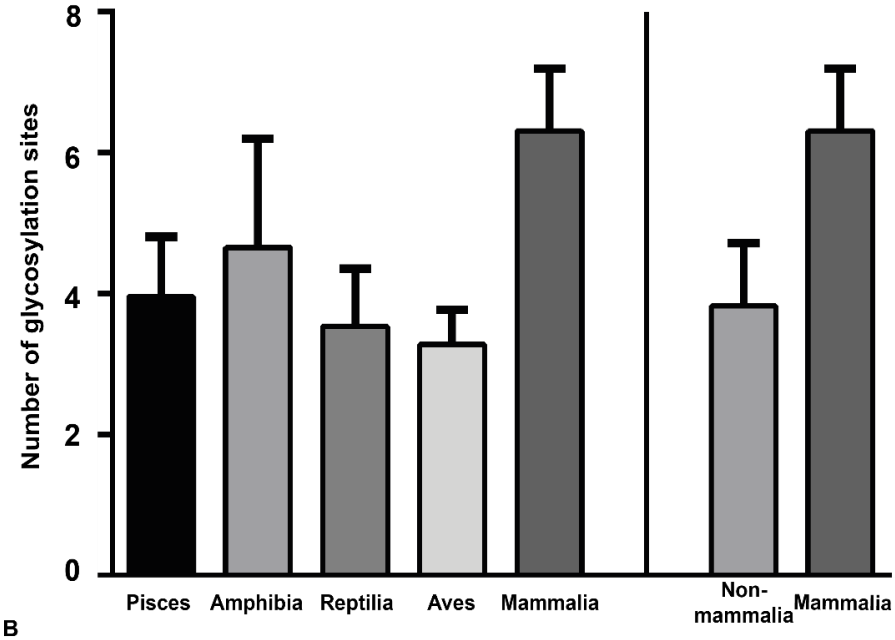

B

Classes tested	Amphibia vs. Pisces	Reptilia vs. Pisces	Aves vs. Pisces	Mammalia vs. Pisces	Reptilia vs. Amphibia	Aves vs. Amphibia	Mammalia vs. Amphibia	Aves vs. Reptilia	Mammalia vs. Reptilia	Mammalia vs. Aves	Non-mammalia vs. Mammalia
P-value	0.2204	0.1547	0.0472	< 0.0001	0.1027	0.0511	0.0037	0.4627	< 0.0001	< 0.0001	< 0.0001
P-value summary	ns	ns	*	****	ns	ns	**	ns	****	****	****

Fig.18 Comparison of glycosylation sites of 108 species of various animal classes. (A) Diagram of the amount of putative glycosylation sites calculated with NetNGlyc 1.0. (B) Statistical evaluation of differences. The error bars correspond to the mean±standard deviation. Data were analyzed by using an unpaired, two-tailed Student's t test (****P<0.0001; ***P<0.001; **P<0.01; *P<0.05).

Comparable to the above discussed FC recognition sites, an evolutionary tendency even in the case of the glycosylation sites is observable. The average number of glycosylation sites beside mammals is at highest in the case of amphibians (4.7), whereas this class also shows the lowest number of species tested (only three species tested). The average number of glycosylation sites is 4.0 (fish), 3.6 (reptiles) and 3.3 (birds). One exception once more are mammals with an average amount of 6.6 potential glycosylation sites. Only *Monodelphis domestica* (Marsupialia) has an expected number of glycosylation sites lower than 5. Other exceptions are *Alligator mississippiensis* and *Alligator sinensis* with 5, as well as *Xenopus laevis* with 5 and *Bufo gargarizans* with 6 glycosylation sites. *Scleropages formosus* displays the lowest amount of glycosylation sites with 2 potential N-glycosylation located on the α-chain. Taken together: Increased glycosylation of CLU is presumably a mammalian-specific feature.

5.1.2.7 Comparison of *Callorhinchus milli* and *Homo sapiens*

Finally, it was of interest whether a direct comparison of distantly related species confirms the concept of an evolutionary conservation of basic CLU features. For this purpose, the CLU aa sequence of *Callorhinchus milii* and *Homo sapiens* was compared (Fig.19). Both species displaying an identity in their aa sequence of about 35%. *Callorhinchus milii* belongs to the class of Chondrichthyes which is separated from the remaining vertebrates about 425 to 460 million years ago [214, 218]. *Callorhinchus milii* in particular, belongs to the order of Holocephali which have followed their own evolutionary route distinct from the remaining Chondrichthyes about 400 million years ago [214, 218]. Intriguingly, the first primates emerged in the history of life about 63 million years ago and the first man-like animals/monkeys are not older than 20 million years [214]. That means in turn that there are more than 425 million years of separate evolution between the CLU protein of *Callorhinchus milii* and *Homo sapiens*. Fig.19 shows the result of the comparison.

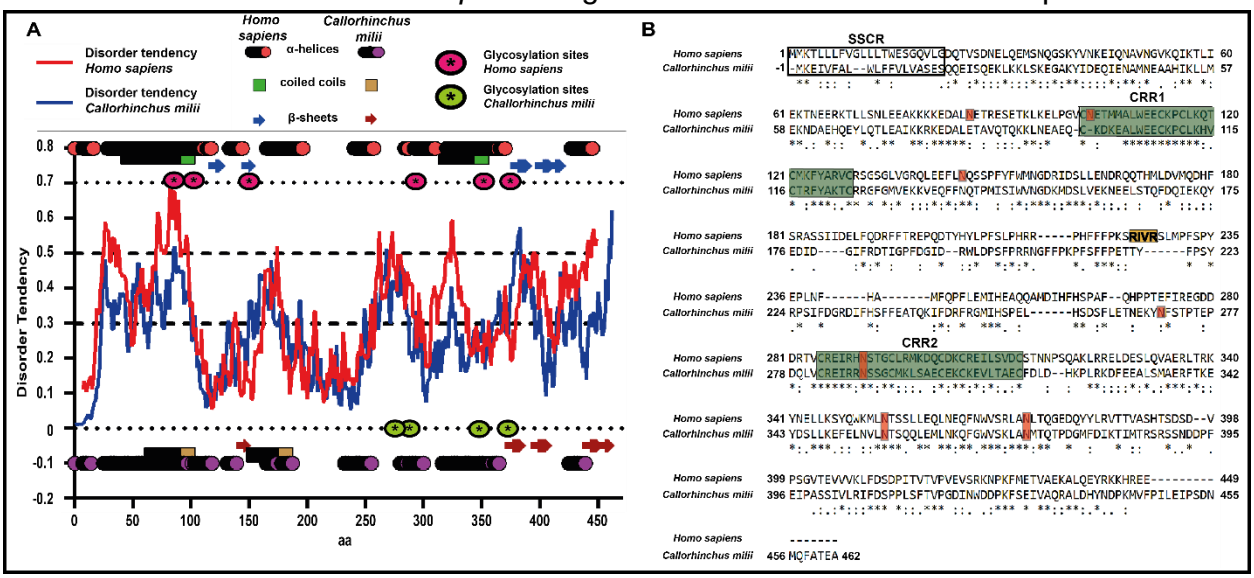

Fig.19 Prediction of disorder tendency and secondary structures. The full-length aa sequence of *Callorhinchus milii* and *Homo sapiens* was used for the analyses as described above. (A) Prediction of disorder tendency and secondary structures using UIPred and JPred. Glycosyaltion sites were predicted with NetNGlyc and are red highlighted. (B) Alignment of the aa sequence using Clustal Omega. Concerning prediction of SSCR (signal sequence coding region), CCR (cysteine-rich region) please see 4.4.

The comparison of disorder tendency between *Callorhinchus milii* revealed a similar tendency as described above. Nevertheless, the average disorder tendency of *Callorhinchus milii* CLU is about 0.27 vs. 0.32 in the case of *Homo sapiens*. It is important to note that *Callorhinchus milii* displays the lowest disorder tendency of 84 animals tested. The next relative to *Callorhinchus milii* used in the analysis is *Chiloscyllium plagiosum* which display an average disorder tendency of 0.35. The average disorder tendency among the animal classes are: 0.32 Mammalia, 0.36 Osteichthyes, 0.31 Chontrichthyes, 0.31 Amphibia, 0.34 Reptilia and 0.32 Aves. Therefore, *Callorhinchus milii* is an exception of all animals tested concerning its disorder tendency. Moreover, *Callorhinchus milii* and *Chiloscyllium plagiosum* do not show the putative coiled-coil domain at the C-terminus but a comparable distribution of the remaining secondary structures. Furthermore, as already mentioned above, both Chontrichthyes do not bear the putative FC recognition site and display glycosylation sites only in the section of the usual β-chain. Nonetheless, in both cases a SSCR and both CCRs are present. Taken together, even though CLU of *Homo sapiens* and *Callorhinchus milii* are separated by more than 425 million years, both are 1) potential secretory glycoproteins, 2) may form five disulfide bonds, 3) have extended α-helices/coiled-coil domains at the N-terminus and a stretch of β-sheets at the C-terminus, 4) show comparable peaks of higher disorder tendency at approximately the same position within the aa sequence and 5) share three equal N-glycosylation sites.

5.1.3 Role of FC cleavage & glycosylation for sCLU chaperone activity

The proteolytic maturation and the high glycosylation are apart from the disulfide bonds the most prominent structural elements of sCLU. Nevertheless, the role of these two features are poorly investigated. This section will therefore shed light on the dependence of sCLU chaperone activity from its glycosylation and proteolytic maturation.

5.1.3.1 FC cleavage is no prerequisite for secretion & chaperone activity of sCLU

Fig. 20 illustrates an approach for the creation of uncleaved sCLU and its behavior in chaperone activity assays. To find out whether the proteolytic maturation is a prerequisite for processing, secretion and chaperone activity of sCLU, mutant constructs in the putative recognition site for furin-like proprotein convertases (FC recognition site) were created and transiently transfected into HEK-293 cells (Fig. 20A-C). Subsequently,

overexpressing cells were selected, sufficient amounts were purified and chaperone activity assays were performed (Fig. 20D).

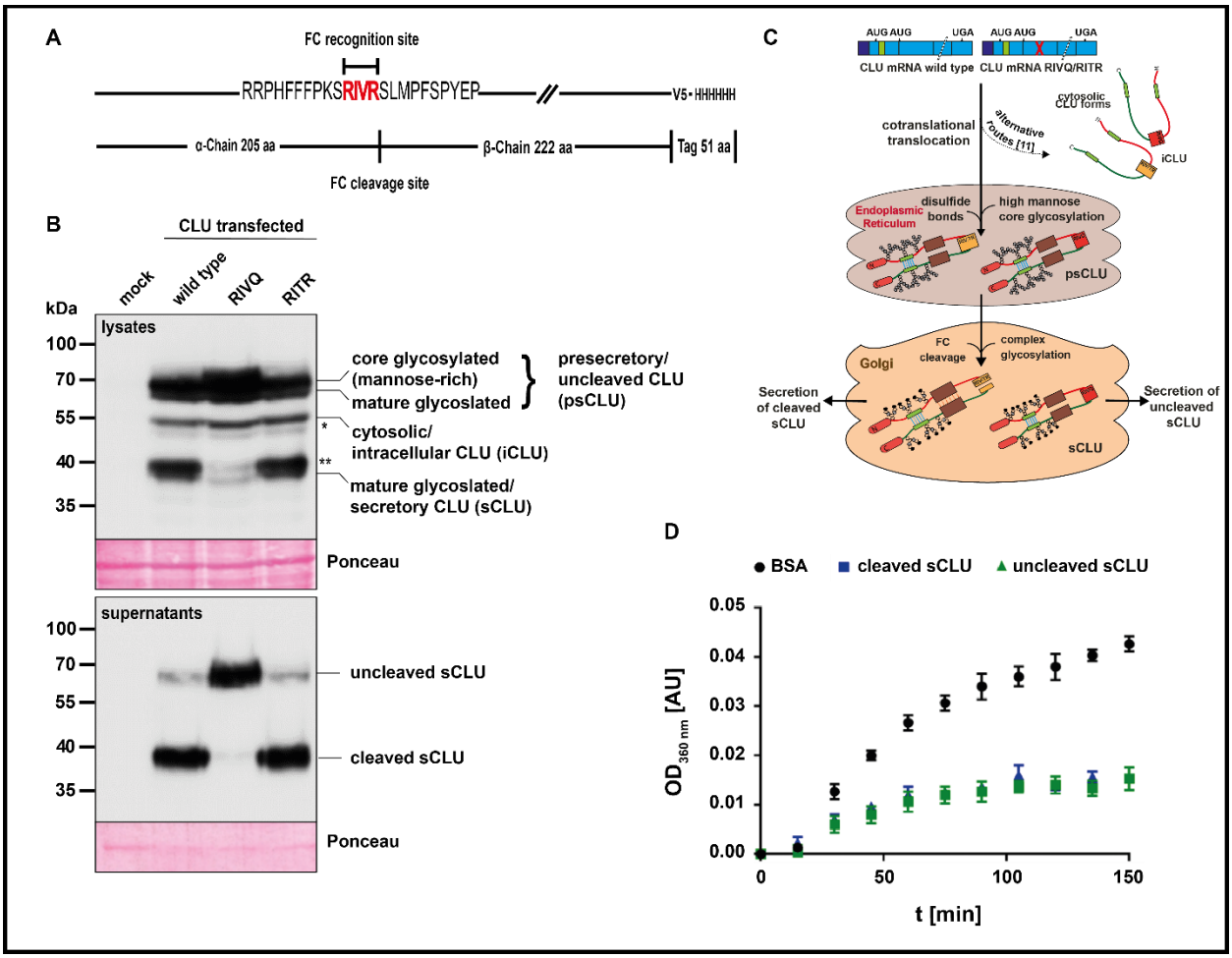

Fig.20 Generation of uncleaved sCLU and verification of its chaperone activity. (A) Schematic depiction of key features of recombinant CLU construct and indication of the furin-like proprotein convertase (FC) recognition and cleavage site. (B) Transient transfection of HEK-293 cells for 18 hours and subsequent serum-free cultivation for additional 24 hours. Finally, cell culture lysates and supernatants were collected and 10% reducing SDS-PAGEs and Western blots were performed using the anti-V5 antibody. As loading control Ponceau staining was carried out (* alternative iCLU form; ** cleaved high-mannose precursor). (C) Illustration of the cross-road of representative protein bands (D) HEK-293 cells were transfected as described above but were set on serum-rich medium afterwards. After reaching full confluency the cells were passaged to fresh 6-well plates and selected using 10 µg/mL Blastidicin. Eventually, mutant sCLU (RIVQ, uncleaved) and wild type sCLU (cleaved) were purified and chaperone activity assays were performed. Briefly, 75 µg/mL sCLU or 83 µg/mL BSA was incubated with 750 µg/mL necrotic cell lysates under non-reducing conditions. Data plotted in intervals of 15 min. The represented data were obtained from a single experiment using triplicates. Error bars correspond to standard deviation. The data shown are representative for at least three independent experiments.

Importantly, the proteolytic maturation is neither required for sCLU protein maturation nor for secretion. Furthermore, the lack of proteolytic maturation is no prerequisite for sCLU chaperone activity. As expected, the C-terminal arginine residue of the RIVR motif is the key aa for FC recognition [195] as the RITR mutation does not affect the proteolytic

maturation. Apart from the notions to be evolutionary conserved (5.1.2) no necessity of the proteolytic cleavage was detectable.

5.1.3.2 Terminal carbohydrates are no prerequisite for chaperone activity of sCLU

To further assess whether the glycosylation is involved in sCLU chaperone activity, in a first approach the distal carbohydrates were trimmed (Fig. 21).

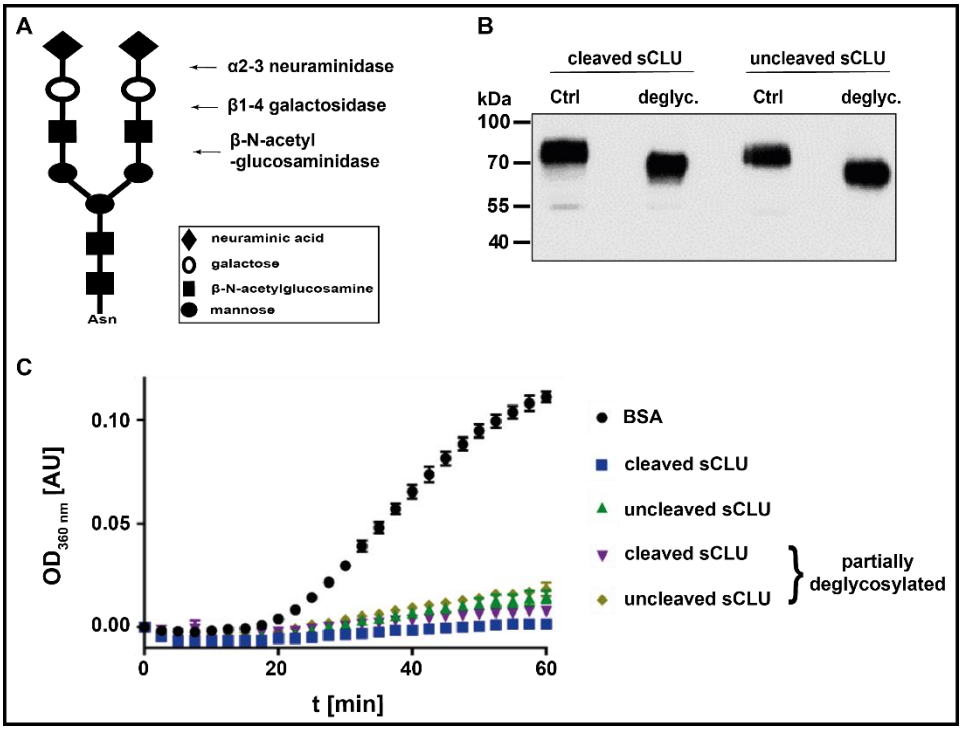

Fig.21 Partial deglycosylation of the distal carbohydrates and determination of remaining chaperone activity. (A) Schematic depiction of sCLU glycosylation and indication of the cleavage site of glycosidases used. (B) Western blot analyses of partially deglycosylated cleaved and uncleaved sCLU on 9% SDS-PAGEs with 200 ng protein per lane under non-reducing conditions using the anti-V5 antibody. (C) Chaperone activity assay with 1 mg/mL Catalase as client protein, 75 µg/mL sCLU and 83 µg/mL BSA as control under non-reducing conditions. Data plotted in intervals of 5 min. The represented data were obtained from a single experiment using duplicates to triplicates. Error bars correspond to standard deviation. The data shown are representative for two to three independent experiments.

As shown in Fig. 21 cleaved and uncleaved sCLU retains its chaperone activity after removal of the distal carbohydrates. Even though a slight increase in chaperone activity of cleaved and uncleaved as well as of full and only partially deglycosylated sCLU is visible, distal glycosylation is no prerequisite for sCLU to act as a molecular chaperone.

5.1.3.3 PNGase F treatment diminishes sCLU chaperone activity

For complete deglycosylation the endoglycosidase PNGase F was used and the success concerning residual glycosylation, chaperone activity and folding were assessed (Fig.22).

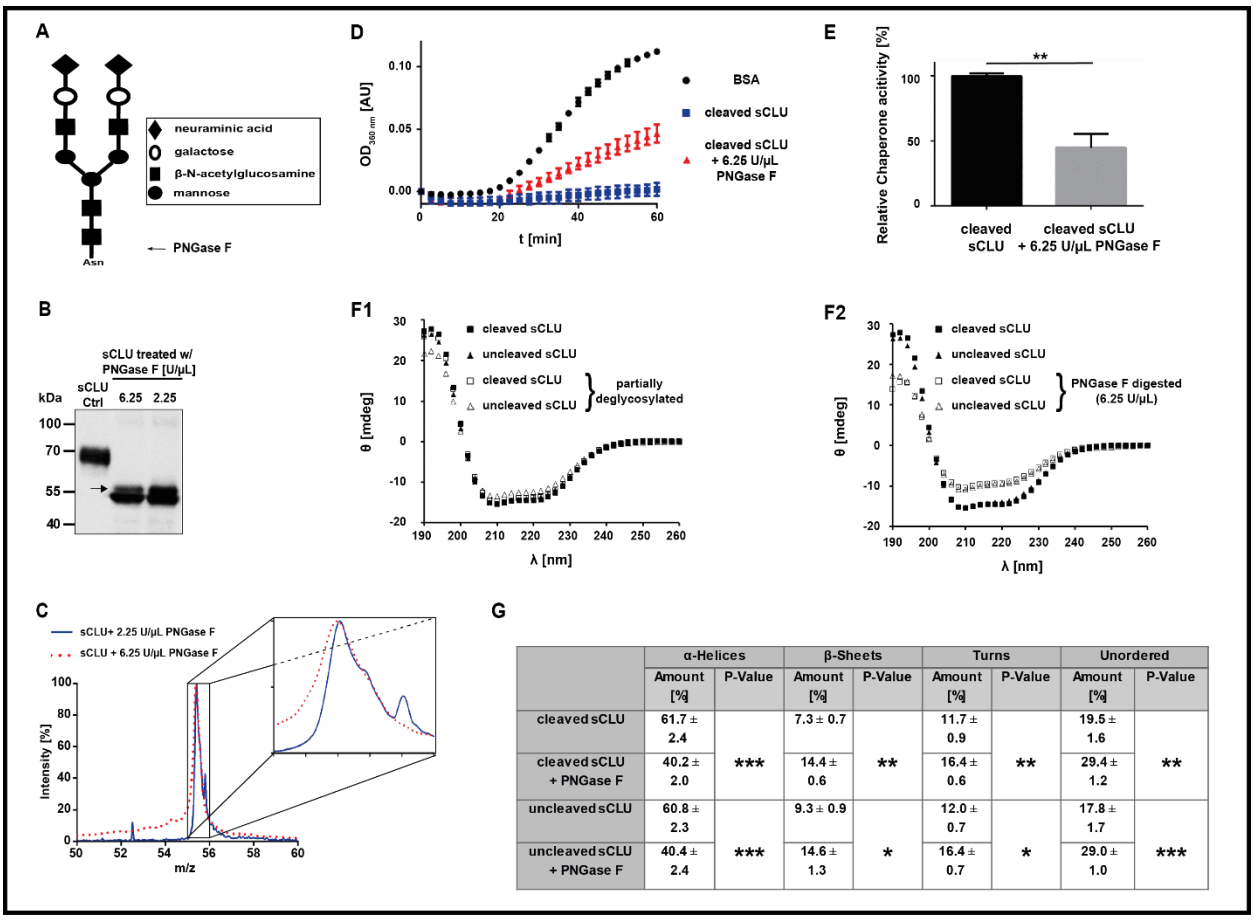

	α-Helices		β-Sheets		Turns		Unordered	
	Amount [%]	P-Value	Amount [%]	P-Value	Amount [%]	P-Value	Amount [%]	P-Value
cleaved sCLU	61.7 ± 2.4		7.3 ± 0.7		11.7 ± 0.9		19.5 ± 1.6	
cleaved sCLU + PNGase F	40.2 ± 2.0	***	14.4 ± 0.6	**	16.4 ± 0.6	**	29.4 ± 1.2	**
uncleaved sCLU	60.8 ± 2.3		9.3 ± 0.9		12.0 ± 0.7		17.8 ± 1.7	
uncleaved sCLU + PNGase F	40.4 ± 2.4	***	14.6 ± 1.3	*	16.4 ± 0.7	*	29.0 ± 1.0	***

Fig. 22 Approach for complete deglycosylation of sCLU using PNGase F (A) Schematic depiction of the PNGase F cleavage site. (B) Western blot analyses of cleaved sCLU deglycosidation using PNGase F at various concentrations after 12 hours of digestion. 200 ng protein was applied to a 9% SDS-PAGE under non-reducing conditions and detection of sCLU was carried out using the anti-V5 antibody. The arrow indicates remaing glycosylation. (C) MALDI-TOF MS analyses of cleaved sCLU digested with various concentrations of PNGase F. (D) Chaperone activity assay using 75 µg/mL sCLU untreated or digested with 6.25 U/µL PNGase F or 83 µg/mL BSA with 1 mg/mL catalase as client protein under non-reducing conditions. Data plotted in intervals of 5 min. The represented data were obtained from a single experiment using triplicates. Error bars correspond to the standard deviation. The data shown are representative of three independent experiments. (E) The absorbance data obtained between 90 and 150 min (plateau phase) in chaperone activity assays (see above) was taken as a measure for the relative chaperone activity. The BSA control is regarded as not being active as a molecular chaperone. Relative chaperone activity is expressed in relation to data obtained concerning untreated cleaved sCLU which is assumed to have a chaperone activity of 100%. For the evaluation, the data of three independent experiments, each with the mean of three measurements were used. The error bars correspond to the mean±standard errors. Data were analyzed by using an unpaired, two-tailed Student's t test (***P<0.001; **P<0.01; *P<0.05). (F) CD spectra of cleaved and uncleaved sCLU treated with or without glycosidases. Purified cleaved or uncleaved sCLU was either treated with or without α2,3-neuraminidase, β1,4-galactosidase and β-N-acetylglucosaminidase (F1) or 6.25 U/µL PNGase F (F2). All CD spectra were obtained at wavelengths ranging from 190 to 260 nm in 1 nm intervals. The spectra shown illustrate the means of three consecutive

scans and are representative of several individual experiments. Plotted is the ellipticity θ (mdeg) against the wavelength λ (nm), whereas intervals of 2 nm were chosen for a better illustration. (G) Calculated percentage of secondary structure elements of cleaved and uncleaved sCLU in accordance with CD spectra measurements (±standard errors). The results were obtained from measurements carried out five to six times. Data were analyzed by using one-way ANOVA, followed by Bonferroni multiple comparison test (***P<0.001; **P<0.01; *P<0.05).

Stewart *et al.* 2007 [31] reported that 0.1 U/µL PNGase F is sufficient for sCLU deglycosylation with no adverse impact on folding and activity of sCLU. Due to residual glycosylation in [31], an increase in PNGase F concentration was used as shown in Fig. 22. As demonstrated (Fig. 22B & C) an increase of PNGase F concentration in comparison to [31] up to 2.25 U/µL and 6.25 U/µL still leaves sCLU partially glycosylated. The chaperone activity, however, is impaired by about 50% (Fig. 22D & E). Moreover, tremendous changes in the amounts of α-helices of about 60% to 40% occurs in both, uncleaved and cleaved sCLU, after PNGase F digestion. In contrast, the amounts of β-sheets (about 7% to 14%), turns (about 12% to 16%) and unordered regions (about 19% to 29%) increases (Fig. 22F2 & G). Intriguingly, partially deglycosylation does not promote a significant change in the measured CD spectra (Fig. 22F1). These data indicate a dependence of the chaperone activity and folding of sCLU towards its core-glycosylation.

5.1.3.4 sCLU chaperone activity depends on glycosylation and FC cleavage

Due to remaining residual glycosylation even after digestion with high concentrations of PNGase F (Fig.22), deglycosylation was carried out under reducing conditions to render sCLU glycosylation sites more accessible for deglycosylation. Intriguingly, after use of DTT for 12 hours the β-chain was fully deglycosylated but now the α-chain showed residual glycosylation (Fig.23A). Finally, an incubation for 6 hours in the absence and subsequent incubation in the presence of 40 mM DTT successfully removed all glycosylation on both chains and even on uncleaved sCLU (Fig.23A & B). It is important to note that the deglycosylated uncleaved sCLU has a slightly lower molecular weight than the corresponding 55 kDa band in the lysates of transfected HEK-293 cells (Fig.23B). The CLU band at 55 kDa therefore corresponds to the mistranslocated CLU form 1-449 still bearing the ER leader peptide (see also Fig.20 & [11]). As expected after generating fully deglycosylated sCLU an impairment in chaperone activity by 90% (uncleaved sCU) and 80% (cleaved sCLU) was observable (Fig.23D & F). Most importantly, however, is the finding that uncleaved sCLU shows a tremendous sensitivity towards reducing conditions (Fig.23C & E). Depending on the used quantity of sCLU, the decline in chaperone activity of uncleaved sCLU was between 65% (using 100 µg/mL, Fig.23E) and 85% (using 75 µg/mL, Fig.23F). Intriguingly, even by using 40 mM DTT in case of cleaved sCLU, in comparison the 5 mM DTT in the case of uncleave sCLU, the

sCLU chaperone activity of uncleaved sCLU was abolished more severe (15% vs. 20%) (Fig.23E).

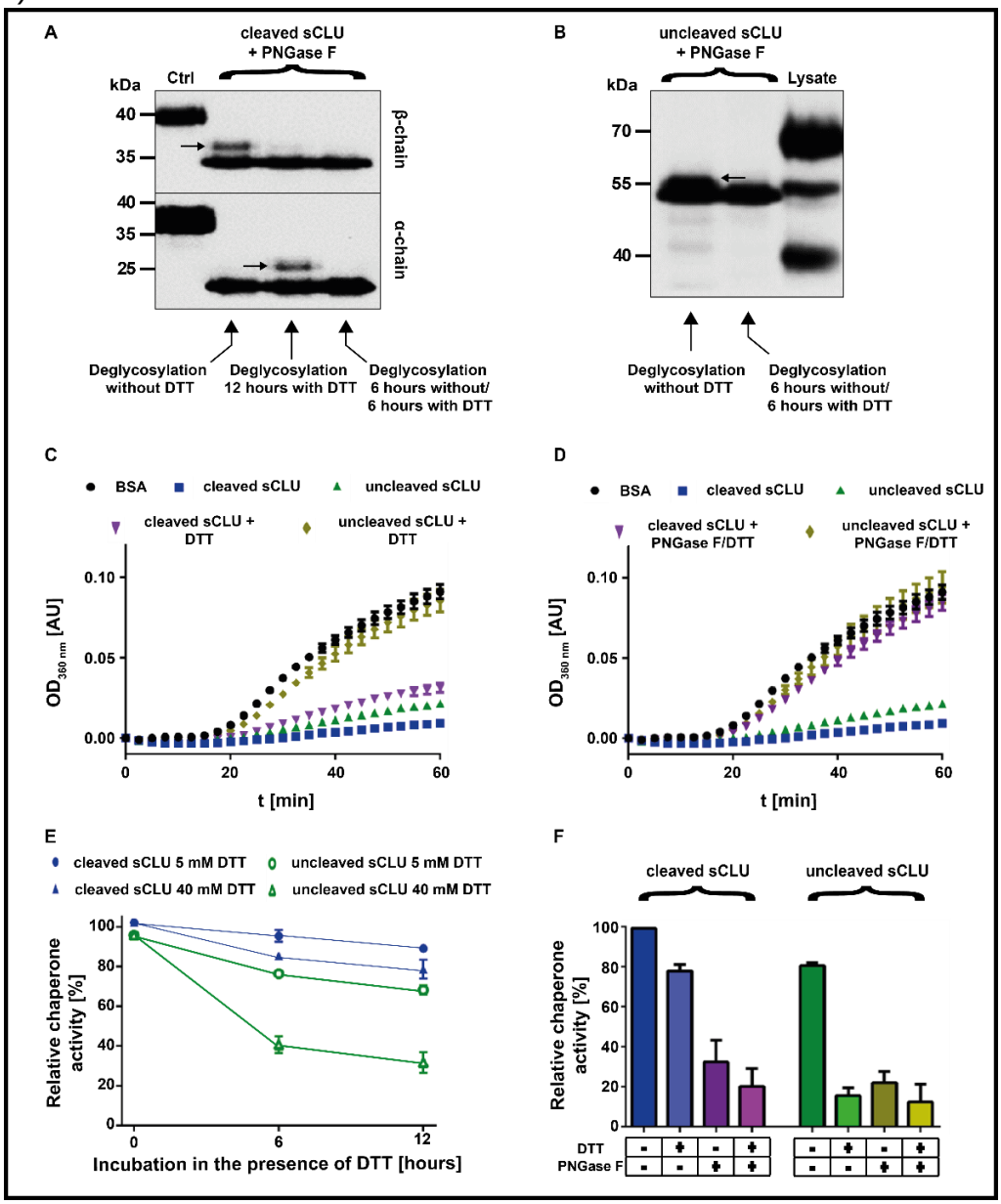

Fig.23 Approach for complete deglycosylation using PNGase F in combination with DTT. For successful full deglycosylation of sCLU, the following approaches were tested: 1) PNGase F treatment in the absence of DTT for 12 hours, 2) with 40 mM DTT for 12 hours, 3) without DTT for 6 hours and subsequent addition of 40 mM DTT for another 6 hours. Remaining glycosylation in Western blot analyses is indicated by black arrows. (A) Full deglycosylation of cleaved sCLU on 12.5% SDS-PAGEs under reducing conditions. To detect the sCLU β-chain, the anti-V5 antibody and for the α-chain the 41D antibody was used. (B) Full deglycosylation of uncleaved sCLU was verified on a 9% SDS-PAGE under reducing conditions. To compare fully deglycosylated uncleaved sCLU with stress-induced unglycosylated non-secreted CLU forms, as described previously [11], 50 µg of whole cell lysates from HEK-293 cells transiently transfected with recombinant wild type CLU constructs, were analyzed (see also Fig.20). The detection of CLU was realized by using the anti-V5 antibody. (C, D) As deglycosylation using PNGase F without DTT for 6 hours and subsequent for another 6 hours in the presence of 40 mM DTT was successful, chaperone activity assays were performed as described (Fig.20 & 21) but under reducing conditions (addition of 5 mM DTT). The represented data

were obtained from a single experiment using triplicates. Error bars correspond to standard deviation. The data shown are representative of three independent experiments. (E) Chaperone activity assays of cleaved and uncleaved sCLU incubated in the presence of 5 or 40 mM DTT for 0, 6 or 12 hours at 37°C. The assays and the analyses were carried out as described above but with 100 µg/mL sCLU (C & D). Data points are means of three measurements, error bars correspond to the standard deviation. The data shown are results of at least three independent experiments. (F) Cleaved and uncleaved sCLU were incubated as described above (A & B). Subsequently, chaperone activity assays were performed (see C & D) and data were analyzed as described in Fig. 22E. For the evaluation, the data of three independent experiments, each with the mean of three measurements were used. The error bars correspond to the mean±standard errors.

Taken together, these data suggest that the chaperone activity of sCLU is dependent on glycosylation and on the proteolytic cleavage after exposure to reducing conditions.

5.1.3.5 Impaired sCLU chaperone activity upon reduction can be restored

The finding that uncleaved sCLU is sensitive to reducing conditions raises the question whether this inhibition is irreversible and whether the decline is associated with severe structural changes in comparison to cleaved sCLU (Fig.24).

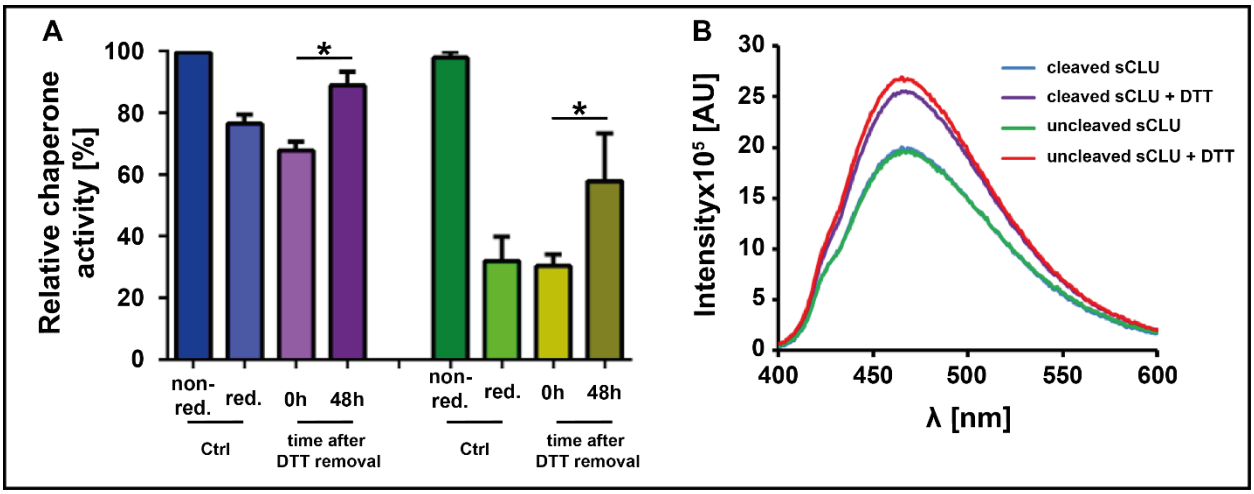

Fig.24 Rescue of the DTT-induced impairment in sCLU chaperone activity. (A) The procedure is in accordance with the approach described in Fig.23E & [19]. After 12 hours of incubation with or without 40 mM DTT at 37°C, sCLU was either subsequently used for chaperone activity assays (Ctrl reducing and non-reducing) or DTT was substituted by PBS using a 5 kDa cut-off filter unit at 4°C and used for chaperone activity assays immediately after buffer exchange or after 48 hours on 4°C. For the evaluation, the data of three independent experiments, each with the mean of three measurements were used. The error bars correspond to the mean±standard errors. Data were analyzed by using an unpaired, two-tailed Student's t test (***P<0.001; **P<0.01; *P<0.05). (B) To figure out whether uncleaved sCLU tends to unfold more severe than cleaved sCLU both sCLU proteins were incubated with 40 mM DTT for 12 hours. Subsequently, the samples were incubated with ANS and measured using a fluorescence spectrometer.

To determine whether DTT-induced inhibition of uncleaved sCLU chaperone activity is irreversible, DTT was removed after 12 hours of incubation and sCLU was further processed/assayed as described in Fig.24. Intriguingly, the chaperone activity of cleaved sCLU can be restored by 20% to about 90% and the activity of uncleaved sCLU by 30%

to about 60% (Fig.24A). However, it was still questionable how the tremendous impairment in chaperone activity of uncleaved sCLU upon DTT treatment was caused. One possibility is a serious unfolding. To test this, fluorescence spectroscopic measurements were carried out (Fig.24B). The fluorescence spectroscopic measurement using ANS indicating that upon DTT treatment cleaved and uncleaved sCLU unfold in a comparable manner. These data suggest that the decline of chaperone activity of uncleaved sCLU has another reason.

5.2 The role of CLU in the face of necrosis

As already mentioned in the Introduction (section 1.7 & 1.8), the occurrence of the CLU protein is often related to situations of “uncontrolled” cell-death, necrosis. The putative role is primarily to act as a molecular chaperone and thus to support the removal of cell debris, misfolded protein and dying cells. Moreover, it has been suggested that CLU promotes cell survival and even proliferation, presumably acting in an oncogenic fashion. Additionally, other reports came across indicating adverse effects, such as promoting cell death. Nevertheless, the process of necrosis, especially the impact on surrounding neighboring cells is currently poorly understood. Furthermore, the mechanism(s) of how CLU is upregulated in vital neighboring cells close to necrosis is barely explored. This section will address effects of necrotic cell lysates on vital cells, if CLU upregulation as a response to necrotic lysates takes place and how CLU potentially affects vital cells. Fig.25 will give a brief overview concerning the basic approach of a necrotic cell death assay.

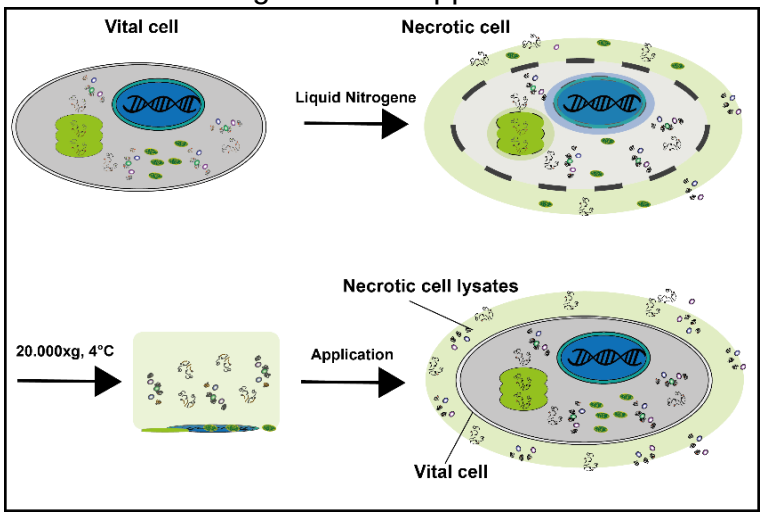

Fig. 25 Preparation of necrotic cell lysates. Further details please see the Methods Section (4.1.1.4).

Please note that the following section contains excerpts of the article: Rohne *et al.* 2017 *“Exposure of Vital Cells to Necrotic Cell Lysates Induce the IRE1α Branch of the Unfolded Protein Response and Cell Proliferation”*.

5.2.1 Necrotic cell lysates induce JNK signaling and CLU upregulation

As described in the Introduction (section 1.5) the CLU promoter bears at least two stress-related elements that might be responsible for CLU upregulation upon cellular stress, which is presumably present in necrotic tissue. At one hand the AP-1 binding site (recognized by AP-1 activated by the JNK signaling pathway) and on the other hand the so-called CLE element (a binding sequence for HSFs). Therefore, it was tested whether the JNK signaling pathway and/or a heat shock response is activated in vital neighboring cells upon treatment with necrotic cell lysates (Fig.26).

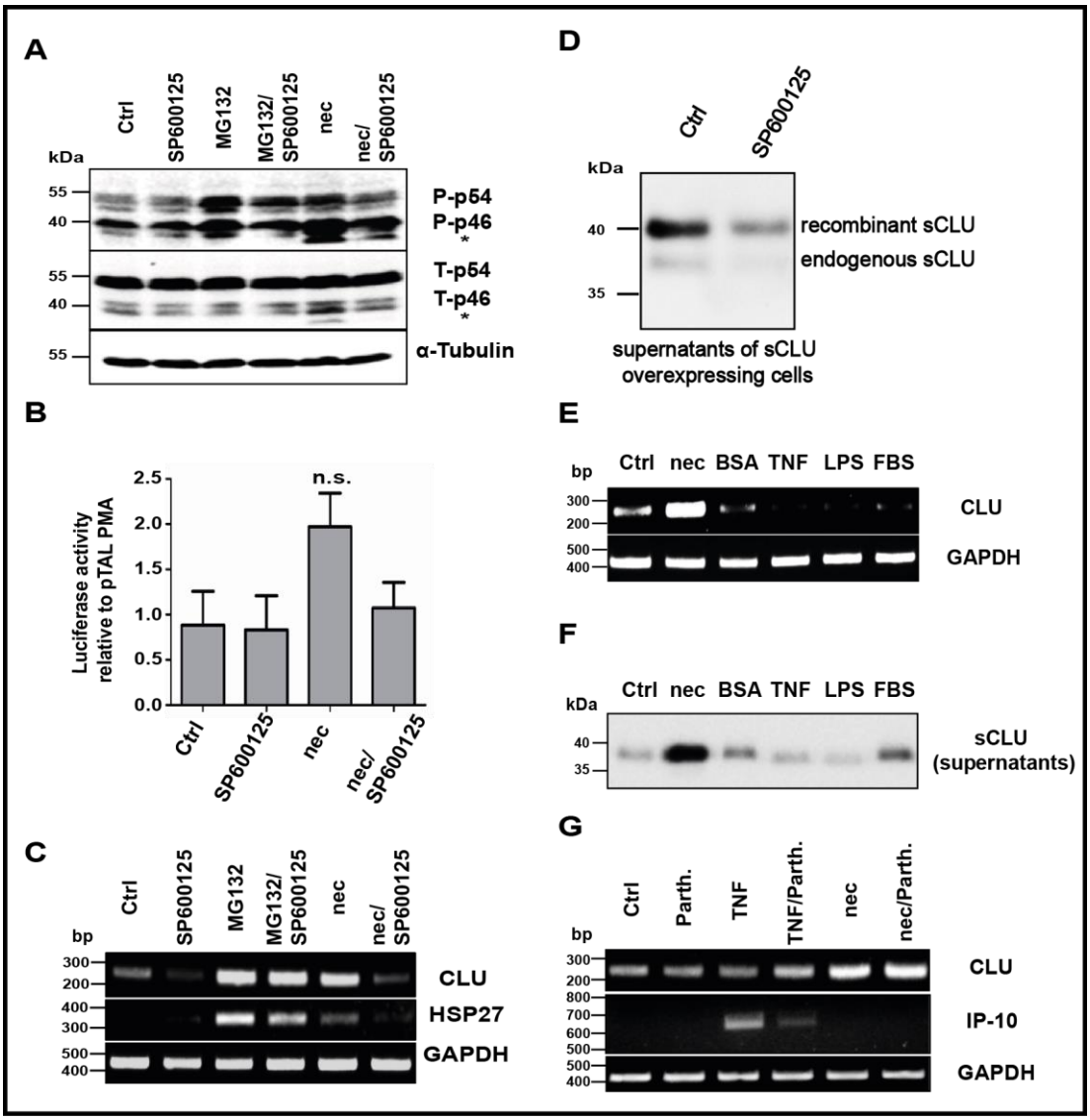

Fig.26 Necrotic cell lysates induce the JNK/SAPK signaling pathway. HEK-293 cells were preincubated with or without 10 µM JNK inhibitor SP600125 for 9 hours. (A-C) After preincubation, cells were stimulated with either 10 µM MG-132 or 1 mg/mL necrotic cell lysates (nec) in the presence or absence of SP600125 for 2 hours (Western blot), 5 hours (reporter assays) or 6 hours (sqRT-PCR). (A) JNK (p46/p54) phosphorylation analyses were carried out by Western blot (n=3). (B) AP-1 luciferase reporter assays: Chemiluminescence was measured and is shown relative to blank vector stimulated with 1 µM PMA. As transfection control pTER-EGFP was co-transfected. Data shown are the

mean±standard errors of three independent experiments. Data were analyzed by using one-way ANOVA, followed by Tukey's multiple comparison test. (D) To test whether SP600125 affects the secretion, sCLU overexpressing HEK-293 cells were incubated initially with 10 µM SP600125 for 4 hours (serum-free) followed by 6 hours of incubation with fresh 10 µM SP600125 containing serum-free medium. Western blot analyses were carried out with 30 µL medium per lane on a reducing SDS-PAGE using the sc-6419 antibody. As control DMSO in equal amounts was applied (n=2-3). (E,F) HEK-293 cells were stimulated with 1 mg/mL necrotic cell lysates (nec), BSA, FBS, 5 ng/mL TNF or 1 µg/mL LPS (under serum-free conditions) for 6 hours after 4 hours serum-free preincubation. (E) sqRT-PCR analyses for CLU transcription with GAPDH as control (n=3) (F) Western blot analyses for secreted sCLU with 30 µL medium per lane (n=3) (G) sqRT-PCR analyses for the transcription of CLU, IP-10 (NF-κB positive control) with GAPDH as loading control were performed in HEK-293 cells preincubated with or without 25 µM NF-κB inhibitor Parthenolide (Parth.) for 4 hours. After preincubation, cells were stimulated with either 5 ng/mL TNF or 1 mg/mL necrotic cell lysates (nec) in the presence or absence of 25 µM Parthenolide for 6 hours (n=2).

After application of necrotic cell lysates to vital HEK-293 cells, elevated JNK phosphorylation (p54/p46), AP-1 reporter activity, CLU transcription upregulation and secretion was found (Fig.26A-C & E-G). In contrast, the increase in transcriptional upregulation and secretion was absent in cells treated with BSA, TNF, LPS or FBS pointing to the specificity of the cellular response (Fig.26E&F). Moreover, the transcriptional upregulation of CLU, JNK (p46/p54) phosphorylation and AP-1 reporter activity was abolished in the presence of the JNK inhibitor SP600125 (Fig.26A-C). Comparable results were obtained after treatment with the proteasome inhibitor MG-132, a potent JNK inducer (Fig.26A&C). Nevertheless, the transcriptional upregulation of CLU after stimulation with MG-132 was not reversed by SP600125 indicating an alternative route (Fig.26C). Indeed, a transcriptional upregulation of HSP27, serving as a marker gene for the heat shock response, was detectable in both MG-132 and necrotic cell lysate stimulated cells (Fig.26C). Nevertheless, the inhibition of the heat shock response by SP600125 in the case of necrotic cell lysates was less robust in the case of MG-132. Additionally, it must be mentioned that SP600125 inhibits the constitutive secretion of sCLU (sCLU overexpressing cells under the control of a CMV promoter) as demonstrated in Fig.26D. It is therefore not possible to connect CLU transcriptional upregulation with its secretion in the presence of SP600125. Taken together, necrotic cell lysates induce the JNK/SAPK-AP-1 signaling pathway and the heat shock response but not the NF-κB signaling pathway, as shown by usage of the NF-κB inhibitor Pathenolide [120] (Fig.26G).

5.2.2 Necrotic cell lysates induce the IRE1α branch of the UPR

To determine which pathway(s) triggers the JNK phosphorylation and thus CLU upregulation, multiple possibilities, such as UV light, growth factors, Src kinases (App.7A) or TNF (Fig.26E-G), were excluded. Nonetheless, the IRE1α branch of the UPR (Section 1.9.2) is also prone to induce the JNK signaling pathway. Even though it has been considered that the activation of an UPR suppresses CLU upregulation and secretion [158], it was tested whether a UPR is activated after application of necrotic cell lysates (Fig.27).

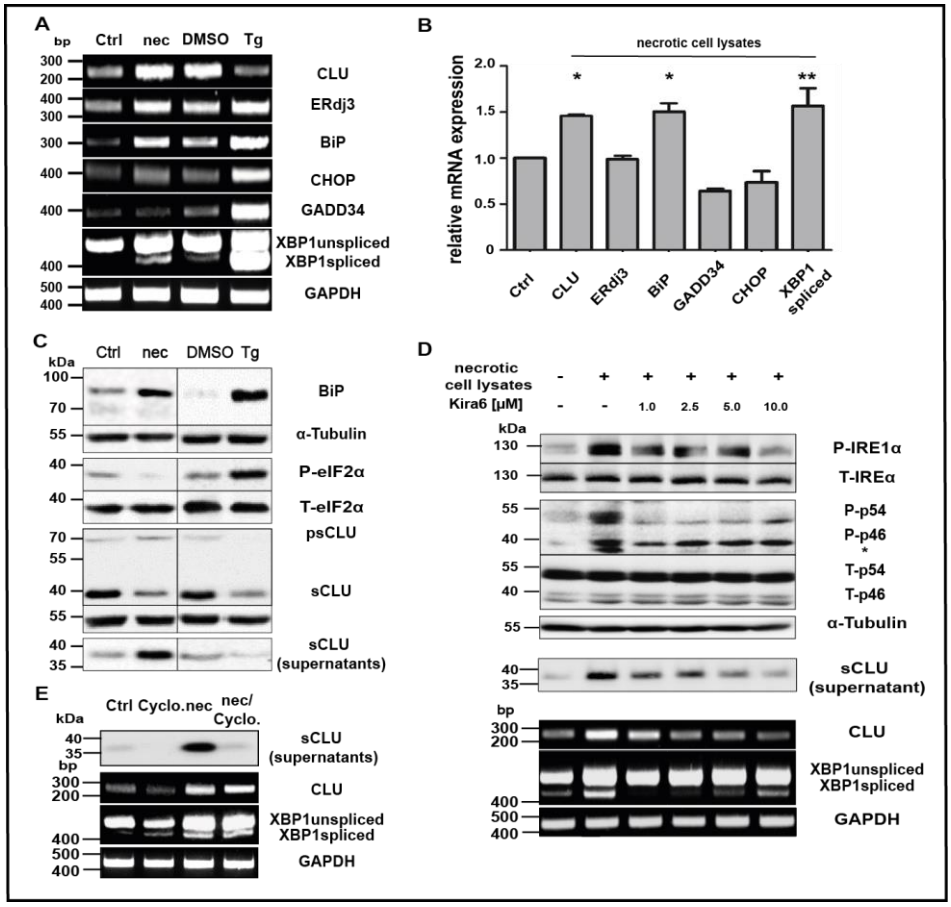

Fig.27 Necrotic cell lysates induce the IRE1α branch of the unfolded protein response (UPR). (A) sqRT-PCR analyses for the transcription of CLU, ERdj3, BiP, CHOP, GADD34 and XBP1 with GAPDH as loading control were performed in HEK-293 cells stimulated with 1 mg/mL necrotic cell lysates (nec) or 1 μM Thapsigargin (Tg) for 6 hours (n=3). (B) qRT-PCR analyses of HEK-293 cells stimulated with 1 mg/mL necrotic cell lysates were carried out. Values are represented as mean±standard errors from three independent experiments. Data were analyzed by one-way ANOVA, followed by Dunnett's test for multiple comparison (***P<0.001; **P<0.01; *P<0.05). (C) Western blot analyses of HEK-293 cells stimulated with 1 mg/mL necrotic cell lysates (nec) or 1 μM Thapsigargin (Tg) for 6 hours (BiP and CLU) or 2 hours (eIF2α) (n=3). (D) HEK 293 cells were preincubated in the presence of various concentrations of the IRE1α kinase inhibitor Kira6 and subsequently stimulated with 1 mg/mL necrotic cell lysates in the presence of Kira6 for 2 hours (Western blot) or 6 hours (sqRT-PCR and cell culture supernatants) (n=3). (E) sqRT-PCRs and Western blot analyses of HEK-293 cells stimulated with 1 mg/mL necrotic cell lysates for 6 hours in presence of 5 μg/mL of the translation inhibitor Cycloheximide (n=3).

To determine whether an UPR is active upon stimulation with necrotic cell lysates, sqRT- and qRT-PCR analyses were conducted encompassing all three branches of the UPR (see section 1.9.2). Intriguingly, after 6 hours of stimulation with necrotic cell lysates, significant XBP1 splicing and transcriptional upregulation of CLU and BiP was observable (see section 1.9.2). In contrast, elevated transcription of ERdj3 (ATF6 branch), GADD34 or CHOP (PERK branch) was not induced (Fig.27A & B). Furthermore, a translational upregulation of BiP (Fig.27C), in accordance with increased sCLU secretion, but no eIF2α phosphorylation (PERK branch) (Fig.27C) was detectable strengthening the notion that

necrotic cell lysates specifically activate the IRE1α branch of the UPR. Nevertheless, the ER stress inducer Thapsigargin (in contrast to necrotic cell lysates) induces the IRE1α and the PERK branch of the UPR as demonstrated by enhanced XBP1 splicing and elevated transcript levels of CHOP and GADD34 (Fig.27A). Further, an increased BiP expression (Fig.27A & C) and eIF2α phosphorylation (Fig.27C), but no CLU transcriptional upregulation and sCLU secretion was observable (Fig.27A & C). Interestingly, after using the validated IRE1α kinase inhibitor Kira6, the transcriptional upregulation and secretion of CLU was impaired in a dose-dependent manner (Fig.27D). In correlation, JNK (p54/p46) and IRE1α phosphorylation was also decreased pointing to a link of the UPR and CLU expression. Intriguingly, at high concentrations of Kira6, XBP1 splicing emerged despite of decreased IRE1α phosphorylation which is possibly a result of increased IRE1α oligomerization [141, 142, 219]. To test whether the XBP1 splicing is driven by a protein overload within the ER the translation inhibitor Cycloheximide was utilized (Fig.27E). Surprisingly, no difference in XBP1 splicing, but impaired sCLU secretion was observed demonstrating no correlation of increased protein load in the ER but rather a direct effect of necrotic cell lysate on the activation of UPR.

5.2.3 The UPR-CLU axis remains elusive

Encouraged by findings that the IRE1α kinase inhibitor Kira6 impairs CLU upregulation, it was of interest to confirm an UPR-CLU axis in other approaches. Fig.28 shows the results of usage of another IRE1α kinase inhibitor (APY29), IRE1α overexpression and IRE1α knockdown. As illustrated in Fig.28 none of the approaches was successful to prove the IRE1α-CLU link. The IRE1α kinase inhibitor APY29 promotes IRE1α and JNK phosphorylation (Fig.28A), as well as XBP1 splicing (Fig.28B) after stimulation with necrotic cell lysates. The later notion has already been reported elsewhere [141, 219], describing APY29 as a drug which promotes IRE1α oligomerization. Nonetheless, APY29 has never been tested in cell culture or animals, there are solely *ex vivo* studies available yet. Intriguingly, at high APY29 concentrations (>0.5 µM), XBP1 is no longer detectable but remains unspliced after application of necrotic cell lysates (Fig.28B). Once more, sCLU is still secreted from the cell up to a concentration of <1.5 µM APY29. The second approach with overexpressed IRE1α recombinant constructs leaves sCLU secretion unaltered but also does not elevates the CLU protein or mRNA level (Fig.28C). Note that the blank transfection of IRE1α does not activate JNK (p46/p54) phosphorylation or CLU upregulation (data not shown). Finally, IRE1α knockdown also not changes CLU upregulation, but prevents BiP upregulation and XBP1 splicing (Fig.28E).

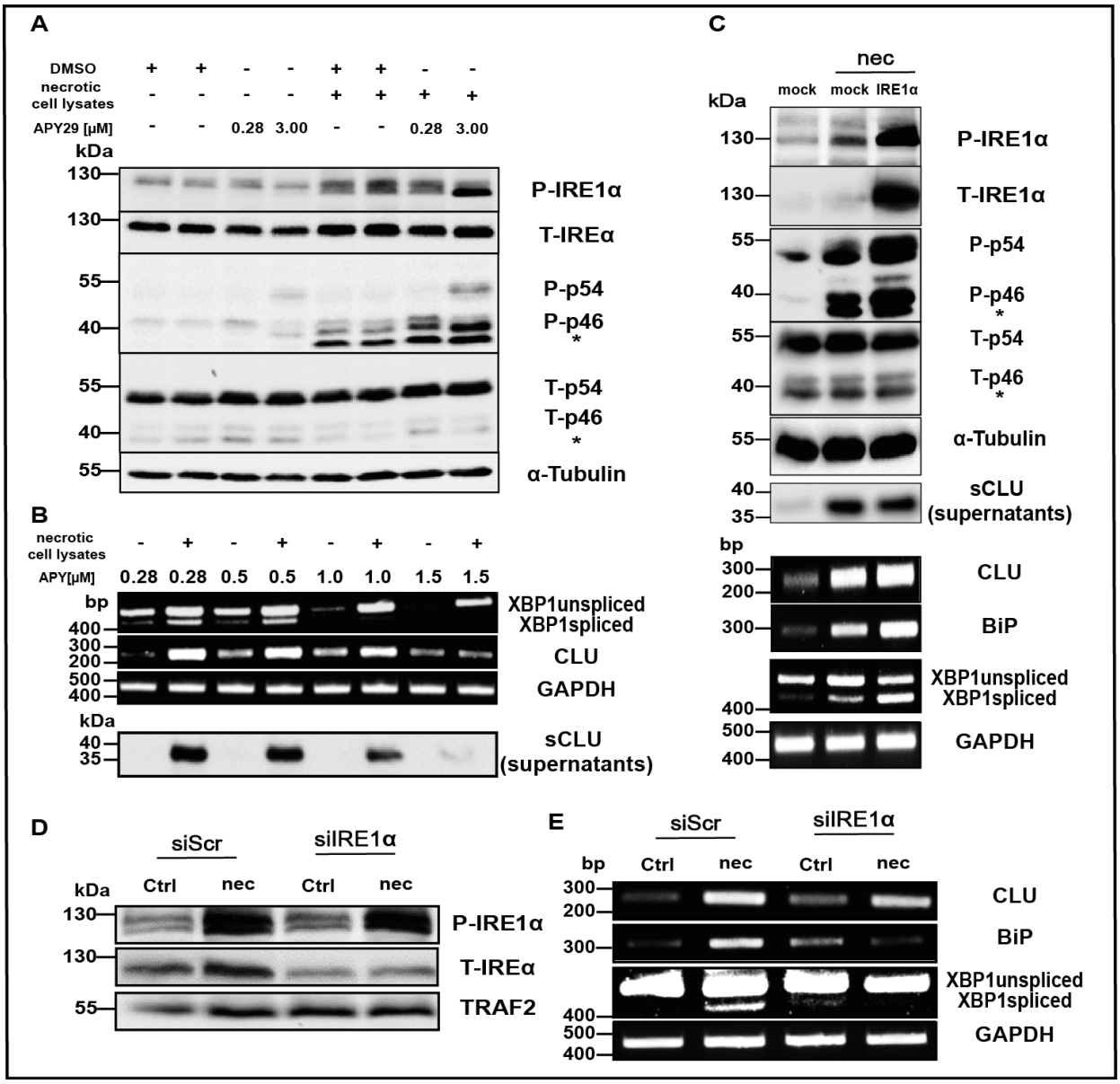

Fig.28 No confirmation for an UPR-CLU axis. (A,B) HEK-293 cells were preincubated with APY29 at various concentrations or DMSO as control and subsequently stimulated with 1 mg/mL necrotic cell lysates (nec) in presence of APY29 or DMSO for 2 hours (A) or 6 hours (B). (A) Western blot analyses conducted on 7.5% (IRE1α) or 10% (JNK, p46/p54) SDS-PAGEs (n=4). (B) sqRT-PCR for CLU expression and XBP1 splicing plus Western blot analyses for sCLU secretion using the sc-6419 antibody (n=3). (C) HEK-293 cells were transfected with pcDNA6 (mock) or pcDNA6-IRE1α full-length (IRE1α) for 6 hours, splitted into fresh 6-well plates and grown for another 40 hours, subsequently the transfected cells were set serum-free for 4 hours and eventually stimulated with 500 µg/mL necrotic cell lysates (nec) for 2 hours (Western blot) or 6 hours (sqRT-PCR & supernatants) (n=5). (D,E) HEK-293 were reverse transfected with siRNA (siScr & siIRE1α) for 40 hours, set serum-free for 4 hours and were stimulated with 1 mg/mL necrotic cell lysates for 2 hours (Western blot) or 6 hours (sqRT-PCR & supernatants) (n=3).

In summary, the approaches to show an UPR-CLU axis were insufficient.

5.2.4 Necrotic cell lysates promote cell proliferation

Due to detection of stress-related pathways induced in cells challenged with necrotic cell lysates, it was of interest whether the affected cells are undergoing apoptosis. Fig.29 shows the results of FACS analyses, MTS and proliferation assays.

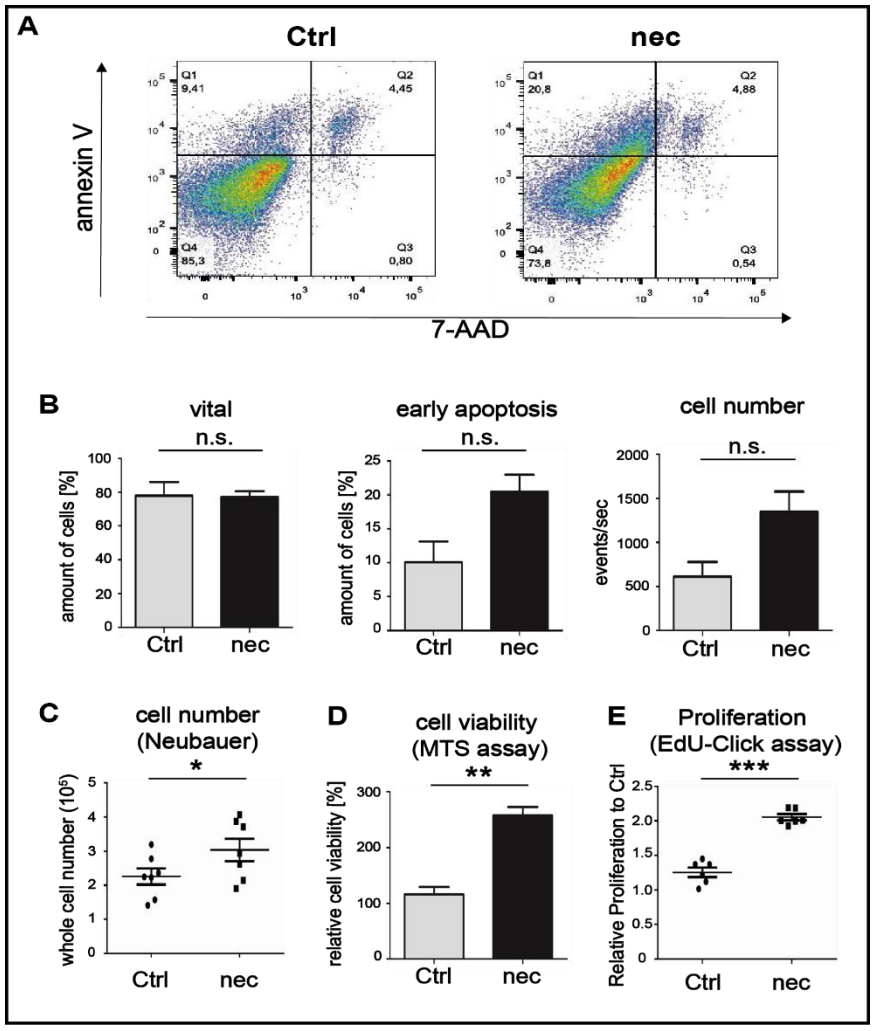

Fig.29 Necrotic cell lysates promote proliferation. (A) FACS analyses of cells stimulated for 24 hours with necrotic cell lysates (nec) were performed using annexin V (apoptosis) or 7-AAD (necrosis) (n=4). (B). Assessment of the ratio of vital cells, early apoptosis and whole cell number (after 24 hours of stimulation with 1 mg/mL necrotic cell lysates, nec). Values shown are the mean±standard errors of three to four independent experiments. Data were analyzed by using an unpaired, two-tailed Student's t test (***P<0.001; **P<0.01; *P<0.05). (C) 100,000 HEK-293 cells were seeded into 24-well plates and grown for 24 hours, subsequently the cells were stimulated with 1 mg/mL necrotic cell lysates (nec) for another 24 hours and finally counted with a Neubauer counting chamber. Values shown are the mean±standard errors of seven independent experiments. Data were analyzed by using an unpaired, one-tailed Student's t test (***P<0.001; **P<0.01; *P<0.05). (D) MTS assays with HEK-293 cells after 24 hours stimulated with 1mg/mL necrotic cell lysates (nec). Values shown are the mean±standard errors of three independent experiments. Data were analyzed by using an unpaired, two-tailed Student's t test (***P<0.001; **P<0.01; *P<0.05). (E) EdU-Click assays with HEK-293 cells after 24 hours stimulated with 1 mg/mL necrotic cell lysates (nec). Values shown are the mean± standard errors of six independent experiments. Data were analyzed by using an unpaired, two-tailed Student's t test (***P<0.001; **P<0.01; *P<0.05).

After testing whether cells are more apoptotic after treatment with necrotic cell lysates it was surprising that there was no significant difference in the amount of vital cells compared to control cells in FACS analyses using annexin V and 7-AAD (Fig.29A). Intriguingly, an elevated number of cells was found in samples stimulated with necrotic cell lysates (Fig.29B & C). This result was supported by a 2.5-fold increase in metabolic activity measured by MTS assays (Fig.29D) and cell proliferation assay using the EdU-Click system (Fig.29E). These results are indicating that necrotic cell lysates facilitate a contribution instead of an adverse effect on vital neighboring cells.

5.2.5 Elevated cell proliferation is not caused by IRE1α, CLU or AiF

The surprising result that cell viability and proliferation are elevated after application of necrotic cell lysates raises the question concerning underlying mechanisms. At first it is of interest whether CLU, UPR or the mechanism of apoptosis-induced proliferation (AiF) [220, 221] is responsible. To address this question, stable CLU knockdowns, IRE1α overexpression and Caspase-3 inhibition were carried out (Fig.30).

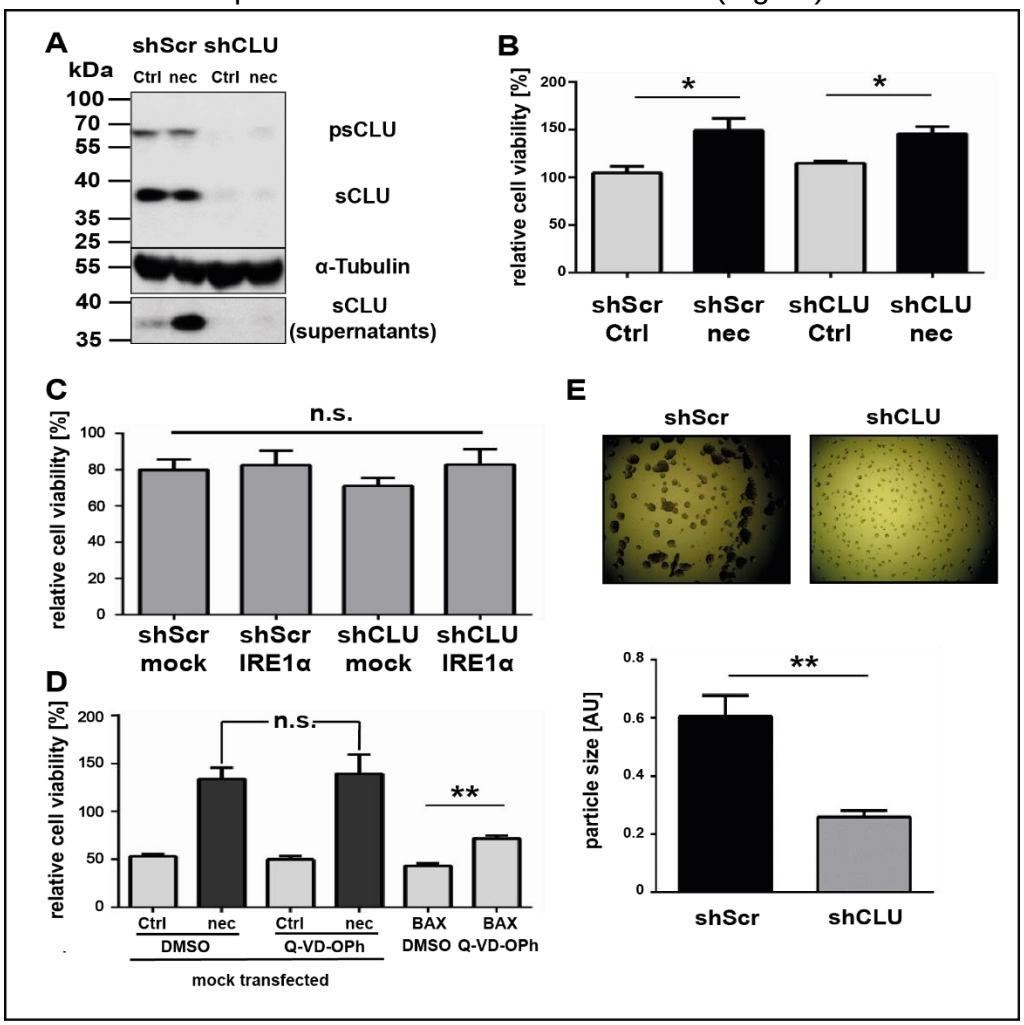

Fig.30 CLU, IRE1α and AiP does not contribute to elevated cell viability/proliferation. HEK-293 cells stable transfected with pTER-EGFP encoding CLU shRNA (shCLU) or scramble (shScr), stimulated with 1 mg/mL necrotic cell lysates (nec) for 6 hours (Western blot analyses, A) or 12 hours (MTS assays, B) (n=3) (C) 10,000 HEK-293 cells stable transfected with shCLU or shScr (see above) were seeded into 96-well plates and grown for 24 hours. Afterwards, the cells were transfected with pcDNA6 (mock) or IRE1α-pcDNA6 (IRE1α) for 6 hours. Subsequently, the cells were set serum-free for 12 hours and finally a MTS assay was performed (n=3). (D) 10,000 HEK-293 were seeded into 96-well plates and grown for 24 hours. Subsequently, the cells were transfected with pcDNA6 (mock) or BAX-pcDNA6 (BAX) for 18 hours with concomitant stimulation of 1 mg/mL necrotic cell lysates (nec) for 12 hours in the presence of 5 μM Q-VDOPh (n=3). (E) Cell aggregation assays with 20,000 HEK-293 cells in 96-well plates for 48 hours (n=4). (B-E) All values shown are the mean±standard errors. Data were analyzed by using an unpaired, two-tailed Student's t-test (***P<0.001; **P<0.01; *P<0.05).

CLU and IRE1α are known to exert cytoprotective and even cell proliferative functions [19, 72, 74, 80, 95, 105, 106, 108, 128, 152, 168]. Furthermore, it is known that Caspase 3-mediated apoptosis can trigger cell proliferation in neighboring cells, a mechanism which is known as apoptosis-induced proliferation (AiP) [220, 221]. To test whether CLU, IRE1α and/or AiP contribute to the observed proliferation, stable CLU knockdowns (Fig.30A & B), IRE1α overexpressing constructs (Fig.30C) and the pan caspase inhibitor QVD-OPh (Fig.30D) were used. Eventually, in none of the approaches a modulation in cell viability was observable pointing to an alternative mechanism. Interestingly, by subjecting the CLU knockdown cells to a cell aggregation assay a decline in cell aggregation was observable in the case of CLU knockdown cells, which is in accordance with [2].

5.2.6 The mTOR- and ERK1/2 signaling contribute to increased cell viability

Thus, CLU, IRE1α and AiF failed to be responsible for the observed advantage effects to cell viability, it was of interest whether the mTOR and the ERK1/2 signaling pathway, two pathways which are described as promoting cell proliferation [222], are involved (Fig.31). Since ERK1/2 and mTOR signaling is known to stimulate cell proliferation the involvement of these pathways was tested. In cells treated with necrotic cell lysates elevated levels of phosphorylated ERK1/2, mTOR, p70- & p85S6 ribosomal kinase (p70/p85S6K), and S6 ribosomal protein (S6) were found (Fig.31A). Surprisingly, phosphorylation of all targets was inhibited using the IRE1α kinase inhibitor Kira6, implying a rather broad spectrum of Kira6 target molecules (Fig.31B). As expected, necrotic cell lysates-induced phosphorylation of p70/p85S6K, and S6 was successfully prevented in cells treated with the mTOR inhibitor Rapamycin (Fig.31C). To determine how Kira6 and Rapamycin alter the viability of the necrotic cell lysate stimulated cells, MTS assays were performed. Kira6 drastically masked the enhanced viability of cells stimulated with necrotic cell lysates, whereas Rapamycin was less efficient (Fig.31D & E).

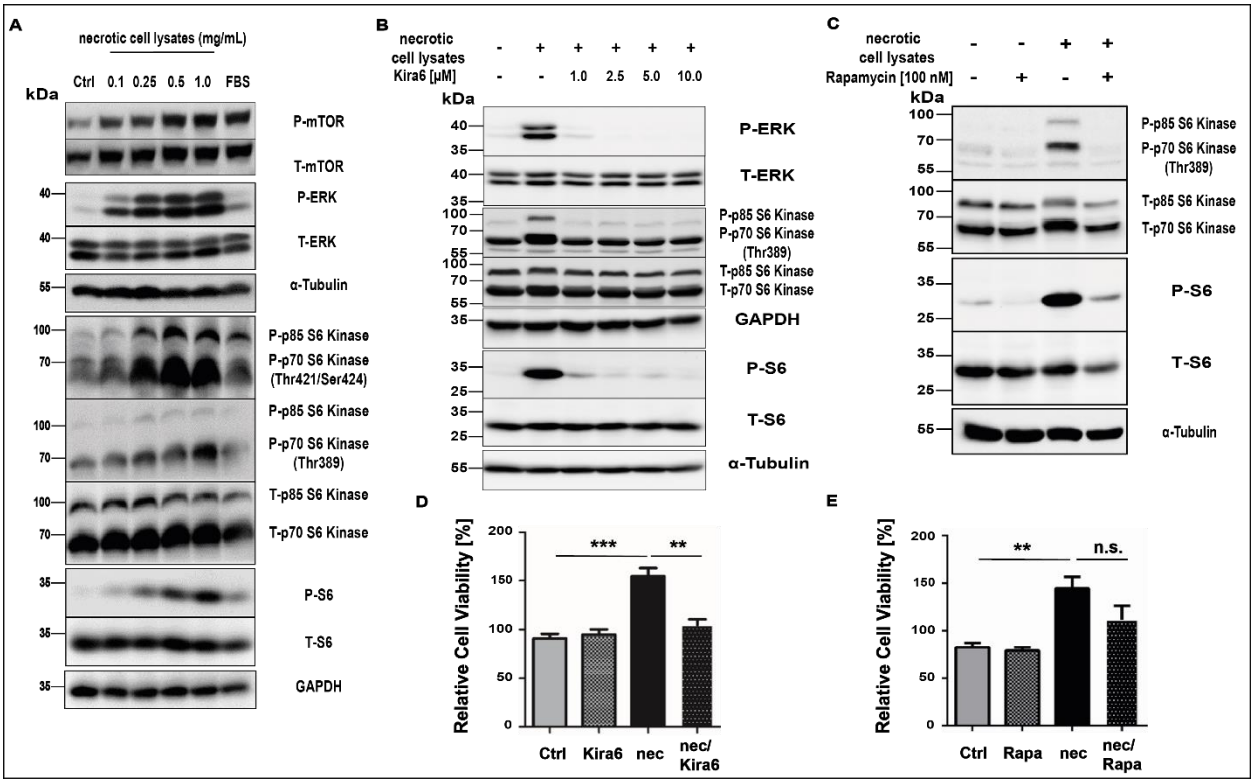

Fig.31 ERK1/2 and the mTOR signaling pathways contribute to elevated cell viability/proliferation. (A) HEK-293 cells were incubated with various concentrations of necrotic cell lysates (nec) for 2 hours and Western blots were performed. (n=3) (B, C) HEK 293 cells were preincubated in the presence of various concentrations of the IRE1α kinase inhibitor Kira6 or Rapamycin (100 nM) and subsequently stimulated with 1 mg/mL necrotic cell lysates (nec) in the presence of Kira6 or Rapamycin for 2 hours. (D,E) MTS assays with HEK-293 cells stimulated with 1 mg/mL necrotic cell lysates (nec) were performed in the presence of 10 μM Kira6 or 20 nM Rapamycin for 12 hours. Values shown are the mean±standard errors of three independent experiments. Data were analyzed by using one-way ANOVA, followed by Tukey's multiple comparison test (***P<0.001; **P<0.01; *P<0.05).

Taken together, these data indicate that necrotic cell lysates promote cell proliferation and viability by activating ERK1/2 and mTOR signal transduction pathways in vital cells. This mechanism can be summarized under the term: Necrosis-induced Proliferation (NiP).

5.2.7 A protein factor is responsive for UPR, CLU upregulation and NiP

To further shed light on the origin of the observed effects, necrotic cell lysates were digested with RNase A (data not shown) and Chymotrypsin (Fig.32). The protease Chymotrypsin was used since no adverse effects of Chymotrypsin were observable to the cells (data not shown). Intriguingly, after digesting necrotic cell lysates with Chymotrypsin ERK1/2, p70/p85S6K, S6 and JNK (p46/p54) phosphorylation, as well as CLU transcriptional upregulation and XBP1 splicing was impaired. Nevertheless, mTOR

phosphorylation and sCLU secretion (Fig.32B, red arrow) were almost unaltered indicating separate mechanisms apart from the remaining effects.

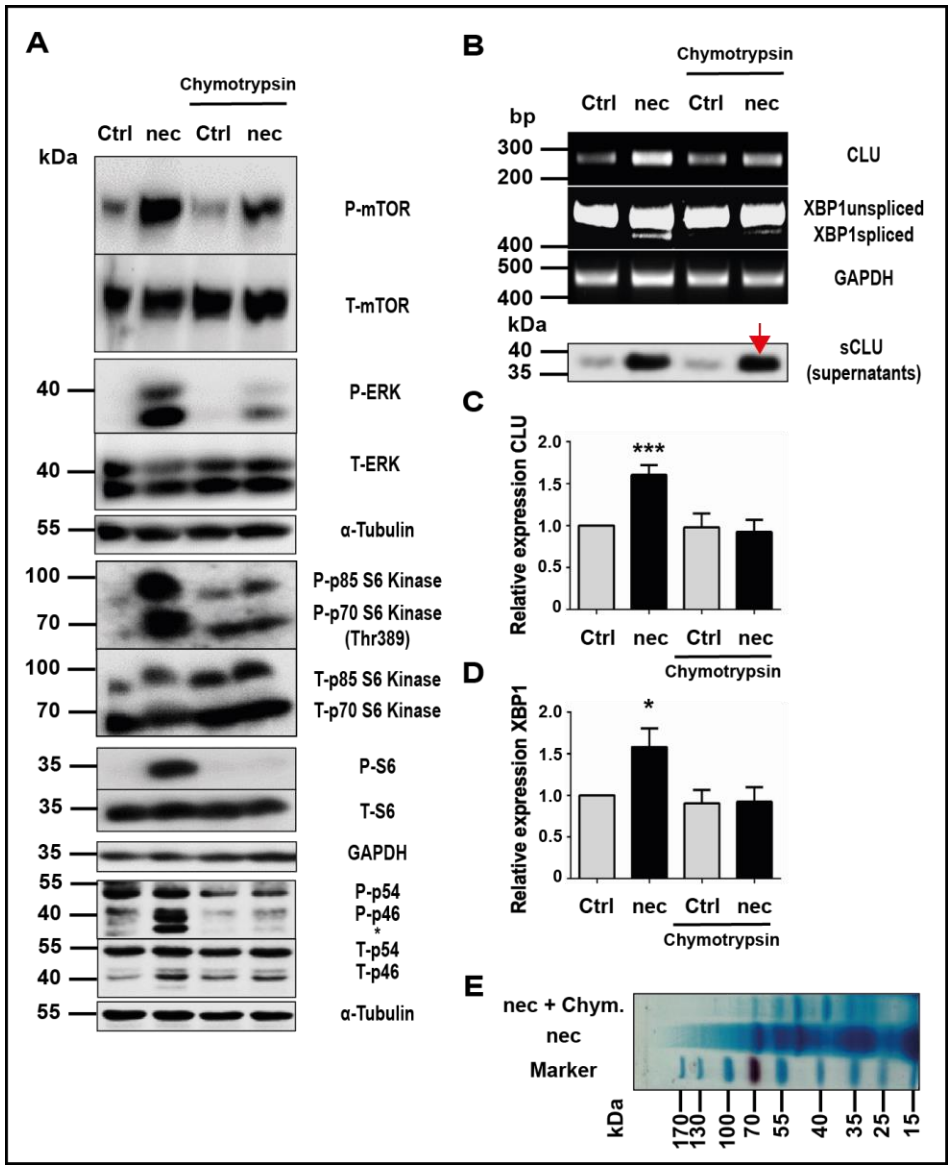

Fig.32 A protein drives the phosphorylation of mTOR, ERK1/2, p70/p85S6K, as well as CLU upregulation and XBP1 splicing. Fully confluent HEK-293 cells were set serum-free for 4 hours and subsequently stimulated for 2 hours (Western blots) or 6 hours (sqRT-PCR, qRT-PCR or supernatants) using necrotic cell lysates (nec) digested with or without Chymotrypsin. (A) Western blot analyses on 6% SDS-PAGE (mTOR), 15% p70/p85S6K and 10% (ERK1/2, S6 & JNK) SDS-PAGEs (n=4). (B) sqRT-PCR for CLU upregulation and XBP1 splicing with GAPDH as control (n=3), as well as Western blot for sCLU secretion in supernatants detected with sc-6419 antibody (n=3). (C,D) qRT-PCR analyses of CLU upregulation and XBP1 splicing. All values shown are the mean±standard errors of three independent experiments. Data were analyzed by using an unpaired, two-tailed Student's t test (***P<0.001; **P<0.01; *P<0.05). (E) Digestion control on 10% SDS-PAGE loaded with 30 µg protein and stained with Coomassie brilliant blue (n=3).

Taken together, these data suggest that the responsible factor is a protein.

5.2.8 sCLU secretion is uncoupled from the not-ubiquitous expressed factor

Encouraged by the surprising findings that the digestion of the wanted proteinogenic factor does not hamper necrotic cell lysate-mediated increased sCLU secretion, it was of interest 1) whether the factor is ubiquitously expressed, 2) whether the factor belongs to the known group of danger-associated molecular patterns (DAMPs) and 3) whether sCLU secretion and transcriptional upregulation are indeed not correlated. The results of the addressed questions are shown in Fig.33.

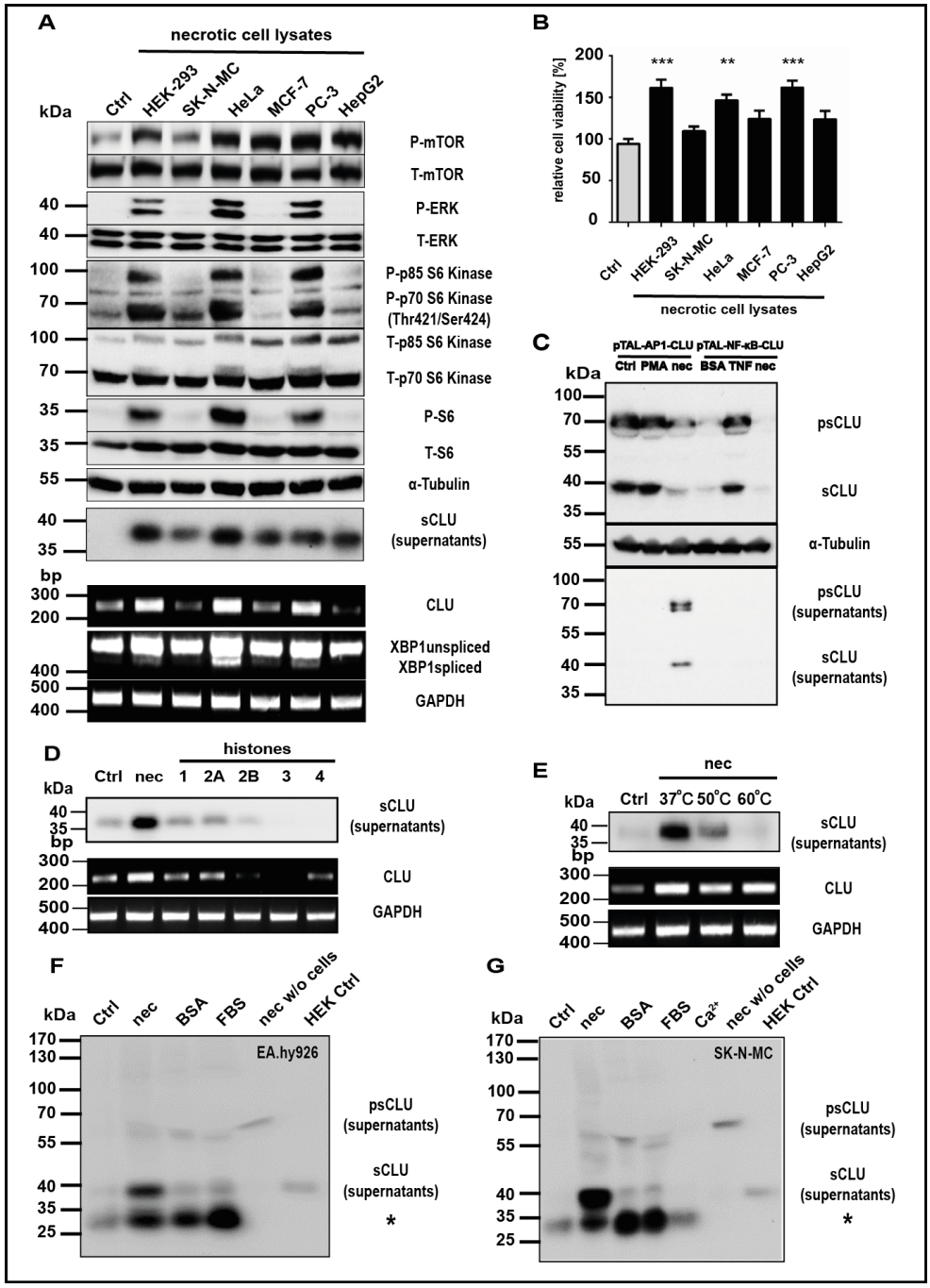

Fig.33 Cell lines expressing the wanted factor as well as correlation of CLU transcriptional upregulation and sCLU secretion. (A) HEK-293 cells fully confluent were set serum-free for 4 hours and subsequently were stimulated with 500 µg/mL necrotic cell lysates obtained from various cell lines (see Figure) for 2 hours (Western blots) or 6 hours (sqRT-PCR, and Western blot of supernatants, detecting antibody sc-6419) (n=3). (B) MTS assays with HEK-293 cells stimulated with 1 mg/mL necrotic cell lysates obtained from various cell lines for 12 hours. Values shown are the mean±standard errors of three independent experiments. Data were analyzed by using one-way ANOVA, followed by Tukey's multiple comparison test (***P<0.001; **P<0.01; *P<0.05). (C) $1.0*10^6$ HEK-293 cells were seeded in 6-well plates and were transfected with the vectors pTAL-AP-1 or pTAL-NF-κB, where the luciferase-coding region was substituted by full-length CLU as described in the Material and Method Section, for 6 hours. Subsequently the cells were passaged 1:3 in fresh 6-well plates and grown for another 36 hours. After reaching full confluency, the cells were set serum-free for 4 hours and finally stimulated with 1 µM PMA, 5 ng/mL TNF, 5 ng/mL BSA, 500 µg/mL necrotic cell lysates (nec) for 6 hours. Western blot analyses were conducted with the anti-V5 antibody (n=3). (D,E) Confluent HEK-293 cells were set serum-free for 4 hours and were stimulated with 1 mg/mL necrotic cell lysates (nec, untreated or heated for 30 minutes at 50°C or 60°C, respectively) or 1 µg/mL histone proteins for 6 hours. Finally, Western blot analyses of supernatants using the antibody sc-6419 and CLU sqRT-PCRs with GAPDH as loading control were carried out. (F,G) Fully confluent SK-N-MC or EA.hy926 cells were set serum-free for 4 hours and were stimulated with 25 µM $CaCl_2$, 1 mg/mL necrotic cell lysates (nec, obtained from HEK-293 cells), BSA or FBS for 12 hours. Subsequently, the supernatants were precipitated as described in the Method Section and applied to Western blot analyses using the sc-6419 antibody. To prevent potential false-positive results from endogenous CLU within the necrotic cell lysates (nec), 1 mg/mL necrotic cell lysates was also precipitated as control (nec w/o cells) (n=2-3).

The notion of an independence of the sCLU secretion from its transcriptional upregulation was supported in various experimental settings. First, it was shown that necrotic cell lysates obtained from SK-N-MC, MCF-7 and HepG2 cells are not suitable to induce ERK1/2, p70/p85S6K and S6 phosphorylation (Fig.33A). In accordance with the absence of induction of the investigated signal transduction pathways these lysates also fail to induce significant elevation of cell viability (Fig.33B) as well as XBP1 splicing or CLU transcriptional upregulation (Fig.33A). Intriguingly, an increased accumulation of sCLU was detectable in all supernatants (Fig.33A). Moreover, by conducting reporter assays with NF-κB and AP-1 reporters coupled with the CLU full-length protein coding region, no secretion of sCLU was detectable in the supernatants of the NF-κB reporters after stimulation with TNF even though CLU accumulates in the whole cell lysates (Fig.33C). Note that the NF-κB reporter is not activated in the presence of necrotic cell lysates confirming the above conducted experiments with Parthenolide (Fig.26G). Further, it was detectable that the AP-1 reporter has a basic activity even in its unstimulated state which explains the high variability in the conducted luciferase reporter assays described above (Fig.26B). Nevertheless, sCLU accumulation in the supernatants is solely present in the necrotic cell lysate stimulated lane and not even in the positive control with PMA (Fig.33C). Additionally, an impairment in the basic CLU expression was observable after application of histone H2B and H3. However, a concomitant decrease in sCLU secretion has not been observed in the case of histone H4 implying at least an indirect correlation of histone-mediated decline in CLU expression and sCLU secretion (Fig.33D). Similar findings were made after heating necrotic cell lysates at 50°C and 60°C, respectively (Fig.33E). The higher necrotic cell lysates were heated the more tremendous was the impairment in sCLU secretion (Fig.33E). However, necrotic cell lysates, independently of

the temperature used for heating, still induce transcriptional upregulation of CLU (Fig.33E). Moreover, it was reported that after application of up to 2 µg/mL Actinomycin D, a potent transcription inhibitor, it does not prevent necrotic cell lysate-mediated sCLU secretion [223]. This result was reproducible. Similar to [223], an inhibition of CLU transcriptional upregulation but only minor impairment of sCLU secretion upon stimulation with necrotic cell lysates in the presence of 2 µg/mL Actinomycin D for 6 hours was observable (App.7B). Eventually, stimulation of EA.hy926 and SK-N-MC cells also show an increased sCLU secretion (Fig.33F & G). Nonetheless, CLU transcriptional upregulation has never been observed (data not shown). Taken together, the data are implying at least two routes: one for sCLU secretion (Fig.32 & 33)/mTOR phosphorylation (Fig.32) and another route for ERK1/2 phosphorylation, CLU transcriptional upregulation and UPR induction. In this context, it should be mentioned that besides the histone proteins tested above, S100A8/S100A9, HMGB1 and HSP72 failed to be responsible for the induction of the described pathways (App.7C,E & F). Moreover, interference of TLR4 signaling by using TLR4 blocking antibodies also show no difference (App.7C & D). Therefore, “standard DAMPs” are probably not responsible for the observed effects [113, 114, 120].

5.2.9 Location and size of the responsible protein factor

Of approximately 10,000 and 12,000 different proteins which are expressed in cells [224], and some researchers even estimate that up to 100,000 various proteins might exist in a cell [225], it is indeed difficult to find one distinct protein. Nevertheless, by combining size exclusion chromatography and cell death assays at least rough information can be obtained. The basic concept of fractionizing is illustrated in Fig.34.

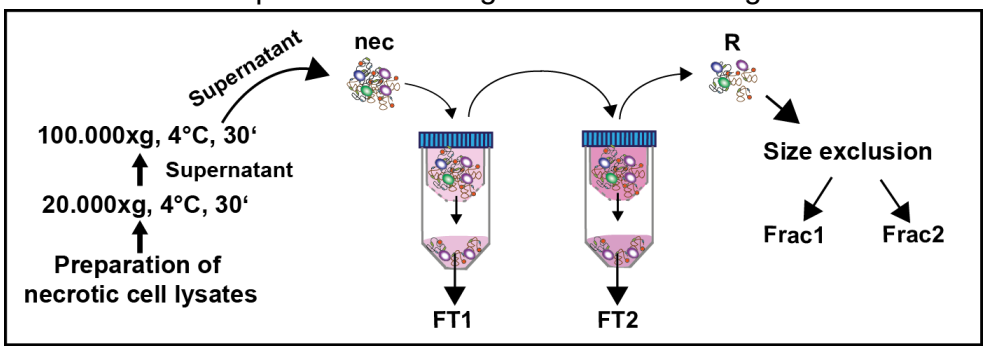

Fig.34 Fractionization of necrotic cell lysates. Illustrated is the procedure with ultracentrifugation. Necrotic cell lysates without ultracentrifugation was solely centrifuged at 20,000xg at 4°C for 30 minutes and directly applied to size exclusion.

Based on the illustration in Fig.34 the necrotic cell lysates were fractionized, results are shown in Fig.35.

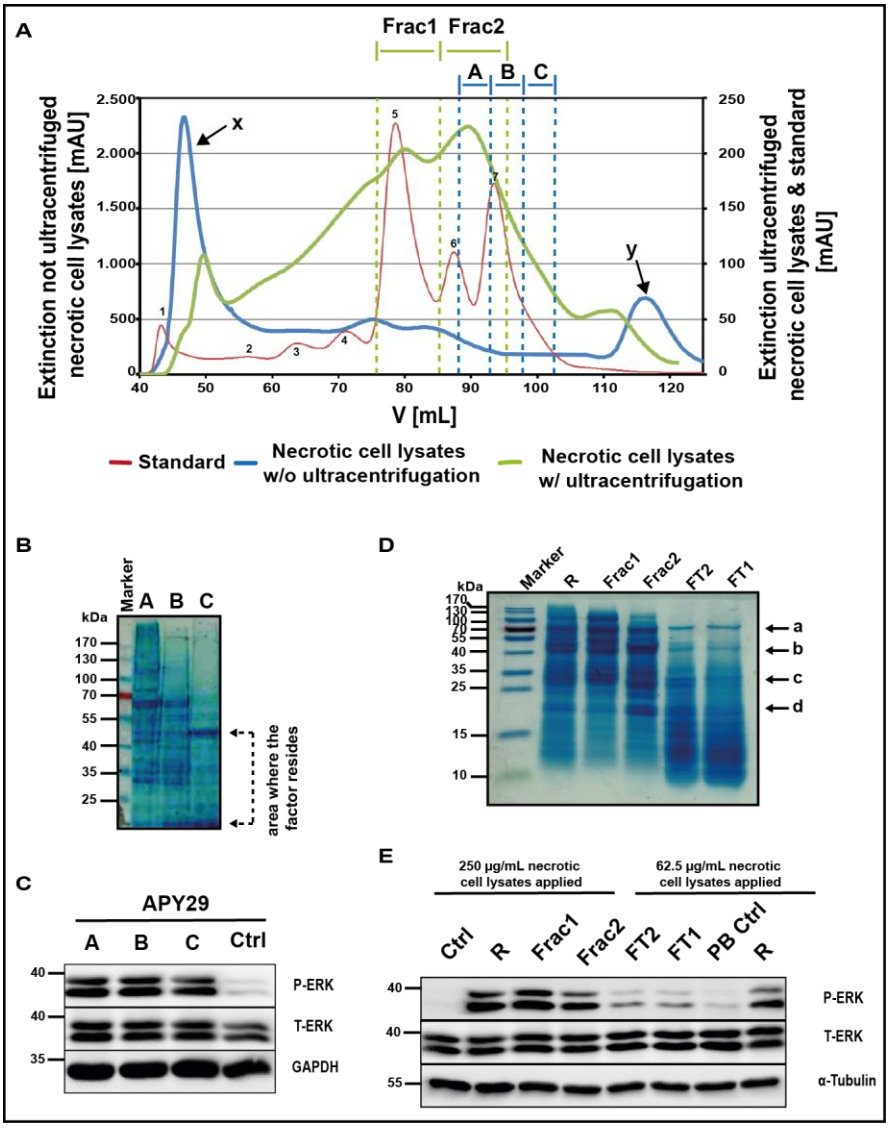

Fig.35 Approximately size of the wanted protein factor. (A) Chromatogram of the size exclusion chromatography as described in Methods (4.3.5.2) and Fig.34. 1 = Blue Dextran (approx. 2,000 kDa), 2, 3 & 4 = Apoferritin (trimer, dimer and 443 kDa monomer), 5 = Conalbumin (75 kDa), 6 = Carbonanhydrase (29 kDa), 7 = Ribonuclease (13.7 kDa). (B) Coomassie-stained SDS-PAGE (10%) of precipitated fractions from size exclusion chromatography carried out with necrotic cell lysates which have not been ultracentrifuged (see also Fig.34). (C) Fractions depicted in (B) were applied to fully confluent HEK-293 cells (approximately 0.1 mg/mL, 6-well plates, preincubation and stimulation in the presence of 3 µM APY29) for 2 hours and ERK1/2 phosphorylation was detected using Western blot. (D) Coomassie-stained SDS-PAGE (15%) of precipitated fractions from size exclusion chromatography carried out with necrotic cell lysates which have been ultra-centrifuged (see also Fig.34). (E) Western blot analyses (ERK1/2 phosphorylation) of HEK-293 cells (fully confluent and 4 hours on serum-free) stimulated with the fractions of the separation of necrotic cell lysates (nec) as shown in see (D) for 2 hours.

As shown in Fig.35A ultracentrifugation successfully removes higher molecular aggregates (x, approximately 2,300 mAU). Further, the use of Amicon centrifugal filter tubes also removes lower molecular species (y). The collected fractions were further applied to Coomassie-stained SDS-PAGEs and cells (Fig.35B & C, D & E). Interestingly,

it was detectable that the protein within the necrotic cell lysates which potentially drives NiP is below 45-50 kDa (see ERK1/2 phosphorylation). Please note, that also an increase in phosphorylation of IRE1α, p70/p85S6K and S6 phosphorylation was detectable (data not shown). However, it is important to note that even proteins of 50 kDa or higher, for instance 70 kDa (Fig.35D, arrow a), are passing the Amicon filters (Fig.35D). However, these bands might also correspond to SDS-resistant protein aggregates. Nevertheless, proteins below 35 kDa are in the majority (Fig.35D). Moreover, by testing the fractions obtained from Amicon filtration on HEK-293 cells, at least low ERK1/2 phosphorylation occurs which however could be caused due to low protein concentration (Fig.35E). Nonetheless, the remaining necrotic cell lysates (R) which were not applied to the size exclusion chromatography are more suitable to induce ERK1/2 phosphorylation at the same concentration as the Amicon flow through (Fig.34, 35 D & E). These data implying that the desired factor is not a high molecular weight factor but is probably larger than 20 kDa. In a similar study, it was found that a factor leading to comparable effects as described (increased cell viability and CLU upregulation) must be between 130 and 190 kDa [185]. This notion can be excluded based on the findings of this study. In summary, the wanted protein factor is approximately between 20 and 50 kDa in size. Potential distinct protein weights are >40 kDa, 30 kDa or 20 kDa (Fig.35D, arrows). Please note that sCLU secretion was detectable in any fraction (data not shown; arrows b, c d).

To further obtain information concerning the cellular location of the wanted protein factor, HEK-293 cells were heated up to 45°C for 10 minutes and kept in culture afterwards for another 3 hours. Subsequently, the cells were centrifuged and the supernatant was applied to fresh vital HEK-293 cells (Fig.36A). Intriguingly, this approach revealed an increased ERK1/2, mTOR and S6 phosphorylation in the vital cells stimulated with supernatants obtained from dying cells but not with supernatants obtained from unheated living control cells (Fig.36B). Importantly, in the supernatants collected, α-Tubulin (cytoskeleton), GAPDH (cytosol/mitochondria) or Calreticulin (ER) was not detectable (Fig.36B).

In summary, the wanted protein factor is probably between 20 and 50 kDa in size and located either in the plasma membrane, the extracellular matrix/space or will be secreted upon cell stress.

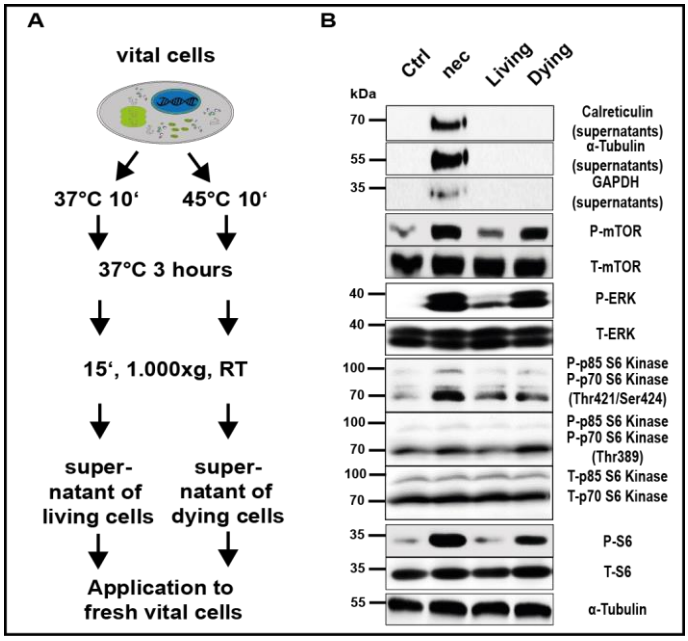

Fig.36 Cell dying assay for evidence of the cellular location of the wanted protein factor. (A) Schematic depiction of a cell dying assay. (B) Western blot analyses of HEK-293 cells stimulated with supernatants obtained from dying cells as described in (A) for 2 hours after 4 hours on serum-free. The Western blots were conducted on 6% (mTOR), 15% (p70/p85S6K) and 10% SDS-PAGEs for the remaining targets.

5.2.10 Transcriptomic approach to find the wanted protein factor

Encouraged by evidences of the molecular weight and the potential location of the wanted protein factor, transcriptome data of the cell lines (except of HEK-293) tested in Fig.33 (A&B) were obtained by TRON and comparison analyses were conducted (Fig.37).

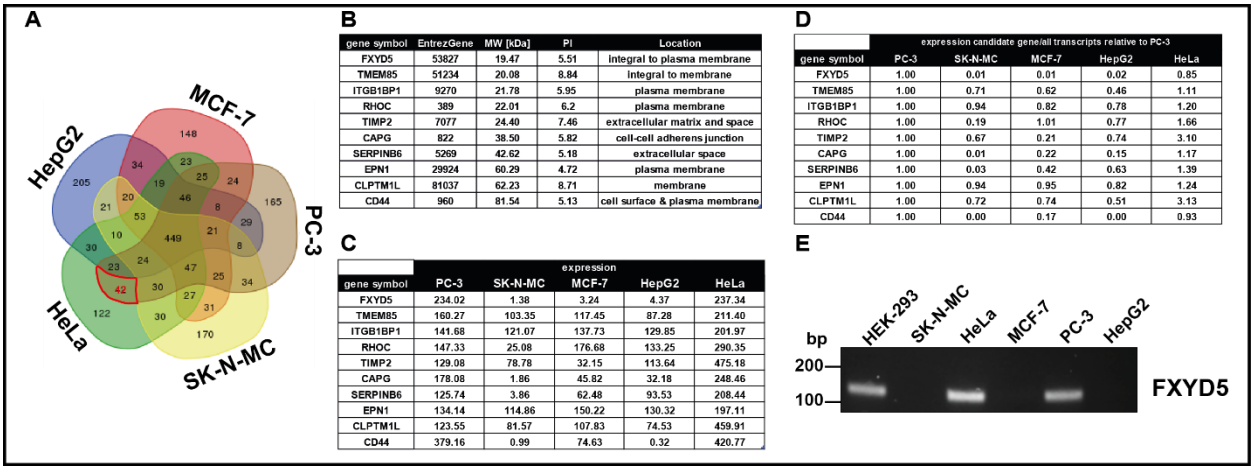

B

gene symbol	EntrezGene	MW [kDa]	PI	Location
FXYD5	53827	19.47	5.51	integral to plasma membrane
TMEM85	51234	20.08	8.84	integral to membrane
ITGB1BP1	9270	21.78	5.95	plasma membrane
RHOC	389	22.01	6.2	plasma membrane
TIMP2	7077	24.40	7.46	extracellular matrix and space
CAPG	822	38.50	5.82	cell-cell adherens junction
SERPINB6	5269	42.62	5.18	extracellular space
EPN1	29924	60.29	4.72	plasma membrane
CLPTM1L	81037	62.23	8.71	membrane
CD44	960	81.54	5.13	cell surface & plasma membrane

C

	expression				
gene symbol	PC-3	SK-N-MC	MCF-7	HepG2	HeLa
FXYD5	234.02	1.38	3.24	4.37	237.34
TMEM85	160.27	103.35	117.45	87.28	211.40
ITGB1BP1	141.68	121.07	137.73	129.85	201.97
RHOC	147.33	25.08	176.68	133.25	290.35
TIMP2	129.08	78.78	32.15	113.64	475.18
CAPG	178.08	1.86	45.82	32.18	248.46
SERPINB6	125.74	3.86	62.48	93.53	208.44
EPN1	134.14	114.86	150.22	130.32	197.11
CLPTM1L	123.55	81.57	107.83	74.53	459.91
CD44	379.16	0.99	74.63	0.32	420.77

D

	expression candidate gene/all transcripts relative to PC-3				
gene symbol	PC-3	SK-N-MC	MCF-7	HepG2	HeLa
FXYD5	1.00	0.01	0.01	0.02	0.85
TMEM85	1.00	0.71	0.62	0.46	1.11
ITGB1BP1	1.00	0.94	0.82	0.78	1.20
RHOC	1.00	0.19	1.01	0.77	1.66
TIMP2	1.00	0.67	0.21	0.74	3.10
CAPG	1.00	0.01	0.22	0.15	1.17
SERPINB6	1.00	0.03	0.42	0.63	1.39
EPN1	1.00	0.94	0.95	0.82	1.24
CLPTM1L	1.00	0.72	0.74	0.51	3.13
CD44	1.00	0.00	0.17	0.00	0.93

Fig.37 Comparison analyses of transcriptome data obtained by TRON. (A) Venn Diagram of cell lines tested above. The red 42 indicates candidate genes which are only present in HeLa and PC-3 cells. (B) Candidate genes in HeLa and PC-3 cells which are located at the plasma membrane, the extracellular matrix or other areas close to the cell surface which allows a spontaneous release without complete destruction of the cell. (C) Expression of the candidate genes in all cell lines. (D) Expression of genes relative to the expression of all transcripts relative the expression of the corresponding gene in PC-3 cells. (E) sqRT-PCR of the candidate gene FXYD5.

After comparison of all cell lines (Fig.37), 42 candidate genes were remained which fulfill the requirements listed above (molecular weight, cellular location, expressed only in PC-3 and HeLa). Eventually, only the candidate gene FXYD5 survives all exclusion criteria. Unfortunately, due to closing of the work group it was not possible to test FXYD5 in cell culture even though its cloning was successful. The FXYD5 in pcDNA6 constructs can be obtained upon request from the author of this thesis.

6 Discussion

The extracellular molecular chaperone secretory Clusterin (sCLU) is described as the most abundant extracellular chaperone ever found. Nevertheless, its precise function is considered “enigmatic”. Over time, a plethora of additional roles suggested, superelevate CLU as a key player in cellular settings such as cell death and survival. The initial idea of this thesis was to understand how CLU might exactly be involved in these mechanisms, especially in the modulation of signal transduction pathways. Unfortunately, initial observations finally failed to be proved (App.8), concluding that potential effects might be the result of side effects or experimental artifacts. Encouraged from these findings it was of interest to find alternative routes for understanding CLUs’ role in the cellular homeostasis.

6.1 The evolution of the CLU protein

The importance of a protein is clearly correlated with its occurrence and conservation among various species. Surprisingly, only few studies have addressed the expression of the CLU proteins beside higher mammalians. Still less studies have addressed the evolution of the *clu* gene or CLU protein. Additionally, it has never been determined whether the sCLU protein of other animals, except of humans, displays chaperone activity.

6.1.1 Mouse vs. human CLU (sCLU)

In a first approach the CLU protein of one of the close relative to humans, the mouse, was cloned, expressed, purified and basic characterizations were conducted. The identity in the aa sequence of mice and humans is about 77%. Nonetheless, equal CD spectra were obtained and both proteins display a chaperone-like activity (Fig.13B&C), even though the activity of mouse sCLU was slightly impaired which might be correlate with the observations that both chains are only loosely connected with one another (Fig.12A). However, predictions of the secondary structure of mouse vs. human CLU using the full-length aa sequence (JPred) revealed: 55.8% vs. 52.8 α-helices and 4.9% vs. 9.1% β-sheets. The CD spectra measurements however, show in both species approximately 60% α-helices and 9% β-sheets, the remaining secondary structures are 12% turns and approximately 19% unordered or random coiled structures (Fig.13B & 22G). Moreover, the basic structural components such as cysteine-rich regions (CRRs), the furin-like proprotein convertase recognition site (FC recognition site), coiled-coil domains, position of α-helices and β-sheets are all located at approximately the same site. However, the glycosylation varies in the case of mouse sCLU with only two glycosylation sites on the α-chain and four on the β-chain (humans display three glycosylation sites on both chains).

Intriguingly, in human sCLU one glycosylation site is located upstream of CRR1, this glycosylation site does not occur in mouse. Nonetheless, it remains to be figured out whether this glycosylation is involved in the slightly improved chaperone activity of human sCLU. Taken together, it was shown for the very first time that sCLU except of human origin is a conserved extracellular chaperone.

6.1.2 CLU, a conserved extracellular chaperone among vertebrates?

Encouraged of the above findings, it was of interest how conserved the CLU protein is. Indeed, the *clu* gene is not existent in Invertebrata (no hit in the data base). Interestingly, it is assumed that CLU has evolved as result of a gene duplication of a common ancestor gene leading to the *clu* and the *clul1* gene [226, 227]. Furthermore, using the genome browser (https://genome-euro.ucsc.edu/) the *clu* and the *clul1* gene was neither found in *Ciona intestinalis* (Urochordata) and *Branchiostoma lanceolatum* (Cephalochordata) nor in *Petromyzon marinus* (Cyclostomata). Therefore, CLU and its family member the Clusterin-like protein 1 (CLUL1) are not older than about 450 million years and solely present in Gnathostomata [214, 218]. In contrast to the almost ubiquitous expressed CLU [19, 35, 228], CLUL1 (Clusterin-like protein 1) for its part is nowadays primarily expressed in the retina [226, 229]. Initial studies of CLUL1 in dogs [230] have revealed that CLUL1 bears the putative SSCR, CRRs and N-glycosylation sites, also renders CLUL1 as a secretory glycoprotein (App.3-5). Nonetheless, it has never been addressed whether CLUL1 acts as a secreted molecular chaperone as in the case of sCLU. Intriguingly, by analyzing features within the CLUL1 protein (10 birds, 23 mammalians, 13 fishes and 3 reptiles) further similarities to CLU have been found (App.3-5). CLUL1 also bears regions of low conservation (RLCs) at approximately the same positions as CLU (App.4&5, Fig.14&15). The RLC-I in CLUL1 is an extended area in the center of the aa sequence (approximately between 175 and 275 aa) and it has an extended high disordered tendency (App.4&5). CLU in comparison displays a higher order within the RLC-I (Fig.15). Intriguingly, after predicting putative FC recognition sites within CLUL1 only six species show a conserved FC recognition site in the RLC-I and four more species show a FC recognition site downstream and upstream of the RLC-I, respectively (App.3). The most important finding however is, that except of *Crotalus adamanteus* (snake) only fishes show a putative FC recognition site in the RLC-I of CLUL1 (App.3). In contrast, in the case of 108 CLU-expressing species tested, only three species show no indication for a FC recognition site (all fishes, see Fig.17C & App.1). These data suggest that either the putative FC recognition site was not present in the ancestor gene of *clu* and *clul1* or has been secondarily regressed. However, the strong presence of the FC recognition site in CLU coupled with its far expression pattern (ubiquitous!) makes it more likely that the FC recognition site is beneficial for the functioning of the protein. It is therefore unlikely that this feature has been regressed during evolution. It is more likely that both proteins were

in an “evolutionary competition”, whereas CLU has triumphed because of particularities, such as the FC recognition site. Intriguingly, the RLC-II displays in both (CLU and CLUL1) a high disorder tendency and a noticeable stretch of β-sheets (Fig.15, App.4). Moreover, CLU and CLUL1 also show an extended α-helical stretch at the N-terminus and coiled-coil domains (Fig.15 & App.4). Indeed, the C-terminus of CLUL1 also shows an area with extended α-helices, but these α-helices are not necessarily tending to form coiled-coil domains (App.4). In the case of CLU however, only two-thirds of CLU-expressing species tested show a coiled-coil structure at the C-terminus (App.1). It must be emphasized, that no correlation concerning the absence of the coiled-coil domains at the C-terminus and the animal class was observable in the case of CLU (App.1).
Another predictable component of the CLU protein are the N-glycosylation sites. As shown in Fig.18 ranging from fishes to mammals, the amount of glycosylation sites increases (4.0 in the case of fish to 6.6 in mammals). A comparable observation was made in the case of CLUL1 ranging from 3.5 (fish) over 3.7 (reptiles) and 3.3 (birds) to finally 4.7 in the case of mammals (App.3). It is important to note that both proteins (CLU and CLUL1) have a comparable length of their aa chain (452 vs. 465 aa) but *exempli gratia* mammalian sCLU has a 1.4 higher glycosylation rate than mammalian CLUL1 (App.1&3).
Concerning the predictable protein structures of the CLU protein it can therefore be summarized, that the α-helices at the N- and the C-terminus, the β-sheets at the C-terminus and the coiled-coil domains (primarily!) at the N-terminus are potentially crucial prerequisites for the function of sCLU. Moreover, the conservation of N-glycosylation sites and its higher abundance in mammals indicates that the N-glycosylation is a fundamental feature of sCLU and therefore for sCLU function.

6.1.3 Conserved elements in the CLU structure are important for chaperone activity

To further asses the role of structural components discussed above, the role of N-glycosylation and the putative FC recognition site in the case of human sCLU was tested. By generating uncleaved sCLU (RIVR→RIVQ), subsequent chaperone activity assays and CD spectra analyses it was found that the proteolytic cleavage is neither a prerequisite for the expression and secretion of sCLU nor for the chaperone activity or the secondary structure composition (Fig.20B&D, 21C, 22F&G). Furthermore, it was shown that the removal of terminal glycosylation has also no significant influence on chaperone activity and on secondary structures in both cleaved and uncleaved sCLU (Fig.21C, 22F1&G). Finally, the removal of core-carbohydrates using PNGase F was successful to impair sCLU chaperone activity by about 50% (Fig.22D&E) and to alter the secondary structure composition in both cases (approximately 61% to 40% α-helices, 8% to 15% β-sheets, 12% to 16% turns, 18% to 29% unordered, for exact percentages please

see Fig.22G). This finding was of interest, because of two reasons: 1) Stewart *et al.* 2007 [31] concluded that sCLU is still active as chaperone after PNGase F digestion with concentrations far lower than used in this thesis (0.1 U/µL vs. 2.25 to 6.25 U/µL) and 2) despite of high PNGase F concentrations and 12 hours of digestion sCLU still shows remaining glycosylation (Fig22B&C). Intriguingly, the residual glycosylation was solely present on the β-chain (Fig.23A). For complete deglycosylation, DTT was utilized to reduce the disulfide bonds thus making the N-glycosylation sites potentially more accessible for PNGase F-treatment (Fig.23A). Surprisingly, after 12 hours of co-incubation with DTT the remaining glycosylation was removed from the β-chain but now a residual glycosylation was present on the α-chain. Indeed, which N-glycosylation site remains cannot be explained by the present data. However, it can be taken into consideration that glycosylation sites which are buried further into the protein, e.g. the site downstream of CCR1 or within CCR2 are not accessible (Fig.14&15). Nonetheless, after gradual reduction (6 hours without and 6 hours with DTT), full deglycosylation was successful (Fig.23A&B) displaying heavily impaired chaperone activity in both cases (cleaved and uncleaved sCLU, see Fig.23C-F). Moreover, the tremendous sensitivity of uncleaved sCLU towards reduction became apparent (Fig.23C, E-F). This finding was probably one of the most remarkable observations since it was expected that reduction primarily influences cleaved sCLU. A further approach to figure out whether uncleaved sCLU is more denatured or exposes more hydrophobic aa proved to be incorrect (Fig.24B). In both cases (cleaved and uncleaved sCLU), an elevation in ANS fluorescence was detectable arguing that reduction alters the folding in a comparable manner (Fig.24B). Nevertheless, at least a slight increase was detectable in the case of uncleaved sCLU incubated with DTT. To assess this phenomenon, it is important to illustrate the overall hydrophobicity and secondary structures of all animals tested to find a conclusive explanation (Fig.38).

Basic structural features were already discussed therefore, only additional notable particularities, conspicuous in Fig.38 should be addressed. Basically, the hydrophobicity and secondary structures are extensively conserved among 105 various species (similarity 52%). Intriguingly, within RLC-I an α-helix is conserved which shows a slight increase in hydrophobicity (blue curly bracket). The fact that cleaved sCLU still shows sufficient chaperone activity after reduction implies that the stabilization of the molecule is mediated by other/additional structural elements. Uncleaved sCLU in contrast, loses its chaperone activity after reduction which would indicate that the stabilizing feature (which still stabilizes cleaved sCLU after reduction) does not participate in the stabilization of uncleaved sCLU. Furthermore, the fact that the FC recognition site is extensively conserved but no adverse effect upon chaperone activity was detectable (except under reducing conditions) suggests that the proteolytic cleavage is necessary to allow both chains to establish further intramolecular interactions between areas of the protein which

are conserved in a similar fashion as the FC recognition site, and are located in close proximity. The only features which are in line with the requirements are AH2 and AH3.

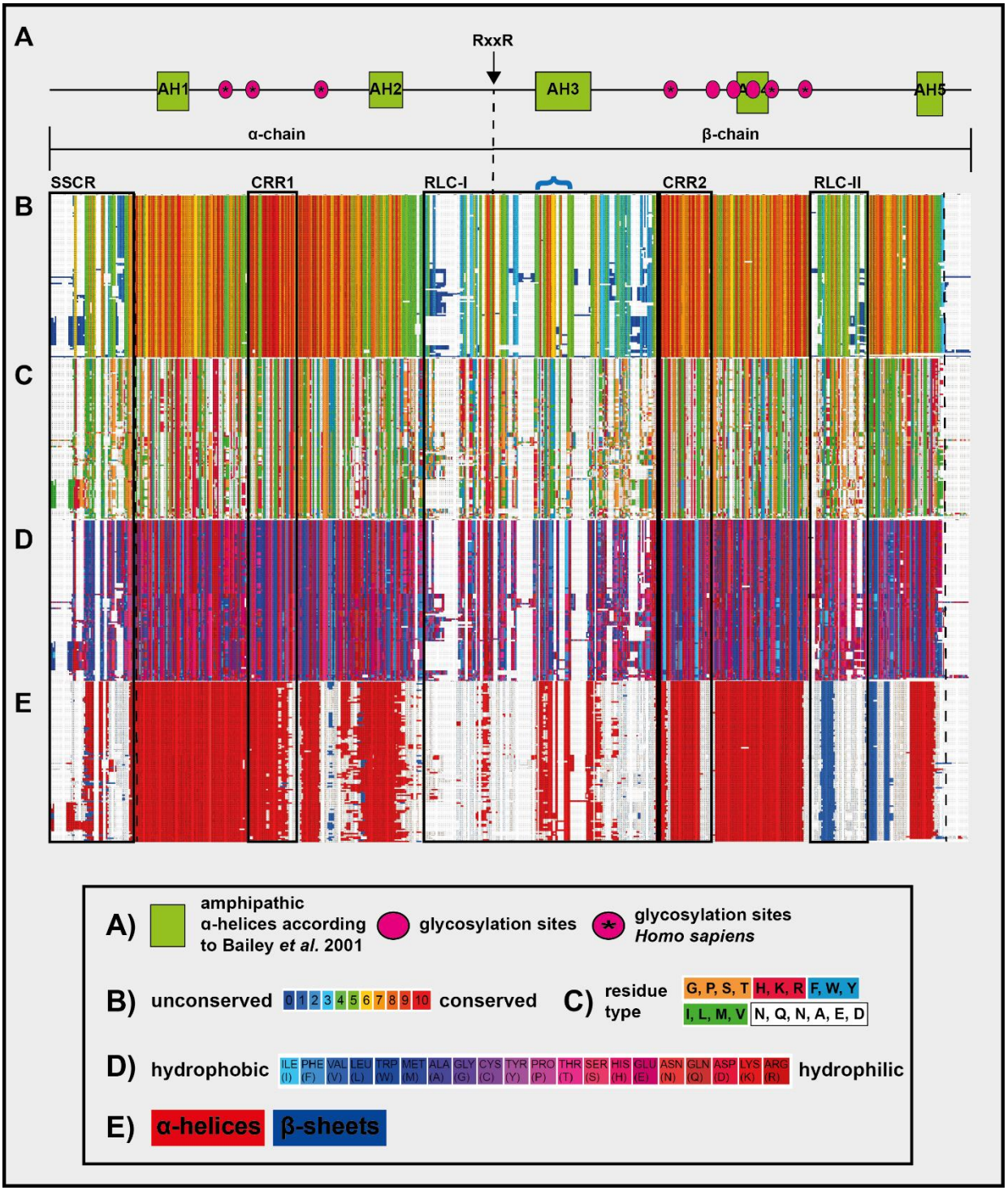

Fig.38 Alignment of the 105 species and calculation/prediction of (B) conservation, (C) residue type, (D) hydrophobicity and (E) secondary structures using PRALINE (see section 4.4). (A) Depiction of full-length CLU with notable features. AH amphipathic α-helix; SSCR signal sequence-coding region; CCR cysteine-rich region; RLC region of low conservation; RxxR FC recognition site. The blue curly bracket indicates the area within AH3 displaying elevated hydrophobicity.

A possible explanation for the observed effect is illustrated in Fig.39 according to Rohne *et al.* 2016 [19].

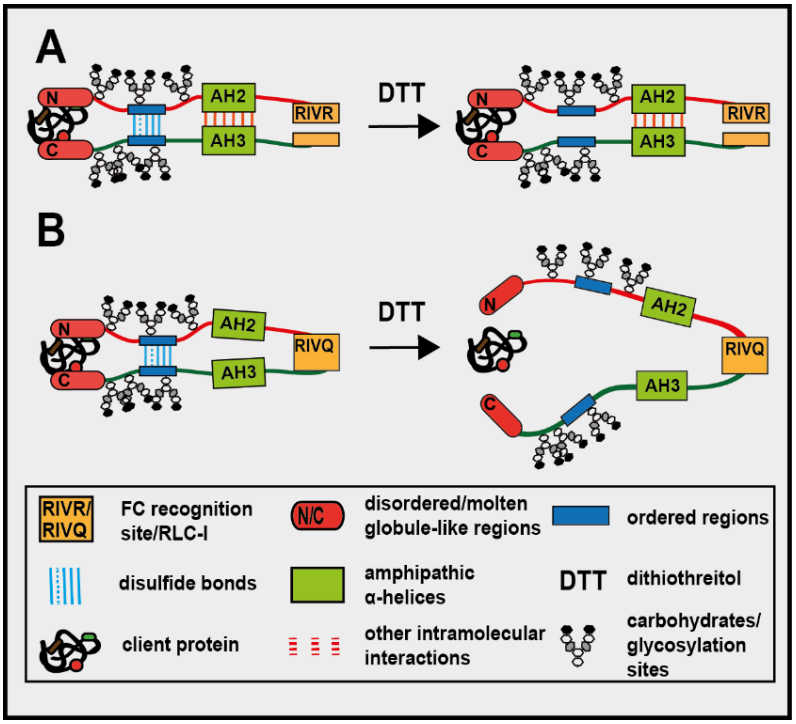

Fig.39 Schematic depiction of sCLU chaperone activity and hypothetical influence of structural elements.

As argued above additional structural elements are involved in sCLU chaperone activity which are no prerequisite under non-reducing conditions but crucial once the disulfide bonds are reduced. The assessment of the complete CLU protein sequence finally revealed that the amphipathic domains or other neighboring regions may be responsible for sCLU protein stabilization (Fig.39A), but will not be established if the proteolytic cleavage is abolished (Fig.39B). The slight increase in fluorescence as measured in Fig.24B. is probably the result of ANS binding to AH3.

6.1.4 sCLU is an evolutionary conserved extracellular chaperone

As shown via bioinformatic and biochemical approaches, sCLU is evolutionary conserved and acts as a molecular chaperone, potentially among all craniate classes. The most crucial elements for sCLU chaperone activity probably are: 1) N-terminal coiled-coil α-helices, C-terminal stretches of 2) α-helices and 3) β-sheets, as well as 4) N-glycosylation. Moreover, under conditions which might reduce the disulfide bonds it was observable that additional elements might be of importance for sCLU chaperone activity. These elements likely are the amphipathic α-helices 2 and 3 (see Fig.38). However, the exact role of these helices has not been figured out experimentally in this thesis but was partially addressed in the thesis of Benjamin Renner (in preparation).

Moreover, it was shown in an additional bioinformatic approach that the CLU-like protein (CLUL1) displays similar structural features as enumerated above (see also App.4&5). Nevertheless, the fact that the proteolytic cleavage within CLUL1 was mainly found in fishes, raises the assumption that the proteolytic cleavage site within the CLU protein was the decisive “structural innovation” which finally led to the ubiquitous expression of the CLU protein whereas CLUL1 is solely expressed in the retina nowadays. However, it is important to note that CLUL1 is poorly investigated (only 5 publications thus far). A biochemical characterization (especially of the chaperone activity) of CLUL1 has not been carried out, and was conducted in the case of the sCLU protein solely in humans (and presently also in mice as seen above). To verify the assumptions discussed in this thesis, it would be of importance to clone, express and purify sCLU of other animals as well as CLUL1 and experimentally confirm the alleged chaperone activity. Moreover, the creation of truncated human sCLU constructs (for instance at the N- and C-terminus) would be proof for the assumed role of the above classified crucial elements. Additionally, it must be noted that in some animals tested (*Oncorhynchus mykiss*, *Alligator mississippiensis*, *Loxodonta Africana* & *Nomascus leucogenys*) no SSCR was found. This notion is of importance since it would imply that sCLU is not necessary a secretory protein in all animals. At least in the case of *Loxodonta Africana* (African elephant) and *Nomascus leucogenys* (Northern white-cheeked gibbon), it is of interest, because a specialization of the CLU protein was implied for mammalians in this thesis (for instance higher glycosylation rate). Nonetheless, it remains speculative until it is experimentally verified whether these CLU forms can be secreted or not. In the case of *Oncorhynchus mykiss* (Rainbow trout, see [231]), a basic characterization was conducted but it was not carried out whether it is secreted from the cell.

6.2 sCLU: A Biomarker of necrotic cell death?

As already described in the Introduction (1.7 & 1.8), CLU (especially sCLU) is an alleged key player in the face of tissue damage, inflammation and necrosis. Especially, its role in necrosis is of increasing interest due to correlations of sCLU expression/secretion in animal models and clinical studies facing “uncontrolled” cell death (see 1.8 and [19, 190]). In context with the above (6.1) discussed necessity of the proteolytic cleavage for sCLU chaperone activity under reducing conditions (please note that the intracellular environment is predominantly reductive [232, 233]), it was further tested how CLU is regulated and sCLU is secreted from the cell in the case of necrosis. In addition, potential influences of CLU on the faith of the cells were investigated but no decisive effect was observable (App.7B-D, data not shown). Nevertheless, a plethora of surprising observations were made concerning CLU regulation and beyond.

Please note that the following section contains excerpts of the article: Rohne *et al.* 2017 *"Exposure of Vital Cells to Necrotic Cell Lysates Induces the IRE1α Branch of the Unfolded Protein Response and Cell Proliferation"*.

6.2.1 CLU is upregulated by JNK signaling upon necrosis even in the presence of UPR

For years sitting on the "back shelf" of cell death research, necrotic cell death now emerges demonstrating to be a more and more coordinated and sophisticated cell death mechanism with a huge potential in biomedical research [112]. Involved in this setting is the extracellular chaperone Clusterin (CLU), which is highly correlated with necrosis, tissue degeneration and apoptosis [19, 85]. CLU is found to exert a cytoprotective role by helping to heal damaged tissue as well as clearing the extracellular space from apoptotic cells, protein aggregates, and cellular debris [66, 67, 70, 74, 100, 234]. To find a regulatory link between these two research fields, it was of interest to characterize the response mechanisms in vital cells to ongoing tissue necrosis. As a model system, necrotic cell lysates obtained from freeze/thawed HEK-293 cells were applied to vital HEK-293 cells (Fig.25). As observed *in vivo*, a transcriptional upregulation of CLU has been demonstrated in this model (Fig.26E). Furthermore, an activation of the JNK/SAPK signaling pathway as well as a heat shock response and evidence for the involvement of these pathways in CLU upregulation by using the JNK inhibitor SP600125 was detected (Fig.26A-C). An involvement of NF-κB as seen in similar experiments by Zhou *et al.* 2015 could not be confirmed (Fig.26E, 26G & 33C).

Furthermore, it was demonstrated in this thesis that cells stimulated with necrotic cell lysates suffer ER stress which results in the specific induction of the IRE1α branch of UPR (Fig.27A, B, D&E). Interestingly, it was shown by Alnasser *et al.* 2016 [168] that CLU might be part of this cellular response. On the basis of decreased IRE1α phosphorylation in CLU knockout cells under ischemic conditions they proposed that CLU might act as a supporting chaperone in the UPR. By using the IRE1α kinase inhibitor Kira6, a decline in CLU expression was indeed observable (Fig.27D). More recently, it was suggested that severe ER stress induced by Thapsigargin abolishes CLU upregulation and prevents its secretion [17, 158], a finding that was also supported in this thesis (Fig. 27A&C). It can therefore be argued, that CLU expression and sCLU secretion can only be present or promoted under "mildly" ER stress encompassing solely the IRE1α branch, but is inhibited by the induction of the PERK branch. Please note that until the findings of Alnasser *et al.* 2016 [168] and the data presented in this thesis, it was assumed that sCLU expression and secretion will be inhibited in the case of UPR [17, 158].

Even though the alleged IRE1α-specific kinase inhibitor Kira6 [140] diminished necrotic cell lysate-mediated CLU upregulation, other approaches to prove the IRE1α-CLU axis

failed. IRE1α overexpression had no adverse or promoting effect on CLU upregulation and sCLU secretion (Fig.28C) which at least confirms the suggestion above that the presence of an UPR does not abolish CLU expression. The usage of another IRE1α kinase inhibitor (APY29) revealed that this inhibitor indeed acts in an opposite manner by enhancing IRE1α and JNK phosphorylation after co-application with necrotic cell lysates (Fig.28A). The reason for this phenomenon is most likely that APY29 promotes IRE1α oligomerization which is a prerequisite for IRE1α autophosphorylation [128, 141, 219]. As in the case of Kira6-specifity, APY29 was (to the knowledge of the author of this thesis) never or solely insufficiently tested on eukaryotic cells. As will be discussed below, Kira6 also inhibits a plethora of other signaling pathways. APY29 for its part, also promotes the phosphorylation of other targets as ERK1/2 and S6 (App.7F). Please note, that to the knowledge of the author of this thesis it has never been shown that IRE1α activates ERK1/2 signaling. Inhibitor-based studies of signal transduction pathways can therefore be assumed to be misleading. Nevertheless, APY29 application increases XBP1 splicing, IRE1α phosphorylation and (once more) has only little impact on CLU upregulation and secretion (declines from a concentration of 1 µM APY29, the ID_{50} however is 280 nM [219], Fig.28A&B). Intriguingly, at the dosage of 1.0 µM APY29, XBP1 was no longer detectable via sqRT-PCR (Fig.28B), indicating that it was either no longer expressed or degraded. IRE1α is capable for unspecific degradation of RNA to prevent an ongoing overload with proteins in the ER upon UPR, a mechanism called RIDD (see 1.9.2). Nonetheless, application of necrotic cell lysates prevents the complete absence of XBP1 but does not keep XBP1 splicing upright (Fig.28B). This finding implies a turning point in UPR where presumed pro-survival XBP1 splicing by IRE1α turns into potential pro-death JNK phosphorylation and RIDD (Fig.7 and [128, 157]). Not surprisingly, APY29 lowers the cell viability in a dose-dependent manner (App.7E). It is important to mention that sCLU secretion is presumably in accordance with CLU mRNA translation (Fig.27E, impaired sCLU secretion after application of Cycloheximide). This result suggests that even under conditions of increasing ER stress CLU is still upregulated, translated and secreted proving once more that CLU upregulation/secretion and UPR is no contradiction (in this context see also 6.2.3). Further experiments using IRE1α-specific siRNA successfully prevents necrotic cell lysate-mediated XBP1 splicing and BiP upregulation but leaves CLU upregulation unaltered (Fig.28D&E). Nonetheless, as shown in Western blot analyses in Fig.28D, IRE1α phosphorylation was almost unaltered allowing therefore no conclusion (please note that a Phospho-IRE1α → JNK mechanisms underlies the present experimental approaches).

Taken together, necrotic cell lysates induce the JNK signaling pathway and the IRE1α branch of UPR, a final confirmation for an UPR-CLU axis is still missing but various approaches prove that CLU upregulation and sCLU secretion can still occur upon UPR which was at least barely confirmed thus far.

6.2.2 Necrosis-induced Proliferation (NiP): A novel mechanism?

The observed induction of stress pathways as described above raises the question whether vital cells exposed to necrotic cell lysates display an elevated level of cell death or apoptosis. Testing whether the necrotic stress causes increased apoptosis, revealed that the cell number and viability was enhanced (Fig.29B, C&D, Fig.31D&E). No significant apoptosis was detectable (Fig.29A&B). In contrast, it was measured that the cells indeed start to proliferate (Fig.29E). Important pathways stimulating cell proliferation are the ERK1/2 and the mTOR signaling pathway [222]. Not surprisingly, it was observed that necrotic cell lysates indeed induce the ERK1/2 and the mTOR signaling pathway, whereas the FBS control solely induces the mTOR signaling pathway (Fig.31A). Moreover, concurrent with mTOR phosphorylation, the phosphorylation of p70/p85S6K and S6 is enhanced (Fig.31A). In this context, it should be mentioned that the ERK1/2 and the mTOR signaling pathway are working together to eventually phosphorylate S6 (see also Fig.40). ERK1/2 phosphorylates the residues Thr421/Ser424 at the autoinhibitory domain of the p70S6 kinase to render the kinase accessible for mTOR-mediated phosphorylation at Thr389 which serves as a platform for PDK1 for full activation of the p70S6 kinase and subsequent S6 phosphorylation (Fig.31A) [235, 236]. The phosphorylation of ERK1/2 however, occurs already at low concentrations of necrotic cell lysates and is accompanied by Thr421/Ser424 phosphorylation of the p70S6 kinase (Fig.31A). This confirms a decisive role of ERK1/2 in the mTOR/p70S6 kinase/S6 signaling pathway (Fig.31A). It is important to note that a decrease in ERK1/2-, p70/p85S6K, and S6 phosphorylation after using the IRE1α kinase inhibitor Kira6 was observable (Fig.31B). Importantly, the use of the mTOR inhibitor Rapamycin indeed prevents p70/p85S6K and S6 phosphorylation, but in contrast to Kira6 (Fig.31D), does not abrogate the entire increase in cell viability (Fig.31E). The viability of cells, therefore, probably relies on ERK1/2 activity. In contrast, no benefit of CLU or IRE1α upon cell viability was observable (Fig.30A-C). These findings are in accordance with previous observations of our group that CLU has no influence on BAX-mediated apoptosis [11]. This notion was supported after observing that CLU, independent of its subcellular location, is not capable to alter cell viability (App.7A-D). Nonetheless, in cell aggregation experiments (Fig.30E) it was reproduced that CLU actually promotes cell aggregation [2]. These data, taken together, imply that the cell viability/cell proliferation-enhancing key pathways are most likely the ERK1/2 and the mTOR signaling pathway.

Intriguingly, it was recently shown in drosophila and in human cancer cells that apoptotic cells release growth stimulating signals into the extracellular fluid resulting in repopulation, a process that might be crucial to tissue reconstruction and remodeling, but is harmful when occurring during tumor therapy [220, 221]. To the knowledge of the author, it has up to now never been considered whether cells undergoing necrotic cell death can likewise directly promote proliferation of surrounding cells. The fact that the

ERK1/2 and the mTOR signal transduction pathway are activated immediately after application of necrotic cell lysates implies that necrotic cells release mitogenic signaling molecules directly into the extracellular space that exert the proliferative effect. Furthermore, inhibiting apoptosis with the pan caspase inhibitor Q-VD-OPh did not suppress the induction of cell proliferation (Fig.30D) demonstrating that it is mediated by components of the necrotic cell lysate rather than being a secondary effect initiated by apoptotic cells. To describe this process, the following term was proposed: Necrosis-induced Proliferation (NiP). For the first time, it was therefore shown that the induction of proliferation of vital surrounding cells initiated by dying neighboring cells is not restricted to caspase 3-dependent apoptosis as a primary stimulus (Fig.30D).
In summary, these results broaden the knowledge on compensatory proliferation induced by apoptotic cells to cells undergoing accidental cell death and therefore have the same profound implications on the therapy of tumors. Along these lines, the most intriguing aspect of these findings are that they suggest promising novel approaches for diagnosis and therapy of unwanted compensatory proliferation by using sCLU as a biomarker in diagnosis and Kira6 resp. derivatives to counteract detrimental compensatory proliferative pathways.

6.2.3 The routes of NiP

After characterizing pathways and targets involved in the mechanisms of the so-called NiP, it was of interest which factors and receptors are involved or more precisely which routes are tracked. In this context, it was at first of interest what kind of substance is responsible for NiP. As depicted in Fig.32 it was found that a protein (necrotic cell lysates digested with Chymotrypsin) is responsible for ERK1/2, p70/p85S6K, S6 and JNK phosphorylation but not for the phosphorylation of mTOR. Moreover, it was shown that after Chymotrypsin digestion, CLU transcriptional upregulation and XBP1 splicing but not sCLU secretion was impaired. These findings imply that at least one route for phosphorylation of EKR1/2 (and others), sCLU upregulation and the IRE1α branch and another route for mTOR phosphorylation and sCLU secretion is induced. The latter case comprises most likely two routes because inhibition of mTOR by Rapamycin does not abrogate sCLU secretion (App.7H). Comparable effects were obtained in SK-N-MC cells (App.6J), indicating that the effects presumably can be expected in other cell lines. Indeed, this was the case. ERK1/2, p70/p85S6K and S6 phosphorylation occurs in SK-N-MC, HeLa, MCF-7 and HEK-293 cells, but not in HepG2 and PC-3 cells (App.7G). A sole macroscopic assessment of the cell culture medium of SK-N-MC cells revealed that after 12 hours of exposure to necrotic cell lysates (obtained from HEK-293 cells) the color of the medium turns yellow (indicates increased accumulation of acid) which was not the case in BSA or FBS controls (App.6I). Nevertheless, it must be mentioned that the factor which induces NiP is not ubiquitous expressed. Nevertheless, the wanted factor

is expressed in HEK-293, HeLa and PC-3 cells, but not in SK-N-MC, MCF-7 or HepG2 cells (Fig.33A&B). However, after testing the respective cell lysates on HEK-293 cells the described NiP effect, CLU transcriptional upregulation and XBP1 splicing was observable (Fig.33A&B). Surprisingly, even in the supernatants of HEK-293 cells stimulated with cell lysates which are not suitable to elevate CLU expression or induce NiP, an increased sCLU secretion was detectable (Fig.33A). The same phenomenon was observable after using CLU reporter constructs (Fig.33C), heating of necrotic cell lysates prior to application (Fig.33E) and in cell lines lacking CLU transcriptional upregulation after stimulation with necrotic cell lysates (Fig.33F&G).
Taken together, these findings imply that the transcriptional upregulation is distinct from sCLU secretion.
The search for the wanted factor was however, not of success. By combining the test of established DAMPs (App.6C-G), size exclusion chromatography (Fig.35), cell dying assays (Fig.36) and transcriptome analytics (Fig.37) the following proposal can be made. The wanted factor is a protein in the size of 20 kDa to 50 kDa, its cellular location is probably close to the cell surface or the factor is secreted. Furthermore, the wanted factor is no DAMP as HSP72, S100A8/S100A9, HMGB1 or Calreticulin [237]. Transcriptome-based analyses further provide one very promising candidate protein, namely the membrane-bound regulatory protein FXYD5 (also known as Dysadherin) which was found to be involved in cancer progression [238]. Interestingly, the sqRT-PCR revealed that FXYD5 is indeed only transcribed in NiP-inducing necrotic cell lysates. After cloning however, our working group has been closed which prevented the further testing and reproduction in cell culture. Nonetheless, the cloned FXYD5 construct and additional information can be obtained upon request. The potential NiP effect and beyond pathways are illustrated in Fig.40.

6.2.4 Is NiP the underlying mechanism of the *“oncogene CLU delusion”*?

Over time, CLU was considered as a key player in tumorigenesis and chemoresistance [239]. The arguments pointing to oncogene-like actions of the CLU protein were predominately based on findings of elevated CLU expression in tumors [86, 87, 90-93], suggested participation of CLU in apoptosis inhibition [126] and an alleged role as a signal transducer which correlates to multiple signal transduction pathways, e.g. induction of the PI3K/AKT [72, 95, 96, 240, 241] and the ERK1/2 [71, 94, 96] signaling pathway, modulation of the NF-κB signaling pathway [242-244], as well as elevated MMP-9 [96, 245] and VEGF [246] expression. Nevertheless, there were also studies published which show no correlation to cancer or cancer-related pathways, and even contradictory results [11, 247, 248]. Intriguingly, phase III clinical studies targeting CLU in various cancers, failed [100]. Moreover, in our group we have found no indication for the promotion of cell survival or increased proliferation in accordance to CLU overexpression or application of

purified sCLU (unpublished data, Fig.30A&B, App.7B-D, [11, 174, 176, 186]). Solely minor modulations of S6 phosphorylation were observed ([176, 249], App.7D). Nonetheless, as already mentioned above, in clinical studies CLU targeting shows no benefit for cancer treatment [100, 250]. These findings imply that CLU is probably no oncogene, a notion which was supported just recently [100]. Moreover, it must be assumed that a mass spectroscopic analyses of sCLU preparations from our lab at the Max Planck Institute for Biophysics in Frankfurt (Main) revealed multiple protein impurities (App.8). Among them are most abundantly histones, Fatty synthase, Tenascin-C and Filamin-A but also heat shock proteins, growth factors as well as DAMPs (such as HSP72, HMGB1 or Calreticulin) were found. Please note, that blank purification never provided sufficient protein yield (5.1.1.2). The indicated proteins are therefore potential sCLU client proteins. Especially, in the case of histones it was recently confirmed that sCLU binds to histone proteins presented on apoptotic cells to mediate their removal [70]. It must be emphasized that none of the publications above ever conducted comparable analyses of their purified sCLU samples and only occasionally conducted control experiments such as sCLU deglycosylation. The possibility of potential side effects has therefore never been excluded.

The most important question therefore is: Why is CLU expression often correlated to cancer? With an *in vitro* necrosis cell death assay it was shown that at least HEK-293 and SK-N-MC cells undergo a novel compensatory mechanism called NiP (Necrosis-induced Proliferation). In accordance with the occurrence of NiP, the cells display increased CLU transcriptional upregulation (HEK-293) and spontaneous sCLU secretion (HEK-293, SK-N-MC & EA.hy926). In the past, it was indeed suggested that necrotic cell death might contribute to tumorigenesis and metastasis [114, 251-253]. Nevertheless, the promotion of necrotic cell death is currently considered as a contributive mode of action for targeting tumors by triggering an immune response [237, 254]. However, it must be taken into consideration that increased necrosis in tumors might induce NiP. NiP in turn, could display CLU transcriptional upregulation and sCLU secretion. The notion that necrotic cell lysates contribute to cell viability has actually already been made in the past [190]. However, this thesis is the first which describe potential contributive signal transduction pathways, such as the ERK1/2 and the mTOR signaling pathway. A schematic depiction of these findings is illustrated in Fig.40.

Nonetheless, challenging questions remain: Which are the underlying receptors involved in the mechanisms as described above? Please note, that TLR4 can be excluded, as shown in App.6C&D. A receptor search using the available transcriptome datasets proved to be difficult. Other questions are: Which further events are responsible for sCLU secretion? As demonstrated in the case of neurons [255], elevated calcium concentrations promote transmitter release. This finding however, was not the case for sCLU secretion (Fig.33G, data not shown). Moreover, it is challenging whether a link of

IRE1α to CLU expression really exists? Furthermore, it is of interest which other cellular programs/mechanisms are affected? Beside the signal transduction pathways described above an inhibition of autophagy caused by necrotic cell lysates was observed by decreased LC3 lipidation (App.6H). One of the most important questions however is, whether this model is applicable to other cell lines and even to the clinic? And most strikingly, is the question concerning which factor(s) facilitates these effects? Especially, the first and the last question are presumably of great importance. As suggested above (5.2.10), FXYD5 could be a promising candidate for NiP and perhaps for the other effects as well. It is fundamental to address this issue to prove whether NiP is indeed adverse in cancer therapy. A determination of NiP-associated molecules in samples of tumor patients would allow to choose therapeutic options which avoid the occurrence of NiP and can therefore improve tumor therapy.

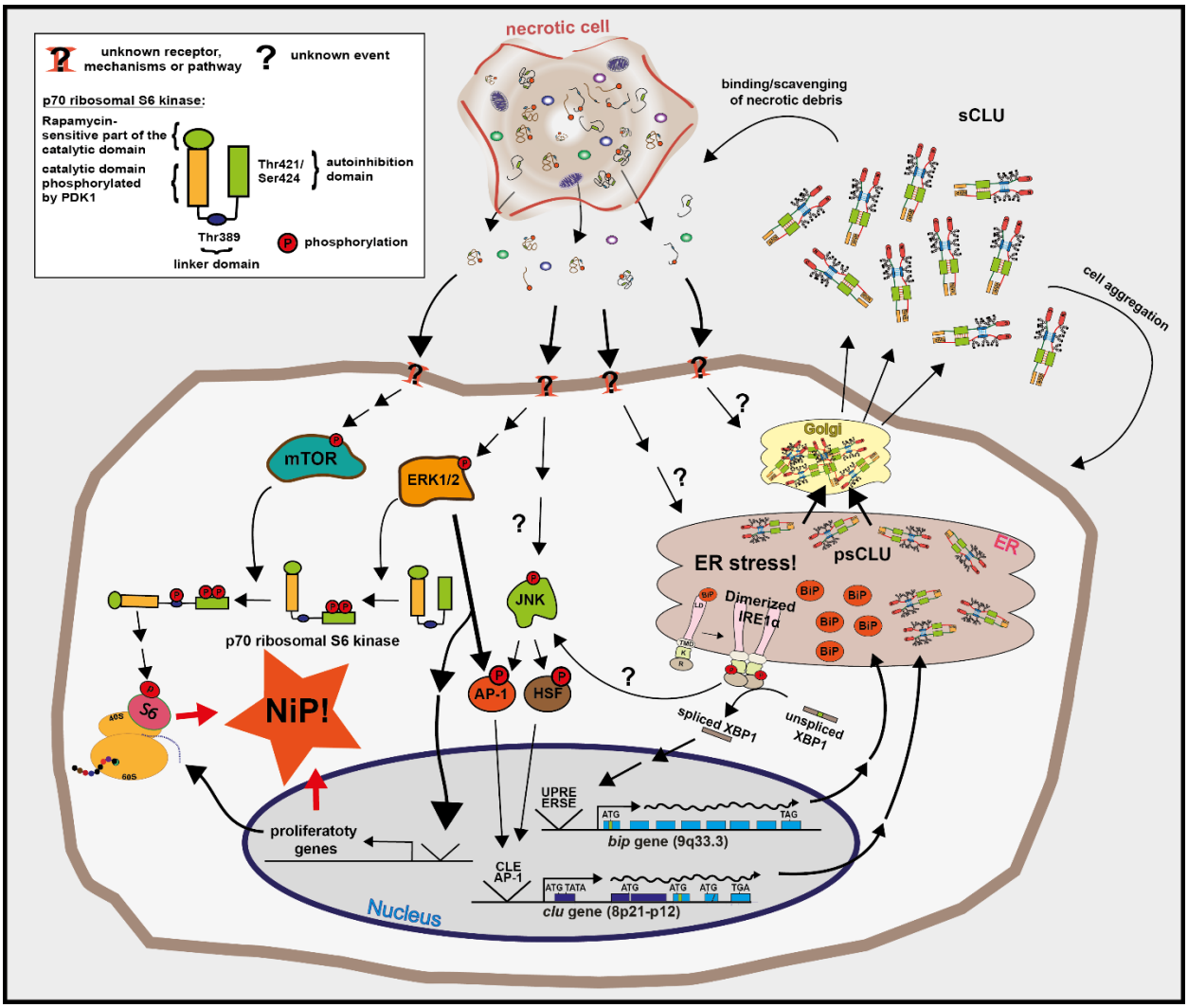

Fig.40 Potential mechanism of NiP and further responses of cells stimulated with necrotic cell lysates.

7 Summary

In this thesis two main issues in CLU biology were addressed: 1st The evolution, structure and chaperone activity of secretory CLU (sCLU) and consequently 2nd the potential role of CLU in molecular cell biology. Concerning the 1st issue it was shown that sCLU is a highly conserved extracellular chaperone whose evolution started more than 425 million years ago. Key components in the CLU protein were elucidated to be crucial for sCLU chaperone activity, namely the proteolytic cleavage and the N-glycosylation. Both features, among additional features, such as N-and C-terminal α-helices, N-terminal coiled-coil domains, C-terminal β-sheets, cysteine-rich regions and areas of high intrinsic disorder, are highly conserved from fishes to humans. The surprising finding that the inhibition of the proteolytic cleavage of sCLU reveals a high sensitivity towards reducing conditions, eventually led to the 2nd issue, namely the assessment of sCLU's role in necrosis (a condition with presumably turns the extracellular space in a more reducing environment). By stimulating vital HEK-293 cells with cell lysates obtained from necrotic cells, increased CLU transcriptional upregulation and secretion was found. Further, it was shown that the upregulation of CLU is in line with the induction of the JNK signaling pathway and the heat shock response. Moreover, the induction of the IRE1α branch of the unfolded protein response (UPR) was shown. Nevertheless, the most intriguing finding was a proliferatory response of the cells towards necrotic cell lysates and concomitant activation of the ERK1/2 and the mTOR signaling pathway, a mechanism now termed *Necrosis-induced Proliferation* (NiP). However, no influence of CLU on the cellular response was observable. Nonetheless, it was demonstrated that sCLU binds a plethora of the proteins within necrotic cell lysates and displays a cell aggregating function as described in the very beginning of CLU research (1983) leading to its name. Eventually, it can be concluded that sCLU is a conserved extracellular chaperone, which is secreted from the cell upon cell damage (necrosis) even in the presence of UPR. Additionally, necrotic conditions are capable of enhancing cell proliferation. Secretory CLU for its part presumably plays an important role in removing cellular debris and in promoting wound healing, for instance by mediating cell aggregation.

8 References

1. Hogg, S.D. and G. Embery, *The isolation and partial characterization of a sulphated glycoprotein from human whole saliva which aggregates strains of Streptococcus sanguis but not Streptococcus mutans.* Arch Oral Biol, 1979. **24**(10-11): p. 791-7.
2. Blaschuk, O., K. Burdzy, and I.B. Fritz, *Purification and characterization of a cell-aggregating factor (clusterin), the major glycoprotein in ram rete testis fluid.* J Biol Chem, 1983. **258**(12): p. 7714-20.
3. Fritz, I.B., et al., *Ram rete testis fluid contains a protein (clusterin) which influences cell-cell interactions in vitro.* Biol Reprod, 1983. **28**(5): p. 1173-88.
4. Urban, J., et al., *Constitutive apical secretion of an 80-kD sulfated glycoprotein complex in the polarized epithelial Madin-Darby canine kidney cell line.* J Cell Biol, 1987. **105**(6 Pt 1): p. 2735-43.
5. Jenne, D.E. and J. Tschopp, *Molecular structure and functional characterization of a human complement cytolysis inhibitor found in blood and seminal plasma: identity to sulfated glycoprotein 2, a constituent of rat testis fluid.* Proc Natl Acad Sci U S A, 1989. **86**(18): p. 7123-7.
6. Leger, J.G., M.L. Montpetit, and M.P. Tenniswood, *Characterization and cloning of androgen-repressed mRNAs from rat ventral prostate.* Biochem Biophys Res Commun, 1987. **147**(1): p. 196-203.
7. de Silva, H.V., et al., *A 70-kDa apolipoprotein designated ApoJ is a marker for subclasses of human plasma high density lipoproteins.* J Biol Chem, 1990. **265**(22): p. 13240-7.
8. Fritz, I.B. and B. Murphy, *Clusterin Insights into a multifunctional protein.* Trends Endocrinol Metab, 1993. **4**(2): p. 41-5.
9. Dietzsch, E., et al., *Regional localization of the gene for clusterin (SP-40,40; gene symbol CLI) to human chromosome 8p12-->p21.* Cytogenet Cell Genet, 1992. **61**(3): p. 178-9.
10. Tobe, T., et al., *Assignment of a human serum glycoprotein SP-40,40 gene (CLI) to chromosome 8.* Cytogenet Cell Genet, 1991. **57**(4): p. 193-5.
11. Prochnow, H., et al., *Non-secreted clusterin isoforms are translated in rare amounts from distinct human mRNA variants and do not affect Bax-mediated apoptosis or the NF-kappaB signaling pathway.* PLoS One, 2013. **8**(9): p. e75303.
12. Burkey, B.F., H.V. deSilva, and J.A. Harmony, *Intracellular processing of apolipoprotein J precursor to the mature heterodimer.* J Lipid Res, 1991. **32**(6): p. 1039-48.
13. Choi-Miura, N.H., et al., *Identification of the disulfide bonds in human plasma protein SP-40,40 (apolipoprotein-J).* J Biochem, 1992. **112**(4): p. 557-61.
14. Kapron, J.T., et al., *Identification and characterization of glycosylation sites in human serum clusterin.* Protein Sci, 1997. **6**(10): p. 2120-33.
15. Lakins, J., et al., *Clusterin biogenesis is altered during apoptosis in the regressing rat ventral prostate.* J Biol Chem, 1998. **273**(43): p. 27887-95.
16. Sabatte, J., et al., *Semen clusterin is a novel DC-SIGN ligand.* J Immunol, 2011. **187**(10): p. 5299-309.
17. Nizard, P., et al., *Stress-induced retrotranslocation of clusterin/ApoJ into the cytosol.* Traffic, 2007. **8**(5): p. 554-65.
18. Li, N., et al., *GRP78 regulates clusterin stability, retrotranslocation and mitochondrial localization under ER stress in prostate cancer.* Oncogene, 2013. **32**(15): p. 1933-42.
19. Rohne, P., H. Prochnow, and C. Koch-Brandt, *The CLU-files: disentanglement of a mystery.* Biomol Concepts, 2016. **7**(1): p. 1-15.

20. Dunker, A.K., et al., *Intrinsically disordered protein.* J Mol Graph Model, 2001. **19**(1): p. 26-59.
21. Humphreys, D.T., et al., *Clusterin has chaperone-like activity similar to that of small heat shock proteins.* J Biol Chem, 1999. **274**(11): p. 6875-81.
22. Poon, S., et al., *Clusterin is an ATP-independent chaperone with very broad substrate specificity that stabilizes stressed proteins in a folding-competent state.* Biochemistry, 2000. **39**(51): p. 15953-60.
23. Poon, S., et al., *Clusterin is an extracellular chaperone that specifically interacts with slowly aggregating proteins on their off-folding pathway.* FEBS Lett, 2002. **513**(2-3): p. 259-66.
24. Bailey, R.W., et al., *Clusterin, a binding protein with a molten globule-like region.* Biochemistry, 2001. **40**(39): p. 11828-40.
25. Wilson, M.R. and S.B. Easterbrook-Smith, *Clusterin is a secreted mammalian chaperone.* Trends Biochem Sci, 2000. **25**(3): p. 95-8.
26. Carver, J.A., et al., *Small heat-shock proteins and clusterin: intra- and extracellular molecular chaperones with a common mechanism of action and function?* IUBMB Life, 2003. **55**(12): p. 661-8.
27. Dabbs, R.A. and M.R. Wilson, *Expression and purification of chaperone-active recombinant clusterin.* PLoS One, 2014. **9**(1): p. e86989.
28. Hochgrebe, T., et al., *pH-dependent changes in the in vitro ligand-binding properties and structure of human clusterin.* Biochemistry, 2000. **39**(6): p. 1411-9.
29. Wyatt, A.R., J.J. Yerbury, and M.R. Wilson, *Structural characterization of clusterin-chaperone client protein complexes.* J Biol Chem, 2009. **284**(33): p. 21920-7.
30. Calero, M., et al., *Functional and structural properties of lipid-associated apolipoprotein J (clusterin).* Biochem J, 1999. **344 Pt 2**: p. 375-83.
31. Stewart, E.M., et al., *Effects of glycosylation on the structure and function of the extracellular chaperone clusterin.* Biochemistry, 2007. **46**(5): p. 1412-22.
32. Jordan-Starck, T.C., et al., *Mouse apolipoprotein J: characterization of a gene implicated in atherosclerosis.* J Lipid Res, 1994. **35**(2): p. 194-210.
33. Atlas-White, M., B.F. Murphy, and H.W. Baker, *Localisation of clusterin in normal human sperm by immunogold electron microscopy.* Pathology, 2000. **32**(4): p. 258-61.
34. Law, G.L. and M.D. Griswold, *Activity and form of sulfated glycoprotein 2 (clusterin) from cultured Sertoli cells, testis, and epididymis of the rat.* Biol Reprod, 1994. **50**(3): p. 669-79.
35. Rosenberg, M.E. and J. Silkensen, *Clusterin: physiologic and pathophysiologic considerations.* Int J Biochem Cell Biol, 1995. **27**(7): p. 633-45.
36. Choi, N.H., et al., *Sandwich ELISA assay for quantitative measurement of SP-40,40 in seminal plasma and serum.* J Immunol Methods, 1990. **131**(2): p. 159-63.
37. O'Bryan, M.K., et al., *Human seminal clusterin (SP-40,40). Isolation and characterization.* J Clin Invest, 1990. **85**(5): p. 1477-86.
38. Cheng, C.Y., et al., *Rat clusterin isolated from primary Sertoli cell-enriched culture medium is sulfated glycoprotein-2 (SGP-2).* Biochem Biophys Res Commun, 1988. **155**(1): p. 398-404.
39. Michel, D., et al., *Stress-induced transcription of the clusterin/apoJ gene.* Biochem J, 1997. **328 (Pt 1)**: p. 45-50.
40. Loison, F., et al., *Up-regulation of the clusterin gene after proteotoxic stress: implication of HSF1-HSF2 heterocomplexes.* Biochem J, 2006. **395**(1): p. 223-31.
41. Jin, G. and P.H. Howe, *Transforming growth factor beta regulates clusterin gene expression via modulation of transcription factor c-Fos.* Eur J Biochem, 1999. **263**(2): p. 534-42.

42. Cervellera, M., et al., *Direct transactivation of the anti-apoptotic gene apolipoprotein J (clusterin) by B-MYB.* J Biol Chem, 2000. **275**(28): p. 21055-60.
43. Shaulian, E. and M. Karin, *AP-1 as a regulator of cell life and death.* Nat Cell Biol, 2002. **4**(5): p. E131-6.
44. Shaulian, E., et al., *The mammalian UV response: c-Jun induction is required for exit from p53-imposed growth arrest.* Cell, 2000. **103**(6): p. 897-907.
45. Schiff, R., et al., *Oxidative stress and AP-1 activity in tamoxifen-resistant breast tumors in vivo.* J Natl Cancer Inst, 2000. **92**(23): p. 1926-34.
46. Oh, I.H. and E.P. Reddy, *The myb gene family in cell growth, differentiation and apoptosis.* Oncogene, 1999. **18**(19): p. 3017-33.
47. Wong, P., et al., *Genomic organization and expression of the rat TRPM-2 (clusterin) gene, a gene implicated in apoptosis.* J Biol Chem, 1993. **268**(7): p. 5021-31.
48. Schepeler, T., et al., *Clusterin expression can be modulated by changes in TCF1-mediated Wnt signaling.* J Mol Signal, 2007. **2**: p. 6.
49. Shiota, M., et al., *Clusterin is a critical downstream mediator of stress-induced YB-1 transactivation in prostate cancer.* Mol Cancer Res, 2011. **9**(12): p. 1755-66.
50. Kim, G., et al., *SREBP-1c regulates glucose-stimulated hepatic clusterin expression.* Biochem Biophys Res Commun, 2011. **408**(4): p. 720-5.
51. Takeuchi, A., et al., *Insulin-like growth factor-I induces CLU expression through Twist1 to promote prostate cancer growth.* Mol Cell Endocrinol, 2014. **384**(1-2): p. 117-25.
52. Wong, P., et al., *Molecular characterization of human TRPM-2/clusterin, a gene associated with sperm maturation, apoptosis and neurodegeneration.* Eur J Biochem, 1994. **221**(3): p. 917-25.
53. Li, X., et al., *IKKalpha, IKKbeta, and NEMO/IKKgamma are each required for the NF-kappa B-mediated inflammatory response program.* J Biol Chem, 2002. **277**(47): p. 45129-40.
54. Lymar, E.S., et al., *Clusterin gene in rat sertoli cells is regulated by a core-enhancer element.* Biol Reprod, 2000. **63**(5): p. 1341-51.
55. Rosemblit, N. and C.L. Chen, *Regulators for the rat clusterin gene: DNA methylation and cis-acting regulatory elements.* J Mol Endocrinol, 1994. **13**(1): p. 69-76.
56. Park, J., et al., *Hypoxia inducible factor-1alpha directly regulates nuclear clusterin transcription by interacting with hypoxia response elements in the clusterin promoter.* Mol Cells, 2014. **37**(2): p. 178-86.
57. Cochrane, D.R., et al., *Differential regulation of clusterin and its isoforms by androgens in prostate cells.* J Biol Chem, 2007. **282**(4): p. 2278-87.
58. Rauhala, H.E., et al., *Clusterin is epigenetically regulated in prostate cancer.* Int J Cancer, 2008. **123**(7): p. 1601-9.
59. Bonacini, M., et al., *Distinct promoters, subjected to epigenetic regulation, drive the expression of two clusterin mRNAs in prostate cancer cells.* Biochim Biophys Acta, 2015. **1849**(1): p. 44-54.
60. Nuutinen, T., et al., *Induction of clusterin/apoJ expression by histone deacetylase inhibitors in neural cells.* Neurochem Int, 2005. **47**(8): p. 528-38.
61. Suuronen, T., et al., *Epigenetic regulation of clusterin/apolipoprotein J expression in retinal pigment epithelial cells.* Biochem Biophys Res Commun, 2007. **357**(2): p. 397-401.
62. Sylvester, S.R., et al., *Localization of sulfated glycoprotein-2 (clusterin) on spermatozoa and in the reproductive tract of the male rat.* Biol Reprod, 1991. **45**(1): p. 195-207.
63. de Silva, H.V., et al., *Purification and characterization of apolipoprotein J.* J Biol Chem, 1990. **265**(24): p. 14292-7.

64. Danik, M., et al., *Human gliomas and epileptic foci express high levels of a mRNA related to rat testicular sulfated glycoprotein 2, a purported marker of cell death.* Proc Natl Acad Sci U S A, 1991. **88**(19): p. 8577-81.
65. Palmer, D.J. and D.L. Christie, *Identification of molecular aggregates containing glycoproteins III, J, K (carboxypeptidase H), and H (Kex2-related proteases) in the soluble and membrane fractions of adrenal medullary chromaffin granules.* J Biol Chem, 1992. **267**(28): p. 19806-12.
66. Bartl, M.M., et al., *Multiple receptors mediate apoJ-dependent clearance of cellular debris into nonprofessional phagocytes.* Exp Cell Res, 2001. **271**(1): p. 130-41.
67. Baiersdorfer, M., et al., *Toll-like receptor 3 mediates expression of clusterin/apolipoprotein J in vascular smooth muscle cells stimulated with RNA released from necrotic cells.* Exp Cell Res, 2010. **316**(20): p. 3489-500.
68. Wyatt, A.R., et al., *Clusterin facilitates in vivo clearance of extracellular misfolded proteins.* Cell Mol Life Sci, 2011. **68**(23): p. 3919-31.
69. Merlotti, A., et al., *Fucosylated clusterin in semen promotes the uptake of stress-damaged proteins by dendritic cells via DC-SIGN.* Hum Reprod, 2015. **30**(7): p. 1545-56.
70. Cunin, P., et al., *Clusterin facilitates apoptotic cell clearance and prevents apoptotic cell-induced autoimmune responses.* Cell Death Dis, 2016. **7**: p. e2215.
71. Shim, Y.J., et al., *Epidermal growth factor receptor is involved in clusterin-induced astrocyte proliferation.* Neuroreport, 2009. **20**(4): p. 435-9.
72. Ammar, H. and J.L. Closset, *Clusterin activates survival through the phosphatidylinositol 3-kinase/Akt pathway.* J Biol Chem, 2008. **283**(19): p. 12851-61.
73. Tung, P.S., et al., *Competition between cell-substratum interactions and cell-cell interactions.* J Cell Physiol, 1992. **152**(2): p. 410-21.
74. Viard, I., et al., *Clusterin gene expression mediates resistance to apoptotic cell death induced by heat shock and oxidative stress.* J Invest Dermatol, 1999. **112**(3): p. 290-6.
75. Zlokovic, B.V., et al., *Glycoprotein 330/megalin: probable role in receptor-mediated transport of apolipoprotein J alone and in a complex with Alzheimer disease amyloid beta at the blood-brain and blood-cerebrospinal fluid barriers.* Proc Natl Acad Sci U S A, 1996. **93**(9): p. 4229-34.
76. Bauskar, A., et al., *Clusterin Seals the Ocular Surface Barrier in Mouse Dry Eye.* PLoS One, 2015. **10**(9): p. e0138958.
77. Schottler, S., et al., *Protein adsorption is required for stealth effect of poly(ethylene glycol)- and poly(phosphoester)-coated nanocarriers.* Nat Nanotechnol, 2016. **11**(4): p. 372-7.
78. Kreuter, J., et al., *Apolipoprotein-mediated transport of nanoparticle-bound drugs across the blood-brain barrier.* J Drug Target, 2002. **10**(4): p. 317-25.
79. Leskov, K.S., et al., *Synthesis and functional analyses of nuclear clusterin, a cell death protein.* J Biol Chem, 2003. **278**(13): p. 11590-600.
80. Zhang, F., et al., *Clusterin facilitates stress-induced lipidation of LC3 and autophagosome biogenesis to enhance cancer cell survival.* Nat Commun, 2014. **5**: p. 5775.
81. Hochgrebe, T.T., et al., *A reexamination of the role of clusterin as a complement regulator.* Exp Cell Res, 1999. **249**(1): p. 13-21.
82. Polihronis, M., et al., *Elevation of human cerebrospinal fluid clusterin concentration is associated with acute neuropathology.* J Neurol Sci, 1993. **115**(2): p. 230-3.
83. Hammad, S.M., et al., *Interaction of apolipoprotein J-amyloid beta-peptide complex with low density lipoprotein receptor-related protein-2/megalin. A mechanism to prevent pathological accumulation of amyloid beta-peptide.* J Biol Chem, 1997. **272**(30): p. 18644-9.

84. Yerbury, J.J., et al., *The extracellular chaperone clusterin influences amyloid formation and toxicity by interacting with prefibrillar structures.* FASEB J, 2007. **21**(10): p. 2312-22.
85. Woody, S.K. and L. Zhao, *Clusterin (APOJ) in Alzheimer's Disease: An Old Molecule with a New Role*. Update on Dementia. 2016.
86. Kadomatsu, K., et al., *Expression of sulfated glycoprotein 2 is associated with carcinogenesis induced by N-nitroso-N-methylurea in rat prostate and seminal vesicle.* Cancer Res, 1993. **53**(7): p. 1480-3.
87. Redondo, M., et al., *Overexpression of clusterin in human breast carcinoma.* Am J Pathol, 2000. **157**(2): p. 393-9.
88. Chen, X., et al., *Clusterin as a biomarker in murine and human intestinal neoplasia.* Proc Natl Acad Sci U S A, 2003. **100**(16): p. 9530-5.
89. Xie, M.J., et al., *Expression of clusterin in human pancreatic cancer.* Pancreas, 2002. **25**(3): p. 234-8.
90. Xie, D., et al., *Up-regulated expression of cytoplasmic clusterin in human ovarian carcinoma.* Cancer, 2005. **103**(2): p. 277-83.
91. Kang, Y.K., et al., *Overexpression of clusterin in human hepatocellular carcinoma.* Hum Pathol, 2004. **35**(11): p. 1340-6.
92. Parczyk, K., et al., *Gp80 (clusterin; TRPM-2) mRNA level is enhanced in human renal clear cell carcinomas.* J Cancer Res Clin Oncol, 1994. **120**(3): p. 186-8.
93. July, L.V., et al., *Nucleotide-based therapies targeting clusterin chemosensitize human lung adenocarcinoma cells both in vitro and in vivo.* Mol Cancer Ther, 2004. **3**(3): p. 223-32.
94. Chou, T.Y., et al., *Clusterin silencing in human lung adenocarcinoma cells induces a mesenchymal-to-epithelial transition through modulating the ERK/Slug pathway.* Cell Signal, 2009. **21**(5): p. 704-11.
95. Wang, C., et al., *Clusterin facilitates metastasis by EIF3I/Akt/MMP13 signaling in hepatocellular carcinoma.* Oncotarget, 2015. **6**(5): p. 2903-16.
96. Shim, Y.J., et al., *Clusterin induces matrix metalloproteinase-9 expression via ERK1/2 and PI3K/Akt/NF-kappaB pathways in monocytes/macrophages.* J Leukoc Biol, 2011. **90**(4): p. 761-9.
97. Trougakos, I.P., et al., *Intracellular clusterin inhibits mitochondrial apoptosis by suppressing p53-activating stress signals and stabilizing the cytosolic Ku70-Bax protein complex.* Clin Cancer Res, 2009. **15**(1): p. 48-59.
98. Park, D.C., et al., *Clusterin interacts with Paclitaxel and confer Paclitaxel resistance in ovarian cancer.* Neoplasia, 2008. **10**(9): p. 964-72.
99. Gleave, M. and H. Miyake, *Use of antisense oligonucleotides targeting the cytoprotective gene, clusterin, to enhance androgen- and chemo-sensitivity in prostate cancer.* World J Urol, 2005. **23**(1): p. 38-46.
100. Wilson, M.R. and A. Zoubeidi, *Clusterin as a therapeutic target.* Expert Opin Ther Targets, 2016: p. 1-13.
101. Hamada, N., et al., *Loss of clusterin limits atherosclerosis in apolipoprotein E-deficient mice via reduced expression of Egr-1 and TNF-alpha.* J Atheroscler Thromb, 2011. **18**(3): p. 209-16.
102. Schwarz, M., et al., *Potential protective role of apoprotein J (clusterin) in atherogenesis: binding to enzymatically modified low-density lipoprotein reduces fatty acid-mediated cytotoxicity.* Thromb Haemost, 2008. **100**(1): p. 110-8.
103. McLaughlin, L., et al., *Apolipoprotein J/clusterin limits the severity of murine autoimmune myocarditis.* J Clin Invest, 2000. **106**(9): p. 1105-13.
104. Van Dijk, A., et al., *Intravenous clusterin administration reduces myocardial infarct size in rats.* Eur J Clin Invest, 2010. **40**(10): p. 893-902.

105. Nguan, C.Y., et al., *Promotion of cell proliferation by clusterin in the renal tissue repair phase after ischemia-reperfusion injury.* Am J Physiol Renal Physiol, 2014. **306**(7): p. F724-33.
106. Li, S., et al., *Reduction of cold ischemia-reperfusion injury by graft-expressing clusterin in heart transplantation.* J Heart Lung Transplant, 2011. **30**(7): p. 819-26.
107. Guan, Q., et al., *Decrease in donor heart injury by recombinant clusterin protein in cold preservation with University of Wisconsin solution.* Surgery, 2012. **151**(3): p. 364-71.
108. Wehrli, P., et al., *Inhibition of post-ischemic brain injury by clusterin overexpression.* Nat Med, 2001. **7**(9): p. 977-9.
109. Imhof, A., et al., *Sustained astrocytic clusterin expression improves remodeling after brain ischemia.* Neurobiol Dis, 2006. **22**(2): p. 274-83.
110. Han, B.H., et al., *Clusterin contributes to caspase-3-independent brain injury following neonatal hypoxia-ischemia.* Nat Med, 2001. **7**(3): p. 338-43.
111. Rosenberg, M.E., et al., *Apolipoprotein J/clusterin prevents a progressive glomerulopathy of aging.* Mol Cell Biol, 2002. **22**(6): p. 1893-902.
112. Vanden Berghe, T., et al., *Regulated necrosis: the expanding network of non-apoptotic cell death pathways.* Nat Rev Mol Cell Biol, 2014. **15**(2): p. 135-47.
113. Rock, K.L. and H. Kono, *The inflammatory response to cell death.* Annu Rev Pathol, 2008. **3**: p. 99-126.
114. Srikrishna, G. and H.H. Freeze, *Endogenous damage-associated molecular pattern molecules at the crossroads of inflammation and cancer.* Neoplasia, 2009. **11**(7): p. 615-28.
115. Kalyanaraman, B., *Teaching the basics of redox biology to medical and graduate students: Oxidants, antioxidants and disease mechanisms.* Redox Biol, 2013. **1**(1): p. 244-57.
116. Chen, G.Y. and G. Nunez, *Sterile inflammation: sensing and reacting to damage.* Nat Rev Immunol, 2010. **10**(12): p. 826-37.
117. Mari, M., et al., *Redox control of liver function in health and disease.* Antioxid Redox Signal, 2010. **12**(11): p. 1295-331.
118. Calvo, E.L., et al., *Clusterin overexpression in rat pancreas during the acute phase of pancreatitis and pancreatic development.* Eur J Biochem, 1998. **254**(2): p. 282-9.
119. Bach, U.C., et al., *Apoptotic cell debris and phosphatidylserine-containing lipid vesicles induce apolipoprotein J (clusterin) gene expression in vital fibroblasts.* Exp Cell Res, 2001. **265**(1): p. 11-20.
120. Zhou, J., et al., *HMGB1 induction of clusterin creates a chemoresistant niche in human prostate tumor cells.* Sci Rep, 2015. **5**: p. 15085.
121. Deegan, S., et al., *Stress-induced self-cannibalism: on the regulation of autophagy by endoplasmic reticulum stress.* Cell Mol Life Sci, 2013. **70**(14): p. 2425-41.
122. Marino, G., et al., *Self-consumption: the interplay of autophagy and apoptosis.* Nat Rev Mol Cell Biol, 2014. **15**(2): p. 81-94.
123. Hetz, C., E. Chevet, and S.A. Oakes, *Proteostasis control by the unfolded protein response.* Nat Cell Biol, 2015. **17**(7): p. 829-38.
124. Niforou, K., C. Cheimonidou, and I.P. Trougakos, *Molecular chaperones and proteostasis regulation during redox imbalance.* Redox Biol, 2014. **2**: p. 323-32.
125. Richter, K., M. Haslbeck, and J. Buchner, *The heat shock response: life on the verge of death.* Mol Cell, 2010. **40**(2): p. 253-66.
126. Trougakos, I.P., et al., *Non-enzymatic post-translational protein modifications and proteostasis network deregulation in carcinogenesis.* J Proteomics, 2013. **92**: p. 274-98.
127. Wyatt, A.R., et al., *Extracellular chaperones and proteostasis.* Annu Rev Biochem, 2013. **82**: p. 295-322.

128. Hetz, C., *The unfolded protein response: controlling cell fate decisions under ER stress and beyond.* Nat Rev Mol Cell Biol, 2012. **13**(2): p. 89-102.
129. D., R., *The endoplasmic reticulum unfolded protein response and neurodegeneration*, in *Protein Quality Control in Neurodegenerative Diseases, Research and Perspectives in Alzheimer's Disease*, R.I.M.a.Y. Christen, Editor. 2013, Springer-Verlag Berlin Heidelberg.
130. Kozutsumi, Y., et al., *The presence of malfolded proteins in the endoplasmic reticulum signals the induction of glucose-regulated proteins.* Nature, 1988. **332**(6163): p. 462-4.
131. Cox, J.S., C.E. Shamu, and P. Walter, *Transcriptional Induction of Genes Encoding Endoplasmic-Reticulum Resident Proteins Requires a Transmembrane Protein-Kinase.* Cell, 1993. **73**(6): p. 1197-1206.
132. Mori, K., et al., *A Transmembrane Protein with a Cdc2+/Cdc28-Related Kinase-Activity Is Required for Signaling from the Er to the Nucleus.* Cell, 1993. **74**(4): p. 743-756.
133. Sidrauski, C. and P. Walter, *The transmembrane kinase Ire1p is a site-specific endonuclease that initiates mRNA splicing in the unfolded protein response.* Cell, 1997. **90**(6): p. 1031-9.
134. Sidrauski, C., J.S. Cox, and P. Walter, *tRNA ligase is required for regulated mRNA splicing in the unfolded protein response.* Cell, 1996. **87**(3): p. 405-13.
135. Nikawa, J., et al., *Saccharomyces cerevisiae IRE2/HAC1 is involved in IRE1-mediated KAR2 expression.* Nucleic Acids Res, 1996. **24**(21): p. 4222-6.
136. Cox, J.S. and P. Walter, *A novel mechanism for regulating activity of a transcription factor that controls the unfolded protein response.* Cell, 1996. **87**(3): p. 391-404.
137. Tirasophon, W., A.A. Welihinda, and R.J. Kaufman, *A stress response pathway from the endoplasmic reticulum to the nucleus requires a novel bifunctional protein kinase/endoribonuclease (Ire1p) in mammalian cells.* Genes Dev, 1998. **12**(12): p. 1812-24.
138. Shamu, C.E. and P. Walter, *Oligomerization and phosphorylation of the Ire1p kinase during intracellular signaling from the endoplasmic reticulum to the nucleus.* EMBO J, 1996. **15**(12): p. 3028-39.
139. Welihinda, A.A. and R.J. Kaufman, *The unfolded protein response pathway in Saccharomyces cerevisiae. Oligomerization and trans-phosphorylation of Ire1p (Ern1p) are required for kinase activation.* J Biol Chem, 1996. **271**(30): p. 18181-7.
140. Ghosh, R., et al., *Allosteric inhibition of the IRE1alpha RNase preserves cell viability and function during endoplasmic reticulum stress.* Cell, 2014. **158**(3): p. 534-48.
141. Korennykh, A.V., et al., *The unfolded protein response signals through high-order assembly of Ire1.* Nature, 2009. **457**(7230): p. 687-U2.
142. Papa, F.R., et al., *Bypassing a kinase activity with an ATP-competitive drug.* Science, 2003. **302**(5650): p. 1533-1537.
143. Yoshida, H., et al., *XBP1 mRNA is induced by ATF6 and spliced by IRE1 in response to ER stress to produce a highly active transcription factor.* Cell, 2001. **107**(7): p. 881-91.
144. Urano, F., et al., *Coupling of stress in the ER to activation of JNK protein kinases by transmembrane protein kinase IRE1.* Science, 2000. **287**(5453): p. 664-6.
145. Bertolotti, A., et al., *Dynamic interaction of BiP and ER stress transducers in the unfolded-protein response.* Nat Cell Biol, 2000. **2**(6): p. 326-32.
146. Okamura, K., et al., *Dissociation of Kar2p/BiP from an ER sensory molecule, Ire1p, triggers the unfolded protein response in yeast.* Biochem Biophys Res Commun, 2000. **279**(2): p. 445-50.
147. Kimata, Y., et al., *Two regulatory steps of ER-stress sensor Ire1 involving its cluster formation and interaction with unfolded proteins.* J Cell Biol, 2007. **179**(1): p. 75-86.

148. Oikawa, D., et al., *Activation of mammalian IRE1alpha upon ER stress depends on dissociation of BiP rather than on direct interaction with unfolded proteins.* Exp Cell Res, 2009. **315**(15): p. 2496-504.
149. Harding, H.P., Y. Zhang, and D. Ron, *Protein translation and folding are coupled by an endoplasmic-reticulum-resident kinase.* Nature, 1999. **397**(6716): p. 271-4.
150. Harding, H.P., et al., *Regulated translation initiation controls stress-induced gene expression in mammalian cells.* Mol Cell, 2000. **6**(5): p. 1099-108.
151. Novoa, I., et al., *Feedback inhibition of the unfolded protein response by GADD34-mediated dephosphorylation of eIF2alpha.* J Cell Biol, 2001. **153**(5): p. 1011-22.
152. Lin, J.H., et al., *IRE1 signaling affects cell fate during the unfolded protein response.* Science, 2007. **318**(5852): p. 944-9.
153. Haze, K., et al., *Mammalian transcription factor ATF6 is synthesized as a transmembrane protein and activated by proteolysis in response to endoplasmic reticulum stress.* Mol Biol Cell, 1999. **10**(11): p. 3787-99.
154. Ye, J., et al., *ER stress induces cleavage of membrane-bound ATF6 by the same proteases that process SREBPs.* Mol Cell, 2000. **6**(6): p. 1355-64.
155. Shen, J., et al., *Stable binding of ATF6 to BiP in the endoplasmic reticulum stress response.* Mol Cell Biol, 2005. **25**(3): p. 921-32.
156. So, J.S., et al., *Silencing of lipid metabolism genes through IRE1alpha-mediated mRNA decay lowers plasma lipids in mice.* Cell Metab, 2012. **16**(4): p. 487-99.
157. Sano, R. and J.C. Reed, *ER stress-induced cell death mechanisms.* Biochim Biophys Acta, 2013. **1833**(12): p. 3460-70.
158. Genereux, J.C., et al., *Unfolded protein response-induced ERdj3 secretion links ER stress to extracellular proteostasis.* EMBO J, 2015. **34**(1): p. 4-19.
159. Martinon, F., et al., *TLR activation of the transcription factor XBP1 regulates innate immune responses in macrophages.* Nat Immunol, 2010. **11**(5): p. 411-8.
160. Luo, H., et al., *Extracellular deposition of mouse senile AApoAII amyloid fibrils induced different unfolded protein responses in the liver, kidney, and heart.* Lab Invest, 2015. **95**(3): p. 320-33.
161. Muller, C., et al., *HDLs inhibit endoplasmic reticulum stress and autophagic response induced by oxidized LDLs.* Cell Death Differ, 2011. **18**(5): p. 817-28.
162. Xue, X., et al., *Tumor necrosis factor alpha (TNFalpha) induces the unfolded protein response (UPR) in a reactive oxygen species (ROS)-dependent fashion, and the UPR counteracts ROS accumulation by TNFalpha.* J Biol Chem, 2005. **280**(40): p. 33917-25.
163. Teixeira, P.F., et al., *Endoplasmic reticulum stress associated with extracellular aggregates. Evidence from transthyretin deposition in familial amyloid polyneuropathy.* J Biol Chem, 2006. **281**(31): p. 21998-2003.
164. Zhu, X.M., et al., *Endoplasmic reticulum stress and its regulator XBP-1 contributes to dendritic cell maturation and activation induced by high mobility group box-1 protein.* Int J Biochem Cell Biol, 2012. **44**(7): p. 1097-105.
165. Karali, E., et al., *VEGF Signals through ATF6 and PERK to promote endothelial cell survival and angiogenesis in the absence of ER stress.* Mol Cell, 2014. **54**(4): p. 559-72.
166. Lipson, K.L., et al., *Regulation of insulin biosynthesis in pancreatic beta cells by an endoplasmic reticulum-resident protein kinase IRE1.* Cell Metab, 2006. **4**(3): p. 245-54.
167. Fonseca, A.C., et al., *Activation of the endoplasmic reticulum stress response by the amyloid-beta 1-40 peptide in brain endothelial cells.* Biochim Biophys Acta, 2013. **1832**(12): p. 2191-203.
168. Alnasser, H.A., et al., *Requirement of clusterin expression for prosurvival autophagy in hypoxic kidney tubular epithelial cells.* Am J Physiol Renal Physiol, 2016. **310**(2): p. F160-73.

169. Senft, D. and Z.A. Ronai, *UPR, autophagy, and mitochondria crosstalk underlies the ER stress response.* Trends Biochem Sci, 2015. **40**(3): p. 141-8.
170. Hirota, M., et al., *Quantitative measurement of spliced XBP1 mRNA as an indicator of endoplasmic reticulum stress.* J Toxicol Sci, 2006. **31**(2): p. 149-56.
171. Sidrauski, C., et al., *Pharmacological brake-release of mRNA translation enhances cognitive memory.* Elife, 2013. **2**: p. e00498.
172. van Schadewijk, A., et al., *A quantitative method for detection of spliced X-box binding protein-1 (XBP1) mRNA as a measure of endoplasmic reticulum (ER) stress.* Cell Stress Chaperones, 2012. **17**(2): p. 275-9.
173. Klug-Micu, G., *Versuche zur Funktion von Clusterin in Humanzellinien durch einen Knockdownansatz. [Diploma Thesis University of Mainz]*. 2010.
174. Prochnow, H., *Charakterisierung und funktionelle Analyse verschiedener Isoformen von Clusterin (Apolipoprotein J). [Doctoral Thesis University of Mainz]*. 2014.
175. Niemeier, A., et al., *Identification of megalin/gp330 as a receptor for lipoprotein(a) in vitro.* Arterioscler Thromb Vasc Biol, 1999. **19**(3): p. 552-61.
176. Rohne, P., *Untersuchung der durch Apolipoprotein J modulierten Signalwege und beteiligten Lipoprotein-Rezeptoren in Dottersackzellen der Maus. [Diploma Thesis University of Mainz]*. 2012.
177. Towbin, H., T. Staehelin, and J. Gordon, *Electrophoretic transfer of proteins from polyacrylamide gels to nitrocellulose sheets: procedure and some applications.* Proc Natl Acad Sci U S A, 1979. **76**(9): p. 4350-4.
178. Müller-Esterl, W., *Biochemie: Eine Einführung für Mediziner und Naturwissenschaftler*. 2004: Spektrum Akademischer Verlag.
179. Gomperts, B., I. Kramer, and P. Tatham, *Signal Transdcution*. Second Edition ed. 2009: Academic Press.
180. Gollan, R., *Mechanisms behind T cell-mediated neuroinflammation. [Doctoral Thesis University of Mainz]*. 2015.
181. Wolf, S., *Einfluss des JNK/SAPK-Signalweges auf die Clusterinexpression in nekrotischem Gewebe. [Diploma Thesis University of Mainz]*. 2014.
182. Chen, C.J., et al., *Identification of a key pathway required for the sterile inflammatory response triggered by dying cells.* Nat Med, 2007. **13**(7): p. 851-6.
183. Debruyne, D., et al., *Cell aggregation on agar as an indicator for cell-matrix adhesion: effects of opioids.* In Vitro Cell Dev Biol Anim, 2009. **45**(8): p. 473-82.
184. Debruyne, D., T. Boterberg, and M.E. Bracke, *Cell aggregation assays.* Methods Mol Biol, 2014. **1070**: p. 77-92.
185. Schmittgen, T.D. and K.J. Livak, *Analyzing real-time PCR data by the comparative C(T) method.* Nat Protoc, 2008. **3**(6): p. 1101-8.
186. Prochnow, H., *Expression und Charakterisierung humaner Apolipoprotein J - Isoformen. [Diploma Thesis University of Mainz]*. 2009.
187. Zhu, B., et al., *In-fusion assembly: seamless engineering of multidomain fusion proteins, modular vectors, and mutations.* Biotechniques, 2007. **43**(3): p. 354-9.
188. Winter, R. and F. Noll, *Methoden der Biophysikalischen Chemie*. 1998, Stuttgart: Teubner Studienbücher.
189. Rohne, P., et al., *The chaperone activity of clusterin is dependent on glycosylation and redox environment.* Cell Physiol Biochem, 2014. **34**(5): p. 1626-39.
190. Baiersdorfer, M., *Charakterisierung der Apolipoprotein J-Genregulation in Fibroblasten und glatten Gefäßmuskelzellen durch nekrotische Zellen und Toll-like Rezeptoren. [Doctoral Thesis University of Mainz]*. 2006.

191. Whitmore, L. and B.A. Wallace, *Protein secondary structure analyses from circular dichroism spectroscopy: methods and reference databases.* Biopolymers, 2008. **89**(5): p. 392-400.
192. Whitmore, L. and B.A. Wallace, *DICHROWEB, an online server for protein secondary structure analyses from circular dichroism spectroscopic data.* Nucleic Acids Res, 2004. **32**(Web Server issue): p. W668-73.
193. Petersen, T.N., et al., *SignalP 4.0: discriminating signal peptides from transmembrane regions.* Nat Methods, 2011. **8**(10): p. 785-6.
194. Gupta, R., *Prediction of N-glycosylation sites in human proteins.* http://www.cbs.dtu.dk/services/NetNGlyc/, 2004.
195. Duckert, P., S. Brunak, and N. Blom, *Prediction of proprotein convertase cleavage sites.* Protein Eng Des Sel, 2004. **17**(1): p. 107-12.
196. Marchler-Bauer, A., et al., *CDD/SPARCLE: functional classification of proteins via subfamily domain architectures.* Nucleic Acids Res, 2017. **45**(D1): p. D200-D203.
197. Marchler-Bauer, A. and S.H. Bryant, *CD-Search: protein domain annotations on the fly.* Nucleic Acids Res, 2004. **32**(Web Server issue): p. W327-31.
198. Marchler-Bauer, A., et al., *CDD: NCBI's conserved domain database.* Nucleic Acids Res, 2015. **43**(Database issue): p. D222-6.
199. Marchler-Bauer, A., et al., *CDD: a Conserved Domain Database for the functional annotation of proteins.* Nucleic Acids Res, 2011. **39**(Database issue): p. D225-9.
200. Pei, J. and N.V. Grishin, *AL2CO: calculation of positional conservation in a protein sequence alignment.* Bioinformatics, 2001. **17**(8): p. 700-12.
201. Simossis, V.A., J. Kleinjung, and J. Heringa, *Homology-extended sequence alignment.* Nucleic Acids Res, 2005. **33**(3): p. 816-24.
202. Simossis, V.A. and J. Heringa, *PRALINE: a multiple sequence alignment toolbox that integrates homology-extended and secondary structure information.* Nucleic Acids Res, 2005. **33**(Web Server issue): p. W289-94.
203. Pirovano, W. and J. Heringa, *Protein secondary structure prediction.* Methods Mol Biol, 2010. **609**: p. 327-48.
204. Dosztanyi, Z., et al., *IUPred: web server for the prediction of intrinsically unstructured regions of proteins based on estimated energy content.* Bioinformatics, 2005. **21**(16): p. 3433-4.
205. Dosztanyi, Z., et al., *The pairwise energy content estimated from amino acid composition discriminates between folded and intrinsically unstructured proteins.* J Mol Biol, 2005. **347**(4): p. 827-39.
206. Drozdetskiy, A., et al., *JPred4: a protein secondary structure prediction server.* Nucleic Acids Res, 2015. **43**(W1): p. W389-94.
207. Anisimova, M. and O. Gascuel, *Approximate likelihood-ratio test for branches: A fast, accurate, and powerful alternative.* Syst Biol, 2006. **55**(4): p. 539-52.
208. Castresana, J., *Selection of conserved blocks from multiple alignments for their use in phylogenetic analysis.* Mol Biol Evol, 2000. **17**(4): p. 540-52.
209. Chevenet, F., et al., *TreeDyn: towards dynamic graphics and annotations for analyses of trees.* BMC Bioinformatics, 2006. **7**: p. 439.
210. Dereeper, A., et al., *BLAST-EXPLORER helps you building datasets for phylogenetic analysis.* BMC Evol Biol, 2010. **10**: p. 8.
211. Dereeper, A., et al., *Phylogeny.fr: robust phylogenetic analysis for the non-specialist.* Nucleic Acids Res, 2008. **36**(Web Server issue): p. W465-9.
212. Edgar, R.C., *MUSCLE: multiple sequence alignment with high accuracy and high throughput.* Nucleic Acids Res, 2004. **32**(5): p. 1792-7.

213. Guindon, S. and O. Gascuel, *A simple, fast, and accurate algorithm to estimate large phylogenies by maximum likelihood.* Syst Biol, 2003. **52**(5): p. 696-704.
214. Dawkins, R., *The ancestor's tale : a pilgrimage to the dawn of evolution*. 2004, Boston: Houghton Mifflin. xii, 673 p.
215. Scott, W.B. and E.J. Crossman, *Freshwater Fishes of Canada. Bulletin 184. Fisheries Research Board of Canada 1973. 966 pp, Bulletin 184: Ottawa, ON; Copy of the property of the Government of Canada*. 1973.
216. *Picture of Callorhinchus milii*. https://upload.wikimedia.org/wikipedia/commons/d/da/Callorhinchus_milii_%28Australian_ghost_shark%29.gif.
217. *Picture of Chiloscylium plagiosum*. https://commons.wikimedia.org/wiki/File:Chiloscyllium_plagiosum2.jpg.
218. Benton, M., *Vertebrate Palaeontology*. Fourth Edition ed. 2015: WILEY Blackwell.
219. Wang, L., et al., *Divergent allosteric control of the IRE1alpha endoribonuclease using kinase inhibitors.* Nat Chem Biol, 2012. **8**(12): p. 982-9.
220. Ryoo, H.D., T. Gorenc, and H. Steller, *Apoptotic cells can induce compensatory cell proliferation through the JNK and the Wingless signaling pathways.* Dev Cell, 2004. **7**(4): p. 491-501.
221. Huang, Q., et al., *Caspase 3-mediated stimulation of tumor cell repopulation during cancer radiotherapy.* Nat Med, 2011. **17**(7): p. 860-6.
222. Mendoza, M.C., E.E. Er, and J. Blenis, *The Ras-ERK and PI3K-mTOR pathways: cross-talk and compensation.* Trends Biochem Sci, 2011. **36**(6): p. 320-8.
223. Hartmann, J., *Vergleichende Charakterisierung der Regulation des Apolipoprotein J in humanen Zelllinien und Primärzellen. [Diploma Thesis University of Mainz]*. 2013.
224. Wilhelm, M., et al., *Mass-spectrometry-based draft of the human proteome.* Nature, 2014. **509**(7502): p. 582-7.
225. Savage, N., *Proteomics: High-protein research.* Nature, 2015. **527**(7576): p. S6-7.
226. Zhang, Q., et al., *Comparative analysis and expression of CLUL1, a cone photoreceptor-specific gene.* Invest Ophthalmol Vis Sci, 2003. **44**(10): p. 4542-9.
227. Siltberg-Liberles, J., *Evolution of structurally disordered proteins promotes neostructuralization.* Mol Biol Evol, 2011. **28**(1): p. 59-62.
228. Aronow, B.J., et al., *Apolipoprotein J expression at fluid-tissue interfaces: potential role in barrier cytoprotection.* Proc Natl Acad Sci U S A, 1993. **90**(2): p. 725-9.
229. Sturgill, G.M., et al., *Mutation screen of the cone-specific gene, CLUL1, in 376 patients with age-related macular degeneration.* Ophthalmic Genet, 2006. **27**(4): p. 151-5.
230. Zhang, Q., et al., *Molecular cloning, characterization and expression of a novel retinal clusterin-like protein cDNA.* Gene, 2000. **243**(1-2): p. 151-60.
231. Londou, A., A. Mikrou, and I.K. Zarkadis, *Cloning and characterization of two clusterin isoforms in rainbow trout.* Mol Immunol, 2008. **45**(2): p. 470-8.
232. Lopez-Mirabal, H.R. and J.R. Winther, *Redox characteristics of the eukaryotic cytosol.* Biochim Biophys Acta, 2008. **1783**(4): p. 629-40.
233. Arunachalam, B., et al., *Enzymatic reduction of disulfide bonds in lysosomes: characterization of a gamma-interferon-inducible lysosomal thiol reductase (GILT).* Proc Natl Acad Sci U S A, 2000. **97**(2): p. 745-50.
234. Lee, S., et al., *Essential role of clusterin in pancreas regeneration.* Dev Dyn, 2011. **240**(3): p. 605-15.
235. Lehman, J.A., V. Calvo, and J. Gomez-Cambronero, *Mechanism of ribosomal p70S6 kinase activation by granulocyte macrophage colony-stimulating factor in neutrophils: cooperation of a MEK-related, THR421/SER424 kinase and a rapamycin-sensitive, m-TOR-related THR389 kinase.* J Biol Chem, 2003. **278**(30): p. 28130-8.

236. Pullen, N. and G. Thomas, *The modular phosphorylation and activation of p70s6k.* FEBS Lett, 1997. **410**(1): p. 78-82.
237. Garg, A.D., et al., *Molecular and Translational Classifications of DAMPs in Immunogenic Cell Death.* Front Immunol, 2015. **6**: p. 588.
238. Nam, J.S., S. Hirohashi, and L.M. Wakefield, *Dysadherin: a new player in cancer progression.* Cancer Lett, 2007. **255**(2): p. 161-9.
239. Koltai, T., *Clusterin: a key player in cancer chemoresistance and its inhibition.* Onco Targets Ther, 2014. **7**: p. 447-56.
240. Riaz, M.A., et al., *Clusterin signals via ApoER2/VLDLR and induces meiosis of male germ cells.* Am J Transl Res, 2017. **9**(3): p. 1266-1276.
241. Leeb, C., C. Eresheim, and J. Nimpf, *Clusterin is a ligand for apolipoprotein E receptor 2 (ApoER2) and very low density lipoprotein receptor (VLDLR) and signals via the Reelin-signaling pathway.* J Biol Chem, 2014. **289**(7): p. 4161-72.
242. Zoubeidi, A., et al., *Clusterin facilitates COMMD1 and I-kappaB degradation to enhance NF-kappaB activity in prostate cancer cells.* Mol Cancer Res, 2010. **8**(1): p. 119-30.
243. Santilli, G., B.J. Aronow, and A. Sala, *Essential requirement of apolipoprotein J (clusterin) signaling for IkappaB expression and regulation of NF-kappaB activity.* J Biol Chem, 2003. **278**(40): p. 38214-9.
244. Essabbani, A., F. Margottin-Goguet, and G. Chiocchia, *Identification of clusterin domain involved in NF-kappaB pathway regulation.* J Biol Chem, 2010. **285**(7): p. 4273-7.
245. Shim, Y.J., et al., *Toll-like receptor 4 signaling is required for clusterin-induced tumor necrosis factor-alpha secretion in macrophage.* Biochem Biophys Res Commun, 2017. **482**(4): p. 1407-1412.
246. Fu, Y., et al., *Overexpression of clusterin promotes angiogenesis via the vascular endothelial growth factor in primary ovarian cancer.* Mol Med Rep, 2013. **7**(6): p. 1726-32.
247. Chayka, O., et al., *Clusterin, a haploinsufficient tumor suppressor gene in neuroblastomas.* J Natl Cancer Inst, 2009. **101**(9): p. 663-77.
248. Bettuzzi, S., et al., *Genetic inactivation of ApoJ/clusterin: effects on prostate tumourigenesis and metastatic spread.* Oncogene, 2009. **28**(49): p. 4344-52.
249. Rövekamp, M., *Untersuchung des LRP1-abhängigen Einflusses von sClu auf die Zellvitalität und die Signaltransduktion in embryonalen Mäusefibroblasten. [Bachelor Thesis University of Mainz]*. 2013.
250. Chi, K.N., et al., *Custirsen in combination with docetaxel and prednisone for patients with metastatic castration-resistant prostate cancer (SYNERGY trial): a phase 3, multicentre, open-label, randomised trial.* Lancet Oncol, 2017. **18**(4): p. 473-485.
251. Vakkila, J. and M.T. Lotze, *Inflammation and necrosis promote tumour growth.* Nat Rev Immunol, 2004. **4**(8): p. 641-8.
252. Leek, R.D., et al., *Necrosis correlates with high vascular density and focal macrophage infiltration in invasive carcinoma of the breast.* Br J Cancer, 1999. **79**(5-6): p. 991-5.
253. Weiss, L., *Some mechanisms involved in cancer cell detachment by necrotic material.* Int J Cancer, 1978. **22**(2): p. 196-203.
254. Vaniet, E., *Gefahrensignale aus sterbenden Zellen*. 2017.
255. Borst, J.G. and B. Sakmann, *Calcium influx and transmitter release in a fast CNS synapse.* Nature, 1996. **383**(6599): p. 431-4.

9 Appendix

App.1a Species used for analyses of identity/conservation, N-glycosylation, FC recognition sites, secondary structures, hydrophobicity and disorder tendency of CLU as well as creation of phylogenetic trees.

ID	name	Class	Order	position of FC recognition sequence/ cleavage site predicted w/ ProP	ProP Score	position cleavage site predicted w/ ProP	Sequence at conserved RxxR position according to Clustal O alignment	most potential recognition site according to Duckert *et al.* 2004	cleavage site according to Duckert *et al.* 2004	No. Of N-glycosylation site according to NetNGlyc	SignalP predic-ted SSCR	aa mature protein	aa prepro-protein	coiled coils at N-terminus	coiled coils at C-terminus	additiona coiled coils
AFN21430.1	*Bufo gargarizans*	Amphibia	Anura	ALKRFKK|EV	0.5	437	HQPSRRERSTLF	RRER	234	6	21	422	443	yes	yes	no
NP_001080775.1	*Xenopus laevis*	Amphibia	Anura	SESRQAR|SP	0.586	233	FSESRQARSPTF	RQAR	233	5	21	426	447	yes	no	no
NP_001004936.1	*Xenopus tropicalis*	Amphibia	Anura	AESRRAR|SP	0.58	231	FAESRRARSPSF	RRAR	231	3	19	426	445	yes	no	no
KQK80821.1	*Amazona aestiva*	Aves	Psittaciformes	n.a.	n.a.	no	RFPLRSERLSRELHP	RLSR	230	4	21	428	449	yes	yes	no
CAA56733.1	*Coturnix coturnix*	Aves	Galliformes	n.a.	n.a.	no	VPRRRLSRELHP	RLSR	230	3	21	430	451	yes	no	no
XP_009562084.1	*Cuculus canorus*	Aves	Cuculiformes	n.a.	n.a.	no	RLIPRSERFSRELHP	RFSR	230	3	21	428	449	yes	yes	no
XP_005443609.2	*Falco cherrug*	Aves	Falconiformes	n.a.	n.a.	no	RFPVRSERFSRELHP	RFSR	230	3	21	429	450	yes	yes	no
AAD17257.1	*Gallus gallus*	Aves	Galliformes	n.a.	n.a.	no	PPRRRLSRELHP	RLSR	231	3	21	427	448	yes	no	no
XP_005146432.1	*Melopsittacus undulatus*	Aves	Psittaciformes	n.a.	n.a.	no	RFPLRSERLSRELHP	RLSR	230	4	21	429	450	yes	yes	no
AAW21812.1	*Numida meleagris*	Aves	Galliformes	n.a.	n.a.	no	PPRRRLSRELHP	RLSR	231	3	21	427	448	yes	no	no
AFM91023.1	*Callorhinchus milii*	Chondrichthyes	Chimaeriformes	n.a.	n.a.	no	FFPETTYFPSYRPSIF	n.a.	n.a.	4	20	442	462	yes	no	yes
ACZ98148.1	*Chiloscyllium plagiosum*	Chondrichthyes	Orectolobiformes	n.a.	n.a.	no	LFPDSSFSPFRHSMF	n.a.	n.a.	4	21	431	452	yes	no	no
XP_014925664.1	*Acinonyx jubatus*	Mammalia	Carnivora	FYARVCR|SG	0.593	129	NPKSRFARNVMP	RFAR	226	7	22	425	447	yes	no	no
XP_002914459.1	*Ailuropoda melanoleuca*	Mammalia	Carnivora	n.a.	n.a.	no	NPKSRFVRNIMP	RFVR	226	7	22	424	446	yes	no	no
XP_007192795.1	*Balaenoptera acutorostrata scammoni*	Mammalia	Artiodactyla	PKSRLAR|NV	0.582	221	NPKSRLARNVMP	RLAR	221	8	20	421	441	yes	yes	no
XP_005909198.1	*Bos mutus*	Mammalia	Artiodactyla	PKSRFAR|NV	0.634	221	NPKSRFARNVMP	RFAR	221	7	20	415	435	yes	yes	no
AAI49633.1	*Bos taurus*	Mammalia	Artiodactyla	PKSRFAR|NV	0.634	221	NPKSRFARNVMP	RFAR	221	7	20	419	439	yes	yes	no
JAB40221.1	*Callithrix jacchus*	Mammalia	Primates	PKSRIVR|SL	0.528	227	FPKSRIVRSLMP	RIVR	227	7	23	426	449	yes	yes	no
XP_010946877.1	*Camelus bactrianus*	Mammalia	Artiodactyla	PKSRFAR|NL	0.519	226	NPKSRFARNLMP	RFAR	226	7	22	423	445	yes	no	no
XP_006194079.2	*Camelus ferus*	Mammalia	Artiodactyla	PKSRFAR|NL	0.519	226	NPKSRFARNLMP	RFAR	226	7	22	423	445	yes	no	no
NP_001003370.1	*Canis lupus familiaris*	Mammalia	Carnivora	n.a.	n.a.	no	NPKFRIARNIIP	RIAR	226	7	23	422	445	yes	no	no
APL97841.1	*Castor fiber*	Mammalia	Rodentia	n.a.	n.a.	no	YPKSRFVRSLRLFPS	RFVR	226	5	22	425	447	yes	yes	no
ADP20553.1	*Cavia porcellus*	Mammalia	Rodentia	n.a.	n.a.	no	YPKSRLVRSILP	RLVR	226	6	22	427	449	yes	yes	no
XP_004433604.1	*Ceratotherium simum simum*	Mammalia	Perissodactyla	PKSRFAR|HI	0.565	226	NPKSRFARHIMP	RFAR	226	6	22	426	448	yes	no	no
XP_007960189.1	*Chlorocebus sabaeus*	Mammalia	Primates	PKSRIVR|SL	0.531	227	FPKSRIVRSLMP	RIVR	227	7	23	426	449	yes	yes	no
XP_012580400.1	*Condylura cristata*	Mammalia	Eulipotyphla	PRSRFAR|DI	0.68	226	SPRSRFARDIVP	RFAR	226	7	22	428	450	yes	no	no
EGW05785.1	*Cricetulus griseus*	Mammalia	Rodentia	n.a.	n.a.	no	YPKSRLVRSLIP	RLVR	226	6	22	425	447	yes	yes	no
XP_012879697.1	*Dipodomys ordii*	Mammalia	Rodentia	n.a.	n.a.	no	FPKSRLVRSLRPLSP	RLVR	226	5	22	426	448	yes	yes	no
XP_014698794.1	*Equus asinus*	Mammalia	Perissodactyla	PKSRFAR|NI	0.521	227	NPKSRFARNIMH	RFAR	227	7	22	427	449	yes	no	no
NP_001075413.1	*Equus caballus*	Mammalia	Perissodactyla	PKSRFAR|NI	0.521	227	NPKSRFARNIMH	RFAR	227	7	22	427	449	yes	no	no
XP_016041118.1	*Erinaceus europaeus*	Mammalia	Eulipotyphla	n.a.	n.a.	no	SPKSRIVRSLLP	RIVR	226	7	22	425	447	yes	yes	no
XP_003984849.1	*Felis catus*	Mammalia	Carnivora	PKSRFAR|NV	0.658	226	NPKSRFARNVMP	RFAR	226	8	22	425	447	yes	no	no
XP_004046873.2	*Gorilla gorilla gorilla*	Mammalia	Primates	PKSRIVR|SL	0.531	227	FPKSRIVRSLMP	RIVR	227	6	23	426	449	yes	yes	no
ADP20516.1	*Heterocephalus glaber*	Mammalia	Rodentia	EYRRKKR|EE	0.555	446	YPKSRLVRSILP	RLVR	226	6	22	426	448	yes	yes	no
NP_001822.3	*Homo sapiens*	Mammalia	Primates	PKSRIVR|SL	0.531	227	FPKSRIVRSLMP	RIVR	227	6	23	426	449	yes	yes	no
tr|I3NHG5|I3NHG5_ICTTR	*Ictidomys tridecemlineatus*	Mammalia	Rodentia	HKSRLAR|SV	0.708	226	YHKSRLARSILP	RLAR	226	5	21	448	469	yes	yes	no
XP_010590652.1	*Loxodonta africana*	Mammalia	Proboscidea	n.a.	n.a.	no	YPKSRVVRNTVPFF	RVVR	179	5	0	396	396	yes	yes	no
NP_001182403.1	*Macaca mulatta*	Mammalia	Primates	PKSRIVR|SL	0.531	226	FPKSRIVRSLMP	RIVR	226	6	22	426	448	yes	yes	no
XP_015354933.1	*Marmota marmota marmota*	Mammalia	Rodentia	HKSRLAR|SI	0.6	226	YHKSRLARSILP	RLAR	226	5	22	426	448	yes	yes	no
XP_012972739.1	*Mesocricetus auratus*	Mammalia	Rodentia	n.a.	n.a.	no	YPKSRLIRSLLP	RLIR	226	6	22	426	448	yes	yes	no
XP_001380037.2	*Monodelphis domestica*	Mammalia	Didelphimorphia	SKQRVVR|DI	0.504	230	FSKQRVVRDIPP	RVVR	230	4	22	436	458	yes	no	no
NP_038520.2	*Mus musculus*	Mammalia	Rodentia	n.a.	n.a.	no	YPKSRLVRSLMS	RLVR	226	6	22	426	448	yes	yes	no
XP_004775167.1	*Mustela putorius furo*	Mammalia	Carnivora	n.a.	n.a.	no	NIKPRFARNIMP	RFAR	226	7	22	424	446	yes	no	no
ELK29388.1	*Myotis davidii*	Mammalia	Chiroptera	FYARVCR|SS	0.53	129	NPKTRFARNLMS	RFAR	223	6	22	424	446	yes	yes	no
XP_008826365.1	*Nannospalax galili*	Mammalia	Rodentia	n.a.	n.a.	no	YPKSRLVRSLLP	RLVR	226	5	22	425	447	yes	yes	no
XP_012363842.1	*Nomascus leucogenys*	Mammalia	Primates	PKSRIVR|SL	0.531	339	FPKSRIVRSLMP	RIVR	339	7	0	560	560	yes	yes	no
XP_004579143.2	*Ochotona princeps*	Mammalia	Lagomorpha	FYARVCR|SG	0.542	129	YPKSRLARHIMP	RLAR	226	7	22	426	448	yes	yes	no
XP_001515556.4	*Ornithorhynchus anatinus*	Mammalia	Monotremata	n.a.	n.a.	no	FSSGRVVRDTSS	RVVR	246	6	36	443	479	yes	no	no
NP_001075518.1	*Oryctolagus cuniculus*	Mammalia	Lagomorpha	QEYRKKK|RV	0.541	444	YAKSRLVRNIMP	RLVR	225	7	22	425	447	yes	yes	no
XP_012663174.1	*Otolemur garnettii*	Mammalia	Primates	PKSRFAR|TI	0.503	227	FPKSRFARTILP	RFAR	227	6	23	429	452	yes	yes	no
tr|W5PZI1|W5PZI1_SHEEP	*Ovis aries*	Mammalia	Primates	PKSRFAR|NV	0.634	221	NPKSRFARNVMP	RFAR	221	6	20	419	439	yes	no	no
JAA39188.1	*Pan troglodytes*	Mammalia	Primates	PKSRIVR|SL	0.531	227	FPKSRIVRSLMP	RIVR	227	6	23	426	449	yes	yes	no
XP_019296395.1	*Panthera pardus*	Mammalia	Carnivora	PKSRFAR|NV	0.658	226	NPKSRFARNVMP	RFAR	226	8	22	425	447	yes	yes	no
XP_007097164.1	*Panthera tigris altaica*	Mammalia	Carnivora	PKSRFAR|NV	0.658	226	NPKSRFARNVMP	RFAR	226	7	22	425	447	yes	yes	no
XP_003902635.1	*Papio anubis*	Mammalia	Primates	PKSRIVR|SL	0.531	227	FPKSRIVRSLMP	RIVR	227	6	23	426	449	yes	yes	no
XP_015862715.1	*Peromyscus maniculatus bairdii*	Mammalia	Rodentia	PKSRLVR|SL	0.517	226	YPKSRLVRSLMP	RLVR	226	5	22	426	448	yes	yes	no
XP_007127925.1	*Physeter catodon*	Mammalia	Artiodactyla	PKSRFAR|NV	0.63	221	SPKSRFARNVMP	RFAR	221	8	20	421	441	yes	yes	no
XP_003777274.1	*Pongo abelii*	Mammalia	Primates	PKSRIIR|SL	0.536	227	FPKSRIIRSLMP	RIIR	227	7	23	426	449	yes	yes	no
NP_444180.2	*Rattus norvegicus*	Mammalia	Rodentia	PKSRLVR|SL	0.517	226	YPKSRLVRSLMP	RLVR	226	6	22	425	447	yes	yes	no
XP_019588724.1	*Rhinolophus sinicus*	Mammalia	Chiroptera	n.a.	n.a.	no	HPKSRIARNIMS	RIAR	226	6	22	426	448	yes	no	no
XP_012396173.1	*Sarcophilus harrisii*	Mammalia	Dasyuromorphia	QKQRVVR|DI	0.59	230	FQKQRVVRDISP	RVVR	230	5	20	380	400	yes	no	no
XP_004614793.1	*Sorex araneus*	Mammalia	Eulipotyphla	GNSRVVR|SL	0.584	229	GGNSRVVRSLLP	RVVR	229	5	20	431	451	yes	yes	no
NP_999136.1	*Sus crofa*	Mammalia	Artiodactyla	PKSRFAR|NI	0.507	227	NPKSRFARNIMP	RFAR	227	7	23	423	446	yes	yes	no
XP_019796892.1	*Tursiops truncatus*	Mammalia	Artiodactyla	PKSRFAR|NV	0.634	221	NPKSRFARNVMP	RFAR	221	8	20	400	420	yes	yes	no
XP_008703334.1	*Ursus maritimus*	Mammalia	Carnivora	PKSRFAR|NI	0.536	226	NPKSRFARNIMP	RFAR	226	7	22	424	446	yes	no	no
XP_006203350.2	*Vicugna pacos*	Mammalia	Artiodactyla	PKSRFAR|NL	0.519	226	NPKSRFARNLMP	RFAR	226	7	22	423	445	yes	no	no

App.1b Species used for analyses of identity/conservation, N-glycosylation, FC recognition sites, secondary structures, hydrophobicity and disorder tendency of CLU as well as creation of phylogenetic trees.

ID	name	Class	Order	position of FC recognition sequence/ cleavage site predicted w/ ProP	ProP Score	position cleavage site predicted w/ ProP	Sequence at conserved RxxR position according to Clustal O alignment	most potential recognition site according to Duckert *et al.* 2004	cleavage site according to Duckert *et al.* 2004	No. Of N-glycosylation site according to NetNGlyc	SignalP predic-ted SSCR	aa mature protein	aa prepro-protein	coiled coils at N-terminus	coiled coils at C-terminus	additiona coiled coils
SBP06891.1	*Aphyosemion striatum*	Osteichthyes	Cyprinodontiphormes	PVTRRSR|SV	0.534	228	APVTRRSRSVH	RRSR	228	5	31	428	459	yes	yes	no
XP_007255478.1	*Astyanax mexicanus*	Osteichthyes	Characiformes	QPARVYR|SP	0.523	225	SQPARVYRSPFQ	RVYR	225	3	20	431	451	yes	yes	no
XP_013870874.1	*Austrofundulus limnaeus*	Osteichthyes	Cyprinodontiphormes	PLSRHSR|SL	0.628	226	APLSRHSRSLRTLFH	RHSR	226	5	31	419	450	yes	yes	no
XP_012684745.1	*Clupea harengus*	Osteichthyes	Clupeiformes	GRSRVYR|SP	0.703	223	LGRSRVYRSPIE	RVYR	223	3	20	433	453	yes	yes	no
XP_008311637.1	*Cynoglossus semilaevis*	Osteichthyes	Pleuronectiformes	PYSRHRR|GI	0.681	230	GPYSRHRRGIRSIFQ	RHRR	233	5	31	433	464	yes	yes	no
XP_015245708.1	*Cyprinodon variegatus*	Osteichthyes	Cyprinodontiphormes	n.a.	n.a.	no	APVTRRARSIHM	RRAR	228	5	31	426	457	yes	yes	no
AAQ56181.1	*Danio rerio*	Osteichthyes	Cypriniformes	FYSRTCR|SG	0.51	128	THAGRIYRSPMH	RIYR	229	4	21	428	449	yes	no	no
XP_010880875.1	*Esox lucius*	Osteichthyes	Esociformes	n.a.	n.a.	no	QLHSRIVRSPLQ	RIVR	234	4	21	440	461	yes	yes	no
JAQ22465.1	*Fundulus heteroclitus*	Osteichthyes	Cyprinodontiphormes	n.a.	n.a.	no	APVTRRARSIHM	RRAR	227	5	30	430	460	yes	yes	no
tr|G3NXP9|G3NXP9_GASAC	*Gasterosteus aculeatus*	Osteichthyes	Perciformes	GPTRSIR|SL	0.522	220	LGPTRSIRSLFQ	RSIR	220	5	22	412	434	yes	yes	no
XP_017312023.1	*Ictalurus punctatus*	Osteichthyes	Siluriformes	n.a.	n.a.	no	FHRPSPIYRSLFHDPQFPDFH	n.a.	?	3	20	422	442	yes	yes	no
XP_017267217.1	*Kryptolebias marmoratus*	Osteichthyes	Cyprinodontiphormes	PMSRHSR|SI	0.686	227	APMSRHSRSIHT	RHSR	227	5	30	424	454	yes	yes	no
KKF27296.1	*Larimichthys crocea*	Osteichthyes	Perciformes	n.a.	n.a.	no	LGPTRQGRSIRSLFR	RQGR	226	5	27	431	458	yes	yes	no
XP_014349227.1	*Latimeria chalumnae*	Osteichthyes	Coelancanthiformes	n.a.	n.a.	no	PKSLRISRASP	RISR	234	4	20	441	461	yes	no	no
XP_015208246.1	*Lepisosteus oculatus*	Osteichthyes	Lepisosteiformes	QRSRVYR|SP	0.631	229	QQRSRVYRSPYY	RVYR	229	3	20	438	458	yes	yes	no
XP_004550621.1	*Maylandia zebra*	Osteichthyes	Cichliformes	RRGRSIR|SL	0.641	233	LSPARRGRSIRSLFH	RSIR	233	4	31	431	462	yes	yes	no
SBP47041.1	*Nothobranchius furzeri*	Osteichthyes	Cyprinodontiphormes	PVMRRSR|SI	0.54	228	APVMRRSRSIHT	RRSR	228	4	31	425	456	yes	yes	no
tr|A0A1A8DV96|A0A1A8DV96_9TELE	*Nothobranchius kadleci*	Osteichthyes	Cyprinodontiphormes	PVMRRSR|SI	0.54	228	APVMRRSRSIHT	RRSR	228	4	31	425	456	yes	yes	no
tr|A0A1A8GQG0|A0A1A8GQG0_9TELE	*Nothobranchius korthausae*	Osteichthyes	Cyprinodontiphormes	PVMRRSR|SI	0.54	227	APVMRRSRSIHT	RRSR	227	4	31	424	455	yes	yes	no
tr|A0A1A8IEU0|A0A1A8IEU0_NOTKU	*Nothobranchius kuhntae*	Osteichthyes	Cyprinodontiphormes	PVMRRSR|SI	0.54	228	APVMRRSRSIHT	RRSR	228	4	31	425	456	yes	yes	no
tr|Q5NDK4|Q5NDK4_ONCMY	*Oncorhynchus mykiss*	Osteichthyes	Salmoniformes	n.a.	n.a.	no	EVHSRVVRSPLK	RVVR	242	4	0	469	469	yes	yes	no
XP_003446372.1	*Oreochromis niloticus*	Osteichthyes	Cichliformes	PYARHGR|SI	0.518	229	SPYARHGRSIRSLFH	RHGRS	229	5	30	431	461	yes	yes	no
XP_019953002.1	*Paralichthys olivaceus*	Osteichthyes	Pleuronectiformes	RHSRSVR|SL	0.633	230	LSPTRHSRSVRSLFH	RSVR	230	4	29	432	461	yes	yes	no
XP_007578572.1	*Poecilia formosa*	Osteichthyes	Cyprinodontiphormes	PAIRRAR|SI	0.501	228	APAIRRARSIHL	RRAR	228	4	31	430	461	yes	yes	no
XP_014906758.1	*Poecilia latipinna*	Osteichthyes	Cyprinodontiphormes	PAIRRAR|SI	0.501	228	APAIRRARSIHL	RRAR	228	3	31	430	461	yes	yes	no
XP_014832717.1	*Poecilia mexicana*	Osteichthyes	Cyprinodontiphormes	PAIRRAR|SI	0.501	228	APAIRRARSIHL	RRAR	228	4	31	430	461	yes	yes	no
XP_005737342.1	*Pundamilia nyererei*	Osteichthyes	Perciformes	RRGRSIR|SL	0.641	232	LSPARRGRSIRSLFH	RSIR	232	5	30	431	461	yes	yes	no
XP_017551221.1	*Pygocentrus nattereri*	Osteichthyes	Characiformes	n.a.	n.a.	no	SMFSRPTRVYRSPVH	RVYR	228	3	20	435	455	yes	yes	no
ACN10851.1	*Salmo salar*	Osteichthyes	Salmoniformes	n.a.	n.a.	no	EAHSRVVRSPLK	RVVR	241	3	21	447	468	yes	yes	no
XP_018597884.1	*Scleropages formosus*	Osteichthyes	Osteoglossiformes	GRSRFYR|SP	0.602	229	FGRSRFYRSPLW	RFYR	229	2	26	433	459	yes	yes	no
tr_M3ZZQ6_M3ZZ	*Xiphophorus maculatus*	Osteichthyes	Cyprinodontiphormes	PAVRHAR|SI	0.595	228	APAVRHARSIHM	RHAR	228	3	31	428	459	yes	yes	no
tr|A0A151N604|A0A151N604_ALLMI	*Alligator mississippiensis*	Reptilia	Crocodylia	n.a.	n.a.	no	LPSTRVVRDLPS	RVVR	231	5	0	467	467	yes	no	no
XP_006033945.1	*Alligator sinensis*	Reptilia	Crocodylia	n.a.	n.a.	no	RSPFRSPRLPSTRVVRDLPS	RVVR	229	5	21	444	465	yes	yes	no
XP_003229606.2	*Anolis carolinensis*	Reptilia	Squamata	VPSRVAR|SV	0.796	226	RVPSRVARSVPP	RVAR	226	3	22	445	467	yes	no	no
JAG68343.1	*Boiga irregularis*	Reptilia	Squamata	THSRVAR|NT	0.507	226	FTHSRVARNTRPFSP	RVAR	226	3	22	437	459	yes	no	no
tr|M7AYN0|M7AYN0_CHEMY	*Chelonia mydas*	Reptilia	Testudines	ANARVVR|DT	0.548	221	FANARVVRDTHP	RVVR	221	3	21	456	477	yes	no	yes
XP_019392802.1	*Crocodylus porosus*	Reptilia	Crocodylia	n.a.	n.a.	no	LPSTRVVRDLPS	RVVR	228	4	20	444	464	yes	yes	no
JAI13821.1	*Crotalus adamanteus*	Reptilia	Squamata	THSRVAR|NV	0.641	226	FTHSRVARNVRPFSQ	RVAR	226	3	22	437	459	yes	no	no
JAG47134.1	*Crotalus horridus*	Reptilia	Squamata	THSRVAR|NV	0.641	226	FTHSRVARNVRPFSQ	RVAR	226	3	22	437	459	yes	no	no
XP_015270667.1	*Gekko japonicus*	Reptilia	Squamata	TGSRVAR|NV	0.679	226	FTGSRVARNVHS	RVAR	226	4	22	426	448	yes	no	no
tr|V8NR93|V8NR93_OPHHA	*Ophiophagus hannah*	Reptilia	Squamata	n.a.	n.a.	no	FTHSRVARNTRPFSQFFS	RVAR	240	3	36	452	488	yes	no	no
XP_013912776.1	*Thamnophis sirtalis*	Reptilia	Squamata	TRSRIAR|NT	0.534	226	FTRSRIARNTRP	RISR	226	3	22	435	457	yes	no	yes

App.2 Phylogenetic trees created after CLU full-length protein truncation

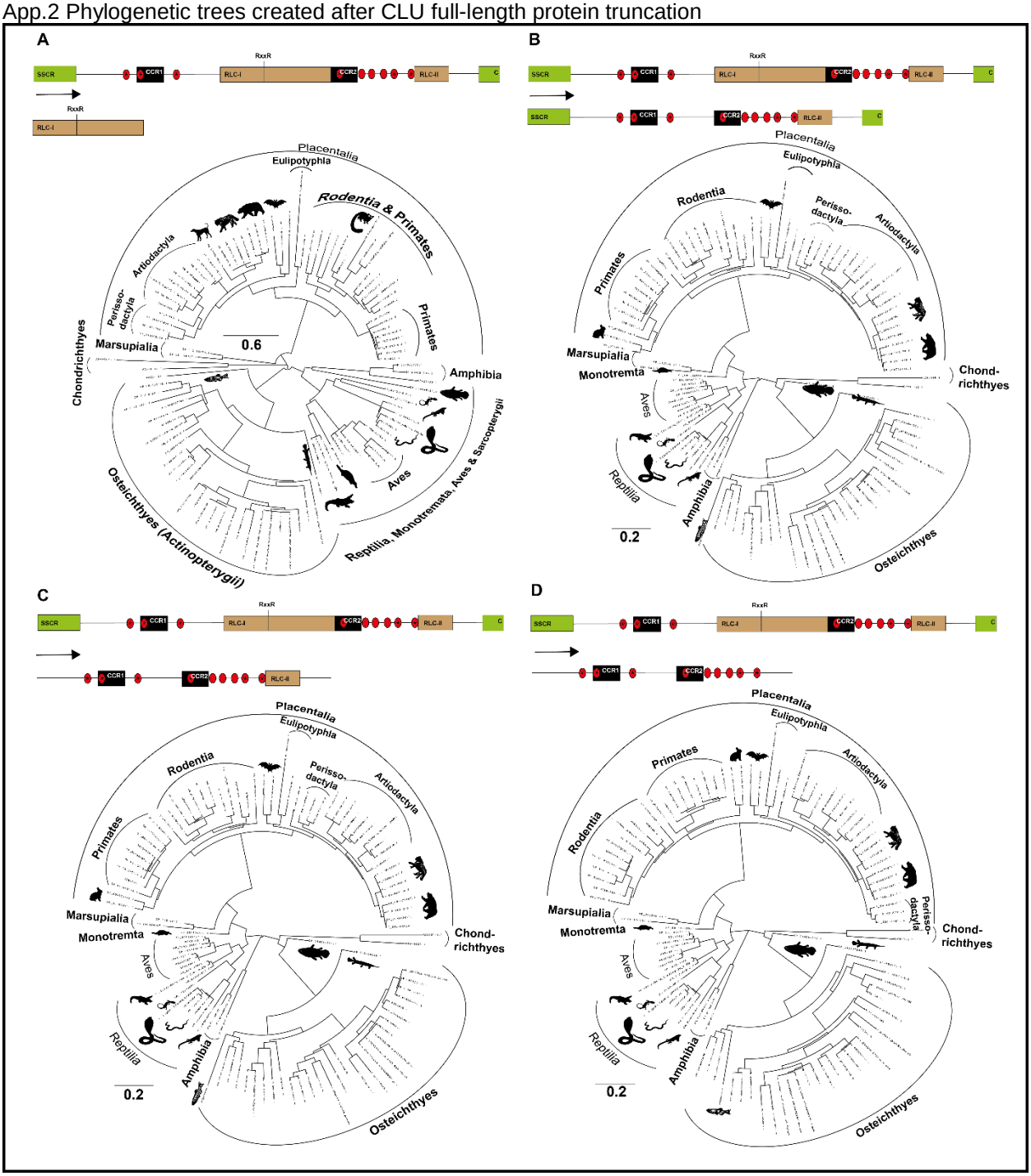

App.3 Species used for analyses of identity/conservation, N-glycosylation, FC recognition sites, secondary structures, hydrophobicity and disorder tendency of CLUL1.

ID	name	Class	position of recognition sequence/ cleavage site predicted w/ ProP	ProP Score	position cleavage site predicted w/ ProP	number of NetNGlyc predicted glycosylation sites	SignalP predicted SSCR	aa mature protein	aa prepro-protein
tr_U3J8K4_U3J8K4_ANAPL	*Anas platyrhynchos*	Aves	n.a.	n.a.	n.a.	3	22	436	458
tr|A0A094K9V9|A0A094K9V9_ANTCR	*Antrostomus carolinensis*	Aves	n.a.	n.a.	n.a.	4	22	434	456
tr|A0A087REG4|A0A087REG4_APTFO	*Aptenodytes forsteri*	Aves	n.a.	n.a.	n.a.	3	19	441	460
tr|A0A091K2I8|A0A091K2I8_COLST	*Colius striatus*	Aves	n.a.	n.a.	n.a.	4	22	446	468
tr_U3JUQ5_U3JUQ5_FICAL	*Ficedula albicollis*	Aves	GVSTFKR|KV	0.527	139	2	20	444	464
tr_F1N8T1_F1N8T1_CHICK	*Gallus gallus*	Aves	n.a.	n.a.	n.a.	3	20	441	461
tr|A0A093QKZ0|A0A093QKZ0_9PASS	*Manacus vitellinus vitellinus*	Aves	n.a.	n.a.	n.a.	4	17	443	460
tr|G1NBT5|G1NBT5_MELGA	*Meleagris gallopavo*	Aves	n.a.	n.a.	n.a.	3	35	444	479
tr|A0A091SZG4|A0A091SZG4_9AVES	*Pelecanus crispus*	Aves	n.a.	n.a.	n.a.	4	17	443	460
tr_H0ZIU4_H0ZIU4_TAEGU	*Taeniopygia guttata*	Aves	GVSTFKR|KV	0.527	136	3	19	439	458
tr_G1LJ79_G1LJ79_AILME	*Ailuropoda melanoleuca*	mammalia	n.a.	n.a.	n.a.	6	29	444	473
sp_Q3ZRW9_CLUL1_BOVIN	*Bos taurus*	mammalia	n.a.	n.a.	n.a.	5	21	444	465
tr_F7GTA9_F7GTA9_CALJA	*Callithrix jacchus*	mammalia	n.a.	n.a.	n.a.	4	21	449	470
sp_Q95KN1_CLUL1_CANLF	*Canis lupus familiaris*	mammalia	n.a.	n.a.	n.a.	6	21	444	465
tr_H0VTN6_H0VTN6_CAVPO	*Cavia porcellus*	mammalia	n.a.	n.a.	n.a.	5	21	445	466
tr_A0A0D9RYF9_A0A0D9RYF9_CHLSB	*Chlorocebus sabaeus*	mammalia	n.a.	n.a.	n.a.	4	21	445	466
tr_F6ZBU7_F6ZBU7_HORSE	*Equus caballus*	mammalia	n.a.	n.a.	n.a.	6	25	444	469
tr_M3WB13_M3WB13_FELCA	*Felis catus*	mammalia	n.a.	n.a.	n.a.	5	26	441	467
tr_G3QG57_G3QG57_GORGO	*Gorilla gorilla gorilla*	mammalia	n.a.	n.a.	n.a.	5	21	445	466
sp_Q15846_CLUL1_HUMAN	*Homo sapiens*	mammalia	n.a.	n.a.	n.a.	5	21	445	466
tr_I3MN97_I3MN97_ICTTR	*Ictidomys tridecemlineatus*	mammalia	n.a.	n.a.	n.a.	5	21	448	469
tr_F7G367_F7G367_MONDO	*Monodelphis domestica*	mammalia	n.a.	n.a.	n.a.	4	24	445	469
sp_Q3ZRW6_CLUL1_MOUSE	*Mus musculus*	mammalia	n.a.	n.a.	n.a.	5	21	443	464
tr_M3Y239_M3Y239_MUSPF	*Mustela putorius furo*	mammalia	n.a.	n.a.	n.a.	5	21	444	465
tr_G1PFW4_G1PFW4_MYOLU	*Myotis lucifugus*	mammalia	n.a.	n.a.	n.a.	4	26	443	469
tr_F6TZ12_F6TZ12_ORNAN	*Ornithorhynchus anatinus*	mammalia	n.a.	n.a.	n.a.	3	20	454	474
tr_G1SVL6_G1SVL6_RABIT	*Oryctolagus cuniculus*	mammalia	n.a.	n.a.	n.a.	4	21	444	465
tr_H0WMM5_H0WMM5_OTOGA	*Otolemur garnettii*	mammalia	n.a.	n.a.	n.a.	5	21	437	458
tr_W5PHW8_W5PHW8_SHEEP	*Ovis aries*	mammalia	n.a.	n.a.	n.a.	5	25	444	469
tr_H2R0C0_H2R0C0_PANTR	*Pan troglodytes*	mammalia	n.a.	n.a.	n.a.	5	21	445	466
tr_A0A096MYI6_A0A096MYI6_PAPAN	*Papio anubis*	mammalia	n.a.	n.a.	n.a.	4	21	444	465
sp_Q3ZRW7_CLUL1_RAT	*Rattus norvegicus*	mammalia	n.a.	n.a.	n.a.	5	21	443	464
tr_G3VEV2_G3VEV2_SARHA	*Sarcophilus harrisii*	mammalia	n.a.	n.a.	n.a.	4	29	444	473
XP_007899164.1	*Callorhinchus milii*	Pisces	n.a.	n.a.	n.a.	2	20	449	469
tr_A5PMY8_A5PMY8_DANRE	*Danio rerio*	Pisces	n.a.	n.a.	n.a.	5	23	443	466
tr_E6ZJ37_E6ZJ37_DICLA	*Dicentrarchus labrax*	Pisces	LCRRLRR|QA	0.592	311	3	20	453	473
tr_W5UK95_W5UK95_ICTPU	*Ictalurus punctatus*	Pisces	n.a.	n.a.	n.a.	4	20	442	462
XP_005995776.1	*Latimeria chalumnae*	Pisces	GSERSKR|DF	0.73	317	1	0	487	487
XP_010793087.1	*Notothenia coriiceps*	Pisces	RRSRSIR|SL	0.696	231	5	29	426	455
tr_I3JFL9_I3JFL9_ORENI	*Oreochromis niloticus*	Pisces	MCRRLRR|QA	0.611	309	4	20	445	465
XP_014060663.1	*Salmo salar*	Pisces	VRSRMVR|SA	0.609	241	5	21	447	468
KPP65294.1	*Scleropages formosus*	Pisces	GRSRFYR|SP	0.602	229	2	26	430	456
XP_016393050.1	*Sinocyclocheilus rhinocerous*	Pisces	n.a.	n.a.	n.a.	4	20	439	459
XP_011619842.1	*Takifugu rubripes*	Pisces	PYSRWGR|SI RWGRSIR|SL	0.570 0.550	226 229	4	28	432	460
tr_H2TI47_H2TI47_TAKRU	*Takifugu rubripes*	Pisces	n.a.	n.a.	n.a.	4	28	445	473
XP_005805221.1	*Xiphophorus maculatus*	Pisces	PAVRHAR|SI	0.595	228	3	31	428	459
tr_G1KHS7_G1KHS7_ANOCA	*Anolis carolinensis*	Reptilia	n.a.	n.a.	n.a.	5	19	440	459
AFJ49715.1	*Crotalus adamanteus*	Reptilia	THSRVAR|NV	0.641	226	3	22	437	459
tr_K7FJW1_K7FJW1_PELSI	*Pelodiscus sinensis*	Reptilia	n.a.	n.a.	n.a.	3	21	445	466

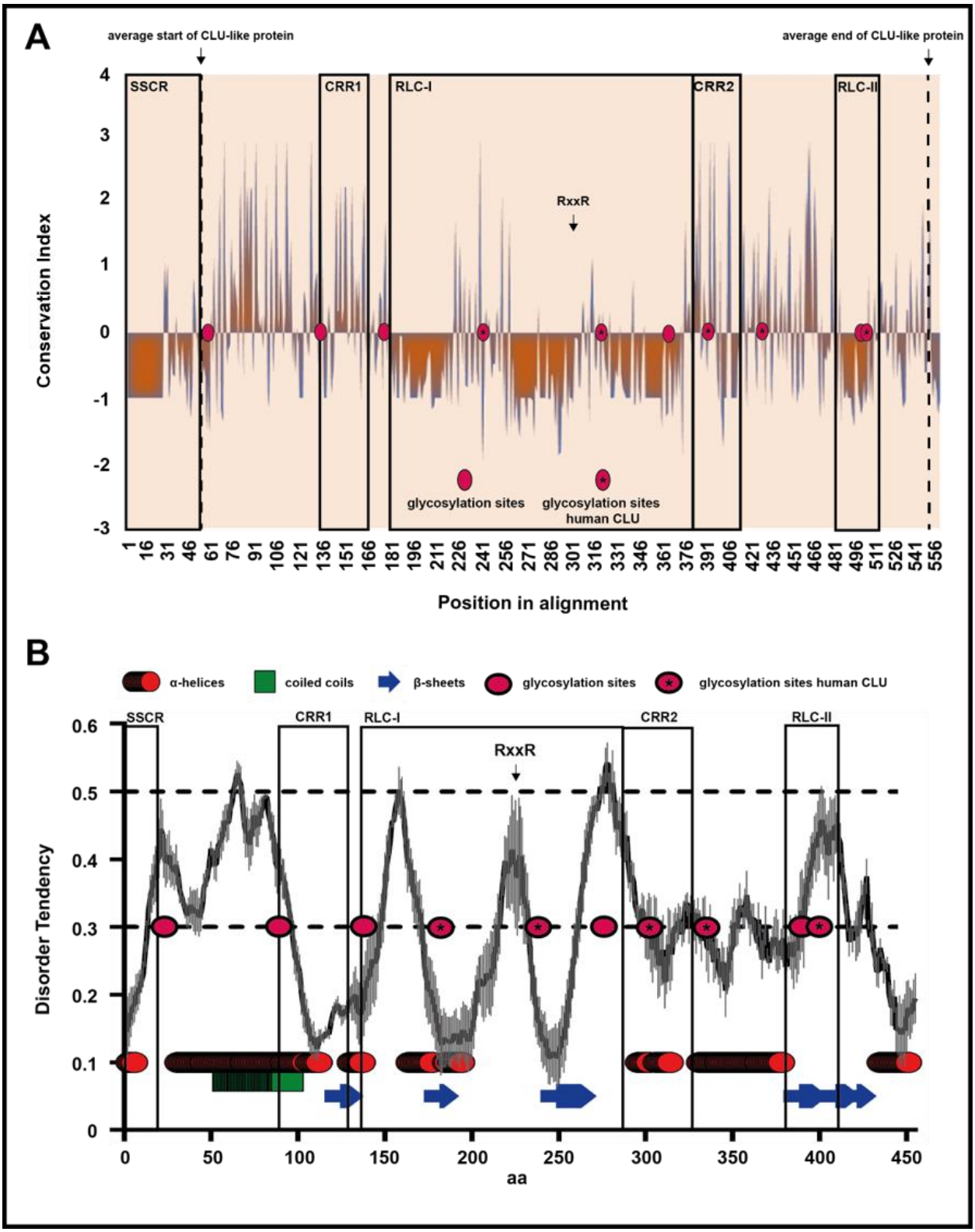

App.4 Identity, disorder tendency and secondary structures of CLUL1. (A) Calculated Conservation Index with 49 species (listed in App.3) according the Method Section (4.4). (B) Disorder tendency and secondary structures predicted from 42 species (455 aa, partially truncated at the N-terminus, all species with a length >470 aa were excluded) according the procedure in 4.4.

App.5 Conservation, residue type, hydrophobicity and secondary structures of CLUL1 aligned, calculated and predicted using PRALINE (see Methods Section 4.4) based on the full-length sequence obtained from 49 various species (see App.3).

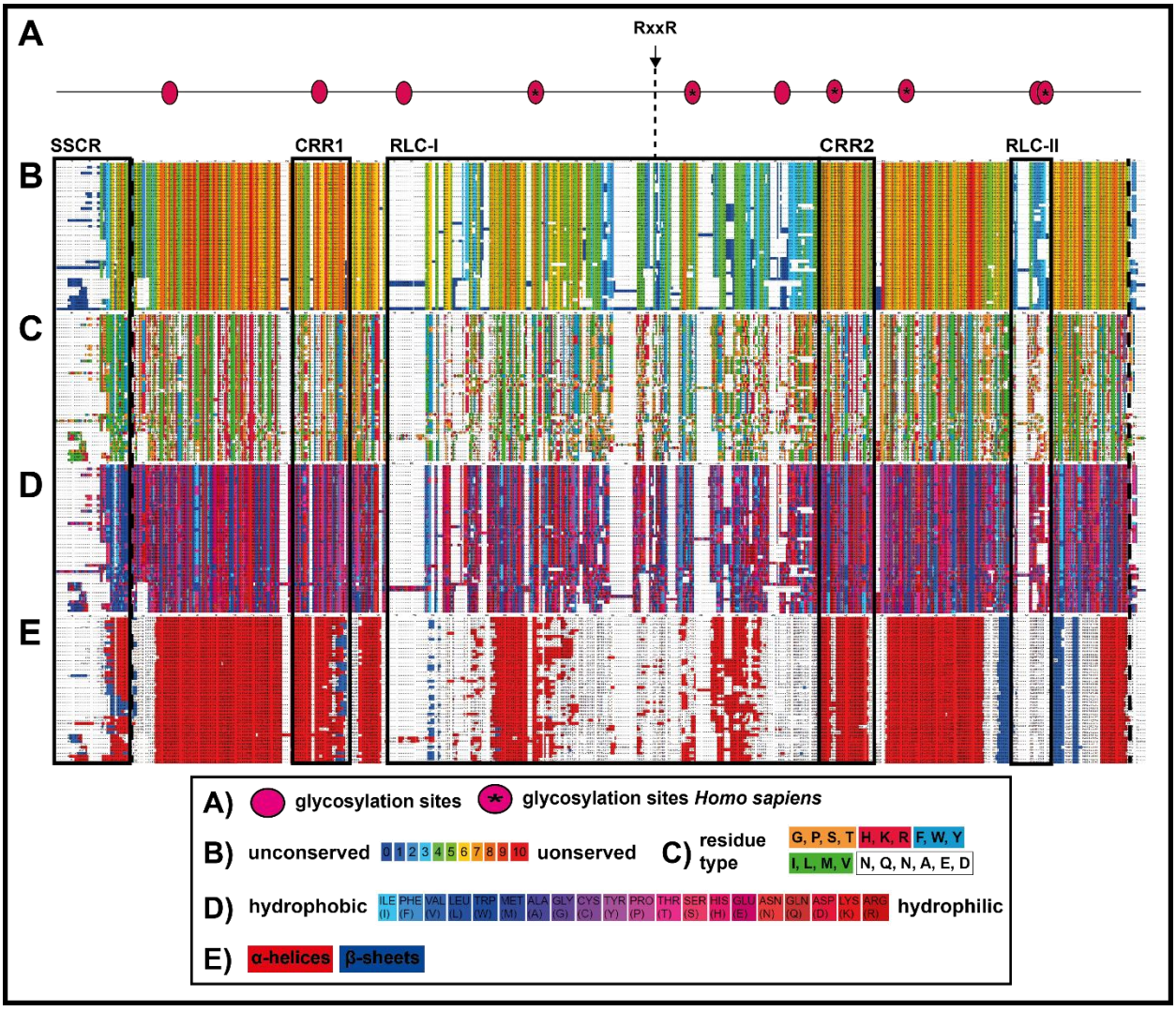

App.6 Supporting experimental files 1. All experiments were conducted according to the standard procedures of comparable experiments shown in the Method and Result Section. (A) HEK-293 were treated with necrotic cell lysates (1 mg/mL) and Src phosphorylation was analyzed by Western blotting (n=3). (B) HEK-293 cells were incubated in presence of Actinomycin D (2 µg/mL) for 6 hours and Western blot analyses and sqRT-PCRs were conducted (n=3). (C-E) HEK-293 were preincubated with 2.5 µg/mL anti-TLR4 blocking antibody (TLR4) or anti-goat isotype control (Iso) and stimulated with 1 mg/mL necrotic cell lysates with subsequent Western blotting and sqRT-PCR (n=3). (F) HEK-293 cells wer stimulated with 5 µg/mL S100A8/S100A9 proteins and respective necrotic cell lysate controls (1mg/mL) with subsequent Western blotting and sqRT-PCR (n=2-3). (G) HSP72 in pcDNA6 (HSP72) and pcDNA6 were transfected into HEK-293 cells for 6 hours, were transferred into fresh 6-well plates, grown for additional 36 hours and cell culture lysates were obtained with standard protocol for generation of necrotic cell lysates. Afterwards, the necrotic cell lysates were applied to vital HEK-293 cells and Western blot analyses were carried out (n=3). (H) Western blot analyses for LC3 lipidation as described in Fig.32A (n=3). (I) Photography of the cell culture supernatants obtained as described in Fig.33G. (J) Experiment with fully confluent SN-N-MC cells according to Fig.32A (n=3).

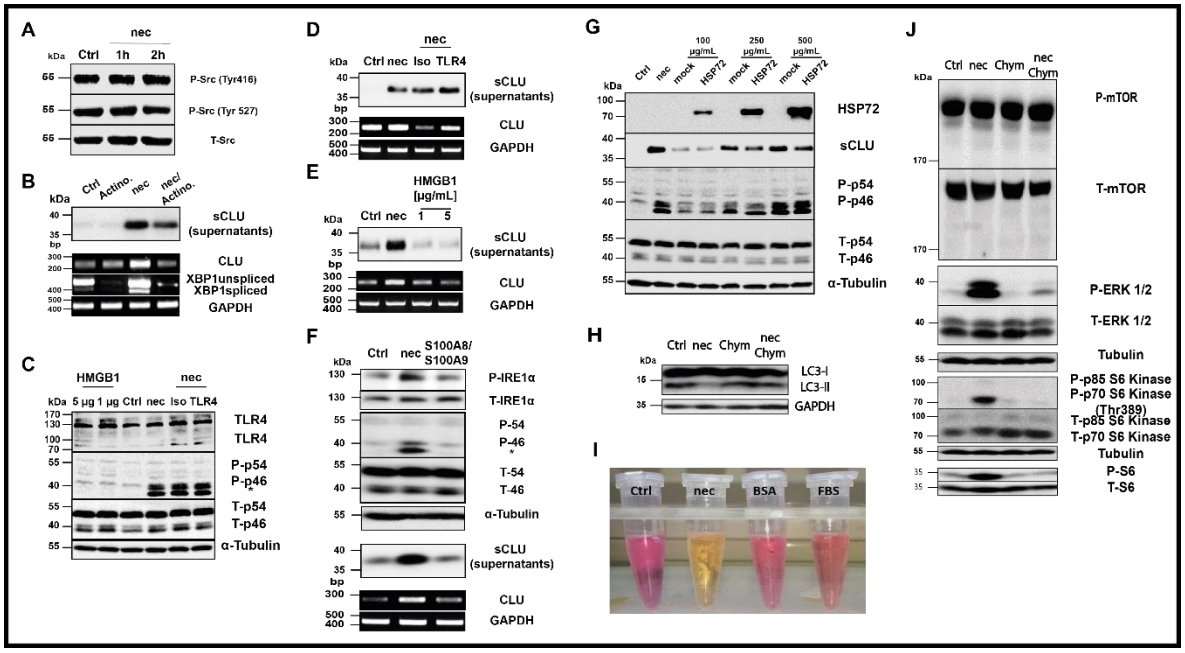

Next page:

App.7 Supporting experimental files 2. All experiments were conducted according to the standard procedures of comparable experiments shown in the Method and Result Section. (A,B) HEK-293 cells were transfected with the indicated constructs cloned in pcDNA6 an 10,000 cells were seeded into 96-well plates (B) and the remaining cells in 6-well plates (A). (A) the cells were set serum-free and Western blot analyses were carried out after 10 hours (n=3). (B) After growing phase the cells were preincubated with 10 µM SP600125 or DMSO for 4 hours and stimulated for 12 hours. Values shown are the mean±standard errors of three independent experiments. Data were analyzed by using one way ANOVA, followed by Tukey's multiple comparison test. (C) Analogue to Fig.31D but with additional stimulation with sCLU or endotoxin-free sterile BSA (n=3). (D) HEK-293 cells were stimulated for 2 hours with 250 µg/mL necrotic cell lysates, in absence (1) or presence of 10 µg/mL of fresh sCLU (2) or sCLU incubated at 37°C without (3) or with 6.25 U/mL PNGaseF for 12 hours (4). Subsequent Western blotting and densitometric analyses using ImageJ were conducted. Values shown are the mean±standard errors of three independent experiments. Data were analyzed by using one way ANOVA, followed by Tukey's multiple comparison test. (E) Experiment analogue to Fig.31D but with various concentrations of APY29 instead of Kira6. Values shown are the mean±standard errors of three independent experiments. (F) HEK-293 were preincubated with 10 µM Kira6 for 4 hours and subsequently stimulated with necrotic cell lysates (1 mg/mL) in presence of absence of 10 µM Kira6 or 3 µM APY29 or both for 2 hours with subsequent Western blotting (n=3). (G) Cell lines as indicated were grown to full confluency and were stimulated after 4 hours on serum-free with 500 µg/mL necrotic cell lysates (nec) obtained from HeLa cells for 2 hours with subsequent Western blotting (n=2-3). (H) Experiment analogue to Fig.31C using supernatants with 6 hours of stimulation and additional sqRT-PCR analyses (n=3).

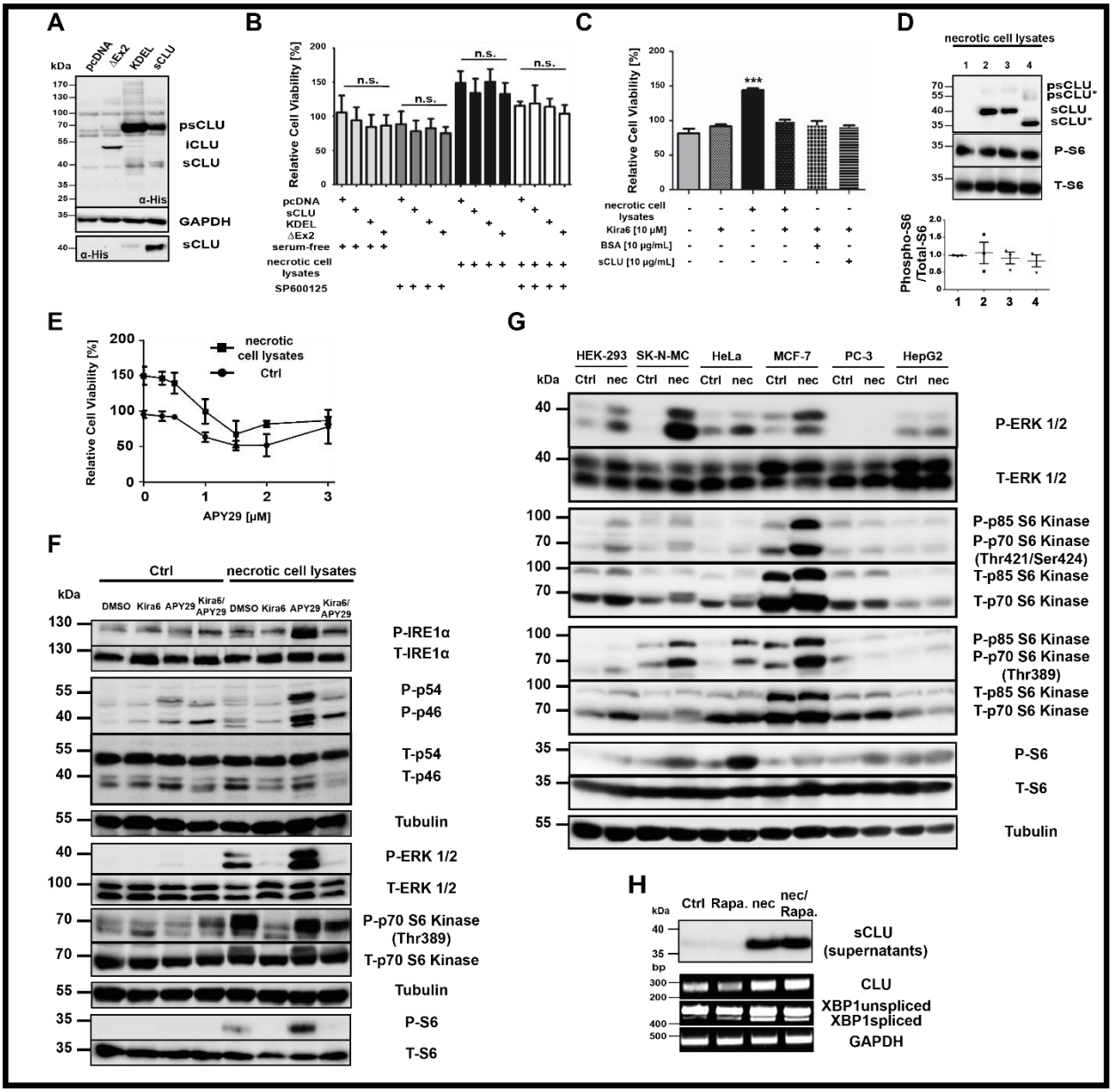
A
kDa
pcDNA
ΔEx2
KDEL
sCLU
psCLU
iCLU
sCLU
α-His
GAPDH
sCLU
α-His
B
Relative Cell Viability [%]
n.s.
pcDNA
sCLU
KDEL
ΔEx2
serum-free
necrotic cell lysates
SP600125
C
Relative Cell Viability [%]
***
necrotic cell lysates
Kira6 [10 μM]
BSA [10 μg/mL]
sCLU [10 μg/mL]
D
necrotic cell lysates
psCLU
psCLU*
sCLU
sCLU*
P-S6
T-S6
Phospho-S6 /Total-S6
E
Relative Cell Viability [%]
necrotic cell lysates
Ctrl
APY29 [μM]
F
Ctrl
necrotic cell lysates
DMSO
Kira6
APY29
Kira6/ APY29
P-IRE1α
T-IRE1α
P-p54
P-p46
T-p54
T-p46
Tubulin
P-ERK 1/2
T-ERK 1/2
P-p70 S6 Kinase (Thr389)
T-p70 S6 Kinase
Tubulin
P-S6
T-S6
G
HEK-293
SK-N-MC
HeLa
MCF-7
PC-3
HepG2
Ctrl
nec
P-ERK 1/2
T-ERK 1/2
P-p85 S6 Kinase
P-p70 S6 Kinase (Thr421/Ser424)
T-p85 S6 Kinase
T-p70 S6 Kinase
P-p85 S6 Kinase
P-p70 S6 Kinase (Thr389)
T-p85 S6 Kinase
T-p70 S6 Kinase
P-S6
T-S6
Tubulin
H
Ctrl
Rapa.
nec
nec/ Rapa.
sCLU (supernatants)
CLU
XBP1unspliced
XBP1spliced
GAPDH

App.8 Result of two mass spectroscopic analyses (mean±standard error) of human sCLU preparations carried out by Dr. Julian Langer at Max Planck Institute for Biophysics in Frankfurt (Main).

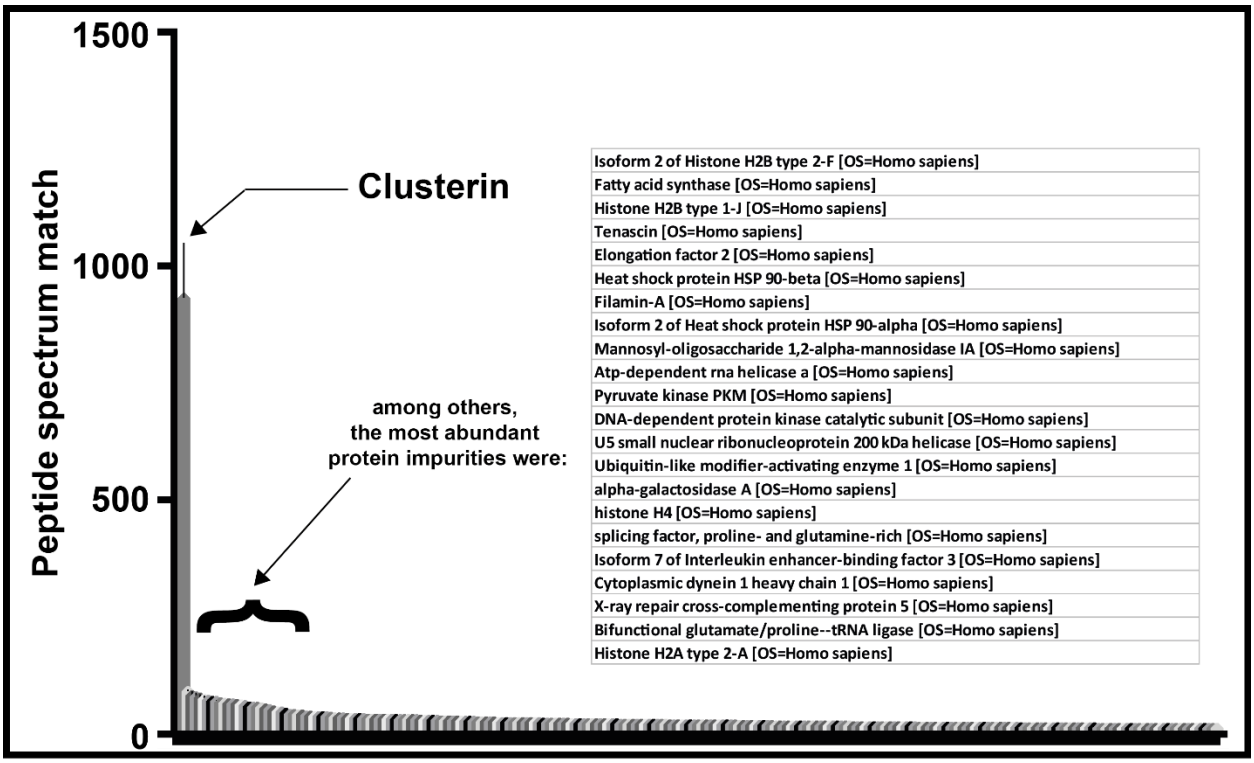

10 Abbreviations

This section contains the most often used abbreviations of this thesis. Additional abbreviations can either found in the respective sections or in associated references.

aa	amino acid
AiP	apotosis-induced Proliferation
AKT	AKT8 virus oncogene cellular homolog
ANOVA	analysis of variance
AP-1	activator protein 1
apoJ	apolipoprotein J
AU	arbitrary unit
Aβ	amyloid beta
BAX	BCL2-Associated X Protein
BiP	binding immunoglobulin protein
bp	base pair
BSA	bovine serum albumin
CD	circular dichroism
CHOP	CCAAT/-enhancer-binding protein homologous protein
CLU	clusterin
CRR	cystein-rich region
DAMP	danger associated molecular patterns
DNA	desoxyribonucleic acid
DMSO	dimethyl sulfoxide
dsRNA	double stranded RNA
eIF2α	eukaryotic Initiation Factor 2 α
ELISA	enzyme-linked immunosorbent assay
ER	endoplasmic reticulum
ERAD	endoplasmic-reticulum-associated protein degradation
ERdj3	endoplasmic reticulum DNA J domain-containing protein 3
ERK	extracellular signal–regulated kinase
FACS	fluorescence-activated cell sorting
FBS	fetal bovine serum
FC	furin-like proprotein cleavage
FPLC	fast protein liquid chromatography
GADD34	growth arrest and DNA damage-inducible protein
Golgi	Golgi apparatus
HDL	high density lipoprotein
HEK-293	human embryonic kidney cells 293
HMGB1	high mobility group box 1
HSF	heat shock factor
HSP	heat shock protein
IRE1α	inositol-requiring enzyme 1α
IRI	ischemia-reperfusion injury
JNK	c-Jun N-terminal kinases
kDa	kilo dalton
LDL	low-density lipoprotein
LEW	lysis equilibration wash
LPS	lipopolysaccharide
LRP	lipoprotein receptor-related protein
mTOR	mechanistic target of rapamycin
nec	necrotic cell lysates
NF-κB	nuclear factor kappa-light-chain-enhancer of activated B cells
NiP	Necrosis-induced Proliferation
nt	nucleotide
p70/p85S6K	p70- & p85S6 ribosomal kinase

PDK1	phosphoinositide-dependent protein kinase 1
PERK	protein kinase RNA-like endoplasmic reticulum kinase
PI3K	phosphatidylinositol-4,5-bisphosphate 3-kinase
PRALINE	PRofile ALIgNEment
psCLU	presecretory Clusterin
qRT-PCR	quantitative Reverse Transcription PCR
RACE	rapid amplification of cDNA ends
RIDD	regulated Ire1-dependent decay
RLC	region of low conservation
RNA	ribonucleic acid
RT	Reverse Transcriptase
sCLU	secretory Clusterin
Scr	cellular sarcoma
SDS-PAGE	sodium dodecyl sulfate polyacrylamide gel electrophoresis
si	rmall interfering
sh	small hairpin
Scr	scrambled
sqRT-PCR	semiquantitative Reverse Transcriptase PCR
SSCR	signal sequence-coding region
Tg	Thapsigargin
TLR	Toll-like receptor
TNF	tumor necrosis factor
TRAF	TNF receptor associated factor
UPR	unfolded protein response
VLDLR	very low density lipoprotein receptor
XBP1	X-box binding protein 1